The role of *Pygopus 2* in Neural Crest

KEVIN ROBERT GILLINDER

A Thesis submitted for the Degree of Doctor of Philosophy

Institute of Genetic Medicine

Newcastle University

April 2012

Abstract

Epidermal neural crest stem cells (EPI-NCSC) are remnants of the embryonic neural crest that reside in a postnatal location, the bulge of rodent and human hair follicles. They are multipotent stem cells and are easily accessible in the hairy skin. They do not form tumours after transplantation, and because they can be expanded *in vitro*, these cells are promising candidates for autologous transplantation in cell replacement therapy and biomedical engineering.

Pygopus 2 (*Pygo2*) is a signature gene of EPI-NCSC being specifically expressed in embryonic neural crest stem cells (NCSC) and hair follicle-derived EPI-NCSC, but not in other known skin-resident stem cells. *Pygo2* is particularly interesting, as it is an important transducer of the Wnt signaling pathway, known to play key roles in the regulation of NCSC migration, proliferation, and differentiation.

This study focuses on the role of *Pygo2* in the development of the neural crest (NC) in vertebrates during development. Three loss-of-function models were utilized to determine the role *Pygo2* in mouse and zebrafish development, and EPI-NCSC *ex vivo*. A Wnt1-specific loss of *Pygo2* in mice causes multi-organ birth defects in multiple NC derived organs. In addition, morpholino (MO) knockdown of *pygo* homologs within zebrafish leads to NC related craniofacial abnormalities, together with a gastrulation defect during early embryogenesis. While *ex vivo* studies using EPI-NCSC suggest a role for *Pygo2* in cellular proliferation. Overall, these results suggest that *Pygo2* is required for the normal development of specific NC derived organs and cell types in a context dependent manner.

Acknowledgements

First and foremost, I would like to take this opportunity to sincerely thank my supervisor, Dr Colin Miles for his endless support, guidance and encouragement. I have especially enjoyed our fruitful scientific discussions and the endless hot chocolates!

Throughout my time at the Institute of Genetic Medicine, I have had the pleasure of working alongside a number of brilliant scientists from numerous laboratories. These have included past and present members of the Miles lab, Sieber-Blum lab, and the Muscle team. I thank them all for their friendship, scientific discussion and technical support.

I would also like to acknowledge my collaborators and students: Dr Oliver Clewes for his assistance with real-time (qPCR) analysis of *Pygo1* expression, Alla Narytnyk (MSc student), for assistance with analyses on the hair and skin, Linda Julian (MSc student), for contributions to analyses on the Me5 and brain, Professor Heather Cordell for assistance with statistical analysis of hair follicle stages, and Dr Owen Hughes and Ian Dimmick for assistance with FACS. Thanks also to Professor Steven Potter and Dr Robert Kelsh for providing the transgenic animal strains used in this study.

Further thanks to Colin, Dr Steve Laval, and Professor Volker Straub for financial assistance towards the end of my studies – it is highly appreciated. In addition, I would also like to thank the many brave souls for manuscript proof reading in the final days, including Colin, Oli, Juliane, Owen, Lee, Carla and Sian.

Finally, very special thanks go to my wife, Sian, for her constant care and support, and most importantly keeping me well fed. I also thank the rest of our families for their love, understanding, and support during this significant endeavour.

TABLE OF CONTENTS

List of Figures

List of Tables

List of Abbreviations

A-P	Anterior to posterior axis
AFD	Acrofacial dysostosis syndrome
ANOVA	Analysis of variance
BLAST	Basic local alignment search tool
CaNCC	Cardiac – Neural Crest Cells
cDNA	Complementary DNA
CNCC	Cranial – Neural Crest Cells
CNS	Central nervous system
Cre	Cre recombinase
CSF	Cerebrospinal fluid
DI	Dentinogenesis imperfecta
DNA	Deoxyribonucleic acid
DORV	Double outlet right ventricle
dpc	Days post coitum
DRG	Dorsal root ganglia
ED1	Emigration Media
EMT	Epithelial to mesenchymal transition
ENS	Enteric nervous system
EPI-NCSC	Epidermal Neural Crest Stem Cell
ESC	Embryonic stem cell
EST	Expressed sequence tag
FACS	Fluorescent activated cell sorting
FSC	Forward scatter
GFP/eGFP	Green fluorescent protein/Enhanced green fluorescent protein
GFP$^+$/GFP$^-$	Isolated GFP fluorescent/non-fluorescent populations isolated using FACS
GI	Gastro intestinal tract
GOI	Gene of interest
H&E	Haematoxylin and Eosin
HEK293	Human embryonic kidney cell line (293)
hpf	Hour post fertilization
hpp	Hours post partum
LongSAGE	Long serial analyses of gene expression
loxP	Locus of X-over P1
Me5	Mesencephalic trigeminal nucleus
MO	Morpholino

mRNA	Messenger RNA
NC	Neural Crest
NCBI	National centre for biotechnology information
NCP	Neural Crest Progeny
NCSC	Neural crest stem cells
neo	Neomycin
NHD	N-terminal homolog domain
NLS	Nuclear localization signal
OFT	Cardiac outflow tracts
Pax3	Paired box 3 gene (*Splotch* is a naturally occurring mutant of *Pax3*)
PBS	Phosphate Buffered Saline
PCP	Planar cell polarity pathway
PCR	Polymerase chain reaction
PFA	Paraformaldehyde
PHD	Plant homology domain
PNS	Peripheral nervous system
PTA	Persistent truncus arteriosus
Pygo/pygo	Pygopus gene
Pygo1/pygo1	Pygopus 1 homolog
pygo1TR	Antisense morpholino targeted to zebrafish *pygo1* (translational blocking)
Pygo2 CKO	Wnt1-Cre conditional knockout of *Pygo2*
Pygo2$^{-/-}$	Homozygous *Pygo2* knockout/*null*
Pygo2/pygo2	Pygopus 2 homolog
Pygo2$^{fl/fl}$	Homozygous *Pygo2* floxed
pygo2TR	Antisense morpholino targeted to zebrafish *pygo1* (translational blocking)
RNA	Ribonucleic acid
RT-PCR	Reverse transcriptase - PCR
SC	Stem cell
SEM	Standard error of the mean
SNCC	Sacral – Neural Crest Cells
SSC	Side Scatter
TNCC	Trunk – Neural Crest Cells
VNCC	Vagal Neural Crest Cells
wg	wingless (*Drosophila* homolog of vertebrate Wnt1)
Wnt	Wnt "wint" pathway
WRE	Wnt Responsive elements
X-gal	5-bromo-4-chloro-indolyl-β-D-galactopyranoside
XP1	Expansion media
β-gal	β–galactosidase

Chapter 1. Introduction

The discovery of epidermal neural crest stem cells (EPI-NCSC) [1,2] has raised the possibility of using an adult stem cell (of neural crest origin) for cell-based therapeutic applications. This is a promising development in regenerative medicine, primarily for three reasons. Firstly, the usage of adult stem cells circumvents many of the ethical difficulties associated with embryonic stem cells. Secondly, with a minimally invasive procedure, EPI-NCSC may be cultivated and thus, present an attractive source of stem cells for autologous transplant. And finally, being a remnant of an embryonic germ layer, EPI-NCSC may potentially be far more amenable to reprogramming than other adult stem cell counterparts, like induced pluripotent stem cells [3].

Nevertheless, a greater understanding of the origin, development and genetic regulation of EPI-NCSC is required for the development of future therapeutic applications utilizing these cells. This research project focuses on analyzing a Wnt pathway cofactor that forms part of the specific molecular signature of EPI-NCSC and its role in the developing neural crest (NC).

1.1 The Neural Crest

1.1.1 Primary and secondary germ layers in vertebrate development

Early in vertebrate development, nearly all species are indistinguishable. While there are obvious variations during development in organism size and developmental timing, they undergo similar developmental stages from fertilization throughout embryogenesis. This observation led Ernst von Baer to conclude that during the early stages of development, all vertebrates share an analogous morphology [4].

Following fertilization, the totipotent zygote is a single, diploid cell that will form the new organism. It undergoes a series of mitotic cell divisions in a stage termed cleavage that results in numerous cells, called blastomeres. The

blastomeres form a compact mass of cells, the morula, which will later expand as blastulation progresses allowing the formation of a blastocoele and enlargement of the blastodisc. The blastocoele is a fluid cavity in the centre of the newly formed blastula. At this stage, some of the differences among vertebrates become obvious. The mammalian, equivalent to the blastocyst, the blastula, is comprised of an outer layer (trophoblast) that will form the placenta, a blastocoele and the inner cell mass, which will develop into the embryo proper [4].

The primitive streak forms along the blastodisc prior to gastrulation and at this stage, there are two primary germ layers, the ectoderm and the endoderm. Importantly, gastrulation creates a third germ layer, the mesoderm, from the existing ectoderm and endoderm. These germ layers will subsequently give rise to all organs and tissues during organogenesis. While all vertebrates undergo gastrulation, the process varies amongst vertebrates and thus, it is another stage at which the diversity amongst vertebrates is apparent. During gastrulation, the embryo is reorganized to internalize the presumptive mesoderm by various mechanisms of cellular movement, including involution or ingression (see Figure 1-1). In mammals and avians it is primarily ingression, whereas other vertebrates utilize both morphogenic cell movements, to achieve the formation of the three germ layers [5].

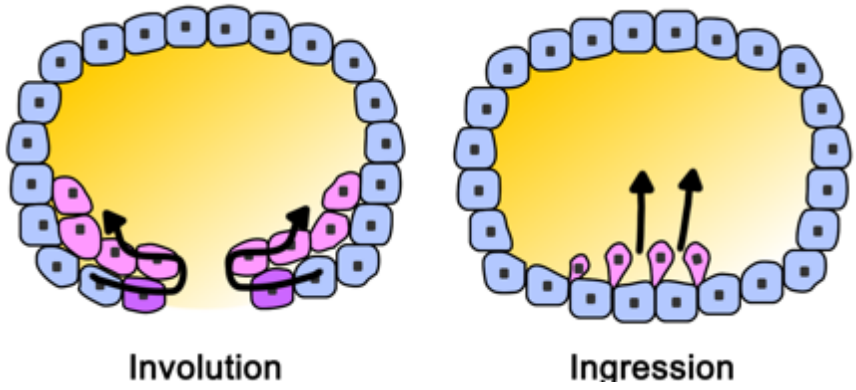

Figure 1-1. Types of cell movements during vertebrate gastrulation
Mammals and avians primarily use ingression of cells to form the mesoderm during gastrulation, whereas other vertebrates use a combination of both involution and ingression. *Adapted from Shook and Keller (2008)*[5].

1.1.2 The fourth germ layer: formation of the NC

The NC was identified independently in 1874 by William His [6], and by Arthur Milnes Marshall in 1879 [7]. Both authors described a band or group of cells that contribute to the formation of adult tissue between the ectoderm and the newly formed neural tube. More recently, Hall has proposed the NC to be an additional fourth germ layer in vertebrate development. This conclusion is based on the definition of a germ layer, and relies upon the inclusion of the mesoderm in germ layer theory. Hall argues that "mesoderm is a secondary germ layer", because it is not specified at the cellular level in the zygote and is formed by inductive interactions between ectoderm and endoderm [8,9]. Like mesoderm, the NC is derived from inductive interactions of a primary germ layer, that is, the neural ectoderm and the non-neural ectoderm. In addition to its derivation from a primary germ layer, the NC independently gives rise to an array of tissue and cell types. Thus by definition, the NC is a secondary germ layer, in addition to the mesoderm [10].

The fourth germ layer, or NC is a transient population of cells that exists for a brief period of time during embryogenesis and its development can be broken down into discrete steps (summarized in Figure 1-2). Near the end of gastrulation, the notochord is formed from the newly created mesoderm at the base of the epiblast. The notochord subsequently induces the ectoderm layer above to thicken, forming the neural plate, as in Figure 1-2A. Following this, the embryo moves into organogenesis, beginning with neurulation and formation of the neural tube. The neural tube is formed from the neural plate by two different processes in all vertebrates in a rostrocaudal wave. Primary neurulation occurs in the cranial region, when the neural plate creases and folds at the lateral borders of the non-neural ectoderm. While in secondary neurulation, the neural tube forms by hollowing out the solid precursor, from the tail bud blastema [10]. In this way, NC may be thought of as having a dual origin, neuroectoderm (primary) and tail bud in caudal NC (secondary). Importantly, neurulation leads to the formation of the neural crest (NC) from the cells at the border of the neural ectoderm and the non-neural ectoderm (see Figure 1-2D)[11].

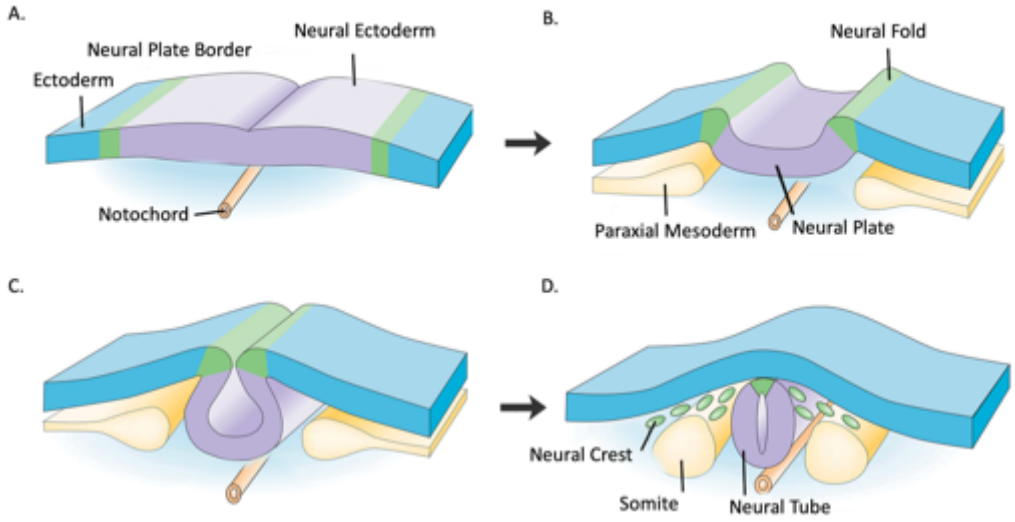

Figure 1-2. NC induction at the border of the neural ectoderm during neurulation
(A-D) Schematic of a transverse section through an embryo with the neural shown in green, neural tube in purple, and ectoderm in light blue. The neural plate border is induced by reciprocal inductions from the non-neural ectoderm and neural ectoderm (A). The neural plates creases and folds during neurulation and comes together to form the neural tube (B-D). Neural crest cells are induced (B) along the neural folds, undergo EMT and subsequently delaminate from the neural folds and dorsal neural tube. *Adapted from Gammill and Bronner-Fraser (2003)*[11].

1.1.3 Specification of the Neural Crest

Specification of the cells fated to become NC occurs during gastrulation [11], by a combination of extracellular signals secreted from the surrounding tissues. The precise timing and interactions of these signals is still unclear, and differs between species. It is also important to recognize that several populations of NC arise along the rostrocaudal axis and this adds further complexity to elucidating the exact genes regulatory network (see recent review [12]). Despite this, attempts have been made to create a generalized overview of the genes involved in the specification process, which may be divided into a number of discrete regulatory modules [13,14].

At the molecular level, specification is reliant upon the expression of *Distal-less homeobox 5* (*Dlx5*) for the formation of border cell types in the non-neural ectoderm [15]. Additionally, Wnt proteins, bone morphogenetic proteins

(BMPs), fibroblast growth factors (FGFs) and *Notch/Delta* all upregulate transcription factors from the *Msx, Pax* and *Zic* gene families along the neural and non-neural ectoderm border [14]. In turn, the following NC specifier genes are induced, *Ap2*, *cMyc*, *Foxd3*, *Id*, *Slug/Snail*, *Twist* and *Sox9* and *Sox10* in pre-migratory NC [16]. Importantly, at the closure of the neural tube, *Wnt1* is transiently expressed within the dorsal neural tube cells, and pre-migratory neural crest [17,18] and has been used in many studies as a marker of neural crest derived cells in tissues other than the central nervous system (CNS) [19,20].

1.1.4 Migration and derivatives of the Neural Crest

Following specification, neural crest stem cells (NCSC) are formed during neurulation along the dorsal aspect of the neural tube. The expression of *cMyc*, *Id* and *Sox9* maintain NCSC in a multipotent state and confer anti-apoptotic properties [21-23]. However, they do not immediately begin proliferation. Instead, they subsequently undergo an epithelial to mesenchymal transition (EMT), and delaminate from the neural tube to migrate along a number of specified pathways [24]. These pathways are determined by the position at which the neural crest cells are first induced in the rostrocaudal sequence of neural tube closure.

EMT is triggered by the integration of extracellular matrix components, such as collagen or hyaluronic acid, and secreted factors, such as TGFβ and FGF families [25]. Subsequent activation of NC specifier genes like *Snail1*, *Snail2*, and *FoxD3* also help to coordinate the EMT process. Interestingly, NC EMT shares three mechanisms also required for metastasis of tumor cells [24]. Firstly, gap junctions replace tight junctions. This leads to a loss of cellular polarity and cell-to cell interactions. Secondly, the levels of specific cadherins are altered from type I to type II, allowing cellular motility. And finally, there is production of metalloproteinase for the digestion of extracellular matrix [26]. While these processes are shared with tumour cells, NC display remarkably little proliferation during EMT.

Premigratory cells are arrested in G_1 phase of the cell cycle and only enter S-phase upon delamination from the dorsal neural tube. This is likely due to the expression of Snail, which represses Cyclin D1 and D2 required for G1/S phase transition [27-29]. Following EMT and delamination, the NCSC begin proliferating and emigrate from the dorsal neural tube. During migration, NCSC are broadly categorized in five groups, based upon the location at which they emigrate from or migrate to as summarized in Figure 1-3. Briefly, these are cranial (CNCC), cardiac (CaNCC), trunk (TNCC), vagal (VNCC) and sacral (SNCC) neural crest cells [30].

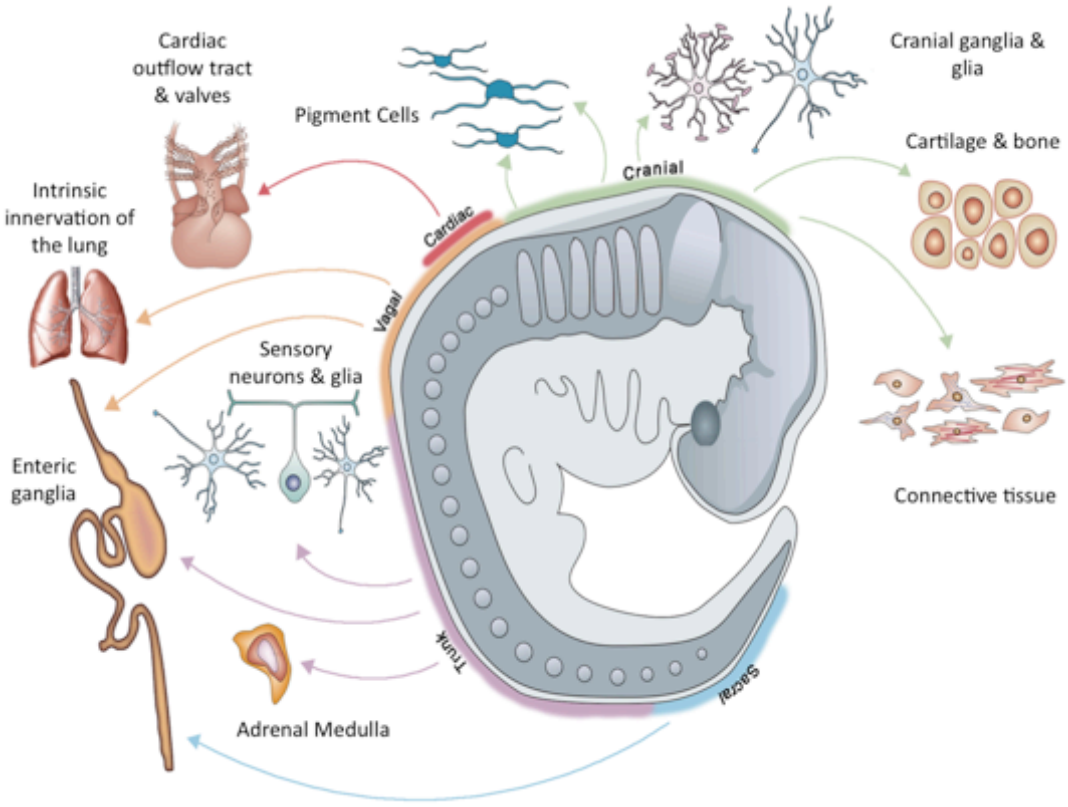

Figure 1-3. Derivatives and emigrational sub-units of the NC
The NC is divided into sub-groups based on the location from which NCC emigrate or migrate to. NCSC can form multiple cell types including, cartilage and bone, connective tissue, pigment cells, sensory neurons, glia, and ganglia, Schwann and chromaffin cells. *Adapted from Hall (2008) and Knecht and Bronner-Fraser (2002)*[10,18].

The CNCC gives rise to bones, cartilage, nerves and connective tissue of the head [31-34]. CaNCC (a subset of VNCC) migrate to the aortic sac, forming the neurons and supporting cells of the cardiac ganglia and participate in septation of the outflow tracts [35-37]. The vagal (VNCC) and sacral neural crest (SNCC) form the peripheral nervous system (PNS), including spinal, cranial and enteric ganglia, intrinsic neurons of organs, Schwann, glial and medullary chromaffin cells [38-40]. While, TNCC predominantly give rise to pigment cells and neurons of the sympathetic nervous system [41].

1.1.5 NCSC are multipotent stem cells

Stem cells are defined as cells with the ability to self-renew, together with the capacity to generate a number of differentiated cell types. In vertebrates, there are two main types of stem cells. Embryonic stem cells are derived from the inner cell mass of the blastocyst/blastula and are termed pluripotent, as they are capable of giving rise to all cell types within the embryo and adult. On the other hand, multipotent stem cells are derived from pluripotent stem cells and help to construct the specific tissues in the embryo. While they maintain cellular turnover or provide regenerative capacity in the adult. However, the differentiation potential of multipotent stem cells is considered more restricted than that of pluripotent stem cells.

Single cell lineage experiments have previously demonstrated the multipotent potential of NC. Dorsal neural tube cells and migrating NC (both in chick) labeled with vital dye show that some of the clones contribute to multiple cell types in the periphery of the organism [42]. Clonogenic cultures of emigrating NC are also multipotent [43-47] with a capacity for self-renewal, at least for a few cell divisions [47-49].

However, the NC is best described as a dynamic heterogeneous population of multipotent and progenitor cells (NCSC). *In vitro* NCSC cultures show a variable capacity for multipotency [50] and clonal cultures from later stage embryos, have shown that commitment to cell fate becomes restricted with both time and location [51]. For example, Quail CaNCC cultures are capable of producing multiple cell types, including smooth muscle, connective tissue, chondrocytes

and neurons. However, during progressive migration towards the cardiac outflow tract, CaNCC loose the ability to give rise to sensory neurons and to pigment cells [52,53].

Yet, late stage NC cells in zebrafish, are still able to fill the role of early NC progenitors following their ablation [54,55]. In addition, heterotopic transplants between different axial levels of NC (chick) reveals that TNCC can produce normal cranial derivatives, and CNCC can form trunk derivatives, with the partial exception of cartilage [56-60]. These experiments highlight that there is some flexibility in fate, and that it is largely dependent upon the microenvironment in which the NC is examined.

1.1.6 Neurocristopathies: when things go wrong

Due to the range of tissues that the neural crest contributes to (refer to Figure 1-3), it is not surprising that there are many syndromes, tumors and dysmorphologies involving the NC. These have collectively been given the name of neurocristopathies. Some neurocristopathies occur as tumours. Neuroblastoma is of the most common neurocristopathy and accounts for 15% of cancer deaths in children [61-64]. Neurofibromatosis Type 1 (NF1) is another form of NC related tumour. These tumours cause multiple pigmentation abnormalities, appear in early childhood, and increase in both size and number with age. This can subsequently lead to the development of tumors along nerves in the skin, brain, and other parts of the body [65-67].

Abnormal development of the NC can also lead to complex dysmorphologies. DiGeorge syndrome is characterized by cardiac conotruncal malformations, aortic arch defects, craniofacial abnormalities and hypoplasia of the thymus and parathyroid; all attributed to defects in NC [68]. In addition, a failure of NC migration can lead to a loss of enteric ganglia in the distal colon, leading to Hirschsprung's disease [69,70].

1.1.7 Unifying features of the neural crest

In summary, the NC is an important secondary germ layer in vertebrate development. The NC is specified at the border of the neural and non-neural

ectoderm, by a combination of BMP, Wnt, FGF, and Delta/Notch signaling. NCSC migrate to many different regions of the embryo, proliferate and contribute to a vast array of tissue and cell types. In addition, NCSC are a heterogeneous population of multipotent stem cells and their developmental options become restricted with progressive migration due to their microenvironment. And finally, deficiencies in NC development can lead to severe diseases and syndromes of early childhood. Thus, NCSC represent an important and unique population of multipotent progenitor cells capable migration and proliferation throughout development. Importantly, three primary features unify the NC and by extension NCSC. That is, they are highly migratory, proliferative and multipotent.

1.2 Epidermal Neural Crest Stem Cells

1.2.1 EPI-NCSC are multipotent stem cells

Recently, multipotent stem cells derived from the NC have been identified, isolated and characterized from the bulge of rodent and human hair follicles [71,72]. These cells were demonstrated to be remnants of the embryonic NC using the lineage tracing to identify and label derivatives of the NC [1,73]. Cells were specifically found residing within the bulge, dermal papillae and outer root sheath of the adult whisker follicle. In addition, neural crest derived cells were also identified in the facial dermis and connective tissue, but not within the epidermis [1].

Ex vivo culturing of micro-dissected bulges from mouse whisker follicles promoted the emigration of EPI-NCSC from explants. These cells were again confirmed as neural crest in origin, expressing Sox10, a marker of neural crest cells [74]. Clonal culturing of EPI-NCSC shows that they are multipotent. Extended cultures of EPI-NCSC can differentiate into multiple cell types including neurons, smooth muscle cells, pigment cells and Schwann cells. EPI-NCSC can undergo directed differentiation into chondrocytes, osteocytes, melanocytes and Schwann cells. EPI-NCSC are capable of rapid division and

expansion *in vitro* and serial cloning has shown that they are capable of self-renewal [71,75].

Taken together, these results suggest that EPI-NCSC are multipotent stem cells capable of differentiation into cranial neural crest cell types. In addition they share unifying characteristics of NCSC in their ability to migrate, proliferate and differentiate into multiple cell lineages [1,2].

1.2.2 Therapeutic applications of EPI-NCSC

Given that EPI-NCSC are multipotent somatic stem cells that can be expanded *ex vivo*, and which can undergo directed differentiation [72], these cells are promising candidates for autologous transplantation in cell replacement therapy and biomedical engineering. The location of EPI-NCSC is not limited to the whisker follicles of mice, as they can be cultured from both human and mouse hairy skin [2,71,72]. They can also be isolated as a highly pure population of stem cells *in vitro*. Thus, they represent an easily accessible, adult source of multipotent stem cells.

In a mouse model of lesioned spinal cord, EPI-NCSC grafts were able to integrate into the host without *in vivo* proliferation or tumor formation [76]. Furthermore, EPI-NCSC transplants into contused spinal cord resulted in an increase in sensory connectivity and renewal of touch perception [77,78]. These preliminary experiments highlight the therapeutic potential of EPI-NCSC and reinforce the need for further characterization and understanding of EPI-NCSC biology.

1.2.3 An EPI-NCSC molecular signature

At the molecular level, EPI-NCSC have further been characterized to discern a genetic signature independent from other skin resident stem cells [74,76]. Three long serial analyses of gene expression (LongSAGE) libraries were prepared with mRNA from two-day-old cultures of EPI-NCSC and NC, and seven-day-old cultures of neural crest progeny (NCP) explants. Differentially expressed tags between the NC and NCP LongSAGE libraries were compared to the EPI-NCSC LongSAGE library yielding 91 mRNA sequences common to both

the EPI-NCSC and NC libraries. Genes known to be expressed in epidermal stem cells [79] were subtracted from these 91 common sequences, giving a panel of 19 signature genes specifically expressed in EPI-NCSC and NC, but not in epidermal stem cells. These 19 signature genes are summarized in Table 1-1. This molecular signature of EPI-NCSC was subsequently validated by quantitative reverse transcriptase PCR (RT-PCR) and immunocytochemistry for two genes, Msx2 and myosin10 (Myo10) [74].

The molecular signature contains numerous genes involved in cellular processes such as RNA, protein and lipid metabolism, gene transcription, cell cycle, apoptosis and cytoskeletal regulation. Importantly, *Pygopus 2* (*Pygo2*) is present in this molecular signature. Within the panel of 19 genes, it has one of the highest fold-difference and confidence value ($p<0.0046$) shown by LongSAGE analysis. *Pygo2* is a recently discovered member of the Wnt pathway, yet its exact role remains unclear in mammals. For this reason (and others, discussed later) it is the primary focus of this research project. As such, it will be covered in detail in the following section (See Section 1.3; p12).

Table 1-1. EPI-NCSC Molecular Signature

Unigene	Gene Symbol/ID	Gene
Mm.286394	Pcbp4	Poly(rC)-binding protein 4
Mm.1763	Msx2	Msh homeobox 2
Mm.33796	H1fx	H1 histone family, member X
Mm.26995	Thop1	thimet oligopeptidase
Mm.28420	Vars2	Valyl-tRNA synthetase,
Mm.60590	Myo10	Myosin X
Mm.259293	2700094K13 Rik	Expressed sequence tag (EST)
Mm.292415	Ets1	V-ets erythroblastosis virus E26 oncogene homolog 1
Mm.22521	Pygo2	Pygopus 2
Mm.323601	Adam12	ADAM metallopeptidase domain 12
Mm.1971	Calr	Calreticulin
Mm.200898	AU041707	1-acylglycerol-3-phosphate O-acyltransferase 6
Mm.21065	5730449L18Rik	Expressed sequence tag (EST)
Mm.14768	Rex3	Brain expressed gene 1
Mm.320575	Peg10	Paternally expressed 10
Mm.178	Cryab	Crystallin, alpha B
Mm.288924	Ube4b	Ubiquitin conjugation factor E4 B
Mm.290995	Crmp1	Dihydropyrimidinase-related protein 1
Mm.3555	Vdac1	Voltage-dependent anion channel 1

Source: Hu et al. (2006)[74]

1.3 Pygopus: discovery & function

In 1999, Prieve and Waterman reported that an additional component of the Wnt signaling pathway was required for gene activation [80]. This conclusion was based on the discovery that nuclear localization of the transcriptional units, β-catenin and T cell factor/lymphoid enhancer factor (TCF/LEF), are not sufficient to initiate transcription. This prompted numerous groups to search for the 'missing component' of the canonical Wnt signaling pathway. In 2002, multiple groups simultaneously identified the *pygopus* gene (*pygo*) in *Drosophila melanogaster* (fruit fly) as a binding partner of both β-catenin and TCF/LEF [81-84]. Since then, it has been demonstrated that Pygo is a nuclear protein, with two conserved domains, the plant homology domain (PHD) and the N-terminal or N-box homology domain (NHD), which together act as a transcriptional co-activator in Wnt signaling.

1.3.1 The importance of the Wnt pathway

The Wnt pathway is essential for vertebrate development [85]. It plays an important role during gastrulation, with formation of the embryonic axis, through organogenesis of multiple organ systems, and into maturity of the adult form [86-90]. For example, normal development of the NC relies upon the Wnt pathway for specification, and migration [91,92]. While in mature vertebrates, the Wnt pathway is required for limb regeneration, fracture repair and healing [93-96]. At the cellular level, it controls cell proliferation, maintenance, differentiation, migration and tissue polarity [97]. In addition, the Wnt pathway has been implicated in human degenerative diseases, such as Alzheimer's disease and osteoarthritis, and is linked to the aetiology of cancer [98-100]. For instance, when β-catenin is mutated or components of the destruction complex fail to destroy β-catenin, it can lead to malignancy, as is the case for colon carcinoma [101]. Thus, β-catenin and the Wnt pathway as a whole, represent an important potential target for drug and stem cell therapies [102,103]. However, the reality of this is far more complicated.

The Wnt pathway is a complex signaling network (see Figure 1-4 & Figure 1-5). The ligands and receptors of the Wnt pathway are represented by large multi-gene families, providing numerous ligand-receptor combinations that contribute to a range of signaling outputs [104]. Within the Wnt pathway, the precise arrangement and state of ligands and receptors can activate multiple signaling cascades. Binding of a particular receptor and or co-receptor allows the cell to discriminate which cascade is to be activated in a context specific manner [105] as summarized in Figure 1-4.

Classically in Wnt biology, these cascades have been described as the canonical and non-canonical pathways depending on their functional ability to induce an ectopic axis in Drosophila [106]. Recently van Amerongen and Nusse (2009) have proposed that these linear views of signaling cascades are misleading and the Wnt pathway should be studied in context of its multiple outcomes, cross-talk and regulatory inputs [105]. However, these descriptions are still relevant

to define the activated signaling cascade and final downstream outcomes of the Wnt pathway.

Activation of these signaling cascades begins with the Wnt ligand. Wnt proteins form a family of secreted glycoproteins that bind to the Frizzled family of G protein-coupled receptors and the low-density lipoprotein receptor-related protein 5 (LRP5) or LRP6 [107]. They may also independently bind Ror2 and RYK [108,109]. Binding of a particular receptor and or co-receptor is the first step in the initiation of either the canonical or the non-canonical pathways.

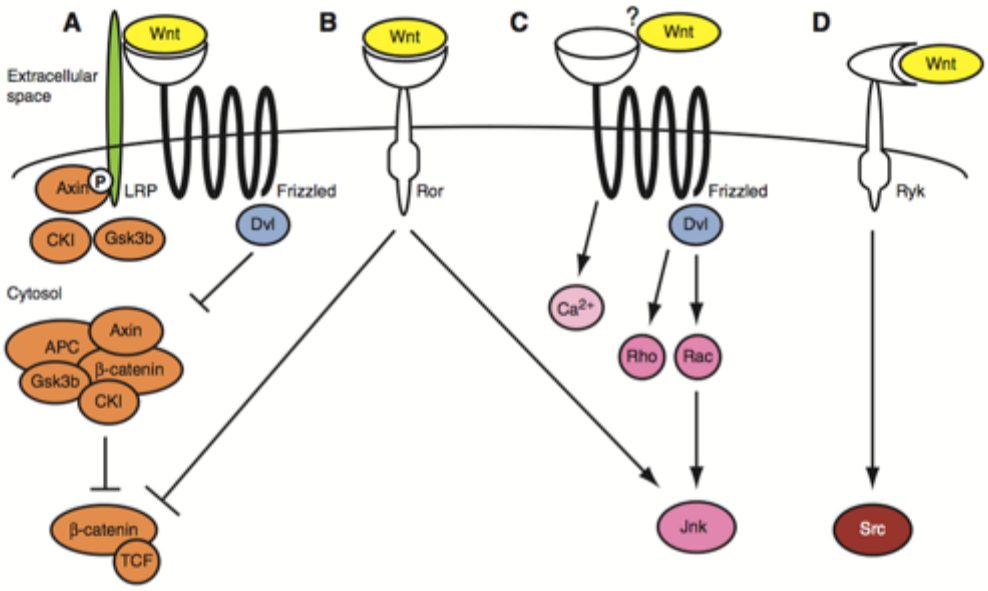

Figure 1-4. Multiple cascades in the Wnt signaling pathway
(A) Normally β-catenin is targeted to the proteasome by the destruction complex of APC, Axin, Gsk3β and CKI. Binding of Wnt family proteins to Frizzled (Fzd) and low density lipoprotein receptor (LRP) families activates Dishevelled (Dvl), which in turn rescues β-catenin from the proteasome. This leads to an accumulation of β-catenin in the cytoplasm, that is subsequently translocated to the nucleus. (B) Wnt ligands can bind Ror2 and repress β-catenin signaling and activate the Jnk cascade. (C) The planar cell polarity pathway is activated by binding of Wnt ligands to Fzd receptors. Downstream cascades include the Calcium dependent pathway, and the Rho and Rac cascades. (D) Wnt ligands can also bind Ryk in neuronal settings. *Source: van Amerongen and Nusse (2009)*[105].

1.3.2 The canonical Wnt signaling cascade

The canonical cascade requires the binding of a Wnt ligand to a Fzd receptor and either LRP5 or LRP6 co-receptors Figure 1-4A. This binding activates Dishevelled (Dvl) phosphoproteins, which inhibit the degradation of β-catenin. In the absence of Wnt ligands, cytoplasmic β-catenin is immediately marked for degradation by phosphorylation [110]. This destruction of β-catenin is mediated by a complex consisting of actin, adenomatous polyposis coli (APC) tumour suppressor protein, glycogen synthase kinase 3β (GSK3β), casein kinase 1 (CK1) and protein phosphatase 2A (PP2A) [110]. Thus, with the activation of Dvl, β-catenin accumulates in the cytoplasm and translocates to the cell nucleus. Inside the nucleus, β-catenin is recruited to replace repressors of the TCF/LEF, for example Groucho [111]. It subsequently targets TCF/LEF to initiate a transcriptional complex by binding to the promoters of Wnt target genes through Wnt responsive elements (WRE) [110]. β-catenin mediated responses include cell fate, proliferation and self-renewal of stem and progenitor cells [97] summarized in Figure 1-5.

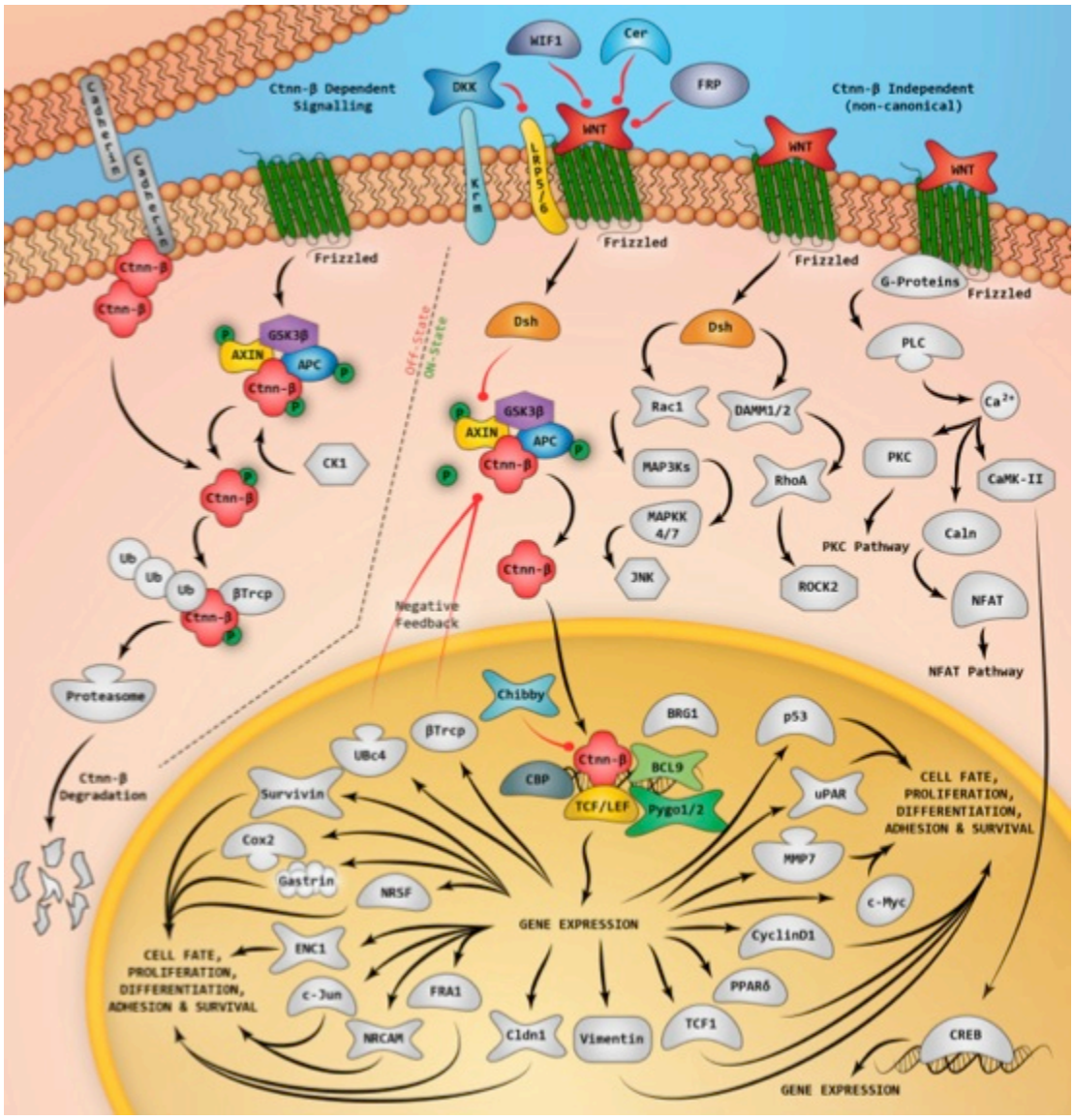

Figure 1-5. Multiple signaling cascades lead to multiple outputs
The Wnt pathway is a complex network of signalling cascades that mediates multiple cellular responses including cell fate, proliferation, differentiation, adhesion and survival. Transduction of the Wnt signal may be mediated by β-catenin (Ctnn-β) in the canonical pathway or independent of β-catenin in the non-canonical pathways. TCF/LEF is important for the output of canonical Wnt signaling. Binding of Wnt ligands leads to nuclear localization of β-catenin and target gene transcription. Without Wnt ligands β-catenin is targeted for degradation. Activation of the JNK, ROCK, PKC and NFAT cascades is mediated by Dvl after Wnt binding of Fzd, independently of LRP5/6. Pygo1/2 is a transcriptional co-activator in the Wnt signaling pathway. *Adapted from: SA Biosciences Wnt Signalling Poster*

1.3.3 Non-canonical Wnt signaling

While alternative Wnt cascades are possible, they are independent of TCF/LEF. This would suggest they are also likely to be independent of *Pygo2*. Briefly, they include the planar cell polarity pathway (PCP) and the calcium dependent cascade. The combined effects of which lead to spatial organization of tissues, remodeling of the cytoskeleton, microtubule signaling (via stabilization of Gsk3β), cell movement and basal body docking [112]. Cells require these functions during convergent extension movements in gastrulation, regulation of cilia, and axonal outgrowth in developing neurons [113-115].

They are activated by direct or indirect binding of ROR2, RYK, and Frizzled receptors in the absence of the co-receptors LRP5 or LRP6 (Figure 1-4B-D). Interestingly, a recent review by Gao and Chen (2010) highlights the importance of Dvl in transducing the input signals from receptors to the appropriate cascades in both canonical and non-canonical signaling [112].

A complex of Frizzled, Dvl and Diversin is initiated in the Planar Cell Polarity (PCP) cascade that polarizes the location of another membrane bound complex, consisting of Vang-like (Vangl) and Prickle (Pk). PCP is important for cell direction and lies in the plane perpendicular to basal/apical polarity. Mutually repressive interactions between the two complexes setup their asymmetric distribution [88]. Additionally, Dvl can associate with Rac1 (ras-related C3 botulinum toxin substrate) and Damm1 (Dvl associated activator of morphogenesis 1) leading to an activation of JNK (C-Jun N-terminal kinase) and ROCK (RhoA kinase) pathways respectively. Collectively these interactions and are grouped within the PCP cascade. The combined effects of which lead to spatial organization of tissues, remodeling of the cytoskeleton, microtubule signaling (via stabilization of Gsk3β), cell movement and basal body docking [112].

Finally the calcium dependent cascade is induced by Wnt binding Frizzled and mediated independently of β-catenin and Dvl through phospholipase C (PLC). Ultimately this increases intracellular Ca^{2+} levels that activate Ca^{2+}/calmodulin-dependent protein kinase (CAMkII), protein kinase C (PkC) and nuclear factor of

activated T cells (NFAT). This cascade regulates dorsoventral patterning and tissue boundary formation, and can lead to inhibition of the β-catenin dependent Wnt pathway [107].

1.3.4 Differential expression and conservation of Pygopus

While there are multiple homologs of *pygo* in vertebrates, they display a high degree of sequence conservation from fly, to frog, mouse and human [82,116-118]. In particular, the greatest sequence identity is found in the terminal PHD and NHD, and a region nearby the nuclear localization sequence (NLS), adjacent to the NHD. The Pygo homologs also appear to be conserved functionally. Human *PYGO1* and *PYGO2* are both capable of providing a rescued phenotype in *Drosophila* with a *pygo* null mutation [82]. Despite this, the expression pattern of *pygo* homologs differs within and between all species studied to date.

In *Drosophila* there exists only one *pygo* gene that is ubiquitously expressed within the embryo [84]. While in *Xenopus laevis* (frog) there exist two homologs of *pygo,* namely *pygo2α* and *pygo2β,* although initial descriptions of the gene were limited to a single homolog [83,118,119]. In the frog, both protein sequences are identical, except *pygo2α* contains an additional 21 amino acids at the N-terminal region. Interestingly, both homologs are differentially expressed in *Xenopus*. The expression of the *pygo2α* transcript is found early in the anterior neural plate and later within the anterior neural tube, mid-hindbrain and forebrain. While, *pygo2β* expression is present throughout the blastula stage and later becomes restricted to the retinal field and derivatives (forebrain and eyes) [118].

In mouse and human there are also two homologs of *pygo, Pygo1/PYGO1* and *Pygo2/PYGO2* respectively. The expression of these homologs has been analysed by northern blot from adult mouse tissues [116]. *Pygo1* expression was shown to be restricted to the heart in adult mice and weakly expressed through later stages of embryonic development. In contrast, *Pygo2* is strongly expressed

throughout embryonic development and in all adult tissues analysed[1,2], except skeletal muscle.

More recently contributions to online databases of gene expression have shown specific expression of *Pygo1* in developing brain, lens of the eye, pharyngeal arches, limbs, kidney and gonads [120-122]. In addition, *Pygo2* expression has been demonstrated in the developing lens, kidney, gonads, brain, pelage and whisker follicles, lung and the intestine [123-125]. This recent evidence does provide some support for a shared expression pattern between the frog and mouse, albeit dynamic.

1.3.5 Pygo is essential for Drosophila development

Pygo is essential for development in *Drosophila*. Knockout studies have shown that a *null* allele of *pygo* is embryonic lethal and recapitulates the phenotype of a loss of *Wingless* (*Wg;* vertebrate *Wnt1*)*, arm* (vertebrate *β-catenin*) or *TCF* [81-84]. For this reason, the role of *pygo* in *Drosophila* development has been extensively studied with a strong focus on the function of the two conserved domains (PHD and NHD) in Wnt signaling.

The two Pygo protein domains confer separate and essential functional ability (see Figure 1-6). The PHD forms part of a family of cysteine rich zinc fingers that are capable of binding DNA/RNA or providing protein-protein interactions. It is suggested that the role of a PHD within large multi-protein complexes is to act as a 'glue' and possibly regulate chromatin structure and binding [126]. Mutational studies of the *Pygo* PHD have shown that it is essential for binding of Pygo to Arm/β-catenin and TCF/LEF through the adapter Lgs/BCL9 [82] and that it exists *in vivo* as a complex with Lgs/BCL9 [81]. Point mutations introduced into the Pygo PHD are sufficient to phenocopy the *pygo* mutant [83].

---

1. Expression within the adult mouse was observed in the following tissues: brain, heart, kidney, liver, lung, skin, small intestine, spleen, stomach, testis and thymus.

2. It should be noted there exists a splice variant of Pygo2 (omitted by Li et al. 2004) within the testis, a known location of high splice variant expression (He et al. 2007).

In addition to this, Kramps *et al.* (2002) have shown that Pygo without a PHD and fused directly to the Lgs HD2 (which binds Arm/β-catenin) was able to rescue both *pygo* and *lgs* mutant animals [82]. Thus demonstrating the primary role of the PHD is to tether Pygo to Lgs and in turn bind Arm/β-catenin following activation and translocation of Arm/β-catenin to the nucleus.

Yet, the Pygo NHD contains a nuclear localization signal (NLS) and is also required for normal function of Pygo [83]. It has the ability to initiate transcription without the PHD. This was shown by Thompson and colleagues, using a fusion protein of the Pygo NHD with the yeast GAL4 DNA binding domain, demonstrated by luciferase and TopFlash reporter assays [127]. While in other *in vitro* assays, the NHD displays transcriptional activity and a single point mutation of the NHD is sufficient to ablate Wg signaling [128,129], albeit an *in vivo* a reduction of Wg output is observed. These results strongly suggest the role of the NHD is in transcriptional co-activation domain.

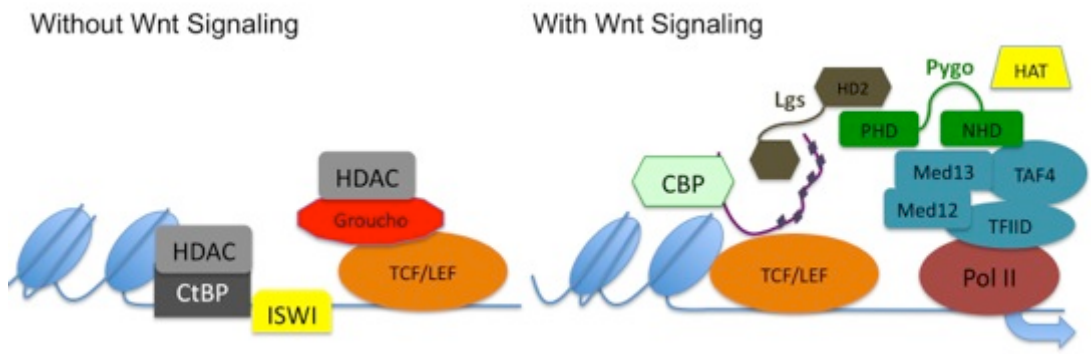

Figure 1-6. Model of Pygo function in transcriptional co-activation
In the absence of Wnt signaling, TCF/LEF represses transcription through binding of Groucho and Histone deacetylase (HDAC). In addition, ISWI and CtBP bind independently to Wnt responsive elements (WREs) and lead to localised deactylation. After Wnt signaling is activated, β-catenin accumulates in the nucleus displaces the repressor Groucho. The histone acetyltransferase CBP is recruited and ISWI and CtBP bind less favorably. β-catenin subsequently recruits Lgs and Pygo. Pygo then contact the Med12 and Med13 subunits of the Mediator complex. In addition, Pygo also recruits TAF4 and TFIID of the basal transcription complex and target gene transcription is initiated. Pygo may also bind HAT and HMT to enhance transcription through changes in methylation status. *Adapted from Cadigan and Peifer (2009)*[130]

1.3.6 The dorso-ventral axis in Xenopus requires Pygopus

Functional studies of *pygopus* in *Xenopus* are limited. However, Belenkaya *et al.* (2002) conducted knockdown analysis of *pygo* in early *Xenopus* development via maternal *pygo* depletion, which resulted in a ventralized phenotype and a reduction in the dorsal markers *chordin*, *Xnr3*, *siamois* and *goosecoid* [83]. Initiation of the dorsalization axis is mediated by Wnt signaling and this result suggests a role for *Xenopus pygo* in Wnt signaling and specifically the Wnt dorsalization pathway during early embryonic development. Subsequently, Lake and Kao (2003) identified a second homolog of *pygo*, which they have renamed to *pygo2α* and *pygo2β.* It was suggested these isoforms represented orthologs of *PYGO2* based on sequence alignment to both human homologs [118]. Knockdown analysis using morpholinos targeted to *pygo2α* and *pygo2β* in later development displayed brain patterning abnormalities within the forebrain and mid-hindbrain [118].

Interestingly, injection of RNA for both full-length genes and *pygo2α* PHD had no effect on *Xenopus* embryos, while a shortened *pygo2α* NHD RNA displayed axis formation abnormalities [118]. This is a similar effect to that of the earlier maternal depletion performed by Belenkaya et al. (2002) and again confirmation of the ability for the NHD to drive transcription of Wnt target genes [83,127-129]. However, not all Wnt target genes were upregulated, suggesting that the NHD functions in a promoter specific manner.

Further evidence for the requirement of *pygopus* in early axis formation has been provided by Kennedy and colleagues, with a simultaneous knockdown of both *pygo2β* and *lgs* in *Xenopus*. In addition, they also show that Pygo2β is required for Lgs nuclear localization; presumably due to the NLS in the NHD of Pygo2β [119].

Taken together, these results indicate that the role of pygo2α/β is dynamic throughout development, it is required by different tissues at different time points. Additionally it highlights that the NHD is the functional unit of the mature protein (capable of acting in a dominant negative manner) and that the PHD is largely required for binding or tethering of Lgs.

1.3.7 A functional redundancy of Pygopus in mouse models

Schwab and colleagues describe the role of *Pygopus* in mouse as a 'quantitative transducer' or modulator of Wnt signal intensity [131]. *Pygo1 null* mice are reportedly viable with no detectable phenotype [123,131]. In contrast, *Pygo2* null mutants usually die shortly after birth and display a range of growth abnormalities summarized in Table 1-2. In these studies double *Pygo1* and *Pygo2* knockout mice did not display any synergistic effect, that is, they did not display enhanced or additional phenotypes over the *Pygo2 null* alone. These studies have led to the suggestion that *Pygo1* is redundant and not required for development in mice [131].

In double knockouts (*Pygo1* and *Pygo2*), Wnt signaling is reduced in a tissue specific manner [123,131]. However, using differential gene expression analysis, Schwab et al. (2007) were unable to show a reduction in more than a few Wnt target genes [131]. In addition, *Pygo2* is crucial for induction of the lens in eye development. Interestingly, it is required by multiple tissues during this process, including the neural crest derived ocular mesenchyme. *Pygo2* was found to function independently of β-catenin and this role may be entirely independent of the Wnt pathway [123].

Table 1-2. Reported phenotypes in *Pygo1* and *Pygo2* knockout models (mouse)

Observed phenotypes	
Neonatal lethality	[116,123,131]
- Rare exceptions survive past birth	
Growth retardation	[116,123,131]
- Reduction in pup weight	
- Reduction in pup length	[116,123,131]
Lens agenesis	
- Reduction in Pax6 expression in lens placode	
- In combination with failure of eyelid formation and closure	
Altered kidney development	[131]
- Increase in nephron cap mesenchyme	
- Decrease in branching of ureteric tips	
Exencephaly or domed head	[116,131]
- 14%-20% of mutants carrying null gene	
Cleft palate	[131]
- 60% of mutants carrying null gene	
Reduction in Wnt signaling	[116,131]
- Tissue specific reduction of Wnt signaling assayed by BAT- gal	
Hair follicle	[116]
- Reduction in follicle density	
- Arrest of follicle development at bud stage	
Lung	[116]
- Pale and smaller	
- Reduction in distal airway branching	
Reduction in small intestine length	[116]
- Likely to be non-specific effect of smaller pup size	

1.3.8 A revised role of Pygopus in the Wnt pathway

More recently, the 'chain of adapters' model initially proposed for Pygo has recently been revised by Cadigan and Peifer (2009) [130]. Originally the model hypothesized that the primary function of *Pygopus* was in binding to Lgs and in turn, binding β-catenin [128]. It was suggested that Pygo supplied an accessory role to β-catenin as transcriptional co-activator in accompaniment to TCF. However, new evidence suggests that this model underestimates the role of *Pygo* homologs.

In a *Pygo2* conditional null mouse created by Nair and Dai (2008), homozygous floxed males are sterile, while development of somatic tissues appears normal [125]. Pygo2 expression was found in the nucleus of elongating spermatids associated primarily with chromatin. The possibility that alternative splicing of the *Pygo2* conditional allele is adversely affected was not explored. However, the hypomorphic allele produces less Pygo2 in spermatids and leads to arrest of spermiogenesis [125]. This study provides evidence that Pygo2 is involved in chromatin remodeling and possibly in a β-catenin independent process. In addition, it also provides circumstantial evidence for an important alternatively spliced transcript of *Pygo2* within the mouse testis.

It has been shown that the PHD exists as a dimer, consisting of two Pygo proteins [132] and with the addition of Lgs/BCL-9 it undergoes a structural conformational change to enhance its affinity to histones [133]. Pygo2 is also capable of expanding mammary progenitor cells through methylation of histone H3 K4 and interacts directly with MLL2 histone methyltransferase (HMT) and GCN5 histone acetyltransferase (HAT) through the NHD [134-136]. Thus, adding further evidence that Pygopus is capable of epigenetic regulation of target gene transcription [137].

In addition to the evidence for chromatin regulation, Pygo is capable of binding directly to TCF [138] and acting as an anti-repressor of the TCF repressor Groucho [111]. Pygo can also recruit subunits (med12, med13) of the mediator complex that are essential for transcription of RNA polymerase II-dependent genes [139]. During transcriptional initiation it has also been linked to the recruitment of the TFIID complex, comprised of the TATA-binding protein (TBP) and TBP-associated factors (TAFs) [140]. And finally, recruitment of the polymerase associated factor 1 (PAF1) relies on binding of Parafibromin to Pygo during transcription initiation [141,142].

1.3.9 Pygopus in disease

As previously discussed, the Wnt pathway is important in the pathology of disease and cancer. It follows that the *Pygo* genes would also be important, due to their pivotal role in transduction of the Wnt signal.

Recently PYGO2 and von Willebrand factor A domain-containing protein 1 (VWA1) were proposed as the candidate genes for a patient with mandibulofacial dysostosis or Treacher Collins syndrome, microtia (loss of outer ear), and limb abnormalities. The combined presentation of these defects is unique, and it suggested they represent a new form of acrofacial dysostosis syndrome (AFD). Using comparative genomic hybridization techniques, the patient was found to carry two chromosomal duplications containing the two candidate genes, *PYGO2* and *VWA1* [143].

In an *in vitro* setting, it has been shown that PYGO2 is highly expressed in breast cancer cells, is essential for growth [144] and is activated downstream of the retinoblastoma tumor suppressor (via E74-like factor-1; [145]). In addition, *Pygo2* is located in an amplified chromosome region upregulated in hepatocellular carcinoma [146]. Popadiuk *et al.* (2006) have demonstrated that PYGO2 is required for malignant growth of epithelial ovarian cancer cells [147]. Importantly these studies demonstrate that the *Pygo* genes may be genuine therapeutic targets. In addition, *β*-catenin does not contribute to the aetiology of these tumours, thus adding further evidence that *PYGO2* can act outside of the canonical Wnt pathway.

Other studies have proposed the homologs of *Pygo* as target candidates for attenuation of malignant cells. This is because TCF transcriptional targets are known to drive tumour progression [148]. In human colorectal cancer cells, knockdown of PYGO1 and PYGO2 by RNA interference caused a reduction in TCF transcriptional output of more than 50% [81]. A decrease in cell growth and proliferation of gliomas was achieved through RNA interference with short hairpin RNA (shRNA) targeted to the expression of Pygo2 [149]. Finally, in a screen of Wnt pathway inhibiting drugs, it was found that a small molecule, pyrvinium is a potent inhibitor. It was discovered that the drug stabilizes Axin, and promotes the degradation of both β-catenin and Pygopus [150].

1.3.10 Summary

In summary, *pygo* is a recently discovered member of the Wnt pathway. It has been suggested to have possible roles in chromatin remodeling and epigenetic

regulation, in addition to its role in transduction of the Wnt signal. While the sequence of Pygo1/2 is highly conserved between invertebrates and vertebrates, its absolute requirement for Wnt signaling is apparently not. In vertebrates, a loss of *Pygo1/2* leads to a reduction in transduction of the Wnt signal, not ablation. In addition, vertebrate expression is dynamic in a spatio-temporal manner, and many of the ascribed functions in development do not appear to be conserved. However, further studies on the role of *Pygo1/2* in vertebrates may yet reconcile these differences.

1.4 Project aims

The discovery of EPI-NCSC as an easily accessed adult source of multipotent stem cells may have significant importance for future cellular based therapies. However, further characterization at both the molecular and technical level is required to bring about their usage in the clinic. To achieve this goal, a thorough understanding of EPI-NCSC genetic regulation and cell signaling factors, which may be utilized to promote *in vitro* differentiation, is required. In addition, an understanding of the genetic pathways that lead to their normal development *in vivo* will also aid in the development of future EPI-NCSC applications.

The discovery of *Pygo2*, both as an EPI-NCSC signature gene, and as an important member of the Wnt pathway is also extremely relevant to future applications of EPI-NCSC. The Wnt pathway plays a key role in the regulation of NCSC differentiation, adhesion, migration and proliferation. In addition, the Wnt pathway is known to be involved in cancer and disease. Given that *Pygo* is important in Wnt signaling and represents a possible therapeutic target for cancer, it is important to fully understand its role in EPI-NCSC. Taken together, this leads to the following hypothesis to be tested:

"Pygopus 2 is required for the normal formation, maintenance, migration, development and differentiation of neural crest stem cells."

To test this hypothesis, a number of strategies involving the use of animal models and *in vitro* cell based assays have been undertaken. Specifically, the objective of this project was to provide an accurate assessment of the following aims:

(i) A broader understanding of the evolutionary context of Pygo homologs

Currently, discrepancies exist in the number of *Pygo* homologs in vertebrates. Frogs have two isoforms of *pygo2*; yet, higher vertebrates have single forms of two separate genes. We know that the protein products of these genes are highly conserved. However, in the mouse, the function of *Pygo1* is apparently redundant. Despite this, there are clear examples of conservation in their roles, the requirement for development of the eye in frog and mouse is one example of this. To gain a greater understanding of the seemingly divergent roles of these genes, a broader screening of Pygo homologs was undertaken across multiple taxa. Using bioinformatics databases and protein alignment tools, previously unreported homologs were identified in both the frog and zebrafish.

(ii) The role of Pygo2 in zebrafish development

Amongst the vertebrate species studied to date, it is the frog that stands out, having a single genetic homolog, which produces two protein isoforms, with differential expression and functions during development. This makes consoling the differences between mammals and invertebrates even more difficult. To address this, a functional study was undertaken in zebrafish to identify if the possible roles of *pygo* homologs in zebrafish development, in particular development of the NC. From the studies performed in frog, it was evident that pygo2α/β expression were largely restricted to the neural tube and NC derived tissues. In this study, morpholino knockdown of both *pygo* homologs has revealed a surprising NC and early gastrulation phenotype.

(iii) The role of Pygo2 in mouse NC development.

While studies have already shown in mice that the role of *Pygo1* is redundant, the *Pgyo2* null mouse exhibits a number of defects in neural crest derived

tissues. Given the reliance of NC on the Wnt pathway, it would seem likely that a number of these reported phenotypes may be neural crest related, and additionally, there may be other abnormalities masked by the ubiquitous knockout of *Pygo2*. To investigate this possibility, the role of *Pygo2* in mouse NC development, was analysed using a compound transgenic model to knockout *Pygo2* expression within the NC. This model displayed multi-organ defects in perinatal mice, which lead to death within a few hours. Importantly, this study has highlighted the context dependent nature of *Pygo2* function and suggests thee may still yet be a non-redundant role for *Pygo1* in mouse development.

(iv) The role of Pygo2 in EPI-NCSC

Finally, the role of Pygo2 in EPI-NCSC maintenance, migration and migration was explored. Other studies *in vitro* have revealed a role for *Pygo2* in cell cycle and proliferation regulation. Utilizing EPI-NCSC from the transgenic mouse model, the loss of *Pygo2* was studied in migration, stem cell maintenance, and proliferation assays. Surprisingly, this study has provided further evidence for a role in cell cycle maintenance and proliferation.

In summary, these studies are of fundamental importance in understanding the role of *Pygo2* in vertebrate and NCSC development and may serve as a paradigm for the development of cell-based therapies, in general.

Chapter 2. Materials and Methods

2.1 Bioinformatics

2.1.1 Database mining

Internet databases held by the National Centre for Biotechnology Information (NCBI) were routinely mined to identify DNA/RNA/Protein accession numbers and their related sequences, specifically matching the inputted gene of interest (GOI). Both metadata (for example, gene annotations, chromosome, gene ID and descriptions) and sequence data (raw sequence, region/feature labels) were recovered from the following databases:

(i) *Homologene; http://www.ncbi.nlm.nih.gov/homologene/*

(ii) *Gene; http://www.ncbi.nlm.nih.gov/gene*

(iii) *Protein; http://www.ncbi.nlm.nih.gov/protein*

(iv) *Nucleotide; http://www.ncbi.nlm.nih.gov/nuccore*

(v) *Expressed Sequence Tag (EST); http://www.ncbi.nlm.nih.gov/est*

(vi) *RefSeq; http://www.ncbi.nlm.nih.gov/RefSeq/*

The following sequence comparisons and searches were performed against the above databases using the Basic Local Alignment Search Tool (BLAST) with accession numbers/sequences for the GOI; located on the NCBI website: http://blast.ncbi.nlm.nih.gov/Blast.cgi.

(i) *Searches for pygo homologs using translated nucleotide sequences*

Translated BLAST searches were performed using the tblastx program with the default general parameters (Expect threshold = 10, Word size = 3, Matrix = BLOSUM62) and no filtering/masking.

(ii) Searches for pygo homologs pygo protein or consensus sequences

Translated BLAST search were performed using the tblastn program with the default general parameters (Expect threshold = 10, Word size = 3, Matrix = BLOSUM62) and no filtering/masking.

2.1.2 Protein Alignments

The following alignment and comparative analyses of protein sequences were routinely performed using the Geneious v5.1 software [151].

(i) Consensus sequence

The pygo consensus sequence was generated conducting a MUSCLE [152] multiple sequence alignment of all pygo homolog proteins (Accession numbers: NP_056432, NP_612157, NP_082392, NP_081145, AAN41447, AAN41448, NP_651872) with 20x iterations. Alignment gaps and ambiguous residues were removed to produce the pygo consensus sequence.

(ii) Putative pygo protein alignments & pygo consensus sequence

Alignments of each of the putative zebrafish pygo homologs were aligned and analysed conducting the MUSCLE alignment tool with 20x iterations. Global and local pairwise identity was calculated by restricting the analysis region within the output pane.

(iii) Pairwise protein alignments and homology

Pairwise protein alignments of pygo homologs were performed using ClustalW (Blosum Matrix, Gap open cost = 10, Gap extended cost = 0.1) with no free end gaps [153].

(iv) Multiple protein alignments

Multiple protein alignments and the unrooted dendrograms of protein homology were produced using the Geneious Tree Builder. Homology was calculated with a global alignment (without free end gaps) using the Blosum62

matrix (Gap open penalty = 12; Gap extension penalty = 3) [153], Jukes-Cantor genetic distance and the neighbour-joining method of tree building. No out-group was specified, because no single species was known prior to this study to be distantly related to all other species.

2.2 Zebrafish Techniques

2.2.1 Colony maintenance & embryo collection

The zebrafish colony was maintained under license from the Home Office (United Kingdom) in accordance with the guidelines and regulations for the care and use of laboratory animals outlined by the Animals (Scientific Procedures) Act 1986. The sox10:egfp transgenic zebrafish strain has previously been described by Carney *et al.* (2006) [154] and was a kind gift from Dr Robert Kelsh. Embryos for colony maintenance and microinjection were obtained from natural crosses. Adult male and female sox10:egfp zebrafish were separated overnight (O/N) and mated on the morning of collection. Embryos were collected and staged according to Kimmel *et al.* [155].

2.2.2 Morpholino stock solutions

Morpholinos obtained from Gene Tools (Philomath, USA) were designed to target *pygo1* and *pygo2* gene expression. For *pygo1,* a translational blocking morpholino was designed, pygo1TR 5'- TGTGGACATTACAGTCTCCCTCACA-3' to knockdown pygo1 expression.

While, pygo2TR 5'- TTCCTTGCTGCTGCTGTCCCGCCAT-3' was targeted to the translational start site and pygo2SP 5'- GCCCCCTAAGACAAATTCAGTGAGA-3' to function as a splice blocking inhibitor as previously described by Eisen and Smith [156]. Morpholinos were suspended in 1x Danieau buffer (58mM NaCl; 0.7mM KCl; 0.4mM $MgSO^4$; 0.6mM $Ca(NO^3)_2$; 5.0mM HEPES, pH7.6) supplemented with 1% Phenol Red (Sigma-Aldrich Cat# P3532) as described by Nusslein-Volhard and Dahm (2002) [157].

2.2.3 Microinjection of zebrafish embryos

Needles were prepared from glass capillaries with a filament (Hilgenberg Cat#1403517) using a micropipette puller (Sutter Instruments, Model# P-97). Needle drop size was first calibrated using a horizontal stage micrometer (Zeiss Cat# 474026-0000-000) before performing injections using a micromanipulator and femtojet transjector (Zeiss Cat# 5171) under a microscope (Leica Model# MZ95). Injections were performed at the 1-cell stage in E3 medium (5mM NaCl; 0.17mM KCl; 0.33mM $CaCl_2$; 0.33mM $MgSO_4$) supplemented with 1 x 10^{-5}% Methylene blue (Sigma-Aldrich Cat# M4159). Embryos were held in position using a customized silicone mould (Ellsworth Adhesives Cat# 184 SIL ELAST KIT). Embryos were subsequently incubated at 28.5°C.

2.2.4 Live zebrafish imaging

Zebrafish embryos were anaesthetized in 0.005% (wt/vol) tricaine/E3 media solution (Sigma-Aldrich Cat# A-5040) briefly, while microphotographs were captured using a fluorescence stereomicroscope (Leica Model# MZ16). Embryos were again stabilized using the customized silicone elastomer mould. The time taken for photography was minimized to prevent developmental delay of the zebrafish embryo.

2.3 Mouse husbandry

2.3.1 Colony maintenance

The *Pygo2* conditional mouse line [131], a kind gift from Prof. Steven Potter, was crossed with the Wnt1-Cre [158] or the R26R reporter strain [159] to generate double transgenic Wnt1-Cre::Pygo2$^{+/-}$ and R26R::Pygo2$^{fl/+}$ mice. Double transgenic mice were subsequently crossed to produce triple transgenic, or *Pygo2 CKO* (Wnt1-Cre::R26R::Pygo2$^{-/-}$) litters. In these mice *Pygo2* is deleted and β-gal expression (from the *lacZ* gene) is activated permanently and specifically within cells having previously expressed Cre under the control of the 5.5kb cis-acting *Wnt1* promoter enhancer. All transgenic lines were maintained on the inbred C57Bl6/J background (The Jackson Laboratory). All mouse work was performed under license from the Home Office (United

Kingdom) in accordance with the guidelines and regulations for the care and use of laboratory animals outlined by the Animals (Scientific Procedures) Act 1986.

2.3.2 Genotyping

Genotyping of mice was routinely conducted using tissue samples collected from the ear (adults), tail (neonates), or yolk sac (embryos) of transgenic mice and immediately frozen. Genomic DNA preparation and PCR methods are described in Section 2.8.2. PCR conditions and primers for all mouse lines used have been described previously [123,158,159] and are listed in Table 2-1.

2.4 Histology

2.4.1 Whole mount Alcian Blue & Alizarin Red S skeletal preparations

Skeletal preparations were conducted using a modified protocol from Mcleod M.J., (1980)[160]. Newborn pups were sacrificed by decapitation, de-skinned and placed in 100% EtOH for 1 week to fix the skeletal tissue. Fixed preparations were transferred to 100% acetone for a further week and subsequently stained for another 3-4 weeks in staining solution (0.015% Alcian Blue 8GX, Sigma-Aldrich Cat# A3157; 0.01% Alizarin Red S, Sigma-Aldrich Cat# A5533; 0.05% Acetic Acid; 70% EtOH). Preparations were cleared under continual surveillance (with micro-dissection of cleared tissue) in 1% KOH/20% glycerol. Finally preparations were taken through a glycerol series (30%, 50%, 80%, 100% glycerol) for photography and storage.

2.4.2 Tissue fixation

Micro-dissected neonatal mouse tissues were routinely collected in ice cold PBS (Phosphate Buffered Saline) from sacrificed pups and immediately fixed in 4% paraformaldehyde (PFA) at 4°C for varying lengths of time, depending on the tissue; 5hr (embryos), 1hr (GI tract), O/N (brain; except for X-gal staining of brain, which was fresh frozen), or 6hr (all other tissues). Specifically for preparation of neonatal brain, the cranial skin and skull plates were also removed for greater penetration of the fixative.

2.4.3 Whole mount X-Gal staining of murine tissue

X-gal staining was performed as described previously [161] with several modifications. Fixed mouse tissue was washed 3x 15mins in X-gal wash buffer (PBS, 0.02% Tergitol® type NP-40, Sigma-Aldrich Cat# NP40S; 0.01% sodium deoxycholate, Sigma-Aldrich Cat# D6750; 2mM $MgCl_2$) and stained in X-gal staining solution (0.2M potassium hexacyanoferrate(II) trihydrate, Sigma-Aldrich Cat# P9387; 0.2M potassium ferricyanide(III), Sigma-Aldrich Cat# 702587; 20mg/ml X-galactosidase, Roche Cat# 11680293001; in X-gal wash buffer). Following O/N staining, tissue was washed 3x 1hr in X-gal wash buffer and fixed in 4% PFA O/N. Following fixation, all specimens were stored in PBS at 4°C in the fridge. Colons were cut longitudinally; the internal mucosa was removed and finally mounted in PBS on a cavity microscope slide for microphotography. All other tissues were either analysed as whole mount specimens, or processed for paraffin embedding and sectioning.

2.4.4 Sectioned on-slide X-gal staining of mouse brain

For X-gal staining of mouse brain, the entire head was fresh frozen in Optimal Cutting Temperature medium (OCT; Thermo Scientific, Cat# LAMB/OCT) using liquid nitrogen (LN_2). 8µm sections were collected on SuperFrost Ultra Plus® microscope slides (VWR Cat#631-0099) using a cryostat (Microm AG Model# HM 560). Sectioned tissue was allowed to dry for 4 hours. Following fixation in 4% PFA for 15mins, slides were washed 3x 15mins in X-gal wash buffer, before staining for 2 hours with X-gal staining solution. Slides were post-fixed for 1hr with 4% PFA and counter-stained with nuclear fast red solution (Sigma-Aldrich Cat# N3020). Finally slides were dehydrated and mounted as per Section 2.4.6.

2.4.5 Paraffin embedding of tissue

Samples of whole organs/tissues were further dissected and trimmed before dehydration through an ascending series of ethanol (70% EtOH, 30mins; 80% EtOH, 30mins; 95% EtOH, 30mins; 100% EtOH, 2x 30mins) and cleared in 2x 10mins xylene washes at RT. Subsequent paraffin infiltration was performed by the removal of half the xylene volume in exchange for an equal volume of molten paraffin to displace remaining xylene. This was performed at 60°C with

20min intervals and lead to an increasing concentration of paraffin from 50%, through 75% to 87.5%. Finally the remaining xylene/paraffin was removed and the tissue was washed with 3x 30min 100% molten paraffin changes and left O/N in molten paraffin to complete infiltration at 60°C. The following day, tissues were embedded in 35mm dishes under a standard microscope and cooled in ice-cold water.

2.4.6 Tissue sectioning and staining preparation

After tissues were embedded, paraffin blocks were trimmed to size, oriented and mounted for sectioning using a microtome (Leica Model# RM 2235). Sections were cut at 7µm and collected SuperFrost Ultra Plus® microscope slides (VWR Cat#631-0099). To ensure proper adherence of sections, slides were baked at 40°C O/N prior to staining. H&E staining on neonatal skin was performed by Alla Narytnyk (under supervision). Nissl staining on neonatal brain sections was performed by Linda Julian (under supervision).

2.4.7 Histological staining

Before histological staining of tissue sections, slides were first de-paraffinised in xylene (2x 5min) and rehydrated through a series of ethanol (100%, 90%, 70%, 50%, 30%) for 2-3min each, with a final rinse in tap water for 5min at RT.

Haematoxylin and Eosin (H&E) staining was performed on rehydrated tissue sections as follows: Haematoxylin stain for 20sec, rinsed in tap water, blued for 10sec in Scott's tap water substitute (TCS Biosciences, Cat# HS735), rinsed again in tap water, followed by eosin stain for 20sec, tap water rinse and dehydrated through a series of ethanol (50%, 70%, 100%) for 1min each.

Nissl staining was performed by immersing rehydrated tissue sections in 0.45µm filtered cresyl violet stain, pH 3.7-3.9 (0.5% wt/vol cresyl violet acetate, Sigma-Aldrich, US, Cat# C5042; 50mM glacial acetic acid) for 10min. Finally, slides were briefly washed in tap water.

After staining, slides were mounted by washing in ethanol for 1min, followed by 2x 3min washes with xylene and coverslipped using DPX mounting media

(Fisher, Cat# D/5319/05). Subsequently slides were dried in a fume exhaust hood O/N before examination and photography using a bright field microscope.

2.5 Immunohistochemistry

2.5.1 Whole mount immunohistochemistry of mouse embryos

Immunostaining of cranial nerves in transgenic mouse embryos was performed on tissue collected from time-mated pregnant females at 10.5dpc. Embryos were collected, fixed and stained as described previously (Section 2.4.2)[162] and all steps were carried out at 4°C unless otherwise stated. To begin, embryos were washed 3x 1hr in 50mM ammonium chloride/PBS at 4°C. This was followed by blocking with a 0.1% hydrogen peroxide/TS-PBS (1% Triton-X, Sigma-Aldrich, Cat# T8787; 10% foetal calf serum; PBS) and incubated for 16hr. Embryos were then incubated with the primary antibody (anti-neurofilament 2H3 concentrate; Developmental Studies Hybridoma Bank, Iowa, Cat# 2H3) in TS-PBS for 3 days. Following 3x 1hr TS-PBS washes; incubation with the conjugated secondary antibody (HRP conjugated goat anti-mouse IgG; Stratech, Cat# 115-035-003) was performed for 20hr. Again, 3x 1hr TS-PBS washes were performed. Embryos were stained with substrate solution (1% 4-chloro-1-naphthol, Sigma-Alrich, Cat# C8890/EtOH) by subsequent incubations at 24°C with Solution A (0.004% substrate solution added drop-wise to 0.1% Triton-X 100; 1M Tris-HCL, pH 7.6) for 15min, followed by 3x 10min Solution B (0.004% substrate solution added drop-wise to 1M Tris-HCL, pH 7.6) and finally 3min with Solution C (0.25% substrate solution/40% EtOH prepared immediately before use). Finally stained embryos were washed 3x 1hr in 30% EtOH, 16hr in 30% EtOH, and infiltrated with 3x 1hr 1:1 EtOH/glycerol washes before storing in 100% EtOH at 4°C before analysis and photography.

2.5.2 Indirect immunofluorescence of sectioned mouse tissue

Immunofluorescence of the mesencephalic trigeminal nucleus (Me5) was performed by Linda Julian (under supervision), on neonatal mouse brain sections following rehydration as per Section 2.4.6. Sections were quickly washed in PBS before proceeding to the antigen retrieval step whereby slides

were subsequently boiled for 5min in citrate buffer (0.01M tri-sodium citrate pH 6.0). Cooled slides were washed in PBS containing 0.02% Triton-X for 15mins followed by 4x 10min washes in PBST (0.05% Tween-20, Sigma-Aldrich, Cat# P7949; PBS). Sections were then blocked with goat serum (1:20 in PBS) for 1hr, at RT in a humidified chamber, to block non-specific binding. Primary antibody to the Low-affinity nerve growth factor receptor (anti-NGF receptor p75; Millipore, Cat# AB1554) was applied to sections (1:200 in PBS) and incubated O/N at 4°C in a humidified chamber. After O/N incubation, slides were allowed to come to RT and washed with 6x 10min changes of 0.02% Triton-X/PBS, before addition of the secondary antibody, DyLight-488 conjugated goat anti-rabbit IgG (Jackson Laboratories, Cat# 111-485-144) was applied (1:200 in PBS) and incubated, protected from the light 2hr at RT. Slides were coverslipped and mounted using Vectashield Mounting Medium with DAPI (Vector Laboratories, Cat# H-1200). Finally coverslips and slides were sealed with nail varnish, and allowed to dry, before subsequent fluorescence analysis and photography.

2.6 Microscopy and image analysis

2.6.1 Image capture

All photomicrograph images used for quantification analyses and illustrations were captured with an AxioCam HR camera, using AxioVision 4.7.1 software (Carl Zeiss Inc.), saved in .zvi format, and exported to .tif format, unless otherwise stated.

Fluorescent and bright field photomicrographs of slides (sectioned tissue) were acquired with a Zeiss Axioplan 2 microscope. Phase contrast and fluorescent photomicrographs of live cultured cells were captured using a Zeiss Axiovert 200 microscope with XL-3 incubator and heated stage (Carl Zeiss Inc.). Bright field photomicrographs of dissected and stained tissues, and cultured cells were captured using a Zeiss Stemi 2000-CS fluorescence stereomicroscope (Carl Zeiss Inc.). Photographs of adult mice were taken using an Olympus C-8080 WZ wide zoom digital camera securely mounted above the bench.

Microscope objectives used for this work included: Plan-Neofluar 2.5x/0.075; Plan-Neofluar 5x/0.15; Plan-Neofluar 10x/0.3; Plan-Neofluar 20x/0.5. Filter sets used for fluorescence work were: DAPI (Excitation G 365; Beam Splitter FT 395; Emission LP 420), and FITC (Excitation BP 45-490; Beam Splitter FT 510; Emission LP 515).

2.6.2 Image analysis and quantification

The following image analyses were performed directly on printed images (manually) or using ImageJ Software upon raw .tif files unless otherwise stated. For each new analysis, the ImageJ Software was first calibrated for the current set of image magnification and dimensions using photomicrographs with scale bars applied using AxioVision software.

Calculation of zebrafish gastrulation angles was performed using the angle tool after locating the embryo geometric centre with the ellipse and straight-line tools.

Hair follicle density analysis was performed as described previously by Li *et al.* (2004)[163] in collaboration with Alla Narytnyk (under supervision) and Dr Oliver Clewes. Briefly, cross-sections from the back skin of 3 *Pygo2 CKO* and 3 wild type neonates were taken underneath the skin surface and H&E stained. Hair follicles were counted within gridded field areas ($1 \times 10^4 \mu m^2$; applied using ImageJ Software) to calculate the number of hair follicles per field. In total 31 fields for the *Pygo2* CKO and 33 fields for the control were counted for statistical analysis. In addition, using the freehand selection tool (ImageJ), the area of each hair follicle counted was measured to calculate mean follicle areas. Overall, 676 hair follicles were measured for the control animals and 575 for *Pygo2 CKO*. Morphometrical staging analysis was performed using the basic criteria as described by Paus *et al.* (2009)[164]. Longitudinal H&E sections from the back skin of 3 *Pygo2 CKO* and 3 control neonatal mice were prepared and to avoid staging of the same follicle twice, a space of 100µm between individual sections from the same sample was maintained. Altogether, 300 *Pygo2 CKO* and 307 control hair follicles were staged.

Measurements of cardiac wall thickness and skull bone lengths were performed using the measurement tool (ImageJ) on calibrated images.

Neurons of the Me5 and GI tract were scored, in collaboration with Linda Julian (under supervision), on the area of p75 and X-gal staining from optimum stained sections. For p75 analysis, 3 representative colour images from 3 *Pygo2* CKO and 3 control mice, were converted to 8-bit grayscale and the upper and lower threshold values were set to 0 and 140 respectively with the particle size lower limit set to 20 and the upper limit set to infinity. A single representative image from 9 *Pygo2* CKO and 8 control X-gal stained colons were colour thresholded between hue values 115 and 160. The area of stain was identified and calculated using the particle tool.

Cell migration counts were performed on mosaic images constructed in Adobe Photoshop CS5 from raw .tif files. The automatic photomerge tool (reposition setting) was used to align images automatically based on pixel intensities, without altering or distorting original image dimensions. A calibrated grid consisting of a series of concentric circles with an additional 600μm diameter was placed over the exclusion zone, and positioned according to scribed scratches on the cell plate. In addition, the mosaic image was further divided into 12x 30° sections to separate the direction of migration.

2.6.3 Diagrams and images

All figure diagrams and images were collated and composed in Adobe Photoshop CS5 software (Adobe) or Microsoft PowerPoint 2011 software (Microsoft). Histograms and statistical representations were produced using Prism 5 statistical software (GraphPad Software Inc.).

2.7 Tissue Culture

2.7.1 Sub-culturing of cell lines

All cells were routinely sub-cultured or split when required for cell maintenance, DNA/RNA extraction, nucleofection, or flow cytometry. Briefly, cell media was removed; cells were washed (except EPI-NCSC cultures) with

Dulbecco's phosphate-buffered saline (DPBS; Invitrgen, Cat# 14040-091), and a small volume of 0.05% trypsin-EDTA with phenol red (Invitrogen, Cat# 25300-054) was added directly to the well to cover cells. Plates were incubated for 5min at 37°C to dissociate cells; yet, EPI-NCSC times were much shorter without any 37°C incubation. An equal volume of regular cell culture medium was added to the cells, for trypsin inactivation, and cells were pipetted repeatedly to achieve a single cell suspension (gently for EPI-NCSC). Cells were then centrifuged for 3min at 500g and re-suspended in standard culture medium. Cell numbers were counted using a hemocytometer and subsequently seeded at the appropriate cell density. For freezing (-80°C/LN_2), cells were suspended into: 10% dimethyl-sulfoxide (DMSO; Sigma-Aldrich, Cat# D2650), 40% FBS and 50% cell medium.

2.7.2 Murine embryonic stem cell maintenance

The murine embryonic stem cell (mESC) line, E14.1 (E14; founder genetic background 129P2/OlaHsd)[165] are routinely cultured within the lab, but were originally provided by the lab of Professor Nicholas Hastie, MRC Human Genetics Unit, Edinburgh. mESC were routinely maintained on 6-well Corning® CellBIND® culture plates (Sigma-Aldrich, Cat# CLS3335) in GTES medium at 37°C with 5% CO_2 in a humidified incubator. GTES media consists of 15% foetal bovine serum (FBS; Invitrogen, Cat# 10437-028), 1x GlutaMax (Invitrogen, Cat# 35050-038), 1mM minimal essential medium (MEM) sodium pyruvate (Invitrogen, Cat# 1136-070), 1x non-essential amino acids (NEAA; Invitrogen, Cat# 11140-050), 1x penicillin/streptomycin (PenStrep; Sigma-Aldrich, Cat# P0781), 1x 2-Mercaptoethanol (βME; Invitrogen, Cat# 21985-023), 1:1000 leukaemia inhibitory factor (LIF; Millipore, Cat# ESG1107), in Glasgow MEM (GMEM, Sigma-Aldrich, Cat# G5154). Cells were routinely sub-cultured every ~48/72 hours for continued culture or for DNA/RNA extraction.

2.7.3 Human embryonic kidney cell maintenance

The human embryonic kidney cell line 293 (HEK), were obtained from the European Collection of Cell Cultures (ECACC, Cat# 85120602). HEK cells were routinely cultured in supplemented Dulbecco's Modified Eagle Medium (DMEM)

on standard 6-well tissue culture treated plates (IWAKI, Cat# 3810-006) at 37°C with 5% CO_2 in a humidified incubator. The supplemented DMEM media consists of 10% FBS, 1x GlutaMax, 1x PenStrep, in DMEM (Invitrogen, Cat# 31966-021). Cells were routinely sub-cultured every ~48/72 hours for continued culture or for DNA/RNA extraction.

2.7.4 Culturing of hair follicle bulge explants

Murine hair follicle bulges were micro-dissected and cultured on CELLstart™ CTS™ (Invitrogen, Cat# A10142-01), coated plates as described previously (Sieber-Blum et al., 2004) with modifications. Briefly, hair follicles from sacrificed adult mice were dissected using sterile forceps and scissors under a lamina flow hood. Sacrificed mice were initially immersed in a 1% Virkon solution for 3min and rinsed with 70% EtOH, before whisker follicles were isolated and collected into 60mm dishes containing dissection buffer (2.5 x 10^{-4}% wt/vol Amphotericin B, Sigma-Aldrich, Cat# A2942; 5 x 10^{-4}% wt/vol gentamicin, Sigma-Aldrich, Cat# G1272; in Hank's balanced salt solution (HBSS), Sigma-Aldrich, Cat# H8264). Connective and lipid tissue was scraped from follicles and discarded, before hair follicle bulbs were removed. The remaining follicle was bisected beneath the ring sinus and the lower portion (containing the bulge) was cut longitudinally to release the bulge.

Before the addition of bulges, 6-well culture plates treated by incubation at 37°C in a tissue culture incubator for 3hr with CELLstart™ CTS™ followed by 1hr with emigration media (ED1). Bulges were subsequently plated onto the treated plates, incubated directly in the well, with no media for 1hr to allow explants to adhere to the substratum. Up to 6 bulges were added per well.

Following adhesion of bulges, 1.5ml of ED1 culture media was added, consisting of 85% MEM α-modified (Sigma-Aldrich, Cat# M8042), 10% FBS (Thermo, Cat# SH30070.02), 5% chick embryo extract (CEE; EGG Tech, Cat# 60650), 2.5 x 10^{-4}% wt/vol Amphotericin B, 5 x 10^{-4}% wt/vol gentamicin, and 1x PenStrep. Bulge cultures were incubated at 37°C with 5% CO_2 in a humidified incubator with media exchanges (1/2 volume) every other day.

Bulge cultures were carefully monitored for outgrowth of EPI-NCSC, normally occurring after 2-3 days in culture. 2-3 days following the onset of emigration, normally day 5 after first explanting the bulge, the bulge was carefully removed with tungsten needle to prevent contaminating growth of keratinocyte cells from the bulge.

2.7.5 Maintenance of EPI-NCSC

After 7 days in culture, nearly 60% of bulges yielded emigrating cultures of EPI-NCSC. At this stage, primary *ex vivo* cultures were sub-cultured, and maintained on CELLstart™ CTS™ coated plates in expansion medium (XP1) at 37°C with 5% CO_2 in a humidified incubator for subsequent nucleofection. XP1 consisted of 85% Neurobasal-A media (Invitrogen, Cat# 108880222), supplemented with 1x B-27 supplement – without Vitamin A (Invitrogen, Cat# 12587), 10% CEE, 1x ITS+3 (Sigma-Aldrich, Cat# I-2771), 1x GlutaMax, 1x PenStrep, 10ng/ml stem cell factor (SCF; R&D Systems, Cat# 455-MC), 20ng/ml neurotrophin-3 (NT-3; R&D Systems, Cat# 267-N3), 25ng/ml epidermal growth factor (EGF; R&D Systems, Cat# 2028-EG), 50ng/ml fibroblast growth factor 2 (FGF-2; R&D Systems, Cat# 3139-FB).

EPI-NCSC were routinely sub-cultured before reaching 50% confluency in XP1 medium at 37°C with 5% CO_2 in a humidified incubator, for continued culture, DNA/RNA extraction, nucleofection or flow cytometry. It was important to maintain low cell density to avoid spontaneous cell differentiation. Culture medium was exchanged every other day, if culture plates were sparsely populated.

2.7.6 Nucleofection of EPI-NCSC

After 7 days of primary emigration culture, EPI-NCSC underwent their first sub-culture. However, before cells were reseeded on CELLstart™ treated plates, they were transfected with the Nucleofector™ device (Lonza, Model# Nucleofector™ II) under the manufacturers directions, using either the Mouse ES Cell Nuceofector® Kit (Lonza, Cat#VAPH-1001) or the Mouse Neural Stem Cell Nucleofector® Kit (Lonza, Cat# VAPG-1004) and the pCAG-Cre:GFP plasmid

vector (Addgene; LabLife, ID#U3478.P38). Briefly, EPI-NCSC cultures from the same mouse were pooled and spun down at 500g. Cells were re-suspended in the nucleofection solution, together with 10ng of plasmid and transferred to a cuvette. Cuvettes were placed in the nucleofector device and the T-020 program was applied (other programs tested were: G-013, O-005, X-001). Cells were then transferred to a pre-treated 6-well plate for 48hrs prior to FACS.

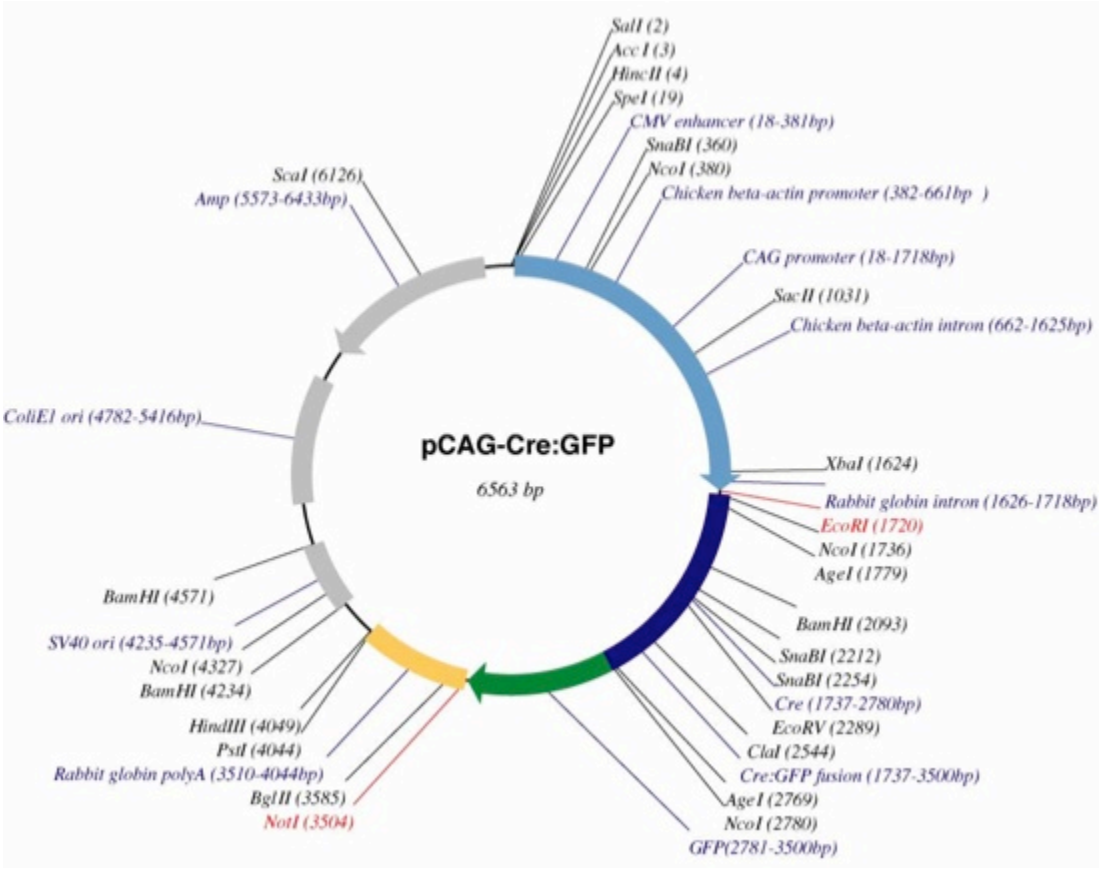

Figure 2-1. Plasmid map of the pCAG-Cre:GFP vector used for nucleofection
The pCAG-Cre:GFP plasmid was constructed by Matsuda and Cepko (2007)[166] and obtained through the Addgene plasmid repository. *Image source: Addgene plasmid 13776 - http://www.addgene.org/13776/*

2.7.7 Fluorescent activated cell sorting (FACS)

EPI-NCSC was harvested 48hr after nucleofection for flow cytometry by first sub-culturing the cells, except cells were retained in media suspension (ED1) and not initially seeded onto 6-well plates. The flow cytometry gating strategy is discussed in Chapter 5. Briefly, only particles with a forward scatter (FSC) and side scatter (SSC) of appropriate cell size were sorted, together with SSC-A (area) and SSC-H (height) to isolate single cells from doublets. EPI-NCSC were sorted based on GFP fluorescence intensity (Filter set: 4-488/530/30-A) and collected for further cell culture using a FACSAria Flow Cytometer (BD Biosciences, Model# FACSAria II). FACS was performed under the direction and assistance of Dr Owen Hughes (Newcastle University) and Ian Dimmick (Newcastle University).

2.7.8 X-gal staining of sorted cells

EPI-NCSC derived from R26R mice were nucleofected and isolated using GFP FACS. After 2 days in culture, cells were fixed for 15min in 4% PFA and washed 3x 15mins in X-gal wash buffer. Cells were subsequently stained in X-gal staining solution. Following O/N staining, tissue was washed 3x 1hr in X-gal wash buffer and fixed in 4% PFA O/N before bright field microphotography.

2.7.9 Alkaline phosphatase staining

Cells were stained for alkaline phosphatase (AP) using a modified protocol from Chang and Moog (1972)[167]. The culture medium was aspirated and cells were briefly washed in PBS, followed by a quick rinse with water. Cells were subsequently stained for 30min at 37°C with AP staining solution before being quickly washed again with water and fixed in 4% PFA for 20min at 4°C. Images of AP staining were captured immediately afterwards, using bright field microscopy to observe red precipitates in positively stained cultures. The AP staining solution was prepared fresh from individual frozen stocks with a final composition of 0.5% barbital (Sigma-Aldrich, Cat# 31995), 0.1% 1-naphthyl phosphate (Sigma-Aldrich, Cat# N7000), 0.5% fast red violet LB (Sigma-Aldrich, Cat# F3381), 0.06% $MgCl_2$.

2.7.10 Sphere assays

Two methods were utilized for sphere formation. Firstly, sub-confluent EPI-NCSC cells were trypsinised, counted and seeded at 1 x 10^4 cells/ml in 1.5ml XP1 medium and allowed to form spheres for up to 14 days at 37°C and 5% CO_2. Alternatively, 10 drops, each containing 100 cells were plated onto the lid of a 6-well plate and cultured as a hanging drop for 24hr prior to plating into a 6-well low adherent plate without CELLstart™ pre-treatment. Hanging drops from the same cell line were combined at this stage and further cultured for a total of 14 days at 37°C and 5% CO_2. To assay their colony forming ability, on the 14th day they were seeded onto CELLstart™ treated 6-well plates and further cultured for another 2 days at 37°C and 5% CO_2. XP1 Medium was exchanged every 48hr by transfer of spheres into 15ml Falcon tubes using a wide-bore pipette, allowing the spheres to settle, aspiration of all but 0.5ml of spent medium, and transferring back into fresh plates containing 1.0ml fresh XP1 medium.

2.7.11 Migration assay

The migration of EPI-NCSC was assayed by seeding 5 x 10^3 cells within 2x glass cloning rings (Sigma-Aldrich, Cat# C2059) on a CELLstart™ pre-treated 6-well plate, in XP1 medium. After allowing cells to adhere for 1hr, cloning rings were removed and the adherent cultures were analysed to verify no cells were outside the seeding zone. A small scratch was marked into each plate, to allow alignment of subsequent images with the overlaid measurement grid. At 6hr, 24hr and 48hr mosaic microphotographs were captured for analysis of cell movement. Images were aligned (see XXX) and a measurement grid consisting of concentric circles with increasing radius (600µm each) and 12 x 30° segments was overlaid and aligned to scratch marks made at the beginning of the assay. Cells in each region of the exclusion zone were counted for each mosaic image, and time point and subsequently analysed. Rose plots or radial histograms, illustrating total cell migration numbers, distance and direction were prepared using the Oriana software package (RockWare Inc.).

2.7.12 Proliferation assay

Viable cell counts were collected using a Vi-CELL XR® instrument (Beckman Coulter Inc.). This instrument incorporates a 0.4% trypan blue stain to isolate viable cells from dead cells and debris. Sorted populations of EPI-NCSC were seeded at 520 cells/cm^2 (5 x 10^3 cells in a 6-well plate) and in high density (cells from the migration assay) at 4 x 10^3 cells/cm^2 (29mm^2) within the same media volume and surface area (1.5ml; 9.6cm^2). After 7 days in culture, cells were analysed for their cellular expansion.

2.7.13 Additional tissue culture techniques

All media and solutions were pre-warmed to 37°C before use. Standard aseptic techniques were observed at all times. Cells counts, where stated, refer to viable cells and were counted using a hemocytometer with 0.4% trypan blue exclusion staining (Invitrogen, Cat# 15250-061) or the Vi-CELL XR Cell Counter (Beckman-Coulter), which can determine viable cells from dead cells and cell debris also using trypan blue exclusion.

2.8 Molecular techniques

2.8.1 Standard PCR and gel electrophoresis

DNA fragments were routinely amplified using the polymerase chain reaction (PCR) from genomic DNA or cDNA preparations. GoTaq® PCR reagents (Promega, Cat# M3175) were used for PCR amplification, typically consisting of: 2µl of template (genomic DNA or cDNA), 10µl 5x GoTaq® buffer, 1µl 10mM dNTPs (each), 0.1µl of each primer (reconstituted oligonucleotide stocks at 100pmol/µl), 0.1µl GoTaq polymerase in a final volume of 50µl ddH_20. PCR reactions were carried out using a G-Storm thermocycler (G-Storm, Model# GS1) together with the cycling conditions and primer sets listed in Table 2-1.

PCR products were analysed using standard 1.5% agarose (Takara, Cat# SeaKem® LE) gel electrophoresis in 1x TAE (10x: 48.4g tris-base, 10.9g glacial acetic acid, 2.92g EDTA, made up to 1 litre with dH20). SafeView (NBS

Biologicals Ltd.) nucleic acid stain was added (5µl/100ml) to agarose gels prior to casting.

2.8.2 Genomic DNA preparation and Genotyping

For the purposes of genotyping, genomic DNA was prepared from cell pellets (spun at 500g and media aspirated) and small soft tissue samples. To extract DNA for use in PCR, samples were boiled at 95°C in 100µl of an alkaline lysis solution (25mM NaOH; 0.2mM EDTA) for at least 30min and neutralised with 100µl 40mM Tris-HCL. 1µl of DNA solution was added to the standard PCR reaction as a template for amplification, as described in Section 2.8.1.

2.8.3 RNA extraction from tissue and cells

RNA was isolated from whole preparations of zebrafish embryos, mouse tissue or cell pellets, using TRIzol® LS reagent (Invitrogen, Cat# 10296-010) as per the manufacturers instructions. Briefly, tissue and cells were homogenized in 1ml of TRIzol reagent using trituration with a syringe and 27G needle, followed by 30G needle. Remaining insoluble material was removed from the homogenate by centrifugation at 12,000g for 10 minutes at 4°C. 200µl of chloroform was added to each tube, with vigorous agitation for 15sec and spun at 12,000g for 15min 4°C. The supernatant (aqueous phase) was aspirated into a new tube with 500µl of propan-2-ol and 0.5µl of glycogen (20µg/ul; Invitrogen, Cat# 10814-010), incubated for 5min at RT and spun at 12,000g for 15min at 4°C. The supernatant was removed and the RNA pellet re-suspended 20µl ddH20, and stored at -80°C. RNA was quantified using the Nanodrop apparatus (Thermo Scientific, Model# ND-8000).

2.8.4 RT-PCR

Reverse transcription PCR (RT-PCR) was performed to produce complementary DNA (cDNA) libraries with the High Capacity cDNA Reverse Transcription Kit (Applied Biosystems, Cat# 4368814) as per the manufacturers instructions. Briefly, the following steps were conducted with the use of a thermocycler PCR machine (G-Storm GS1). Typically 500µg of sample RNA was diluted in a final volume of 10µl and added to 10µl of the reaction master mix (2µl 10x RT buffer;

0.8µl 25x dNTP mix, 100mM; 2µl 10x RT random primers; 1µl MultiScribe™ reverse transcriptase; 4.2µl nuclease-free H2O) on ice. The following steps were performed in the thermocycler: 10min at 25°C; 120min at 37°C; 5min at 85°C and held at 4°C. Typically 3µl of cDNA was used per 50µl in subsequent PCR reactions. Housekeeping genes (ef1α, zebrafish; HPRT and β-actin, mouse) were initially used for cDNA normalisation, at 25 cycles. Table 2-1 lists the different RT-PCR primer sets used in cDNA amplification.

2.8.5 Quantitative PCR (qPCR)

Real-time quantitative PCR was performed by Dr Oliver Clewes using SYBR Green JumpStart qPCR MasterMix (Sigma Cat# S4438). Thermo-cycling conditions were: 95° C, 10 min followed by 40 cycles of 95°C, 15 s, 60°C, 60 s and 70°C, 30 s, performed on an Applied Biosystems 7900HT thermocycler. Melting curve analysis showed a single amplification peak for each reaction. Ct values for targets were normalised to the average Ct values of two housekeeping genes (HKG), Hypoxanthine-guanine phosphoribosyltransferase (HPRT), RPS9 and β-actin.

2.8.6 Plasmid preparation

The pCAG-Cre:GFP plasmid (see Figure 2-1) used for nucleofection was obtained from Connie Cepko (via Addgene plasmid 13776) and prepared from transformed DH5α bacterial cells (Invitrogen, Cat# 18263-012). For transformation, 100µl of were DH5α thawed on ice and added to 50ng of plasmid DNA for 20 minutes on ice. Cells were subsequently heat shocked at 42°C for 30sec and returned immediately to ice for 5min. 1ml of LB-Broth (LB; 10g tryptone, 5g yeast extract, 10g NaCl, made up to 1 litre in dH20, and autoclaved) was added to cells, followed by incubation at 37°C for 1hr with shaking. Cells were then spread onto agar plates (10g tryptone, 5g yeast extract, 10g NaCl, 15g agarose, made up to 1 litre dH_20, autoclaved and cast into 3cm bacterial plates) containing ampicillin (50µg/ml) and incubated O/N at 37°C. Isolate colonies were subsequently used to inoculate 5ml LB-Amp (LB plus ampicillin at 50µg/ml) and this was incubated O/N and subsequently used to inoculate 3 litres of LB-Amp, again for O/N incubation at 37°C with shaking.

Finally, this culture was used for plasmid purification using an endotoxin-free, transfection grade maxi-prep kit (Qiagen, Cat# 12162).

2.8.7 Oligonucleotides (PCR primers)

The following Table 2-1 lists the primers sets used throughout this project for genotyping and RT-PCR analysis of mRNA expression.

Table 2-1. Genomic PCR and RT-PCR Primer Sets

Gene ID	Forward Primer (5' to 3')	Reverse Primer (5' to 3')	Tm °C*
CD34	GAACCGTCGCAGTTGGAGCCC	GGCCGGTCCCGTTCTCCTGA	60°C
Cyclin D1	GGGGCCACCTGCATGTTCGT	TGGCGGCCAGGTTCCACTTG	60°C
HPRT	CACAGGACTAGAACACCTGC	GCTGGTGAAAAGGACCTCT	57°C
ID-3	TCCCGCGAGGCACTCAGCTT	CACCTGCGTTCGGGAGGTGC	60°C
Ki-67	TCTGATGTTAGGTGTTTGAG	CACTTTTCTGGTAACTTCTTG	48°C
Msx2	CAGTCCCGGGCCTCTCGTCA	CTGGCGGAACTTGCGCTCCA	60°C
Nes	GAAGCCCTGGAGCAGGAGAAGCA	TCCAGGTGTCTGCAAGCGAGAGTTC	57°C
PCNA	CGCAACCTAGCCATGGGCGT	TCTGGGATTCCAAGTTGCTCCACA	60°C
Pygo2 FLOX	CCTGGATTCTTGTTGCTGGTATG	AAGGTATTTGGTGCTCCGAGGG	60°C
Pygo2 NULL	TGTCTTGATGACAGCGTTTAGCC	AGATTCAGTAAGCTGAGCCTGGTG	60°C
R26R	AAAGTCGCTCTGAGTTGTTAT	GCGAAGAGTTTGTCCTCAACC	56°C
		GGAGCGGGAGAAATGGATATG	
Snai2	CTGGACCGTTATCCGCCCGC	TGGAGTGGAGCTGCCGACGA	60°C
Sox10	GGCTCCGTCCAGACAAGGCAG	TCGTGAAGAGCCCAACGCCC	60°C
Twist1	GCGTCCCACTAGCAGCGGAG	TGTGCCCCACGCCCTGATTC	60°C
Wnt1-Cre (Cre)	CGTTTTCTGAGCATACCTGGA	ATTCTCCCACCGTCAGTACG	55°C
Wnt1-Cre (RARB)	GTAGCCATCGAGACACAGAGT	TGGTAGCCCGATGACTTGTCC	
β-Actin	ATGAAGATCCTGACCGAGCG	TACTTGGCGCCTCAGGAGGAGC	57°C
RPS9	TGTTGACGCTAGACGAGAAGG	AATGAAGGATGGGATGTTCACC	57°C
ef1α	CTGGAGGCCAGCTCAAACAT	ATCAAGAAGAGTAGTACCGCTAGCATT	57°C

Table outlining oligonucleotide sequences used for standard PCR and (*) PCR annealing temperature.

2.8.8 Additional techniques

Filter pipette tips and nuclease free 1.5ml Eppendorf tubes were used at all times.

2.9 Statistical analyses

Routine statistical analysis of results was performed using Prism 5 statistical software (GraphPad Software Inc.). Where appropriate a two-tailed, unpaired Student's *t*-test or ANOVA with Tukey's multiple comparison post-hoc was used to measure significance between two or more populations. Analysis of hair follicle development staging was performed by Professor Heather Cordell using logistical regression analysis using STATA® software (StataCorp LP).

Chapter 3. Distinct Roles for *Pygo Homologs* in Zebrafish Development: Evolution of *Pygopus*

3.1 Introduction

Loss-of-function and studies represent a classical approach to studying gene function. The use of modified oligonucleotides (morpholinos) to knockdown gene expression combined with the zebrafish model provides a fast, economical and relatively simple approach to determine the role of a gene through loss-of-function. In this study, a morpholino (MO) knockdown of *pygo1* and *pygo2* was conducted, together with an *in silico* examination of the zebrafish *pygo* homologs.

3.1.1 Zebrafish as a model organism

The zebrafish (*Danio rerio*) is a small, tropical, fresh water fish species that inhabits rivers and streams of southern Asia, in particular, India, Nepal and Pakistan. It is characterized by five pigmented horizontal stripes along the side of its body that extend to the end of caudal fin rays and thus give zebrafish its common name.

While studies on zebrafish began as early as the 1930s [168,169], it is only in the last fifteen to twenty years that zebrafish have emerged as a popular model organism, and have now become commonplace in laboratories around the world [170]. This is, in part, due to the early pioneering efforts of George Streisinger [171] and the proliferation of large scale mutation screening and genome sequencing projects in general [172-175]. Together these studies have led to a range of tools allowing relatively easy genetic manipulation of zebrafish and additional research community resources like the zebrafish information network (ZFIN) [176,177].

In addition to these efforts, the zebrafish itself provides a number of unique advantages over other conventional model organisms and this has also

contributed to their rise in popularity. In comparison to mice, zebrafish are relatively cheap to accommodate, breed easily and develop rapidly. Furthermore, zebrafish embryos are transparent, allowing visualization of early developmental process and the usage of labeling tools at the cellular level. Finally, because the embryos are externally fertilized, the eggs may be easily manipulated. For example, at the single cell stage of development, drugs and other genetic modifiers may be injected directly into the zebrafish embryo.

3.1.2 Zebrafish development

The embryonic development of the zebrafish has previously been described in detail by Kimmel et al. (1995) and provides an important reference for the embryonic stages of development in this study. In general, there are seven periods of embryogenesis, beginning with the zygote, followed by cleavage, blastula, gastrula, segmentation, pharyngula and hatching periods [155]. These stages cover the first 3 days post fertilization at which point the hatched larva has largely completed morphogenesis and continues to grow into a sexually mature adult after approximately 90 days.

The zygote is first formed by fertilization of the egg and is rapidly followed by the first cellular cleavage, which occurs within the first hour post fertilization (hpf). These cells continue to divide and after eight zygotic cell cycles, they form the blastula (2¼-5¼hpf). At this point, the blastodisc appears as a ball-like structure and epiboly begins with formation of the yolk syncytial layer, while the blastodisc begins spreading over the yolk cell. At the end of the gastrula period (10 hpf), the yolk cell is completely covered and the primary germ layers are formed via involution, convergent and extension cellular movements.

The segmentation period begins around 10hpf and is marked by the formation of somites and the visibility of primary organs. At the beginning of this period the neural tube is formed by a process known as “secondary neurulation” [178]. In contrast to other vertebrates (avians and mammals) where the neural tube forms through the closing of neural folds, the process in zebrafish occurs entirely through a hollowing of the condensed neural primordium as illustrated in Figure 3-1.

Importantly, in both neurulation processes, the NC forms between the non-neural ectoderm and the developing neural tube. Secondary neurulation begins in the zebrafish at the anterior trunk (11⅔hpf) and continues caudally until near the end of the segmentation period (20 hpf). During this period, the neural crest begins migration near the condensing neural primordium and the dorsolateral wall of the brain (cephalic neural crest; 13hpf). Neural crest migration continues caudally, until after the neural tube has fully developed and into the pharyngula period [179].

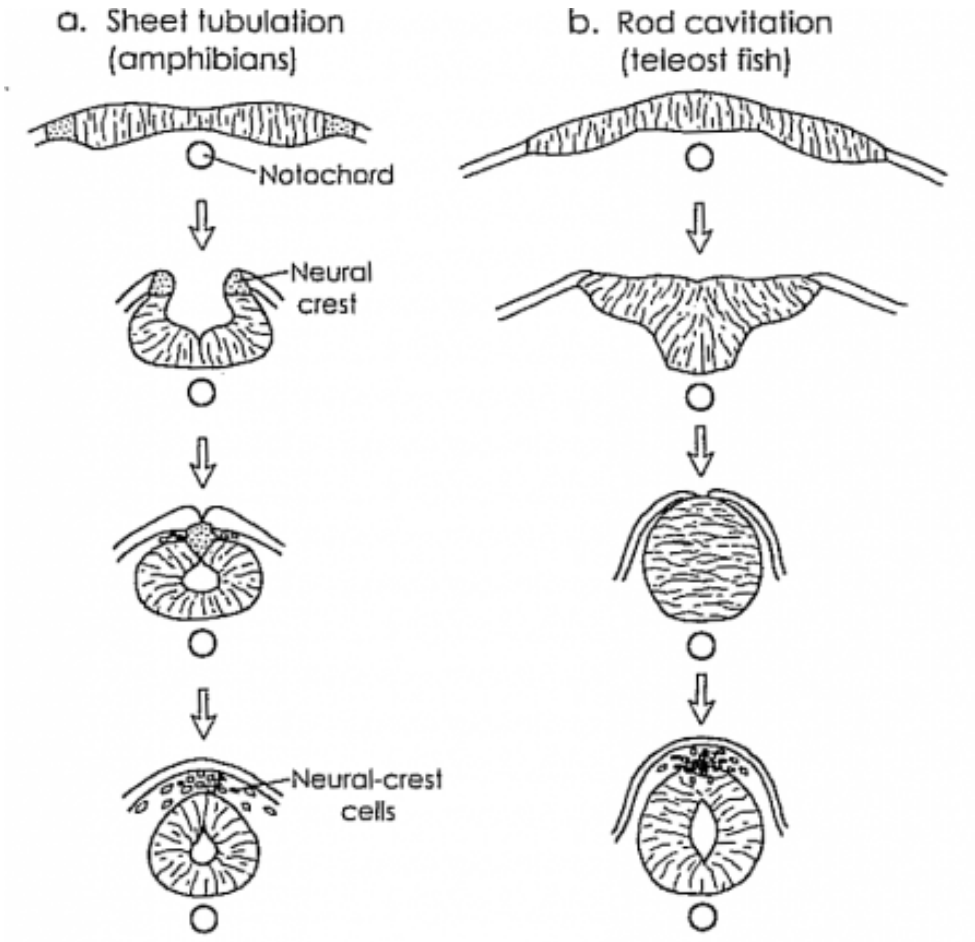

Figure 3-1. Primary and secondary neurulation in frog and zebrafish
Two modes of neurulation in vertebrates. The structure of neural tube is conserved but the developmental process differs between the head and trunk regions. (a) Head and trunk region of most vertebrates and (b) the head and trunk of fishes and caudal regions in other vertebrates. *Source: West-Eberhard (2003)*[180].

The embryo at the beginning of the pharyngula period (24hpf) has a well-developed neural tube, notochord and the full set of somites. As the name suggests, the pharyngeal arches develop during this period alongside the fin rays coupled with differentiation of pigment cells. Also, during this period the irregular heartbeat now develops distinct atrial and ventricular contractions, while the rudimentary heart tube elongates, bends and myocardial cells begin to differentiate into heart cushions (primitive valves).

By the end of the pharyngula period and the beginning of hatching (48hpf), organ morphogenesis is almost complete. The growth rate of the embryo slows down, and hatching occurs sporadically throughout the third day. As pectoral fin development continues, the most prominent changes occur in the pharyngeal region. The mouth and jaws are repositioned and extend anteriorly and eventually protrude beyond the eyes (72hpf).

After the third day, the zebrafish embryo is termed a larva and with most of its morphogenesis completed, it continues to grow rapidly. The swim bladder inflates and the larva begins active swimming and independent feeding (120hpf).

3.1.3 The sox10:egfp model: visualizing early neural crest development

Zebrafish have been used in a wide range of fields including studying developmental processes, the aetiology of disease, cancer, drug screening and genetics [181-185]. Of particular interest, is their use in the study of the development of the NC and its contribution to embryonic development.

During zebrafish embryogenesis, the branchial arches are formed by interactions between the mesodermal mesenchyme, epithelia and migrating NC [186,187]. Subsequently, NC from the branchial arches forms cartilage in the head, jaws and pectoral fins. The NC mesenchyme also contributes to the tail fins. In an evolutionary sense, this is different to higher vertebrates, where the dermal skeleton of the limbs are formed from the mesoderm derived endoskeleton [8].

Like in mammals, the zebrafish NC forms the PNS (ganglia and glia) and pigment cells [188-191]. It may also contribute to the lateral line, a mechanosensory organ used to detect changes in water flow [192]. While the zebrafish heart does not undergo a septation of the outflow tract (like in mammals), there are reports that the NC contributes to all segments of the heart: the bulbous arteriosus, ventricle, atrioventricular junction and atrium [193,194]. Using fluorescently tagged NCC, it has been demonstrated that NCC migrate into the primary heart field during development, participate in heart looping and ventricular function, and additionally contribute to the myocardium [193-196].

In 2006, Carney *et al.* developed a stable transgenic zebrafish line, the sox10:egfp line that allows *in vivo* observation of fluorescent cells within the embryo (see Figure 3-2). In this model, cells that express the transcription factor sox10 also express eGFP from a construct utilizing the *sox10* promoter. This transgenic line was originally created to understand the role of *sox10* in the formation of neurons of the dorsal root ganglia (DRG). However, due to the importance of *sox10* in the development of cell derivatives of the NC, it may be used as a general marker for pre-migratory and migratory NCC [154].

More specifically, the sox10:egfp line faithfully recapitulates the endogenous expression of Sox10 as shown in Figure 3-2. Compare this (Figure 3-2) with the *in situ* expression pattern of *sox10* demonstrated in Figure 2 from Stewart *et al.* (2010)[197]. From these studies, *sox10* is first expressed around 10-11hpf, lateral to the neural plate, and its expression subsequently expands to the neural tube, pre-migratory and migrating NCCs. At 24hpf, expression can be seen in the brachial arch cartilage progenitors, PNS glial precursors and migrating pigment progenitors. Finally at 48hpf, expression begins diminishing rapidly in the sensory neurons. However, transient expression is seen in the brain and persistent expression continues in the glia and begins in the differentiating cartilage of the jaw and pectoral fins [154,198,199].

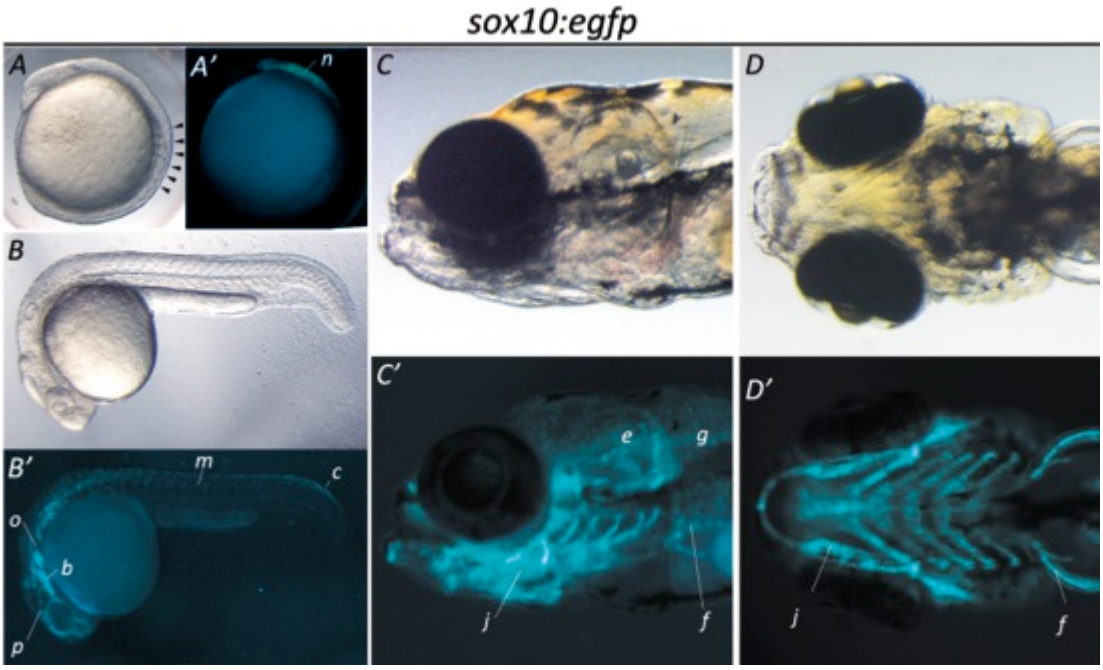

Figure 3-2. Neural crest expression of eGFP in the sox10:egfp zebrafish line during development. Lateral views of transgenic *sox10:egfp* embryos at 12 hpf (A, A'), 24 hpf (B, B') and 120 hpf (C, C') and ventral views of embryos at 120 hpf (D, D'). Fluorescence images show the transient expression of eGFP under UV light (A'-D') and corresponding spatial location in normal bright field images (A-D). Embryos in A are at the 6 somite stage of development, indicated by black arrows. Expression of *egfp* is first seen lateral to the neural plate (*n*) and later in the pigment precursors (*p*), branchial arches (*b*), otic placode (*o*), migrating NCCs (*m*), and pre-migratory NCCs (*c*). Persistent expression is seen in the glia (*g*), ear epithelia (*e*), olfactory neurons (*l*), jaw cartilage (*j*) and pectoral fin cartilage (*f*).

3.2 Aims of this study

As outlined previously there are numerous inconsistencies between the described function of *pygopus* in the fruit fly and that of the homologs in mouse and frog (see Chapter 1). For example, in the fly, *pygo* is essential for transduction of the *wg/Wnt* signal, whereas in the mouse it only modifies the signal intensity or level of transcriptional output. There is also disparity in the number of paralogs and the assumed redundancy between the fly and vertebrates. The fly has one essential *pygo* gene, while the frog genome encodes for two essential splice variants of *pygopus* that represent *pygo2* orthologs. A loss of either leads to severe eye and brain defects. No ortholog of *pygo1* has been reported in the frog. In contrast, there are two separate orthologs, namely

Pygo1 and *Pygo2* in mice. *Pygo1* null mice are viable and display no overt phenotype, while mice lacking *Pygo2* are neonatal lethal. Thus, it is assumed that murine *Pygo1* is largely redundant.

With this in mind, it is tempting to speculate that the additional pygo homologs in higher vertebrates have evolved alongside the NC and Wnt pathways throughout vertebrate radiation. This is supported by the appearance of the NC being a vertebrate innovation [200] and its close association to the NC through the EPI-NCSC molecular signature and the Wnt pathway in general. As such, evolutionary and developmental comparative studies may provide important insight into pygo function and evolution.

To date there are no published studies specifically on the *pygo* gene in *Danio rerio*. However, two reports recently presented an alignment of *Danio* rerio *pygo2* in relation to other orthologs [201,202]. There was no specific discussion of these sequences nor was a *pygo1* homolog reported. Given that the frog has only a single ortholog, it is possible that zebrafish only have a single ortholog too. This would suggest the zebrafish might be devoid of the technical limitations of gene redundancy, as seen in mice. With this in mind, it was anticipated that this study would help to console the role of *pygo* homologs between model organisms, towards a unified understanding of *pygo* homologs in vertebrate development.

Specifically, the aims of this chapter were:

1. *Determine if there exists an additional ortholog of pygopus in zebrafish*
2. *Analyse the evolutionary diversity of the pygopus gene in zebrafish and across other model organisms*
3. *Determine the in vivo expression of pygopus in the zebrafish*
4. *Determine the role of pygopus in zebrafish development*

3.3 Homologs of *pygopus*

3.3.1 Two homologs, pygo1 and pygo2 exist in zebrafish

In order to undertake the first aim of this study, the existence of possible *pygopus* homologs was investigated in the zebrafish genome. Using an *in silico* approach, the method outlined by NCBI [203] was utilized to identify if any reference sequences exist. The HomoloGene [204], Gene [205] and Protein [206] databases were searched for variations on the *pygopus* gene name and symbol. A single annotated sequence was found, *Danio rerio pygopus* homolog 2 with the sequence identifier NM_001033111. This is consistent with previous reports by Kessler *et al* (2009) and Fiedler *et al* (2008). No results were returned from this search for a putative *pygo1* sequence.

To further probe the zebrafish genome, provisional nucleotide reference sequences from human (NM_015617; NM_138300), mouse (NM_028116; NM_026869), frog (NM_001088859) and fly (NM_143615), were obtained from the Nucleotide database [207] to perform a translated BLAST (tblastx) search of the zebrafish expressed sequence tag (EST) and nr (GenBank, RefSeq, EMBL, DDBJ, PDB sequences; excludes genome sequencing projects and ESTs) databases [208]. The translated BLAST algorithm compares the given nucleotide sequence to the target genome allowing for mismatches based upon known redundancy in protein coding sequences [209-211]. In this way, it is possible to analyse if two nucleotide sequences will yield similar protein translations.

From these database queries, positive matches with a bit score (Max value) greater than 40 were collected for further analysis after genomic sequences were removed; leaving only expressed sequences that may be translated to a functional protein homolog. Furthermore, sequences with over 98% homology at the nucleotide level, and expressed from the same chromosome were assumed to be from the same gene and were subsequently filtered from the results. Table 3-1 summarises these remaining 21 unique sequences from the original results pool.

Table 3-1 Resulting sequences from pygopus homology searches in the zebrafish genome

Accession	Sequence Description	Bit Score*
BC171351.1	Danio rerio zgc:172214, mRNA (cDNA clone MGC:198078 IMAGE:9039067), complete cds	161
NM_001033111.2	Danio rerio pygopus homolog 2 (Drosophila) (pygo2), mRNA	130
AL918799.1	AL918799 PJR-Z1+Z2 Danio rerio cDNA clone 053-E12-2, mRNA sequence	76.3
BM533071.1	fx65f06.y1 Zebrafish SJD 5 day embryo Danio rerio cDNA clone IMAGE:5628418 5-similar to SW:CA15_HUMAN P20908 COLLAGEN ALPHA 1(V) CHAIN PRECURSOR. [1] ;, mRNA sequence	45.1
CA470265.1	AGENCOURT_10697357 NCI_CGAP_ZEmb2 Danio rerio cDNA clone IMAGE:6789687 5-, mRNA sequence	43.2
NM_205667.1	Danio rerio small nuclear ribonucleoprotein polypeptides B and B1 (snrpb), mRNA	43.2
BI890427.1	ZF637-2-002182 Zebrafish shield stage whole embryo cDNA library MPMGp637 Danio rerio cDNA clone MPMGp637_7N6;MPMGp637N067 5-, mRNA sequence	42.8
CK681616.1	ZF101-P00025-DEPE-F2_L03 GISZF001_ra Danio rerio cDNA clone IMAGE:7143509 5-, mRNA sequence	41.8
CK361259.1	AGENCOURT_17114219 NIH_ZGC_4 Danio rerio cDNA clone IMAGE:7089465 5-, mRNA sequence	41.4
BI891823.1	ZF637-3-001078 Zebrafish shield stage whole embryo cDNA library MPMGp637 Danio rerio cDNA clone MPMGp637_19G6;MPMGp637G0619 5-, mRNA sequence	40.9
CT650024.2	CT650024 ZF_mu Danio rerio cDNA clone ZF_mu_97a05 5-, mRNA sequence	40.9
CA476609.1	AGENCOURT_10701089 NCI_CGAP_Zemb3 Danio rerio cDNA clone IMAGE:6799773 5-, mRNA sequence	40.8
AL918193.1	AL918193 PJR-Z1+Z2 Danio rerio cDNA clone 044-E08-2, mRNA sequence	40.5
CK361135.1	AGENCOURT_17114189 NIH_ZGC_4 Danio rerio cDNA clone IMAGE:7089152 5-, mRNA sequence	40.5
CK869774.1	AGENCOURT_19404561 NIH_ZGC_16 Danio rerio cDNA clone IMAGE:7214056 5-, mRNA sequence	40.5
DT082349.1	AGENCOURT_56123420 NIH_ZGC_10 Danio rerio cDNA clone IMAGE:8000138 5-, mRNA sequence	40.5
EG585117.1	AGENCOURT_88483876 NIH_ZGC_34 Danio rerio cDNA clone IMAGE:8750262 5-, mRNA sequence	40.5
NM_001128327.1	Danio rerio lysine (K)-specific demethylase 5Ba (kdm5ba), mRNA	40.3
BC100114.1	Danio rerio cDNA clone IMAGE:7174464, partial cds	40
BI887964.1	ZF637-1-002219 Zebrafish shield stage whole embryo cDNA library MPMGp637 Danio rerio cDNA clone MPMGp637_10E8;MPMGp637E0810 5-, mRNA sequence	40
BI890518.1	ZF637-2-002273 Zebrafish shield stage whole embryo cDNA library MPMGp637 Danio rerio cDNA clone MPMGp637_7M13;MPMGp637M137 5-, mRNA sequence	40

*Sequences are listed in order of bit score. The bit score is calculated from the number of gaps and substitutions required to perform an alignment between the query sequence and the result. This higher the score, the more identity between sequences.

To inspect the level of homology between this pool of putative pygopus homologs, a consensus sequence (Figure 3-3) composed from the fly, frog, mouse and human reference sequences was generated using the Geneious software package [151]. Briefly, this was generated using a MUSCLE alignment of the seven sequences with 20x iterations. Gaps and ambiguous residues were removed.

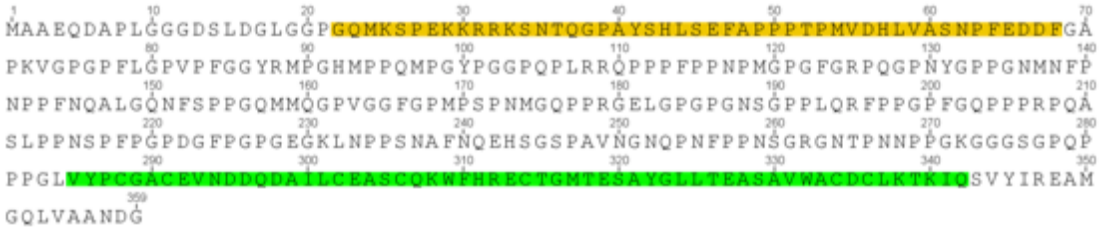

Figure 3-3. Pygopus consensus sequence from fly, frog, mouse and human homologs.
The consensus sequence was generated using *pygo* reference proteins and the MUSCLE alignment algorithm with 20 iterations [212]. Ambiguous residues have been removed, along with sequence gaps. The NHD is highlighted in yellow, and the PHD in green.

The generated consensus sequence was aligned to each of the six possible protein translations from Table 3-1, again using the MUSCLE algorithm. Table 3-2 lists these results including the global pairwise identity of the comparisons, and in addition, local alignment scores from the NHD and PHD regions. Also listed is the chromosome and gene symbol (if known).

To filter these results further, translations containing a stop codon within the alignment between the NHD and PHD were discounted (identified by blue shading), as this would presumably lead to a truncation of the mature protein. Furthermore, a threshold of 30% was applied to further isolate sequences that may represent *pygopus* homologs (shaded red). The threshold was applied to sequence homology in the highly conserved NHD/PHD regions of non-truncated sequences. Sequences over this value are highlighted by red text.

Table 3-2 Homology between the Pygopus consensus sequence and putative homologs

Accession	Gene	Ch.	Region	Open Reading Frame					
				1	1 - Rev	2	2 -Rev	3	3 - Rev
AL918193.1	-	-	global	7.50%	14.80%	9.20%	12.00%	16.20%	9.50%
			NHD	10.60%	10.60%	8.50%	12.80%	17.00%	12.80%
			PHD	6.90%	12.10%	3.40%	13.80%	5.20%	15.50%
AL918799.1	-	-	global	6.10%	5.80%	6.10%	6.70%	6.10%	8.30%
			NHD	10.60%	0.00%	6.40%	14.90%	14.90%	0.00%
			PHD	0.00%	17.20%	10.30%	3.40%	0.00%	40.30%
BC100114.1	-	15	global	8.30%	7.90%	7.20%	8.00%	8.50%	7.50%
			NHD	16.90%	11.20%	10.60%	19.60%	14.70%	10.30%
			PHD	7.50%	12.50%	5.80%	11.10%	10.70%	10.60%
BC171351.1	-	13	global	8.70%	11.00%	**30.20%**	14.00%	11.00%	12.50%
			NHD	6.40%	20.70%	60.40%	14.90%	18.00%	10.40%
			PHD	9.40%	12.10%	71.40%	10.30%	15.50%	16.40%
BI887964.1	-	-	global	23.70%	19.00%	24.60%	18.10%	23.50%	19.30%
			NHD	21.70%	10.60%	19.60%	4.30%	21.80%	10.60%
			PHD	6.90%	5.50%	8.60%	10.70%	12.10%	8.60%
BI890427.1	-	-	global	20.30%	17.50%	22.20%	18.00%	19.70%	18.20%
			NHD	20.90%	6.40%	20.80%	6.40%	15.00%	10.60%
			PHD	5.20%	8.70%	6.90%	13.40%	5.20%	13.60%
BI890518.1	tardbpl	23*	global	22.60%	22.40%	23.10%	21.40%	23.00%	22.20%
			NHD	10.60%	2.20%	12.80%	10.60%	14.30%	17.10%
			PHD	8.70%	19.00%	10.30%	22.40%	5.20%	16.90%
BI891823.1	-	-	global	21.80%	19.60%	22.40%	18.20%	24.00%	18.70%
			NHD	24.00%	4.30%	19.80%	4.30%	23.40%	6.40%
			PHD	1.70%	13.90%	0.00%	8.70%	1.70%	12.10%
BM533071.1	col5a1	21	global	11.40%	12.30%	20.60%	10.60%	10.60%	18.70%
			NHD	17.00%	10.60%	8.50%	14.90%	12.80%	14.90%
			PHD	3.40%	20.70%	12.10%	12.10%	13.80%	1.70%
CA470265.1	ybx1	8*	global	21.60%	22.30%	23.30%	23.40%	20.10%	22.40%
			NHD	12.90%	19.10%	21.30%	23.40%	8.60%	17.00%
			PHD	8.60%	17.20%	15.50%	13.90%	12.10%	22.50%
CA476609.1	kdm5a	-	global	14.00%	12.80%	12.40%	16.90%	13.70%	14.80%
			NHD	8.50%	19.20%	12.80%	22.50%	12.80%	19.10%
			PHD	10.40%	6.90%	10.50%	12.10%	8.60%	12.10%
CK361135.1	-	-	global	20.30%	19.80%	19.50%	19.00%	20.50%	19.70%
			NHD	23.40%	17.00%	25.50%	12.80%	21.30%	10.60%
			PHD	10.30%	5.20%	13.80%	3.40%	8.60%	1.70%
CK361259.1	eif5	20*	global	18.70%	21.20%	16.50%	24.20%	18.10%	23.90%
			NHD	14.90%	21.30%	6.10%	12.80%	17.00%	14.90%
			PHD	10.30%	5.20%	1.70%	6.90%	8.60%	15.50%
CK681616.1	arp1	10	global	15.00%	16.30%	14.40%	15.00%	13.40%	14.20%
			NHD	21.30%	12.80%	12.20%	8.50%	10.60%	22.90%
			PHD	15.50%	15.50%	10.30%	13.80%	12.10%	17.20%
CK869774.1	pklr	16	global	13.00%	13.60%	12.80%	14.80%	13.40%	15.80%
			NHD	12.80%	17.00%	12.80%	12.80%	12.80%	10.60%
			PHD	17.20%	18.60%	15.90%	19.00%	10.30%	12.10%
CT650024.2	-	9	global	10.90%	9.70%	13.10%	10.00%	9.70%	10.00%
			NHD	12.80%	6.40%	10.60%	6.40%	17.00%	12.80%
			PHD	20.70%	12.10%	17.20%	17.20%	17.20%	13.80%
DT082349.1	wdr1	14	global	11.60%	10.20%	12.30%	13.90%	11.70%	10.50%
			NHD	6.40%	8.50%	14.90%	10.60%	8.50%	8.50%
			PHD	11.70%	0.00%	5.20%	12.10%	6.90%	10.00%
EG585117.1	-	14	global	12.50%	10.90%	12.30%	11.40%	10.50%	8.80%
			NHD	19.10%	10.60%	17.00%	8.30%	12.80%	10.60%
			PHD	17.20%	13.80%	12.10%	12.10%	12.10%	13.80%

Table 3-2 – Continued …

NM_001033111.2	pygo2	19	global	9.60%	8.90%	9.60%	12.20%	**19.00%**	9.60%
			NHD	11.20%	13.40%	7.50%	4.90%	87.50%	10.30%
			PHD	10.30%	9.70%	8.00%	11.10%	76.20%	15.10%
NM_001128327.1	kdm5ba	11	global	7.20%	8.50%	7.70%	7.20%	7.60%	7.20%
			NHD	9.50%	8.90%	4.30%	13.00%	12.50%	8.50%
			PHD	5.70%	7.80%	7.70%	6.70%	8.40%	7.40%
NM_205667.1	snrpb	6	global	19.30%	19.70%	10.50%	14.60%	12.70%	11.60%
			NHD	9.80%	12.80%	6.40%	19.10%	16.30%	14.90%
			PHD	12.10%	22.00%	6.80%	17.20%	13.80%	12.10%

* Predicted chromosome location only. Alignments shaded blue contain an in-frame stop codon between the NHD and PHD. Alignments highlighted in red (also in red text) contain >50% homology locally within either the NHD or PHD.

From the initial pool of 21 sequences, two putative homolog sequences were found (Genbank accession: BC171351 & NM_001033111). These have been emphasized (bold & red shading) in Table 3-2. As previously discussed, the first sequence NM_001033111 represents the *pygo2* homolog. However, the sequence '*Danio rerio* zgc:172214, mRNA' sequence (Genbank accession: BC171351) provided evidence for the existence of an additional ortholog of *pygo1* in zebrafish. In corroboration with this initial data, this sequence has recently been included autonomously as the provisional *Danio rerio pygopus* homolog 1 (NM_001113637) reference sequence.

Finally, a subsequent BLAST strategy was conducted on the zebrafish genome to conclusively dismiss the possibility that another homolog of *pygopus* exists in zebrafish. The NHD and PHD consensus sequences (Yellow & Green; Figure 3-3) were used to perform a tblastn query; this time directly on the zebrafish genome. Only two unique 'hits' or sequences from chromosome 13 and 19 were identified. These chromosomal locations agree with those of the two putative homologs, shown in Table 3-2. Thus, it can be safely assumed that no other homolog of *pygopus* exists in zebrafish.

3.3.2 Zebrafish pygo1 and pygo2 are true orthologs

In the early speciation of ray-finned fishes, a genome duplication event led to many genes within the zebrafish genome having multiple copies [213]. Given that frogs have two isoforms of *pygo2* and no *pygo1*, it is entirely possible that the zebrafish *pygo1* sequence previously identified by the BLAST search represents an isoform from a gene duplication event, or specifically a paralog of *pygo2* within zebrafish. Because true orthologs are separated by a speciation event, and not through a gene or genomic duplication event [214].

To test this possibility, protein alignments based on translations of both zebrafish mRNA sequences (BC154591; NM_001033111) were compared to fruit fly (NP_651872), frog (AAN41447; AAN41448), mouse (NP_082392; NP_081145) and human (NP_056432; NP_612157) protein reference sequences. The results from these comparisons have been represented as an unrooted dendrogram (Figure 3-4). In addition, the sequence homology between the zebrafish orthologs and homologs from fly, frog, mouse and human were calculated using a series of pairwise alignments with ClustalW [215]. These results have been summarized in Table 3-3.

Table 3-3 Pairwise percentage identity (global) between pygopus protein homologs

%	Pygo	pygo1	pygo2	pygo2a	pygo2b	Pygo1	Pygo2	PYGO1	PYGO2
Drosophila melanogaster									
pygo	100%	17.0%	28.9%	16.6%	16.3%	14.5%	18.6%	14.9%	18.4%
Danio rerio									
pygo1	17.0%	100%	19.7%	29.6%	31.1%	**43.9%**	30.8%	42.5%	29.6%
pygo2	28.9%	19.7%	100%	35.4%	34.9%	25.0%	**39.0%**	25.4%	36.9%
Xenopus laevis									
pygo2a	16.6%	29.6%	35.4%	100%	98.1%	34.2%	68.8%	33.1%	65.9%
pygo2b	16.3%	31.1%	34.9%	98.1%	100%	38.0%	68.9%	35.5%	69.0%
Mus musculus									
Pygo1	14.5%	43.9%	25.0%	34.2%	38.0%	100%	36.0%	87.4%	35.4%
Pygo2	18.6%	30.8%	39.0%	68.8%	68.9%	36.0%	100%	36.3%	96.5%
Homo sapiens									
PYGO1	14.9%	42.5%	25.4%	33.1%	35.5%	87.4%	36.3%	100%	36.2%
PYGO2	18.4%	29.6%	36.9%	65.9%	69%	35.4%	96.5%	36.2%	100%

The highest percentage identity for each zebrafish pygopus protein is highlighted in bold text (blue background). Percentage sequence identity was calculated by making multiple pairwise comparisons between protein sequences using the ClustalW program (version 2.0.11).

Interestingly, the zebrafish homologs pygo1 and pygo2 cluster with the mouse and human homologs respectively in Figure 3-4, and thus are likely to represent true orthologs of *pygopus.* Both isoforms pygo2α and pygo2β from *Xenopus* cluster independently within the *Pygo2* branch and thus, as previously reported [118] represent paralogs within this study. From Table 3-3 it can be seen that zebrafish pygo1 shares the greatest pairwise identity with mouse Pygo1 (43.9%). And likewise, pygo2 shares its highest sequence identity of 39% with mouse Pygo2. While the sequence homology between zebrafish pygo1 and pygo2 proteins is almost half (19%) that seen with respective mouse orthologs.

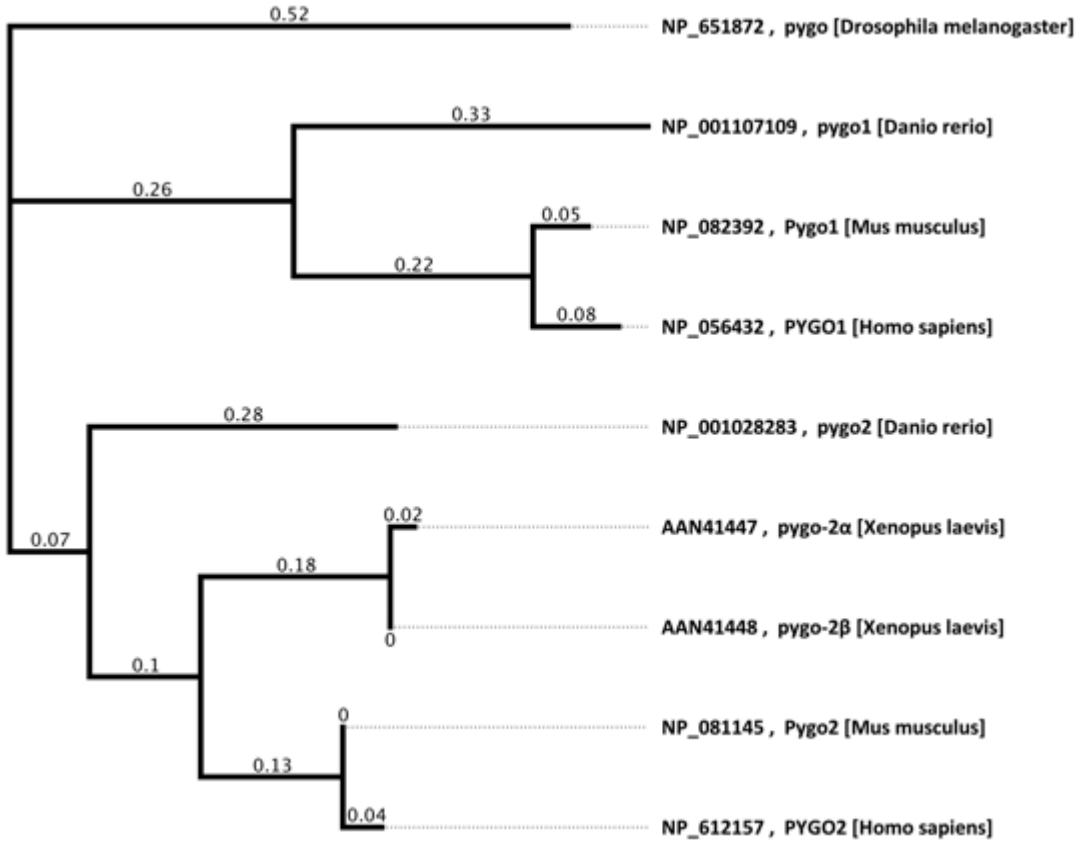

Figure 3-4. Relative genetic distance between *pygopus* homologs.
Protein alignment of reference sequences from fruit fly *(Drosophila melanogaster),* zebrafish *(Danio rerio),* frog *(Xenopus laevis)*, mouse *(Mus musculus)* and human *(Homo sapiens)* were used to construct an unrooted dendrogram. The distance from a common branch point represents the relative genetic distance between two sequences. Numerical labels show the number of substitutions per site from the common branch point. Protein alignments were performed using Neighbor-Joining and the Blosum62 matrice [153].

Genetic linkage is regularly used to infer co-regulation of gene expression [216] and more recently disease association [217], but it also suggests a common or conserved evolutionary history for a gene or chromosomal region. To further explore the evolutionary origins of the zebrafish *pygo* homologs, conserved synteny at the genetic loci was investigated using the NCBI genome browser for zebrafish, mouse and human genome builds. As illustrated in Figure 3-5, both *pygo1* and *pygo2* loci exhibit conserved genetic linkage across the vertebrate species. *pygo1* is immediately flanked in all species by two genes upstream, *neural precursor cell expressed, developmentally down-regulated 4* (*nedd4*) and *protogenin homolog* (*prtg*) and two genes downstream *dyslexia susceptibility 1 candidate 1 homolog* (*dyx1c1*) and *cell cycle progression 1* (*ccpg1*) of the locus.

While *pygo2* is not immediately flanked by conserved linked genes, it is closely flanked by *pre-B-cell leukemia homeobox interacting protein 1* (*pbxip1*) and *CDC28 protein kinase 1B* (*cks1b*). The relatively close linkage of these two genes to *pygo2* is conserved in all three vertebrates. In addition, small clusters of linked genes are also conserved, for example, *ephrin A3a* (*efna3a*), *ephrin A1a* (*efna1a*), *dolichyl-phosphate mannosyltransferase polypeptide 3* (*dpm3*), *tripartite motif containing 46b* (*trim46b*) and *ubiquitin associated protein 2-like* (*ubap2l*), *HCLS1 associated protein X-1* (*hax1*), *aquaporin 10b* (*aqp10b*) (see Figure 3-5). Finally, there also exist a number of genes that retain synteny across the three vertebrate species.

Taken together, the sequence similarity between *pygo* homologs, and the conserved linkage regions across vertebrate evolution strongly suggests that zebrafish *pygo1* and *pygo2* homologs are true orthologs of *pygo*.

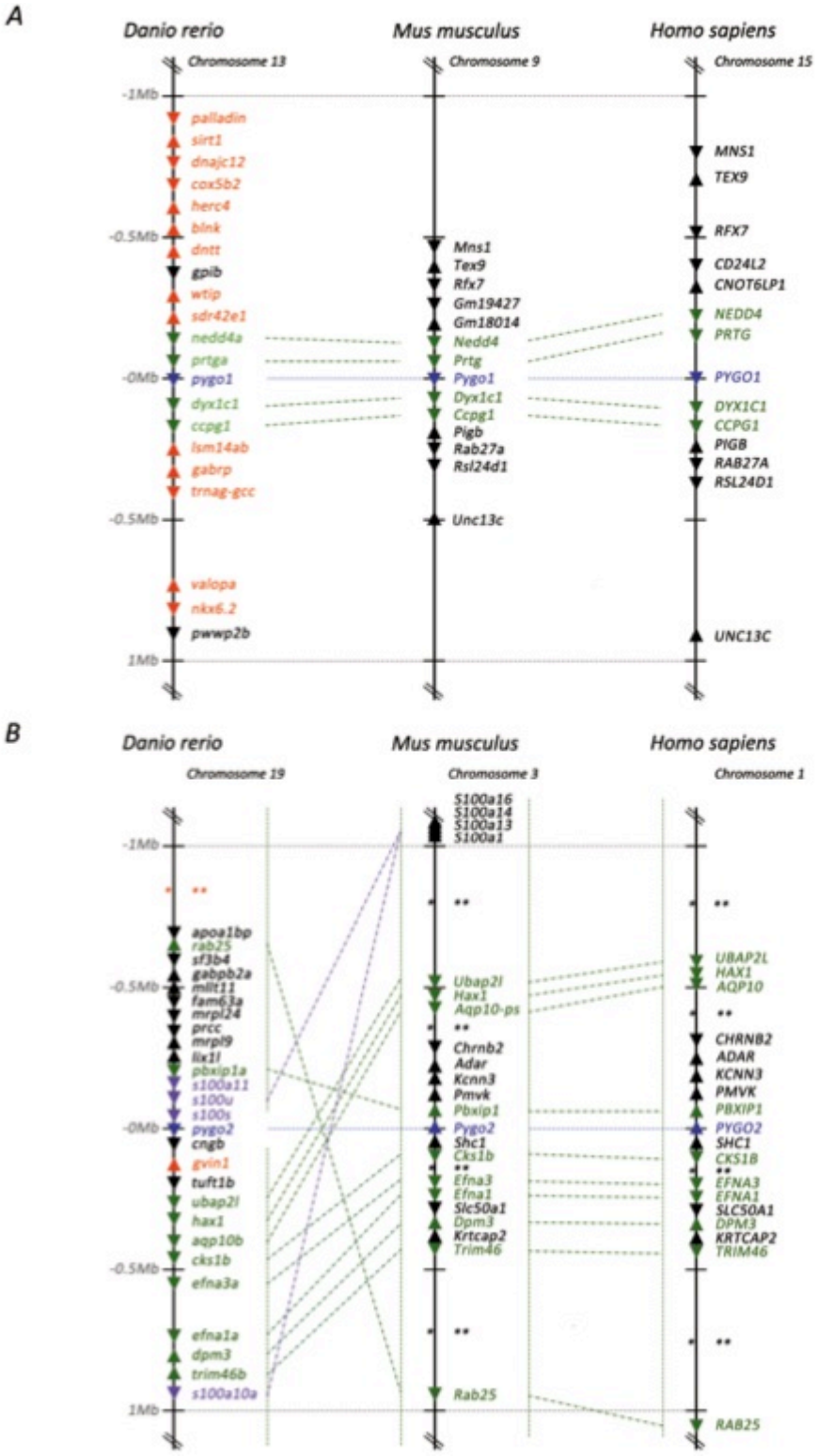

Figure 3-5. Linkage analysis of the Pygo1 and Pygo2 locus in fish, mouse and human
Schematic diagram of genes co-localised to a region within 1 Mb upstream or downstream of the pygo1 (A) or pygo2 (B) locus in zebrafish *(Danio rerio),* mouse *(Mus musculus)* and human *(Homo sapiens)* genomes. Gene order and orientation is indicated by block arrows. Linkage status is indicated by colour; Blue, *pygo* orthologs; Green, conserved linked orthologs; Purple, similar genes (possible paralogs); Red, non-syntenic genes or unknown. Asterisks (*/**) indicate regions where one or more genes have been omitted for clarity. Chromosomal positions of genes are indicative only and not to scale.

3.3.3 The zebrafish pygo1/2 homologs are highly conserved

Pygopus proteins contain two conserved regions, the NHD and PHD. These domains are essential for normal function and interactions of the protein. Importantly, if the putative zebrafish homologs truly represent functional pygopus proteins, then a close inspection of the protein alignments should reveal a high level of sequence conservation between the zebrafish sequences and the conserved NHD and PHD residues.

To assess this possibility, the structural motifs, and interacting residues previously reported within the NHD and PHD were identified within the alignments [128,133,201,202]. As Figure 3-6 demonstrates, there is almost complete conservation across all species, including zebrafish. Residues in the NLS are indicated (labeled beneath in orange) and important interacting residues have been highlighted, including those involved in transcription (Pink), Zn^{2+} binding (Red), histone H3 binding (Purple/Blue) and interactions with the HD1 domain of lgs (Yellow/Blue).

In Figure 3-6, it is interesting to note that both the fly and zebrafish homologs are the longest sequences. It is expected that fish would display a higher level of conservation with invertebrate sequences, given their relative evolutionary position. However, these alignments also suggest that Pygo1 homologs are quite different from Pygo2 and altogether different to pygo. This may further suggest a level of specialty in the function of these homologs.

In addition, there are residues outside of the previously reported NHD and PHD that are highly conserved. Namely residues 157, 186-7, 214, 543 and 625 are all invariant across the sequence alignments. Residues 315-45 are highly conserved as well, and possibly form another domain. It is possible these conserved residues are required to allow the proper tertiary conformation of the protein.

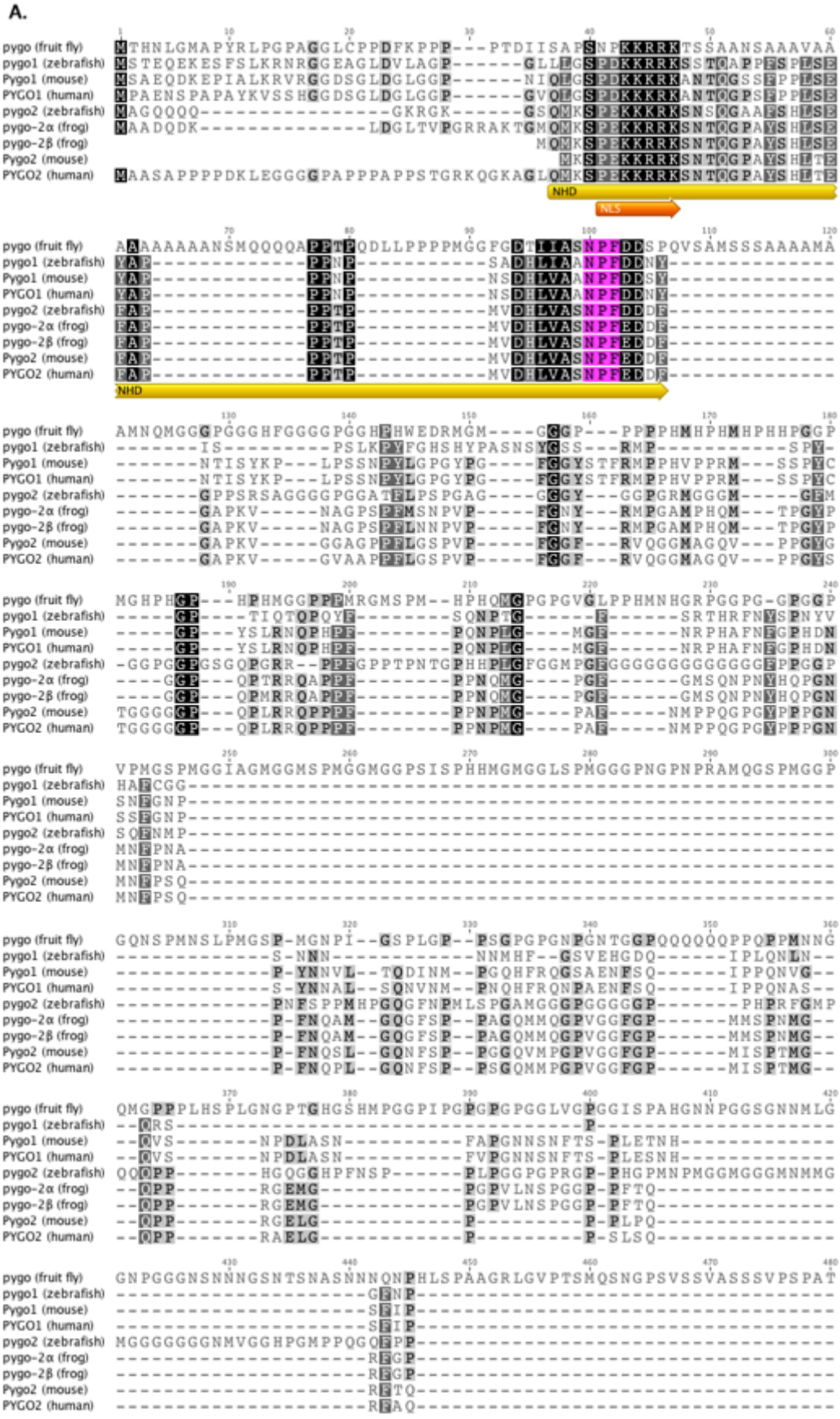
A.
pygo (fruit fly)
pygo1 (zebrafish)
Pygo1 (mouse)
PYGO1 (human)
pygo2 (zebrafish)
pygo-2α (frog)
pygo-2β (frog)
Pygo2 (mouse)
PYGO2 (human)
NHD
NLS

B.

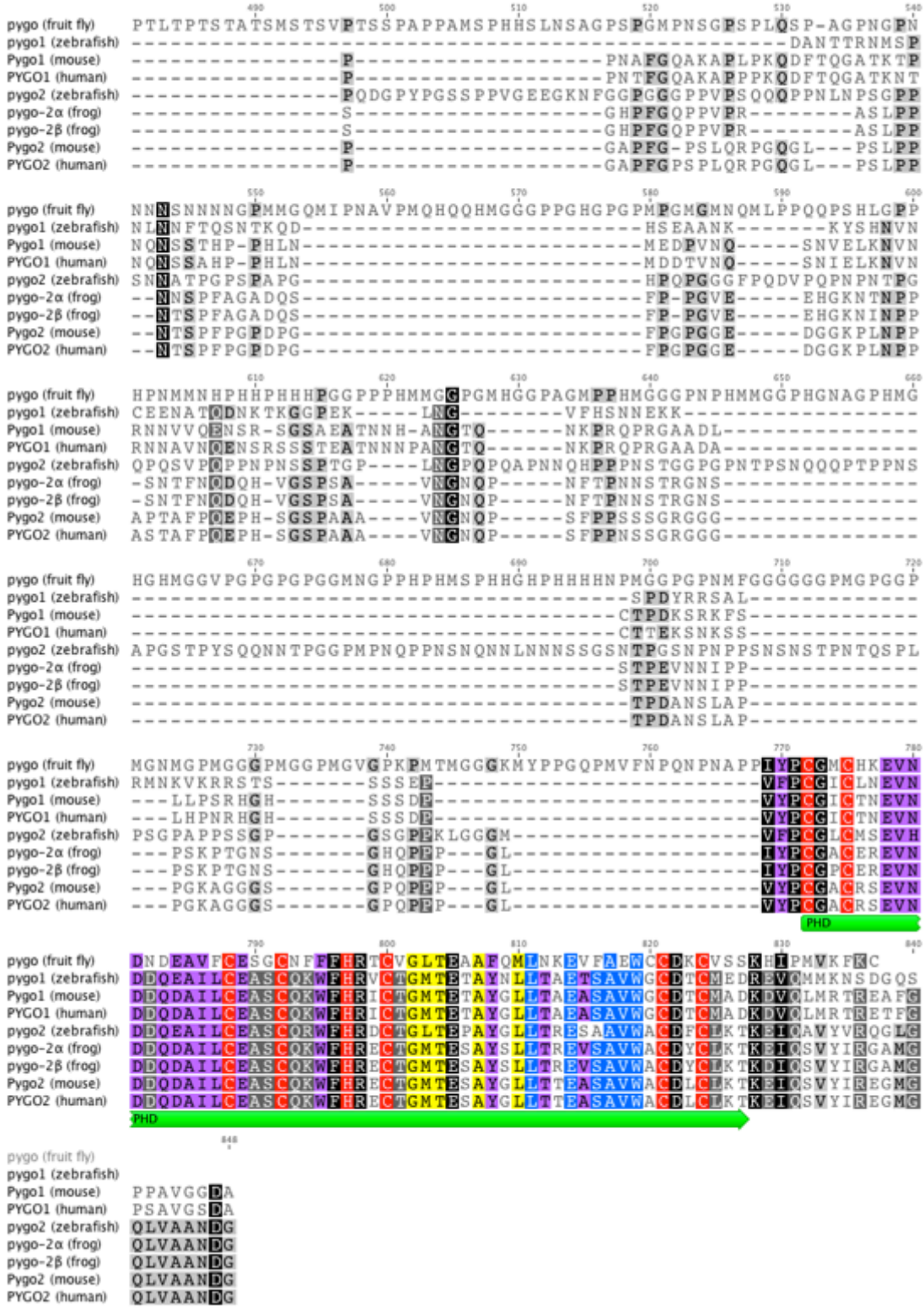
pygo (fruit fly)
pygo1 (zebrafish)
Pygo1 (mouse)
PYGO1 (human)
pygo2 (zebrafish)
pygo-2α (frog)
pygo-2β (frog)
Pygo2 (mouse)
PYGO2 (human)
PHD
PHD

Figure 3-6. Alignment comparison of structural elements and functional residues of pygopus homologs across model organisms.
A and continued in B; protein alignments of pygopus reference sequences from fruit fly (NP_651872), zebrafish (NP_001107109; NP_001028283), frog (AAN41447; AAN41448), mouse (NP_082392; NP_081145) and human (NP_056432; NP_612157) using the MUSCLE alignement algorithm [212]. Gaps in the sequence alignment are represented by dashes. Annotations below alignments are colour coded according to domain; yellow, NHD; orange, NLS; and green, PHD. Residue highlighting indicates sequence homology and key functional residues. Black, invariant residues across all sequences; Dark gray, homologous (similar) residues in >80% aligned sequences; Light gray, semi-conserved residues (60-80% sequences); Pink, NPF residues important for transcriptional activity in the NHD domain [128]; Red, Structural residues (Cys and His) which coordinate the two Zn^{2+} ions [201,202]; Yellow, Conserved residues mediating PHD–HD1 (Lgs/BCL9) interactions [133,201,202]; Purple, Conserved residues important for histone H3 binding [133,201,202]; Blue, Residues involved in both H3 binding and PHD-HD1 interactions.

3.3.4 Multiple pygo homologs exist in higher vertebrates

With the unexpected result that zebrafish have two homologs of *pygo* and the suggestion that they are orthologs, a broader range of species was required to further investigate whether frogs are an exception amongst vertebrates. However, the presence of *pygo* homologs in organisms other than the fly, frog, mouse and human has not previously been reported. In the following study, an *in silico* approach was used to identify if one or more *pygo* gene/s are present in the genomes of other sequenced organisms. Using an approach similar to that described in Section 3.3.1, the Homologene, Gene, RefSeq [208] and Ensembl [218] databases were initially analysed for the search terms '*pygo*', '*pygo1*', '*pygo2*' or '*pygopus*'. These databases provide non-redundant annotations of genomic, and transcribed RNA sequences [210,219]. Organisms in which *a pygo* homolog was found are summarized in the following Table 3-4.

As Table 3-4 demonstrates, homologs of the *pygo* are found only amongst the eukaryotes, specifically within the Kingdom Animalia. While all phyla listed contain species with at least a single homolog, mammals and amphibians predominantly carry two homologs. While amongst the fishes, zebrafish appear to be unique in harboring two homologs.

In some instances, the sequencing and annotation of genomes and cDNA databases is incomplete, thus, it was necessary to verify the existence of additional homologs using a direct approach. For this, the PHD consensus sequence was used to directly perform a translated BLAST search on the species' genome and cDNA databases. In cases where this method was necessary, the homolog number is indicated in Table 3-4 beside an asterisk (*). It is important to recognize these as putative counts, as it is possible that the matching partial genomic sequence may not be transcribed or translated, without the ability for *in silico* or *in situ* verification at this time.

Table 3-4 Organisms with an annotated reference sequence for *Pygopus* homologs

Phyla	Class	Order	Genus & Species	Common Name	Homologs
Annelida	Clitellata	Rhynchobdellida	Helobdella robusta	Leech	1
Arthropoda	Arachnida	Ixodida	Ixodes scapularis	Tick	1
	Crustacea	Cladocera	Daphnia pulex	Water Flea	1*
	Insecta	Diptera	Aedes aegypti	Mosquito	1*
			Drosophila melanogaster	Fly	1
		Hymenoptera	Apis mellifera	Honey Bee	1
			Pediculus humanus corporis	Louse	1
Chordata	Actinopterygii	Beloniformes	Oryzias latipes	Killifish	1
		Cypriniformes	Danio rerio	Zebrafish	2
			Pimephales promelas	Minnow	1
		Gasterosteiformes	Gasterosteus aculeatus	Stickleback	1*
		Salmoniformes	Oncorhynchus mykiss	Trout	1*
		Siluriformes	Ictalurus punctatus	Catfish	1*
		Tetraodontiformes	Takifugu rubripes	Pufferfish	1
			Tetraodon nigroviridis	Green Spotted Puffer	1
	Amphibia	Anura	Xenopus laevis	Frog	2
			Xenopus tropicalis	Frog	2
	Ascidiacea	Enterogona	Ciona intestinalis	Tunicate	1
	Aves	Galliformes	Gallus gallus	Chicken	1
			Meleagris gallopavo	Turkey	1
		Passeriformes	Taeniopygia guttata	Zebra Finch	1
	Mammals	Artiodactyla	Bos taurus	Cattle	2
			Sus scrofa	Boar	2
		Carnivora	Canis familiaris	Dog	2
			Ailuropoda melanoleuca	Panda	2
		Cetacea	Tursiops truncatus	Dolphin	2
		Chiroptera	Myotis lucifugus	Bat	2
		Didelphimorphia	Monodelphis domestica	Short-tailed opossum	2
		Diprotodontia	Macropus eugenii	Wallaby	2*
		Eutheria	Dipodomys ordii	Kangaroo Rat	2*
		Lagomorpha	Oryctolagus cuniculus	Rabbit	2
		Perissodactyla	Equus caballus	Horse	2
		Primates	Callithrix jacchus	Marmoset	2
			Macaca mulatta	Macaque	2
			Gorilla gorilla	Gorilla	2
			Homo sapiens	Human	2
			Pan troglodytes	Chimpanzee	2
			Nomascus leucogenys	Gibbon	2
			Pongo abelii	Orangutan	2
		Proboscidea	Loxodonta africana	Elephant	2
		Rodentia	Cavia porcellus	Guinea Pig	2
			Mus musculus	Mouse	2
			Rattus norvegicus	Rat	2
			Spermophilus tridecemlineatus	Squirrel	2
	Reptilia	Squamata	Anolis carolinensis	Anole	1
Cnidaria	Anthozoa	Actiniaria	Nematostella vectensis	Sea Anemone	1
	Hydrozoa	Anthomedusae	Hydra magnipapillata	Hydra	1
Echinodermata	Echinoidea	Echinoida	Strongylocentrotus purpuratus	Purple Sea Urchin	1
Mollusca	Gastropoda	Lottioidea	Lottia gigantea	Limpet	1*
Nematoda	Secernentea	Spirurida	Brugia malayi	Roundworm	1
Placozoa	Tricoplacia	Tricoplaciformes	Trichoplax adhaerens	Trichoplax	1*

* Species lacking a complete genome assembly and cDNA sequence database. Model organisms in which *pygopus* homologs have previously been reported are indicated by bold typeface.

To further explore the sequence identity amongst these organisms, multiple sequence alignments were performed (as described in Section 3.3). The results from these comparisons have been represented as an unrooted dendrogram in Figure 3-7. From an evolutionary standpoint, it was expected that the mammalian orthologs would cluster together. However, they actually form two of the three major branches, leaving the majority of invertebrate *pygo* in a third more scattered branch. This is similar to what is seen in Figure 3-6. Yet, it is not entirely unexpected, that the majority of invertebrate homologs cluster independently of both the *Pygo1* and *Pygo2* branches. Although, it is interesting that the common branch point for both *Pygo1* and *Pygo2* branches includes the entire phylum chordata and the nematode, *B. malayi.*

However, within the vertebrate clades there are multiple alignments that would appear to be inconsistent with the evolutionary distance between phyla and classes. Surprisingly, avian and reptilian homologs cluster independently alongside the mammalian *Pygo1* and *Pygo2* clades respectively, while homologs belonging to the same genus cluster in completely separate clades. For example, both isoforms of *pygo2 X. laevis* cluster alongside the mammalian *Pygo2's*, while *X. tropicalis pygo1* isoforms cluster with zebrafish *pygo1* alongside the mammalian *Pygo1* clade. Intriguingly, these results provide evidence for an additional homolog in *X. laevis*, namely *pygo1*. This is further supported by X. tropicalis encoding two isoforms of *pygo1* and a single *pygo2*, giving both species alternative isoforms and 2 orthologs.

This is highly important as it helps to console some of the differences observed between the frog and mammals. In addition, the arrangement of these clusters would suggest a common origin for all pygo homologs, and that the separation of *pygo* from *Pygo1* and *Pygo2* orthologs occurred relatively close together in evolutionary history. It is likely this occurred at the same time as the speciation event that led to the separation of vertebrates and invertebrate homologs. The sequence identity between the zebrafish and mammalian homologs corroborates with this notion as in Figure 3-6.

Furthermore, this is interesting in the context of the NC. The NC is a vertebrate structure, providing a fourth germ layer during embryonic development. Gans and Northcutt (1983)[220] have attributed the transition from invertebrates to vertebrates was associated by a shift in complexity of the head structures; many of which are derived from and require the NC. In addition, the speciation from invertebrates to vertebrates has included multiple genome duplication events. With the high conservation of multiple pygo homologs, and their distinct functions within species, it would seem possible that the various vertebrate innovations, like the NC (including its derivatives, the neurogenic placodes, segmented brain, and endoskeleton)[200] have relied upon the retention of these multiple homologs for body plan complexity.

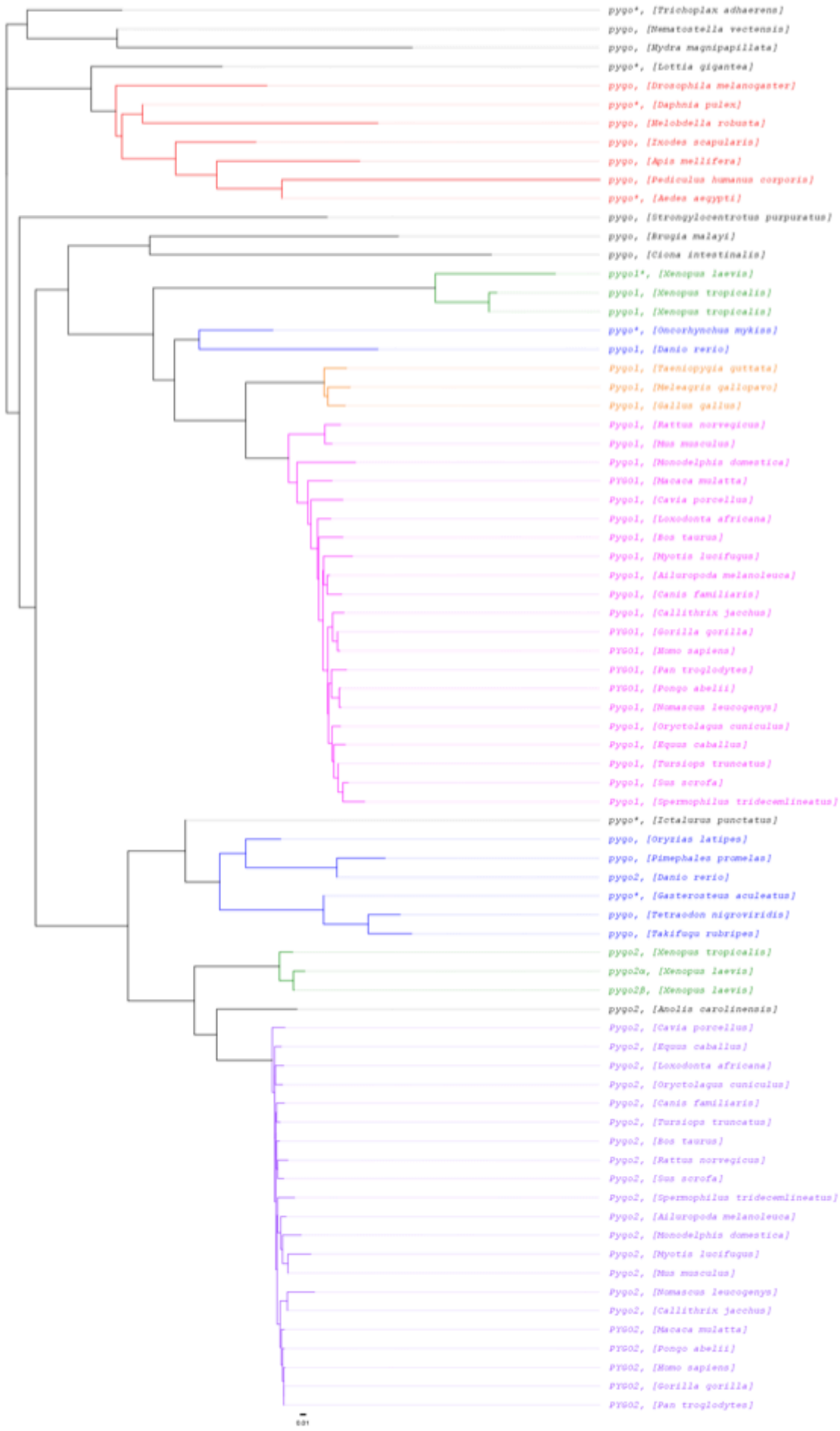
pygo*, [Trichoplax adhaerens]
pygo, [Nematostella vectensis]
pygo, [Hydra magnipapillata]
pygo*, [Lottia gigantea]
pygo, [Drosophila melanogaster]
pygo*, [Daphnia pulex]
pygo, [Helobdella robusta]
pygo, [Ixodes scapularis]
pygo, [Apis mellifera]
pygo, [Pediculus humanus corporis]
pygo*, [Aedes aegypti]
pygo, [Strongylocentrotus purpuratus]
pygo, [Brugia malayi]
pygo, [Ciona intestinalis]
pygo1*, [Xenopus laevis]
pygo1, [Xenopus tropicalis]
pygo1, [Xenopus tropicalis]
pygo*, [Oncorhynchus mykiss]
pygo1, [Danio rerio]
Pygo1, [Taeniopygia guttata]
Pygo1, [Meleagris gallopavo]
Pygo1, [Gallus gallus]
Pygo1, [Rattus norvegicus]
Pygo1, [Mus musculus]
Pygo1, [Monodelphis domestica]
PYGO1, [Macaca mulatta]
Pygo1, [Cavia porcellus]
Pygo1, [Loxodonta africana]
Pygo1, [Bos taurus]
Pygo1, [Myotis lucifugus]
Pygo1, [Ailuropoda melanoleuca]
Pygo1, [Canis familiaris]
Pygo1, [Callithrix jacchus]
PYGO1, [Gorilla gorilla]
PYGO1, [Homo sapiens]
PYGO1, [Pan troglodytes]
PYGO1, [Pongo abelii]
Pygo1, [Nomascus leucogenys]
Pygo1, [Oryctolagus cuniculus]
Pygo1, [Equus caballus]
Pygo1, [Tursiops truncatus]
Pygo1, [Sus scrofa]
Pygo1, [Spermophilus tridecemlineatus]
pygo*, [Ictalurus punctatus]
pygo, [Oryzias latipes]
pygo, [Pimephales promelas]
pygo2, [Danio rerio]
pygo*, [Gasterosteus aculeatus]
pygo, [Tetraodon nigroviridis]
pygo, [Takifugu rubripes]
pygo2, [Xenopus tropicalis]
pygo2α, [Xenopus laevis]
pygo2β, [Xenopus laevis]
pygo2, [Anolis carolinensis]
Pygo2, [Cavia porcellus]
Pygo2, [Equus caballus]
Pygo2, [Loxodonta africana]
Pygo2, [Oryctolagus cuniculus]
Pygo2, [Canis familiaris]
Pygo2, [Tursiops truncatus]
Pygo2, [Bos taurus]
Pygo2, [Rattus norvegicus]
Pygo2, [Sus scrofa]
Pygo2, [Spermophilus tridecemlineatus]
Pygo2, [Ailuropoda melanoleuca]
Pygo2, [Monodelphis domestica]
Pygo2, [Myotis lucifugus]
Pygo2, [Mus musculus]
Pygo2, [Nomascus leucogenys]
Pygo2, [Callithrix jacchus]
PYGO2, [Macaca mulatta]
PYGO2, [Pongo abelii]
PYGO2, [Homo sapiens]
PYGO2, [Gorilla gorilla]
PYGO2, [Pan troglodytes]
0.01

Figure 3-7. Protein alignment of *pygopus* homologs across the animal kingdom.
The relative phylogentic distance of *pygopus* homologs is represented by an unrooted dendrogram. The distance from a common branch point represents the relative genetic distance between two sequences or number of substitutions required, per site, from the common branch point. Protein alignments were performed using Neighbor-Joining and the Blosum62 matrice with the Geneious software [151,153]. Taxonomic classes with more than one species are indicated by colour; Blue, mammals (light blue, Pygo1; dark blue, Pygo2); Red, Actinopterygii; Orange, Aves; Green, Amphibia; Purple, Insecta.

3.4 In vivo expression of *pygo1* and *pygo2*

To verify the expression of the putative zebrafish *pygo1* and *pygo2* sequences *in vivo*, semi-quantitative RT-PCR was performed using cDNA samples from zebrafish throughout the early stages of embryonic development. An initial BLAST search of both mRNA sequences compared to the genomic database revealed that *pygo1* and *pygo2* consist of three exonic regions (see Figure 3-8), a similar gene structure to what is shown previously in the frog, mouse and human homologs [84,118,163]. Subsequently, forward and reverse primers were designed for each homolog as indicated in Figure 3-8 to yield RT-PCR products spanning multiple exons with a size of 612bp for pygo1 and 616bp for pygo2.

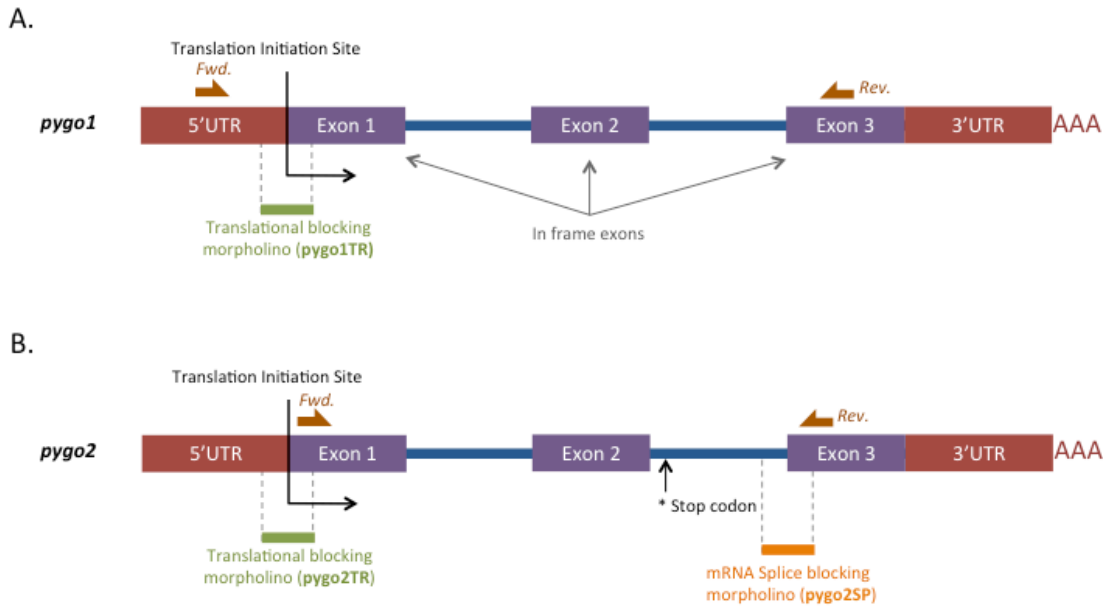

Figure 3-8. Schematic of primer and morpholino binding sites for *pygo1* and *pygo2* in zebrafish. Schematic of gene structure for zebrafish *pygopus* homologs, *pygo1* (A) and *pygo2* (B). Relative positions of forward and reverse primers for both sequences are indicated by arrows. Translational blocking morpholinos are indicated in green and splice blocking morpholino in orange. *Representation - not to scale*.

The results from the RT-PCR of zebrafish cDNA samples during embryogenesis are shown in Figure 3-9. Endogenous gene transcription does not commence in the zebrafish until 4hpf, so transcripts detected in the embryo at this stage are maternally contributed. Thus, it can be seen that both *pygo1* and *pygo2* are maternally contributed to the zebrafish embryo. At 24hpf, expression of both sequences is absent or very weak. At 48hpf, p*ygo2* is expression is strong and persistent up to 120hpf. Conversely, *pygo1* expression gradually increases at the later larval stages of development (72-120hpf).

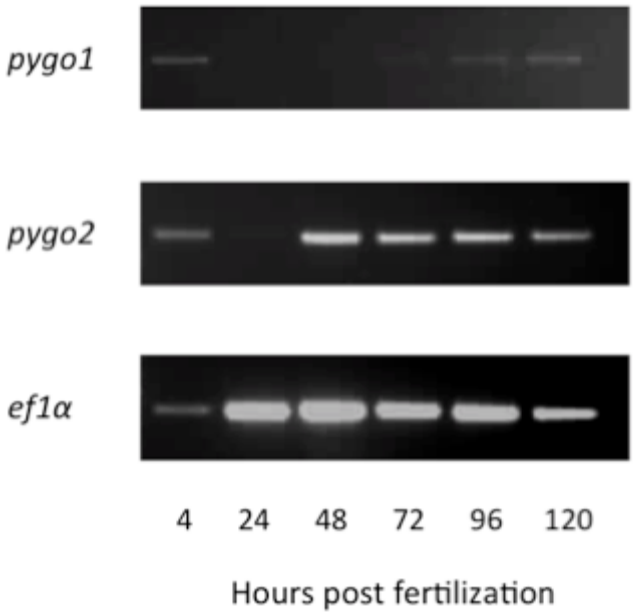

Figure 3-9. Expression of *pygo1* and *pygo2* during zebrafish embryonic development.
RT-PCR gel electrophoresis of *pygo1*, *pygo2* and elongation factor 1α (*ef1α*) using 10µl of cDNA per reaction. 20µl of PCR reaction was loaded per well. *ef1α* provides a housekeeping gene reference sample [221]. Endogenous expression within the embryo at 4hpf has not commenced, thus low expression is expected, within all samples. Expression of gene products at 4hpf is indicative of maternal mRNA contribution to the egg.

3.5 Functional assessment of *pygo1* and *pygo2*

To investigate the possible role of *pygo1* and *pygo2* in zebrafish embryogenesis, a knockdown of both *pygo* homologs was conducted utilizing MO technology. MO targeted to both gene transcripts were injected into *sox10:egfp* embryos at the single cell stage (0.5hpf) and subsequently assessed for resultant phenotypes.

3.5.1 Experimental design of MO injections

MOs are widely employed as a 'reverse' approach to study gene function. They are short antisense oligomers of around 25 nucleotides that block gene expression through RNA interference, by specifically binding an mRNA transcript for a given gene of interest. MO sequences are designed to recognize either the translational start site, and to subsequently block protein translation, or alternatively, to bind splice junctions and disrupt post-transcriptional

processing of mRNA. Either way, the net effect is a knockdown of protein expression from the targeted gene.

For this study, MO oligonucleotides pygo1TR and pygo2TR were designed to knockdown the expression of both *pygo1* and *pygo2* respectively through disruption of protein translation (see Figure 3-8). Additionally, a splice blocking MO (pygo2SP) was designed to disrupt the splicing of the second intron of the *pygo2* transcript. This disruption would presumably lead to retention of the second intron and subsequent truncation of the mature pygo2 protein, via the incorporation of the intronic in-frame stop codon.

In contrast to *pygo2*, it was not possible to design a splice blocking MO to the *pygo1* transcript. All three exons of *pygo1* are in frame, including the introns. Neither of the introns contains an in-frame stop codon, and therefore would lead to an elongated protein. This protein would still encode the relevant PHD and NHD, and evidence from the fly suggests this lengthened protein could remain functional *in vivo* [82]. For example, deletion of the NHD domain in flies, and fusion directly to lgs provided a functional rescue in pygo knockouts.

For any new MO study, the quantity of MO injected must be empirically determined and varies between different sequences. Generally the amount is titrated in small increments, until most embryos display a phenotype without substantial toxicity or non-specific effects. In this study, all MO injections were conducted with consistent drop sizes (⌀16μm) yielding an injected volume of 2.1nl. MO concentrations were adjusted to between 50-500μM, giving final injected amounts of 1ng, 2ng, 4ng and 8ng.

To provide a control for the injection of MOs, the recommended control MO supplied by Gene Tools, LLC was also injected in comparable amounts. The control MO is targeted to Human β-globin pre-mRNA and has been shown to have no significant biological activity in zebrafish. In addition to the control MO, a portion of embryos from each injected clutch of eggs were kept aside to provide a control for variance between lays, breeding pairs and environmental conditions.

Injection of MOs is usually conducted at the single cell stage of development and leads to a ubiquitous knockdown of the gene of interest. Thus, it was possible that resultant phenotypes in this study may have arisen from defects in developmental processes that are not dependent on NC. In addition, given the evidence that *pygopus* may have roles outside of the *wnt* pathway, it is also possible that phenotypes may have occurred that are not related to *wnt* signaling either.

With this in mind, a number of developmental stages and structures were analysed from the injected embryos or morphants. These have been summarised in Table 3-5 and are grouped according to their expected aetiology. In this way, they form a useful set of criteria to assay the morphants during embryogenesis for related phenotypes. In general, these criteria were scored based on gross morphology visualized by light microscopy. However, NC derived tissues were visualized using fluorescence and scored according to their gross morphology, and or relative signal intensity. Mortality rates and somite structure were used as a general marker of morphant health and developmental stage. All analyses of early embryos were performed on stage-matched morphants using the criteria described previously by Kimmel *et al.* (1995).

Table 3-5 Assessment criteria & developmental timeline for *pygopus* morphants

Developmental Stage (Hours post fertilization)	1-3 somites (10-12 hpf)	Prim-5 (24 hpf)	Long-pec (48hpf)	Protruding lip (72 hpf)	Larval period (120 hpf)
General Development					
Mortality rate	✓	✓			
Somite structure		✓	✓	✓	✓
Neural Crest					
Pre-migratory NCC	✓				
Migrating NCC		✓			
PNS:					
- DRG		✓			
- Olfactory		✓			
- Glia / Schwann		✓			
Branchial arches		✓			
Pigment			✓	✓	✓
Cranial cartilage			✓	✓	✓
Jaw cartilage			✓	✓	✓
Tail mesenchyme				✓	✓
Pectoral fin mesenchyme				✓	✓
Wnt Pathway					
Gastrulation	✓				
Heart rate			✓		
Heart looping			✓		
Pericardium			✓	✓	✓
Tail length					✓
Head size					✓
Eyes (size & location)					✓

3.5.2 Optimization of MO injections

Initial injections of pygo1TR and pygo2TR at 8ng lead to high levels (>50%) of toxicity within the first 24hpf. In contrast, pygo2SP (8ng) morphants did not display a significantly higher mortality than the control MO. Lowering the dosage for both translational blocking MOs (pygo1TR & pygo2TR), greatly reduced embryo mortality rates. However, even at 4ng, pygo1TR and 2ng pygo2TR, morphants still displayed mortality rates higher than the control MO injections as shown in Figure 3-10.

Given the mortality rates demonstrated by Figure 3-10 and the presentation of phenotypes, the optimal levels of MO used for each injection were identified as 4ng for pygo1TR and 2ng for pygo2TR. These amounts were derived empirically to achieve a consistent phenotype with minimal embryonic death. While the pygo2SP MO did not contribute to high mortality rates, it was found that excessive amounts of MO (20ng – 30ng) were required to replicate the

phenotype of pygo2TR morphants. Thus, this study focused on the phenotypes from pygo1TR and pygo2TR MO specifically.

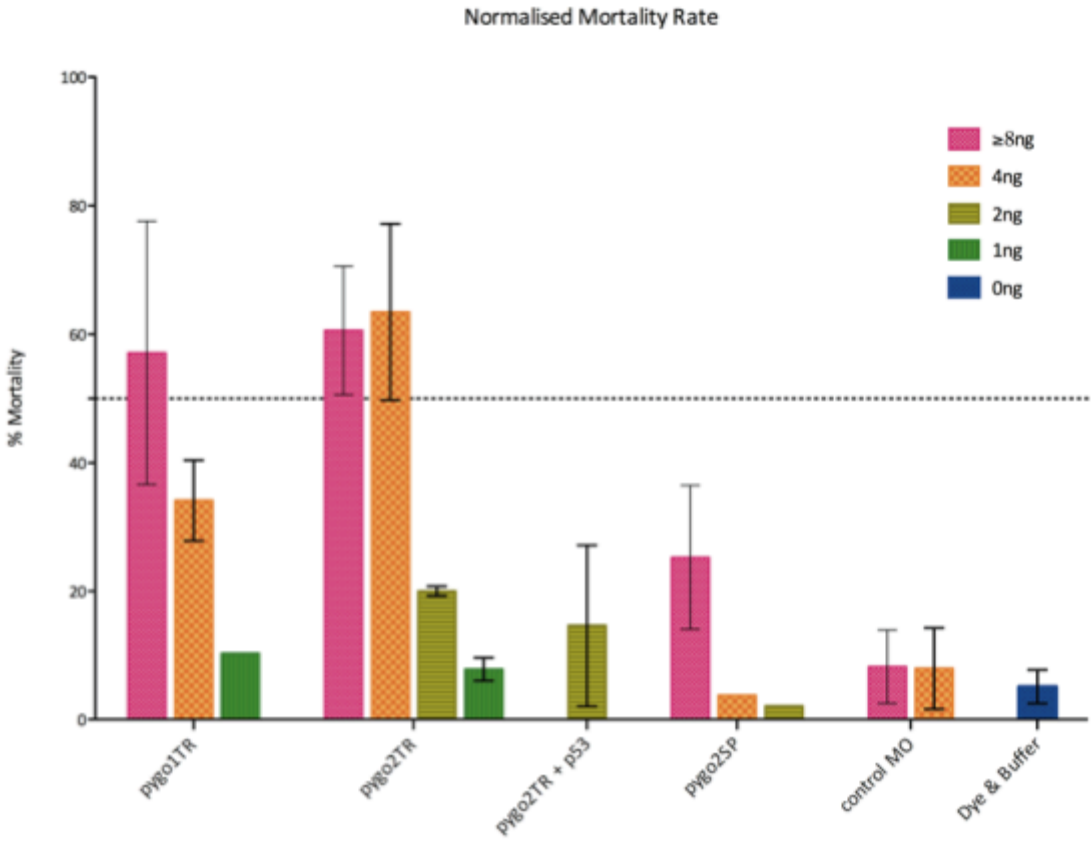

Figure 3-10 Normalized average mortality rate amongst morphants.
Mean mortality rates for each injection condition are presented as a percentage, aggregated from multiple clutches of injected eggs. Mortality rates from each individual condition and clutch were first normalized against the background mortality rate of non-injected eggs from the same clutch, before aggregation of the data.

Non-specific or off-target effects can interfere with mutational screens and loss-of-function studies [222]. In general, these manifest in zebrafish as an overall delay in development, with small eye size, reduced body length and smaller pectoral fins [175]. Specifically in MO screens, it has been shown that phenotypes arising from as many as 1 in 5 different MO are the result of non-

specific effects [223]. Recently, it has been shown that many of these effects are likely to be mediated by p53 activated cell death [224,225]. In these studies, the typical morphant affected by non-specific effects develop extensive neuronal cell death at 24hpf, grow with smaller heads, particularly smaller eyes, display somite and notochord defects, and later develop craniofacial abnormalities.

Following the initial optimization injections, it was observed that pygo2TR morphants displayed a number of phenotypes, similar to the non-specific p53-mediated syndrome described by Robu *et al.* (2007). The pygo2TR morphants developed slowly, were smaller, lacked identifiable structures, like the head, eyes and somites, and presented with extensive regions of darkened tissue. These dark regions were presumed to be apoptotic or necrotic tissue, and were particularly evident in the developing forebrain and midbrain, and along the midline as demonstrated by Figure 3-11. Within these darkened regions, there was also a noticeable loss of NC induction and migration. Finally, it was observed that by 48hpf more than 95% of morphants were dead.

To test the possibility of a p53-mediated effect, co-injections of pygo2TR and p53 MO were performed. While the co-injections did not affect the mortality rate significantly (Figure 3-10), the majority of morphants survived past 48hpf. In addition, the co-injection ameliorated many of the severe phenotypes seen at 24hpf. In particular the co-injection prevented formation of darkened tissue around the head and midline. In addition, the head, eyes and somite structures became recognizable. And finally, the presence of neural crest along the full dorsal aspect was restored. Subsequently, all injections of pygo2TR were performed as a co-injection with the p53 MO.

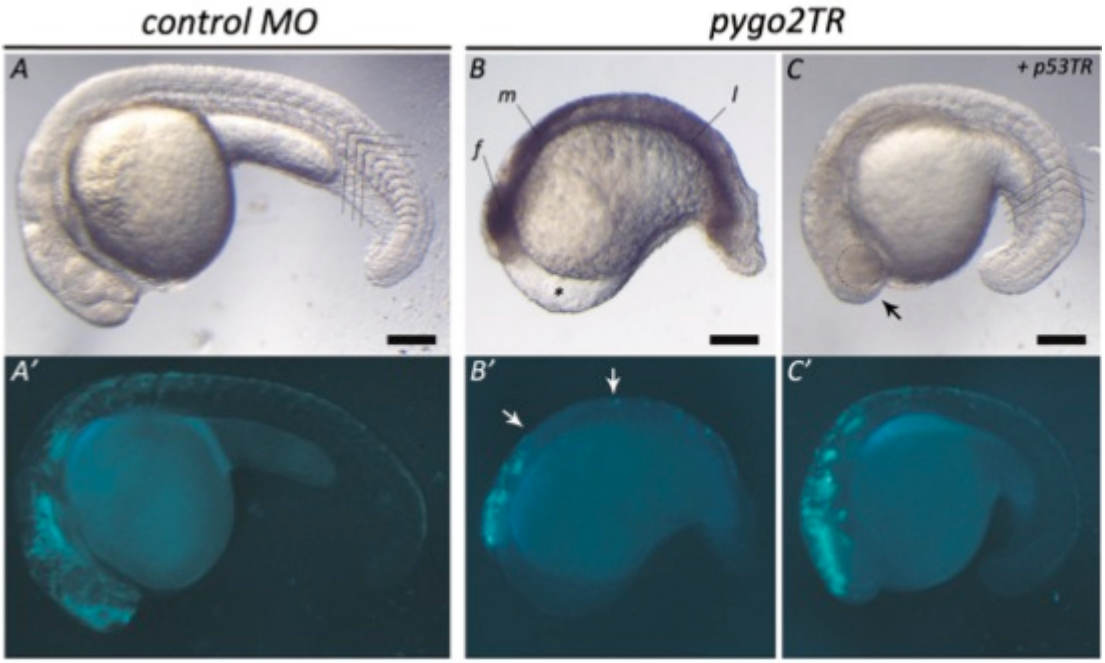

Figure 3-11. Non-specific p53 mediated cell death in pygo2TR morphants.
The injection of the pygo2TR MO induces a p53-mediated effect, particularly in the anterior neural tissue. Lateral views of control MO (A), pygo2TR (B) and co-injected (C) *sox10:egfp* morphants under bright field microscopy at 24 hpf. The same embryos are shown in corresponding panels A'-C' under fluorescence microscopy to visualize pre-migratory and migrating neural crest cells. The non-specific p53-mediated effects include possible apoptotic tissue (brown-black) in the forebrain (f), midbrain (m) and midline (l), and a loss of neural crest induction along the dorsal neural tube in line with the midbrain (between white arrows). Co-injection of pygo2TR and p53 MO ameliorate many of the p53 symptoms and allow recognition of the developing head (arrow), eyes (outlined), and somite structures (dashed lines). *Scale bar = 200μm.*

3.5.3 pygo1 morphants display abnormal hyoid development

While pygo1TR morphants displayed a higher mortality rate than control MO (Figure 3-10), no gross defect was apparent following gastrulation (12 hpf). Nor was there any difference observed in the appearance of pre-migratory neural crest cells in the dorsal neural tube (Figure 3-12). At 24hpf, pygo1TR NC migration was normal, with eGFP expression seen in pre-migratory and migrating NC, in particular the DRG, glia and developing olfactory neurons.

However, analysis of the somite structure was not possible in 37% of pygo1TR embryos (*n=3 clutches)*. This was due to a 'rough' appearance of the skin that

obscured the underlying somite, making it difficult to assess and score the shape. Interestingly, a rough skin phenotype has previously been reported in the Olfactomedin (OLfm1) morphant [226]. Olfm1 is involved in the regulation of NC in chick, and neuronal differentiation in frog [227,228]. However, by 48hpf this phenotype was no longer apparent. Yet, many embryos also presented with a reduction in the head region anterior to the eyes that was apparent in later staged embryos as a reduction in the protruding jaw.

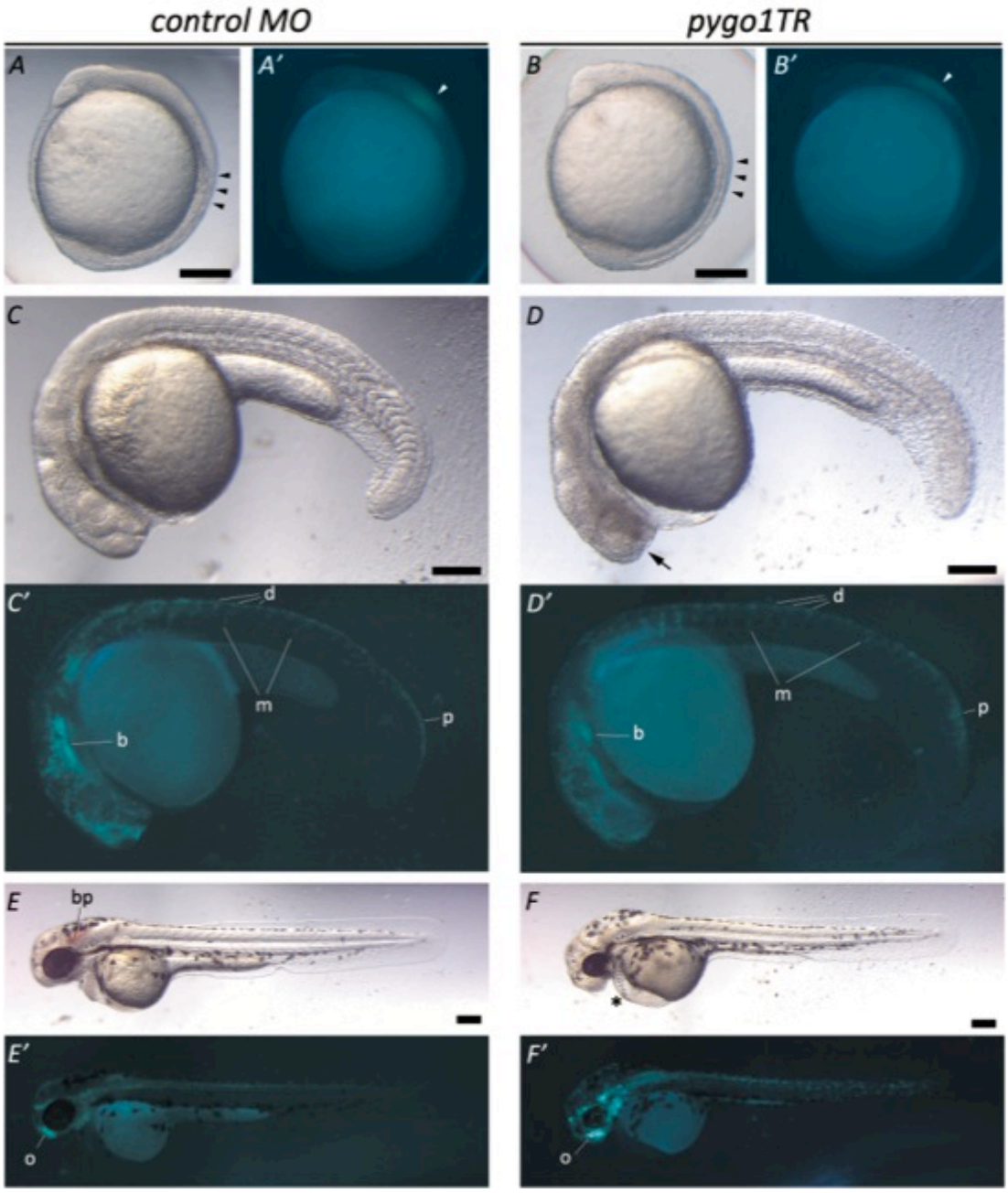

Figure 3-12. Neural crest induction and migration is not affected in pygo1TR morphants.
Lateral view of control MO (A, C, E) and pygo1TR (B, D, F) *sox10:egfp* morphants under bright field microscopy. The same embryos are shown in corresponding panels A'-F' under fluorescence microscopy to visualize pre-migratory (p, white arrowheads) and migrating (m) neural crest cells, branchial arches (b), dorsal root ganglia (d), and olfactory neurons (o). At 12 hpf (A, B) embryos are at the 3 somite stage of development, indicated by black arrowheads. At 24 hpf (C, D) somites are difficult to identify in pygo1TR morphants due to a 'rough' appearance of the skin and embryos show a reduction in the head anterior to the eyes (arrow). While, at 48 hpf (E, F), pygo1TR morphants display a delay in anterior head development and mild cardiac oedema (*). Blood pooling is sometimes observed in control and pygo1TR morphants (bp). *Scale bar = 200μm.*

At the protruding lip stage (72hpf) more than a quarter (27%) of embryos display hemorrhage, or blood pooling in the dorsal forebrain. Morphants continue to display a failure in normal development of the craniofacial region, specifically, the lower jaw fails to elongate and produce the 'protruding lip', characteristic for this stage (see Figure 3-13).

By 120hpf, 41% of pygo1TR morphants display a phenotype that can be broadly classified as either mild or severely affected. Both groups were defined by a failure of the lower jaw to protrude past the eyes. In addition to the jaw phenotype, these morphants develop a syndrome or range of phenotypes, in which, some or all of the following defects are present, kinked pectoral fins, blood pooling in the dorsal anterior head, poor or absent circulation in the tail vein, and cardiac or ocular oedema. In addition to these phenotypes, severely affected morphants were classified by mispatterning of the hyoid bones in the lower jaw (Figure 3-14). This was usually accompanied by more severe oedema in the ocular and cardiac regions.

In the severely affected morphants, the mispatterning of the hyoid bones involves either a failure of the basihyal to extend normally, or alternatively, the basihyal is absent altogether. A failure of basihyal extension has been illustrated in Figure 3-14F. In addition to the basihyal defect, the hyosymplectic bone is also greatly reduced in size and the ceratohyal appears inverted. This inversion is likely due to the shortened/absent basihyal. Together these three bones form the hyoid group of bones, that comparatively in mammals co-ordinate swallowing.

In addition to the hyoid bone defects, the Meckel's cartilage also appears reduced in size, becoming increasingly smaller with severity of the morphant phenotype. The Meckel's cartilage is part of the mandible group of bones in the zebrafish.

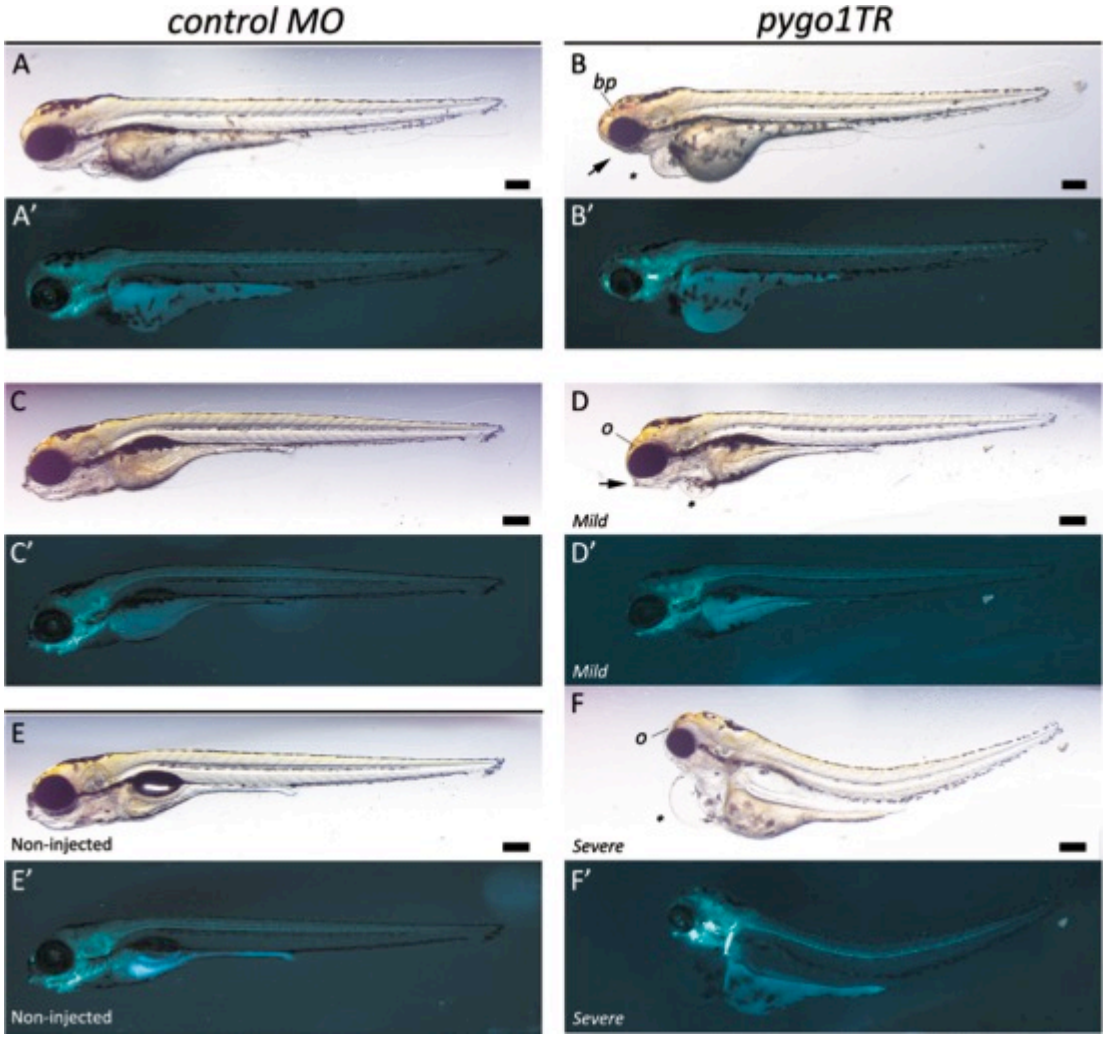

Figure 3-13. Craniofacial development is affected by pygo1TR.
Lateral view of control MO (A, C), pygo1TR (B, D, F) and non-injected (E) *sox10:egfp* morphants under bright field microscopy. The same embryos are shown in corresponding panels A'-F' under fluorescence microscopy to visualize the neural crest derived structures (i.e. cartilage and PNS). At 72 hpf (A, B) pygo1TR morphants fail to develop a protruding lip (arrow) and often have blood pooling on the dorsal surface of the forebrain (b). By 120 hpf, morphants can be classified into mild and severe phenotypes (D, F). Associated phenotypes include ocular oedema (o) and pericardial oedema (p). *Scale bar = 200μm*

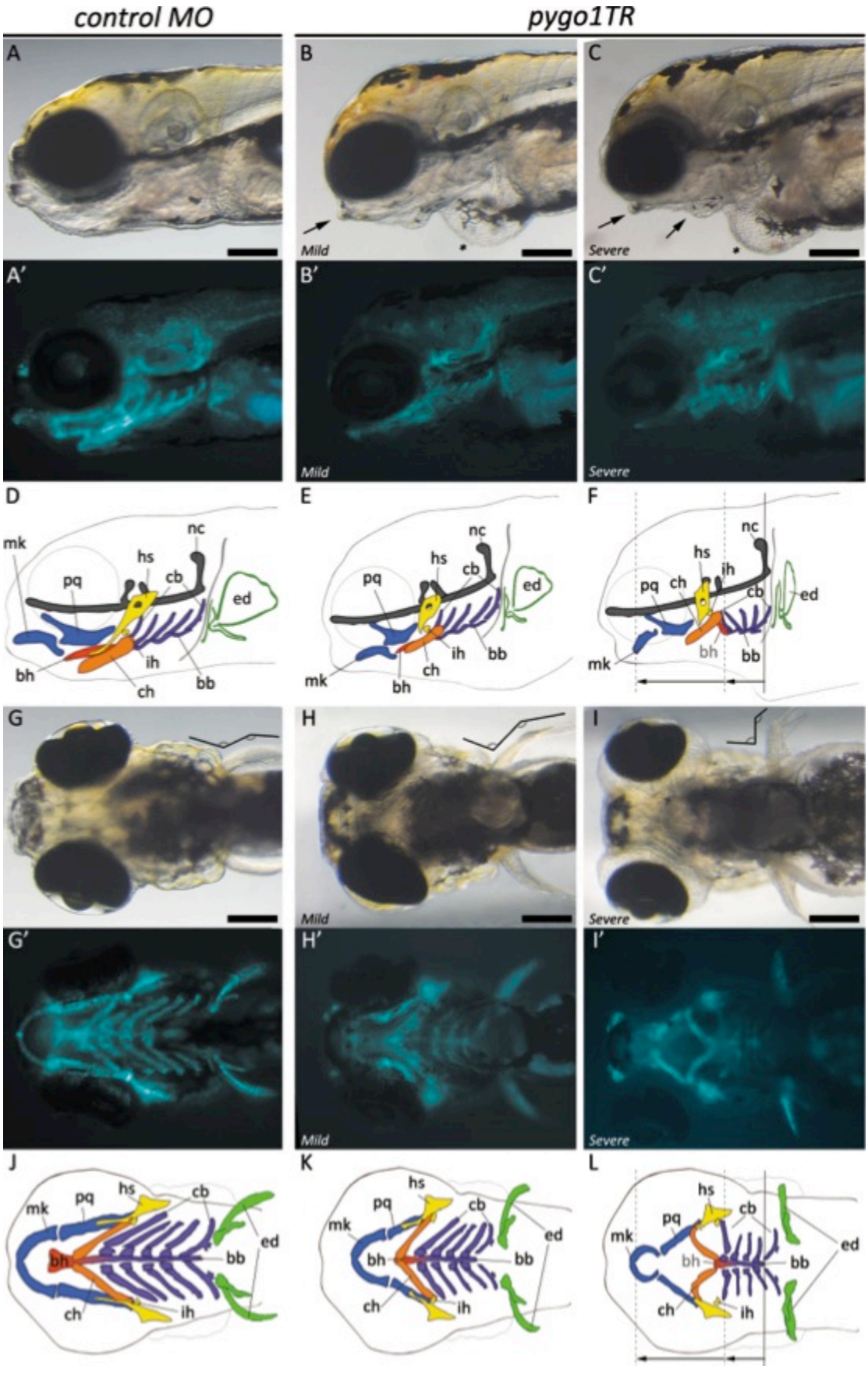
control MO
pygo1TR
A
B
C
Mild
Severe
A'
B'
C'
Mild
Severe
D
E
F
mk
hs
nc
pq
cb
ed
bh
ch
ih
bb
G
H
I
Mild
Severe
G'
H'
I'
Mild
Severe
J
K
L

Figure 3-14. Mispatterning of the hyoid bones in pygo1TR morphants.
Lateral views of control MO (A), mild pygo1TR (B) and severe pygo1TR (C) *sox10:egfp* morphants under bright field microscopy. Corresponding ventral views of the same embryos are also displayed in bright field microscopy (G-I). Again, corresponding lateral and ventral views of fluorescence microscopy have been displayed below bright field images in panels A'-C' and G'-I'. Illustrations of each fluorescent panel have been drawn underneath to clarify the identification of cartilage structures (D-F, J-L). Arrows and lines indicate the failure of the basihyal to extend fully towards the anterior-most region of the head. Cartilages of the same segment share the same colour scheme: the neurocranium is shaded grey; mandibular, blue; hyoid, yellow, orange and red; branchial, purple; mk, Meckel's cartilage; pq, palatoquadrate; bh, basihyal; ch, ceratohyal; ih, interhyal; cb, ceratobranchial; bb, basibranchial; ed, endoskeletal disc. *Scale bar = 200μm*

3.5.4 pygo2TR morphants display an impairment in convergent extension movements during gastrulation

As previously discussed (section 3.5.2; p.81), pygo2TR injections lead to a non-specific p53-mediated cell death by 24hpf. However, even after the addition of p53 MO, co-injected morphants still display a general reduction in body length and eventually arrested development. Subsequently, almost all injected embryos die between 72 and 120hpf, with the exception of rare embryos.

In Figure 3-11, it can be seen that pygo2TR + p53 MO morphants lack the anterior-most features of the head and also exhibit a reduction in tail length at 24hpf. Together, this overall shortened body axis is characteristic of disrupted convergent extension movements during gastrulation and *wnt* genes are known to be key regulators of this process [86,87,229].

As early as 12hpf, following gastrulation, pygo2TR morphants display evidence of a disruption to the normal extension movements prior to segmentation. As Figure 3-15 illustrates, the angle between the anterior and posterior (A-P) structures is increased, indicating a reduction in the A-P axis extension. At 48hpf, the phenotype is generally more severe, as morphants present with a range of developmental defects. At this stage, morphants continue to display general growth retardation and a spectrum of phenotypes. Specifically, they have impaired development of neural structures (PNS), and craniofacial

structures, including the eyes, tail length, tail fins, and normal somite shape. This is in contrast to what is seen in control MO morphants at this stage (Figure 3-15C-D). In addition, many morphants lack peripheral circulation, develop blood pooling in the tail, midline and pericardium, display a reduction in heart rate, and present with severe pericardial oedema. Albeit, many of these defects are likely to be secondary to the primary gastrulation defect prior to segmentation and an overall delayed development.

While this study primarily focused on the pygo2TR MO, injections of pygo2SP MO also produced a similar phenotype. However, between 20-30ng of MO were required to produce a reproducible phenotype. It is interesting to note, that no p53-mediated effects were observed when using this MO.

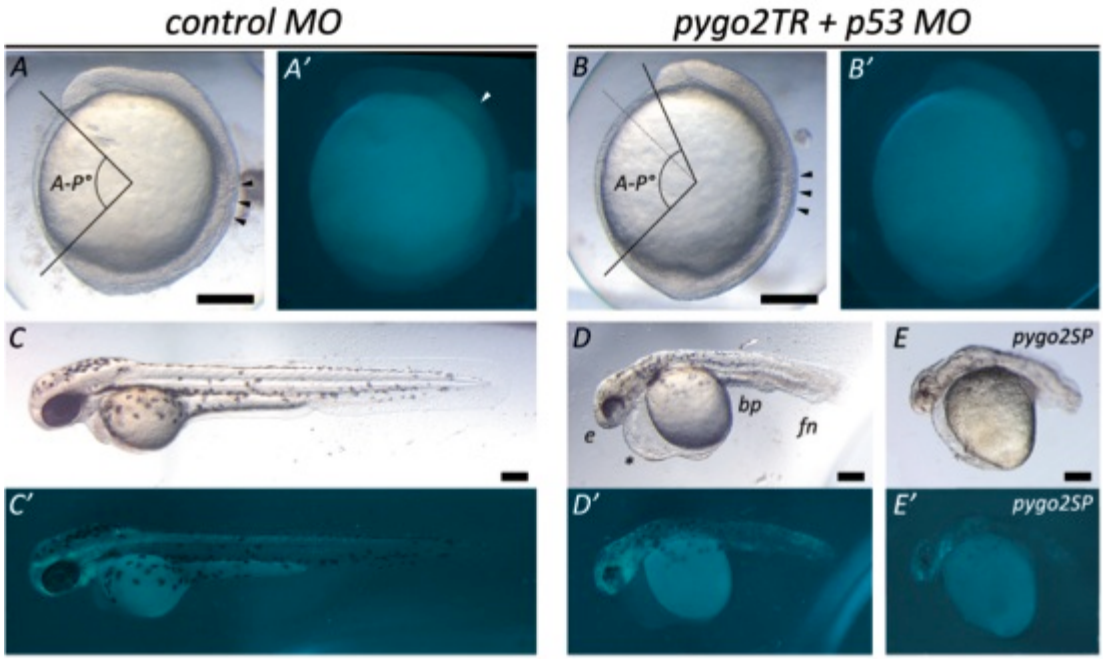

Figure 3-15. Convergent extension movements during gastrulation require *pygo2.*
Lateral views of control MO (A, C), pygo1TR (B, D) and pygo1SP (E) *sox10:egfp* morphants under bright field microscopy. Corresponding lateral views of fluorescence microscopy have been displayed in panels A'-E'. At 12 hpf embryos are have entered the segmentation period of development, with the first 3 somites formed (indicated by black arrowheads; A, B) and pygo2TR morphants show an apparent increase in the anterior-posterior axis angle (A-P°). At 48 hpf, pygo2TR and pygo2SP morphants (D, E) lack development of overall body length, eyes (e), fins (fn), normal somite structure and develop blood pooling (bp) and pericardial oedema (*) in comparison to control MO (C). *Scale bar = 200μm*

3.5.5 pygo2TR morphants display abnormal cardiac function

In addition to the convergent extension phenotype observed in pygo2TR morphant gastrulation, a severe reduction in cardiac function was evident at 48hpf. Following the criteria outlined in Section 3.5.1 (p.78), morphant heart rate, cardiac looping and pericardial oedema were assessed at 48hpf and 72hpf (cardiac looping and oedema only). Heart rates were counted per 30sec, for each embryo and subsequently scored as either looped or straight. While pericardial oedema was scored arbitrarily from 1-5, using a reference chart. For example, if the pericardium extended farther than periphery of the yolk sac or anterior-most structure of the head, it was given the value of 3 or more, dependent upon relative size. Using this method, wild type embryos would normally fall within the range 1-2 decreasing as development proceeds.

The results from these assessments have been displayed in Figure 3-16 and from this it can be seen that pygo2TR morphants and co-injected (pygo1TR + pygo2TR) + p53 have significantly reduced heart rates at 48hpf. In addition to this, they show a sustained failure of cardiac looping and increasing pericardial oedema over time. It is likely that the reduction in heart rate, and reduced looping are specific to the pygo2TR morphants. In Figure 3-16 it can been seen that co-injections with pygo1TR did not alter the phenotype observed with pygo2TR alone. However, as mentioned previously it is likely these defects are secondary to the earlier gastrulation defect.

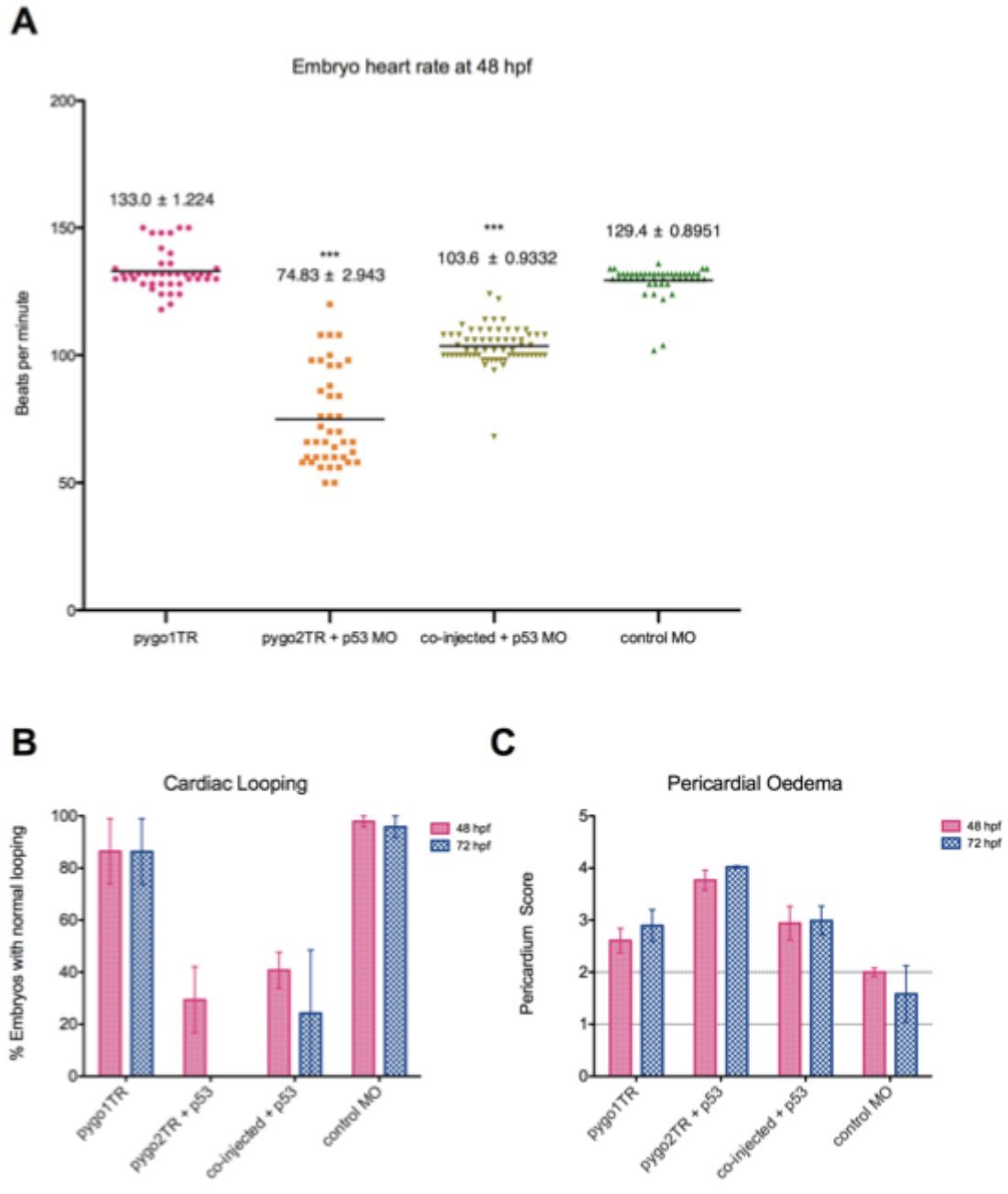

Figure 3-16. Cardiac assessment of injected morphants at 48 hpf and 72 hpf.
Heart rates from injected morphants (A), were counted over a 30 sec interval at 48 hpf and have been presented in beats per minute. Cardiac looping (B) and the size of the pericardial space (C) were scored at 48 hpf and 72 hpf. Morphants were produced by injection of pygo1TR, pygo2TR + p53, co-injections (pygo1TR & pygo2TR + p53), or control MO.

3.5.6 The pygopus homologs are independently required during development

In mice, the role of *Pygo1* is suspected to be redundant with *Pygo2*. While in frogs, the two isoforms show unique expression profiles and independent roles during development. Given the differential temporal expression of zebrafish homologs seen in Figure 3-9, and the unique phenotypes seen with MO knockdown, it is likely that *pygo1* and *pygo2* have unique roles during zebrafish development. However, this does not discount the possibility of some redundancy in the homologs' function or otherwise overlapping roles. To test this possibility, half the optimal dosage required of each MO was co-injected, in combination with p53 MO.

As Figure 3-17 illustrates, the phenotypes achieved by co-injections of pygo1TR and pygo2TR are milder than the single injections alone. In particular, the co-injected morphants display a milder convergent extension phenotype than pygo2TR morphants, and this, in turn, leads to a modest reduction in A-P length. In addition, the severe craniofacial phenotype seen in pygo1TR morphants is absent, although some morphants display the milder jaw phenotype and curvature of the body axis. Taken together, knockdown of the zebrafish *pygo* homologs does not exhibit a synergistic effect, suggesting that their roles are distinct, and that they do not share redundant roles during normal development.

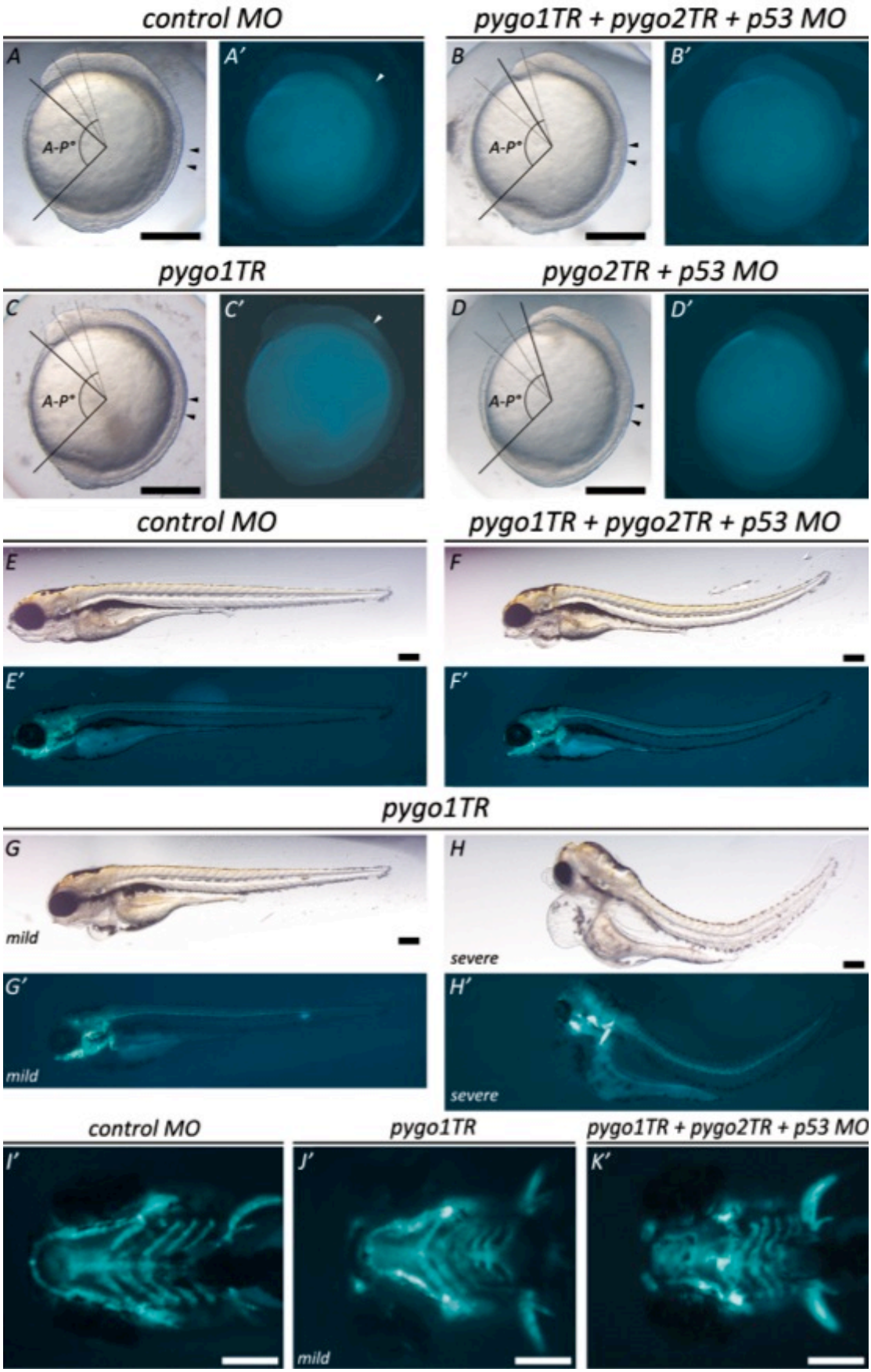
control MO
pygo1TR + pygo2TR + p53 MO
A
A′
A-P°
B
B′
A-P°
pygo1TR
pygo2TR + p53 MO
C
C′
A-P°
D
D′
A-P°
control MO
pygo1TR + pygo2TR + p53 MO
E
F
E′
F′
pygo1TR
G
mild
H
severe
G′
mild
H′
severe
control MO
pygo1TR
pygo1TR + pygo2TR + p53 MO
I′
J′
mild
K′

Figure 3-17. Zebrafish pygopus homologs have distinct roles in embryonic development. Lateral view of control MO (A), co-injected pygo1TR, pygo2TR + p53 MO (B), pygo1TR (C) and pygo2TR + p53 (D) *sox10:egfp* morphants under bright field microscopy. The same embryos are shown in corresponding panels A'-D' under fluorescence microscopy to visualize the neural crest derived structures (i.e. cartilage and PNS). At 12 hpf (A-D) co-injected morphants (B) display a milder defect in convergent extension movements during gastrulation when compared to pygo2TR morphants (D). While at 120 hpf, co-injected morphants (F) display defects similar to a mild pygo1TR syndrome (G) and mild mispatterning in jaw development (K). *Scale bar = 200μm*

3.6 Discussion

The primary aim of this study was to investigate the broader evolutionary context of *pygo* homologs and determine the role of pygo gene(s) in zebrafish development in an attempt to clarify many of the inconsistencies seen between the current fly, frog and murine models. These include the essential requirement for *pygo* in the *wg* pathway versus the suggested 'enhancing' or amplifying role in mice, in addition to the apparent redundancy that is observed in mice, but not in frogs.

Two different approaches were used to investigate these aims. Firstly, a bioinformatics study was undertaken to identify potential homologs of *pygo* in a variety of organisms spanning all three domains of life. It was discovered that the *pygo* gene is unique to metazoans. That is, no evidence was found for a 'pygopus-like' gene in prokaryotes or single celled eukaryotes like yeast. Interestingly *T. adhaerens*, a basal metazoan [230], which arose evolutionarily following the transition from unicellular to multicellular, encodes a single *pygo* homolog. This would appear to corroborate with the appearance of the *wnt* pathway in evolution. To date, *wnt* genes appear to be absent from plants, fungi and protists, and are exclusively found in metazoans [231]. Remarkably this would suggest a closely conserved relationship between the *pygo* homologs and the *wnt* pathway.

It was also shown that zebrafish have two homologs, which make them unique amongst the fishes, but not amongst the vertebrates. However, many of the fish

genome builds are currently incomplete and it is possible that additional homologs may still be identified. To further investigate the possibility that these homologs are true orthologs, sequence comparisons were performed on common model organisms and subsequently on a wider evolutionary range of species.

Three key results suggested that the zebrafish homologs are true orthologs, originating from a speciation event. Firstly, the pygo proteins encode highly conserved domains across all the species studied and importantly the functional residues remain invariant. Secondly, sequence comparisons show a greater sequence homology to other vertebrate homologs than between themselves. Finally, there are multiple homologs found in species from the fishes (Actinopterygii), to the amphibians and the mammals. Taken together, the parsimonious conclusion is that these homologs are derived from a common vertebrate ancestor and the reptiles, avians and some fishes have lost an additional homolog. Simply, *pygo1* and *pygo2* are orthologous to invertebrate *pygo*.

The second approach undertaken in this study was a knockdown of *pygo1* and *pygo2* in zebrafish. The zebrafish was chosen as outlined in Section 3.2 due to its economy, ease of manipulation and evolutionary position. It was hypothesized that this model may clarify our understanding of the redundancy seen in frogs and mice.

During embryonic development, the expression of *pygo1* and *pygo2* was analysed in a temporal manner. It was found that both are maternally contributed; yet *pygo2* is endogenously expressed early on in development, and *pygo1* much later. It would be interesting to conduct *in situ* analysis of their spatial expression pattern. The expression pattern in frogs is increasingly restricted during development, and both *pygo2* isoforms display unique patterns of expression within the eye, brain and neural tube in a stage-dependent manner. However, in mice, *Pygo2* is expressed throughout the entire embryo with regions of higher expression in the brain and spinal cord. Analysis

in the zebrafish may help to reconcile these differences in expression pattern, in similar manner to its functional analysis within this study.

The temporal expression profile of both *pygo* homologs in frogs and the functional differences between frogs and mice would further suggest *pygo* homologs have independent roles in embryonic development. To investigate this, MO injections were performed to knockdown the expression of both zebrafish homologs. Initially, they were targeted independently. It was found that *pygo1* is required for normal jaw development. When MO targeting *pygo1* were injected, the hyoid bones of morphants failed to extend, in particular the basihyal. In addition, morphants also displayed a reduction in the Meckel's cartilage, which is one of the mandible bones.

This phenotype is similar to what is observed with the *chinless* (*chn*) mutation in zebrafish [186,187]. Albeit, in a milder manner. Differentiation of NC is blocked in *chn* mutants and they lack NC derived structures of the jaw. However, in *pygo1* morphants, the structures are mis-patterned, and not absent. This would suggest rather than blocking initial specification of cartilage cells, as with *chn* mutants, the loss of *pygo1* affects the ability of these cells to proliferate or co-ordinate with the surrounding tissue appropriately.

Alternatively, the function of *pygo2* appears broader and earlier, being required during gastrulation for convergent extension movements. This is a similar phenotype to what is observed for a number *wnt* mutations. The *silberblick/wnt11* and *pipetail/wnt5* mutations also display a reduction in the anterior-posterior axis following gastrulation [95,232]. Again, the *pygo2* morphant displays a milder phenotype than seen in these mutations. It is possible this is due to the usage of MOs, providing merely a knockdown, rather than a complete loss of the gene function. Or, as seen in mice, the role of the *pygo* homologs is limited to amplification of the *wnt* signal, and thus not essential for transduction. However, it does, at the very least, infer a role in non-canonical *wnt* signaling.

In addition, the results suggest that *pygo2* is required for normal cardiac looping and heart development. It may be argued that these defects are secondary effects of the primary gastrulation defect, or pericardial oedema. However, *pygo1* morphants show a similar level of oedema to the co-injected morphants, yet do not display a defect in looping or heart rate at 48hpf. On the other hand, co-injected morphants display a mild gastrulation effect and a milder reduction in heart rate than the *pygo2* morphants. Thus it is possible that the heart defect is related to the gastrulation defect, but not the pericardial oedema. However, Li *et al.* (2003) demonstrated a requirement for the NC in zebrafish heart looping, and Sato *et al.* (2006) have shown NCC contribute to cardiomyogenesis. While it is well established that the *wnt* pathway is essential for cardiac development in vertebrates [233,234]. With these studies in mind [193-195], it is possible that the cardiac defect seen in *pygo2* morphants is a primary defect of both NC and *wnt* dependent processes.

It is interesting to note, that both homologs also have distinct roles in embryogenesis. It would appear that *pygo1* is required by NCSC for extension of the jaw bones, specifically the hyoid. While it is likely that *pygo2* is broadly required during gastrulation for transduction of the *wnt* signal that mediates convergent extension movements. Interestingly, no apparent defect was seen in the migration of NCSC, or in the development of the PNS and pigment cells. Yet, overall these results suggest *pygo1* and *pygo2* are required specifically by NC in jaw development and for transduction of the *wnt* signal respectively.

The pygo1/2TR morphants provide an elegant system for a number of future experiments, such as co-injection of MO with a pygo rescue construct. This may also be combined with an overexpression study to directly assess the function of homologs versus paralogs. Additionally, this would unequivocally prove the specificity of the pygo1/2 MO *in vivo*. Subsequently the involvement of *pygo* homologs in NC and the *wnt* could also be validated through screens of putative downstream target genes. Primarily investigating genes involved directly in jaw morphogenesis or convergent extension movements during gastrulation. For example, non-canonical wnt signaling (*wnt5*, *wnt11)* converges on the RhoA pathway for vertebrate gastrulation movements. So the addition of active RhoA

may rescue the *pygo2* phenotype in a similar manner to what has been observed previously [229].

In conclusion, this study has shown that two highly conserved *pygo* homologs exist in the zebrafish, with unique temporal expression profiles. The results suggest *pygo1* and *pygo2* have distinct, non-redundant roles in zebrafish development. These roles include processes that are NC and non-canonical *wnt* pathway dependent. In light of this, the zebrafish is unique amongst the vertebrates studied to date, in having two functionally required homologs of *pygo*.

Chapter 4. Wnt1-Specific *Pygo2* Knockout Mice Display Multi-organ Birth Defects

4.1 Introduction

In the previous chapter, it was demonstrated that MO knockdown of *pygo* homologs yielded phenotypes consistent with defects in NC development or Wnt pathway dependent processes. Whilst MO gene knockdown studies in zebrafish provide a fast, economical and relatively simple approach to studying gene function, they lack the ability to target genes in a tissue specific manner, can have off-target effects [222] and do not ablate gene function entirely. However, murine transgenic models are well established as a system to efficiently knockout gene expression in a precise spatial and temporal fashion, making use of Cre-loxP, and with the use of compound transgenics, tissue specificity can be achieved. Many genes have been targeted with loxP sites to facilitate their inactivation [235], but the limiting step in most studies is the identification/creation of a suitable Cre expressing mouse capable of driving Cre expression to the specific cells/tissue/organ of interest.

4.1.1 The Wnt1 expression domain encompasses the emerging NC

Wnt1 is the prototypical *Wnt* pathway gene. It was originally identified and named *Int-1* (integration locus 1), because it was frequently transcriptionally activated in carcinomas from an adjacent integration of the mouse mammary tumour virus [236]. Subsequently, *Wnt1* was found to belong to a large family of secreted polypeptides with shared homology to the *Drosophila wingless* (*wg*) segment polarity gene [237,238]. Thus, *Wnt* was proposed as a mnemonic name to collectively refer to all members of this gene family [239].

Wnt1 is exclusively expressed during embryogenesis and in maturation of spermatids within the adult mouse testis [240]. Embryonic expression is transient, whereby it is first seen at day 8.5 dpc until 15.5 dpc, and only within the developing CNS [240,241]. Localised regions of expression are observed in

the lateral tips of the neural plate and the dorsal wall of the neural tube, prior and after closure. In addition, other sites include, the ventral wall of the midbrain and the diencephalon, and the lateral walls of the neuroepithelium at the midbrain-hindbrain junction [242].

Targeted mutations of the *Wnt1* gene in the mouse lead to perinatal lethality, loss of the cerebellum and midbrain defects in 90% of homozygotes [243]. In those that survive and in the spontaneous mutant, *swaying*, ataxia and hypertonia is observed associated with a loss of the anterior cerebellum only [244]. It has been suggested this 'milder' phenotype of *Wnt1* mutants is likely due to a functional redundancy with one or more Wnt family members [244-248].

While the expression of *Wnt1* incorporates the dorsal neural tube folds, where the NC emerges during neurulation, the primary function of *Wnt1* appears to be involved in CNS development, and not in the pre-migratory NC. However, it is important to note that the NC first arises exclusively within the domain of *Wnt1* expression.

In 1994, Echelard *et al.* confirmed the expression of *Wnt1* in pre-migratory NC using a Wnt1-lacZ reporter mouse strain [249]. A 5.5kb *cis*-regulatory element cloned from the *Wnt1* promoter was used to drive the expression of β-galactosidase (β-gal) from the *lacZ* transgene, in cells normally expressing *Wnt1*. These cells were subsequently visualized by X-gal staining relying upon the enzymatic actions of β-gal [250]. Furthermore, due to perdurance of *lacZ* expression, it was shown that migrating cells of the NC stained positive for X-gal as they left the dorsal neural tube [249,251,252].

4.1.2 Lineage tracing: The R26R picture

Following the early functional analyses and expression studies of *Wnt1* mutants, Chai *et al.* (2000) utilized a compound transgenic model in which they were able to indelibly mark the appearance and progeny of all Wnt-1 expressing cells [253]. The model utilized two different mouse strains to provide a tool for cell lineage analysis of the NC and its derivatives, outside of the CNS.

Firstly, the Wnt1-Cre mouse strain provided specificity of the *Wnt1* expression domain, expressing Cre recombinase (Cre) from the previously described Wnt1 *cis*-regulatory element [251,252]. In this system, genomic sequences flanked by *loxP* (locus of X-over P1) sites, usher recombination and subsequent removal of the intervening targeted sequence, through the action of Cre. Thus, the Cre-loxP system mediates site-specific recombination and subsequent deletion of targeted genes in mammalian cells and transgenic animals [254,255].

The second mouse strain used was the R26R reporter mouse. This transgenic line ubiquitously express the *lacZ* gene preceded by a loxP flanked (or 'floxed') *neomycin* (*neo*) expression cassette and splice acceptor sequence, from the ROSA26 locus [159]. Downstream of the *neo* cassette are three polyadenylation sequences to prevent transcriptional read-through. These sequences effectively prevent the expression of β-gal (from the *lacZ* gene), except where the *neo* cassette has been deleted, following Cre expression.

Together these transgenic lines provide an elegant solution to studying the fate of the NC outside of the CNS. The Wnt1-Cre::R26R double transgenic mouse model is now well established and has been used to study many derivatives of the NC including, but not limited to, cardiovascular development [93,256], innervation of the lung [257], and formation of cranial bones and teeth [39,253,256-260].

4.1.3 Pygo2 null mice develop defects in NC derived tissues

Previous studies on both *Pygo1* and *Pygo2* knockout mice have revealed a redundant and non-combinatorial function for *Pygo1* in murine development [116,123,131]. *Pygo1 null* mice display no overt phenotype and the adult mice are fertile. In contrast, *Pygo2 null* mice display a range of phenotypes (see Chapter 1). Importantly, these phenotypes incorporate organs that are partially derived from the NC, for example, the brain, palate, skin and intestine.

Interestingly, Song *et al.* (2007) utilized the Wnt1-Cre model together with the *Pygo1* and *Pygo2* floxed models to specifically investigate the lens agenesis observed in the *Pygo1/2 null* study. They were able to identify that NC derived

ocular mesenchyme together with the presumptive lens ectoderm require *Pygo2* (not *Pygo1*) for normal lens induction and development [123]. Thus, this study highlights the possibility that the aetiology of other *Pygo2 null* phenotypes may involve a NC deficiency of *Pygo2*.

4.2 Aims of this study

Pygo2 is a signature gene of EPI-NCSC, which are adult, hair follicle resident, stem cells of NC origin (see Chapter 1). Given that *Pygo2* plays an important role in the transduction of the *Wnt* signal (see also Chapter 1), and in turn, the *Wnt* pathway is important for NC development, it is reasonable to expect that *Pygo2* may also play a substantial part in NC development. Taken together, this would suggest an important role for *Pygo2* in NC and EPI-NCSC development or maintenance within the stem cell niche.

In order to explore the possibility of this role further, a triple transgenic model was developed to specifically ablate *Pygo2* expression and simultaneously label, cells of the NC and their derivatives. This was achieved by combing the Wnt1-Cre, R26R, and conditional Pygo2 mouse lines (described previously in Chapter 1 & 2). Thus, investigation of the resulting triple transgenic mouse model (Wnt1-Cre::R26R::Pygo2$^{fl/fl}$), formed the foundation for this study to broadly assess the role of *Pygo2* in NC development.

Specifically the aim of this chapter was to determine the role of Pygo2 in the development of the murine NC.

4.3 Neural Crest Specificity: The Triple Transgenic Model

The breeding strategy required to obtain the triple transgenic animals used in this study is outlined in Figure 4-1. Briefly, double transgenics were first produced by mating Pygo2$^{fl/+}$ mice to both Wnt1-Cre and R26R mouse strains independently. Double heterozygous offspring from these mating's were subsequently used as breeding pairs to produce triple transgenic litters.

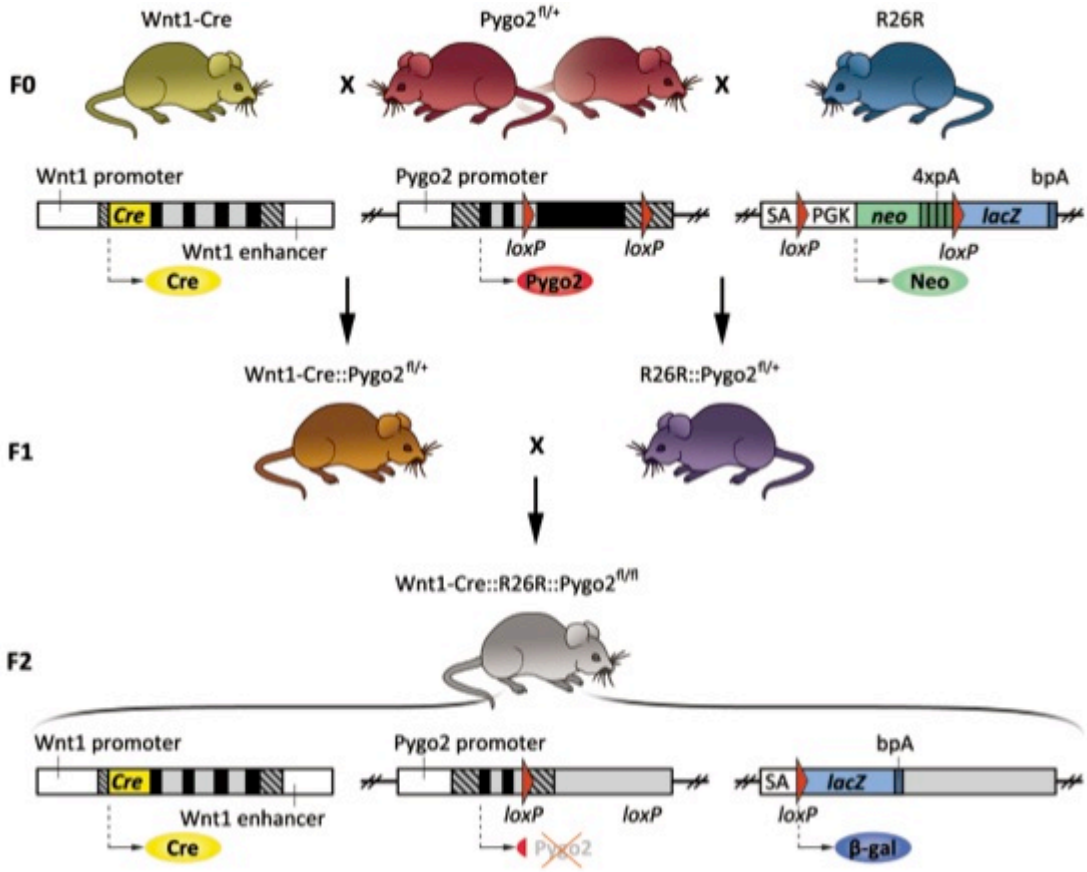

Figure 4-1. Breeding strategy for the Pygo2 conditional knockout triple transgenic model
In the founding generation (F0), Pygo2$^{fl/+}$ mice are mated to both Wnt1-Cre and R26R mouse strains. The Wnt1-Cre mouse carries a random integration that expresses Cre from a Wnt1 promoter and cis-acting element. The R26R carries a targeted insertion of a loxP flanked *neo* expression cassette, preceding an inactive LacZ expression cassette at the ROSA 26 locus. The Pygo2$^{fl/+}$ strain has two *loxP* sites flanking the third exon of *Pygo2*. Double heterozygous F1 progeny are mated to produce triple transgenic *Pygo2* conditional null offspring in F2. These animals express Cre within the normal Wnt1 expression domain. This leads to excision of the neo cassette, and subsequent β-gal expression from the ROSA 26 locus. In addition, the expression of Cre leads to deletion of more than 80% of the coding region of *Pygo2* and effectively leads to a null mutation.

While usage of this triple transgenic model provides a precise tool for assessing the role of *Pygo2* in NC development, it still has a number of technical limitations. Firstly as presented in Figure 4-1, a complex breeding strategy is required to achieve triple transgenic mice. Secondly the number of triple

transgenics produced is low, assuming a purely Mendelian mode of inheritance. As Figure 4-2 illustrates using a modified punnet square, the chance of producing a triple transgenic is one in sixteen (1/16). With the average litter size for C57B6/6J inbred strains averaging eight per litter, these limitations make producing triple transgenic mutants both time consuming and expensive. In order to improve these yields, double transgenic (Wnt1-Cre::Pygo2$^{fl/fl}$) were often incorporated in the study where the identification of NC, and by extension, β-gal mice (R26R) were not required. For example, in the study of skull and mandible length (see Section 4.5.4), data from Wnt1-Cre::R26R:Pygo2$^{fl/fl}$ and Wnt1-Cre::Pygo2$^{fl/fl}$ were pooled to increase the statistical power. However, in these instances, the double and triple transgenic populations were first analysed empirically, and statistically to identify if they differed significantly between R26R positive and negative mice. In all cases, no significant differences were observed between these genotypes.

Figure 4-2. Mendelian segregation of triple transgenic gametes
Modified Mendelian Punnet Square representing the possible genotype combinations from the random integration (Wnt1-Cre), ROSA 26 and *Pygo2* loci. Each box indicates a unique combination for each zygote formed from the possible gametes (columns and rows). In this example, there is a one in sixteen (1/16) chance of producing a Wnt1-Cre::R26R::Pygo2$^{fl/fl}$, triple transgenic *Pygo2* conditional knockout (CKO) zygote.

Further technical limitations exist with the usage of the Cre-loxP system in this model. This may occur in two ways. Firstly, it is possible that incomplete excision at both *pygo2* alleles may occur, leading to a heterozygous state (Wnt1-Cre::Pygo2$^{fl/-}$) within the *Wnt1* expressing cell lineage. Presumably this monoallelic recombination would be equivalent to a heterozygous (Wnt1-Cre::Pygo2$^{+/-}$) mouse and based upon earlier evidence, it may display a milder phenotype or none at all [116,123,125,261]. This outcome could be avoided by initially breeding the double transgenics on a Pygo2$^{+/-}$ background. However, this may also cause additional non-autonomous phenotypes, due to haploinsufficiency (a reduction in Pygo2 expression) from outside of the Wnt1 expression domain.

Secondly, other studies have shown that parental contributions of transgenic Cre protein or mRNA within sperm or oocytes can lead to unrestricted recombination in all tissues of the embryo and subsequently loss of the intended tissue specificity [262-265]. Conversely, persistent expression of the targeted gene is possible following accurate tissue-specific Cre expression and targeted recombination[266]. In a recent study, expression of the targeted gene was proposed to be from the episome by-product of Cre mediated excision [266]. Interestingly, the episome was preferentially retained by slow cycling cells. While these undesirable outcomes are potentially possible with the triple transgenic model, it is unlikely given that the Wnt1-Cre::R26R [19] and CMV-Cre::Pygo2$^{fl/fl}$ [131,267] models have previously been used without complication.

4.4 Conditional deletion of *Pygo2* does not disrupt embryogenesis

The possible defects arising from the *Wnt1*-specific deletion of *Pygo2* were initially studied using mid-gestational embryos. However, the gross morphology of the *Pygo2* conditional knockout embryos (*Pygo2* CKO) appeared normal at 10.5 days post coitum (dpc; see Figure 4-3). This is consistent with the previous study by Song et al. (2007) [123].

4.4.1 The formation and migration of the NC in Wnt1-Cre::R26R::Pygo2$^{fl/fl}$ embryos is unperturbed

To determine if the loss of *Pygo2* had an effect on the establishment and migration of the NC cell population during embryogenesis, conditional *Pygo2* CKO (*n*=4) and control embryos (Wnt1-Cre::R26R::Pygo2$^{+/+}$; *n*=6) were analysed. Embryos from double heterozygous mating's (F1 x F1) were collected at 10.5 dpc and subsequently stained with X-gal to visualize the NC cell lineage (described in Chapter 2). As Figure 4-3 demonstrates, wild type embryos (negative control) do not stain positive for X-gal, suggesting there is neither endogenous β-gal activity, nor background staining in these embryos. However, cells within the *Wnt1* expression domain in Wnt1-Cre::R26R::Pygo2$^{+/+}$ embryos, stain blue, thus confirming the expression and activity of β-gal, as previously reported . In addition, the *Pygo2* CKO embryos also stain positive within the same regions of *Wnt1* expression, in both the pre-migratory and migratory NC.

Importantly, normal staining is observed in the dorsal root ganglion (DRG), the mid-hindbrain boundaries, cranial ganglia, and extensively throughout the pharyngeal arches and developing cranio-facial regions. There is also staining in the migrating cranial (contributing to the cranial ganglia), cephalic crest (colonizing the pharyngeal arches), cardiac, and vagal NC populations. Overall this suggests the first appearance of the NC is normal, in a spatio-temporal manner, and that typical NC migration is underway at this developmental stage.

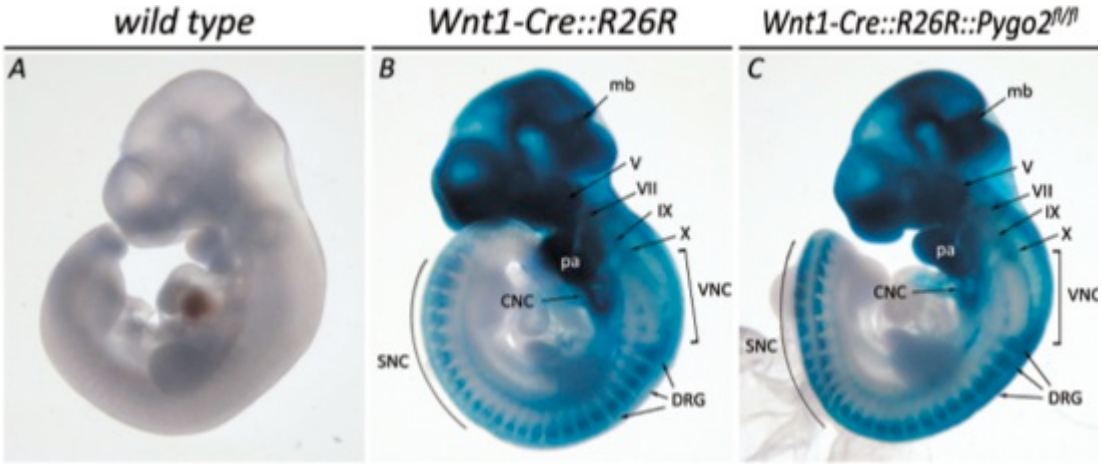

Figure 4-3. The formation and migration of NC is unperturbed in *Pygo2* CKO embryos
Whole-mount staining of 10.5 dpc triple transgenic embryos showing expression of β-gal (blue stain) within the *Wnt1* expression domain. Embryos are presented laterally with anterior to the top and dorsal to the right. Intense staining is seen within NC derived cranial trigeminal (V), facial (VII), glossopharyngeal (IX), and vagus (X) nerve ganglia in both Wnt1-Cre::R26R::Pygo2$^{+/+}$ control (B) and Wnt1-Cre::R26R:Pygo2$^{(fl/fl)}$ (C) knockout embryos. Normal staining is also observed within the pharyngeal arches (pa), mid-hindbrain boundary (mb), dorsal root ganglia (DRG), and migrating NC populations (Cardiac; CNC, Vagal; VNC, Sacral; SNC).

4.4.2 Neuron development proceeds normally in triple transgenic embryos

At this stage of development, the NC is not only migrating, but the NC is also differentiating into glia and neurons of the PNS. While the migration of the NC is highly important, it is also important to assess whether the migratory NC cells are undergoing the normal programs of cell fate. To test this, 10.5 dpc embryos were also stained using an antibody to neurofilament (see Chapter 2). Neurofilaments are intermediate filaments found specifically in neurons and may be used as a marker for neuron development [268].

Briefly, control embryos and *Pygo2* CKO (n=5) embryos were collected and stained overnight with anti-neurofilament antibody. Using a horseradish peroxidase conjugated secondary antibody, the expression of neurofilaments was identified by a black stain from the 4-Chloro-1-naphthol substrate (described in Chapter 2). As Figure 4-4 demonstrates, Wnt1-Cre::Pygo2$^{fl/fl}$ embryos develop neurons in a manner consistent with wild type and control

embryos. Again, this suggests that the formation of the NC is normal, and furthermore, NC cells are capable of differentiating into their specified cell fates.

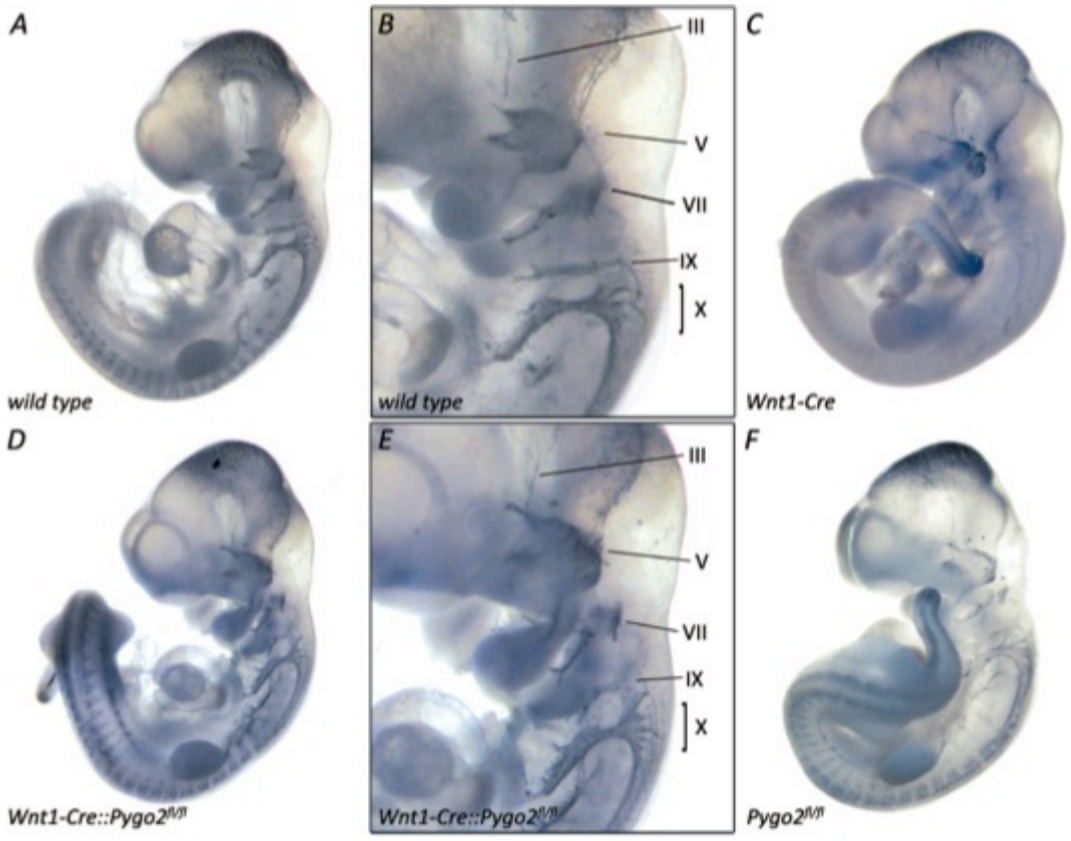

Figure 4-4. Cranial nerves develop normally in Pygo2 CKO embryos
Wholemount immunohistochemistry of neurofilament (2H3) at 10.5 dpc in wild type (A,B), Wnt1-Cre control (C), *Pygo2* CKO (D,E) and Pygo2$^{fl/fl}$ control (F) embryos. Panels B and E, enlarged from wild type and *Pygo2* CKO embryos respectively, show regular cranial ganglia development. Sensory ganglia are located outside the hindbrain and are derived from NC. V, trigeminal nerve; VII, facial nerve; IX, glossopharyngeal nerve; X, vagus nerve.

4.5 Conditional *Pygo2* knockout mice exhibit multiple defects at birth

While conditional *Pygo2* knockout embryos did not display an overt phenotype during embryogenesis within the NC or morphologically, a number of defects were observed shortly after birth. These defects included abdominal bloating and perinatal lethality. In addition, abnormal morphology was observed in

multiple NC derived tissues, including the jaw, gastro-intestinal tract, heart, skin, and trigeminal ganglion. However, many of the phenotypes exhibited in *Pygo2 CKO* appear to be partially penetrant, being evident in only a subset of the mutant population without gender bias.

4.5.1 The loss of Pygo2 from the NC is perinatal lethal

In the ubiquitous *Pygo2* knockout mouse model (*Pygo2 null*), newborn pups die shortly after birth. However, the cause of death remains unknown from studies reported to date [116,123,131,261]. In this study, the Wnt1 dependent deletion of *Pygo2* also leads to perinatal lethality.

Because neonatal lethality precludes the analysis of adult mice, newborn pups were routinely collected as soon as possible following birth, primarily to prevent the degradation of tissue samples required for downstream analysis. As Figure 4-5 illustrates, approximately 20% of newborn pups lacking *Pygo2* (double and triple conditional knockouts) died prior to collection and less than 12 hours postpartum (hpp). However, the immediate collection of pups postpartum also prevented an accurate assessment of the mortality rates amongst the population.

To address this issue, litters born from Wnt1-Cre::Pygo2$^{fl/+}$ and Pygo2$^{fl/+}$ breeding pairs were left undisturbed, except to count the number of pups born and the number of deaths. From 100 pups born, two were missing from subsequent counts and thus, they were presumed to have been cannibalized (genotypes unknown). The final mortality rates from these litters have been added to Figure 4-5. In contrast to the postpartum mortality rates, the true mortality rate amongst *Pygo2* CKO pups increased from 20% to a total of 60%. Interestingly, the 40% rise in mortality occurred exclusively within the following 12-24 hours postpartum. In other words, all pups found alive at 24 hours, survived to at least 10 weeks of age.

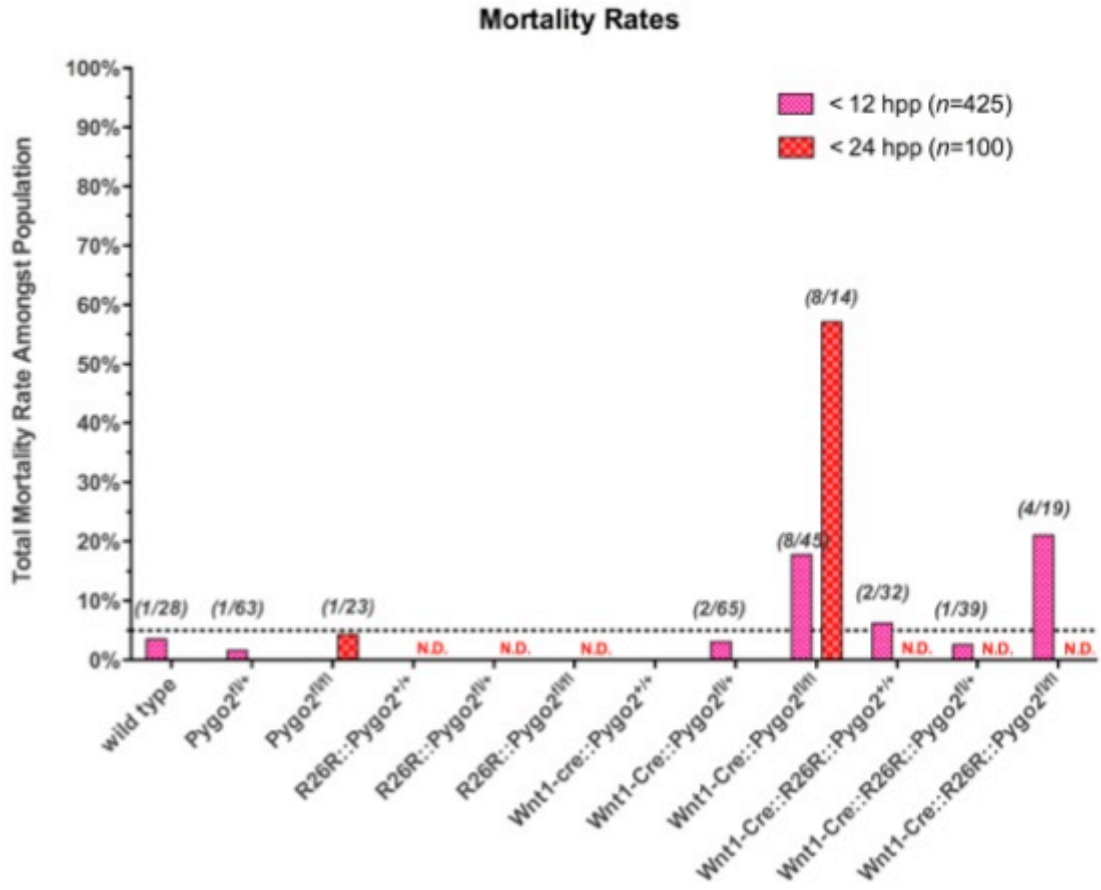

Figure 4-5. Mortality rates amongst triple transgenic litters is greatest between 12-24 hpp
Approximately 20% of conditional *Pygo2* knockout pups (Wnt1-Cre::Pygo2$^{fl/fl}$ & Wnt1-Cre::R26R::Pygo2$^{fl/fl}$) die within 12 hpp (hours postpartum). While between 12-24 hpp, the total mortality increases to approximately 60%. No subsequent deaths were observed between 24 hpp and 10 weeks of age in this study.

Given the high level of mortality seen within the first 24 hours, it was possible that additional *Pygo2* CKO pups may have died *in utero.* To assess this possibility, the genotypes of newborn pups were analysed to identify if there was a bias present in the frequency distribution of genotypes. Assuming independent segregation of each of the transgenic alleles, it is expected that each of the possible sixteen genotypes should be represented equally. That is, each genotype should occur with a frequency of 1/16 or 6.25%, with the exception of *Pygo2* heterozygotes, which are twice as likely at 12.5% (refer to Figure 4-2).

The number of pups born from triple transgenic mating's have been represented by a frequency bar chart in Figure 4-6. Each genotype is largely represented as expected, either 6.25% or 12.5%, with the exception of Pygo2$^{fl/+}$ and Wnt1-Cre::R26R::Pygo2$^{+/+}$, which are slightly under and over represented respectively. Importantly, the conditional *Pygo2* knockouts (coloured red) are both represented at the expected frequency, close to 6.25%. This would suggest that the loss of *Pygo2* in a Wnt1-specific manner does not lead to embryonic lethality.

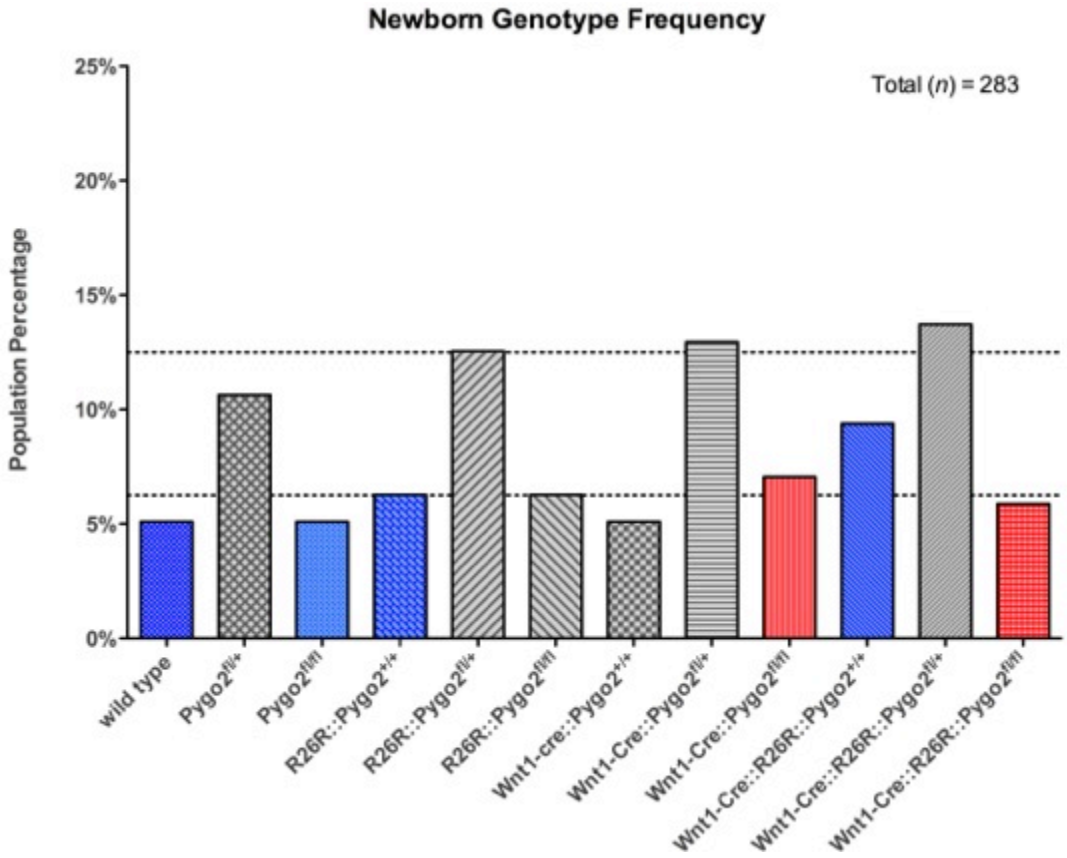

Figure 4-6. The loss of Pygo2 in a Wnt1-specific manner does not lead to embryonic lethality
Frequency histogram representing mortality rates of newborn genotypes from triple transgenic litters. Assuming there is no embryonic lethality in the newborn population, each possible genotype is expected to occur within the population at a frequency of around 6.25%. With Wnt1-Cre::Pygo2$^{fl/+}$ and R26R::Pygo2$^{fl/+}$ breeding pairs, both parents may contribute transgenes to the *Pygo2* locus and therefore Pygo2$^{fl/+}$ offspring are twice as likely, i.e12.5%, irrespective of Wnt1-Cre or R26R genotype. *Pygo2* CKO genotypes (red) are represented at approximately the expected frequency (6.25%), suggesting no embryos are lost before birth. Control genotypes (blue) generally occur in expected frequencies.

In summary, the frequency of genotypes at birth suggest there is no loss of *Pygo2* CKO embryos before birth. This is not surprising, given that *Pygo2 null* mice survive until birth, and Wnt1-Cre::Pygo2$^{fl/fl}$ embryos have been used in studies of lens development [123].

In contrast, 60% of newborn *Pygo2* CKO pups die within the first 24 hpp, fewer than the *Pygo2 null*. This level of mortality is surprisingly high. With the Wnt1-specific knockout of *Pygo2*, the deletion is not ubiquitous and so it was anticipated that some of the original phenotypes may be ameliorated, for example the lethality.

4.5.2 Conditional Pygo2 knockouts do not display a reduction in birth weight nor body length

In addition to the newborn lethality, previous studies on *Pygo2 null* mutants found pups had a shorter body length, and a reduction in birth weight [116,131]. In this study, no statistically significant difference was observed in either length or weight of neonatal pups. Although in general, there was a trend for all transgenic genotypes to weigh less than wild type littermates and significant differences in the variance amongst body lengths were observed.

Statistically, there were no significant differences between mean birth weights for each genotype as determined by one-way ANOVA (F (11,142) = 1.603, p = 0.10). Birth weight results have also been displayed in Figure 4-7 as a scatter dot plot, to illustrate the overall trend for reduced birth weight amongst the transgenic populations compared to wild type. Interestingly, if the weight of the dead *Pygo2* CKO pups is separated from the alive *Pygo2* CKO pups, there is a significant difference in the means determined by ANOVA (F (14,167) = 2.181, p = 0.01). Post-hoc Tukey's multiple comparison test reveals a significant difference (<0.05) between wild type, Pygo2$^{fl/fl}$, R26R::Pygo2$^{+/+}$, R26R::Pygo2$^{fl/+}$, versus the dead *Pygo2* CKO group. This data supports the evidence for a partial penetrance in the range of *Pygo2* CKO phenotypes. Because it is anticipated that severely affected pups would also exhibit greater defects in other phenotypes, for example, dead pups would be lighter. However,

this result should be considered with caution, as it is likely the lower weight may be due to posthumous loss of body fluid.

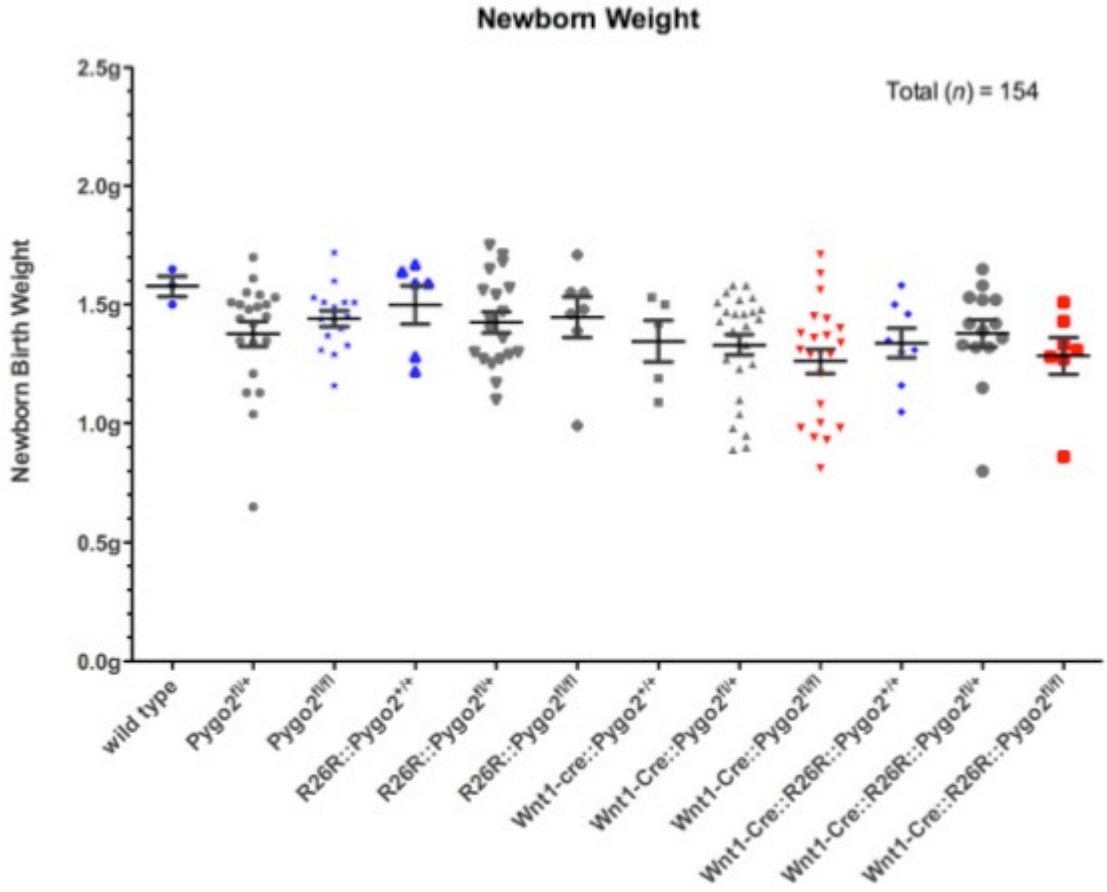

Figure 4-7. Birth weight is unaffected by the loss of Pygo2 in conditional knockout pups
Birth weight for each pup was collected and after genotyping, values were collated according to genotype. Weight was measured in grams, prior to dissection and analysis.

In addition to the birth weight, the body length of newborn pups was measured. Measurements were taken from the ear, to the base of the tail. Similarly to birth weights, a one-way ANOVA was used to test for differences in body length amongst the genotype groups. In contrast to body weight, mean body lengths differed significantly across the genotypes, F (11, 217) = 2.486, p = 0.0059. However, Bartlett's test for equal variances reported a significant variance

amongst the genotypes with a statistic of 21.31, $p = 0.03$. While one-way ANOVA suggested a difference in body length, using Tukey's multiple comparison post-hoc failed to identify any two means that differed significantly.

Taken together, these results suggest that there is a difference between the body lengths, but this is due to a change in the variance within one or more groups. In other words, the distribution of body length within genotypes is non-parametric. To illustrate this point, a box and whisker diagram is provided in Figure 4-8.

In summary, there is no statistical difference in either mean body weight or mean body length. Additionally, a large degree of variance was observed in the newborn body weight and body lengths, with a general trend for Wnt1-Cre genotypes to be lighter, and R26R genotypes to have an increased body length. Overall, it is likely the variation in body length and weight is due to differences between the genetic backgrounds of the transgenic strains and is not specific to the loss of *Pygo2* in this study. It is common for strains of mice to show phenotypic differences over generations of breeding due to genetic drift. For example, simply inbreeding strains of C57BL mice in different locations has led to multiple strains [269,270]. In targeted disruption of the WT1 gene, the background strain can lead to embryonic lethality, with heart defects, or the pups living until birth [271]. There is also a similar case for the EGF receptor mutant [272]. Despite this, dead *Pygo2* CKO pups were significantly lighter than wild type and $Pygo2^{+/+}$ control littermates and it does provide limited support for a partially penetrant phenotype.

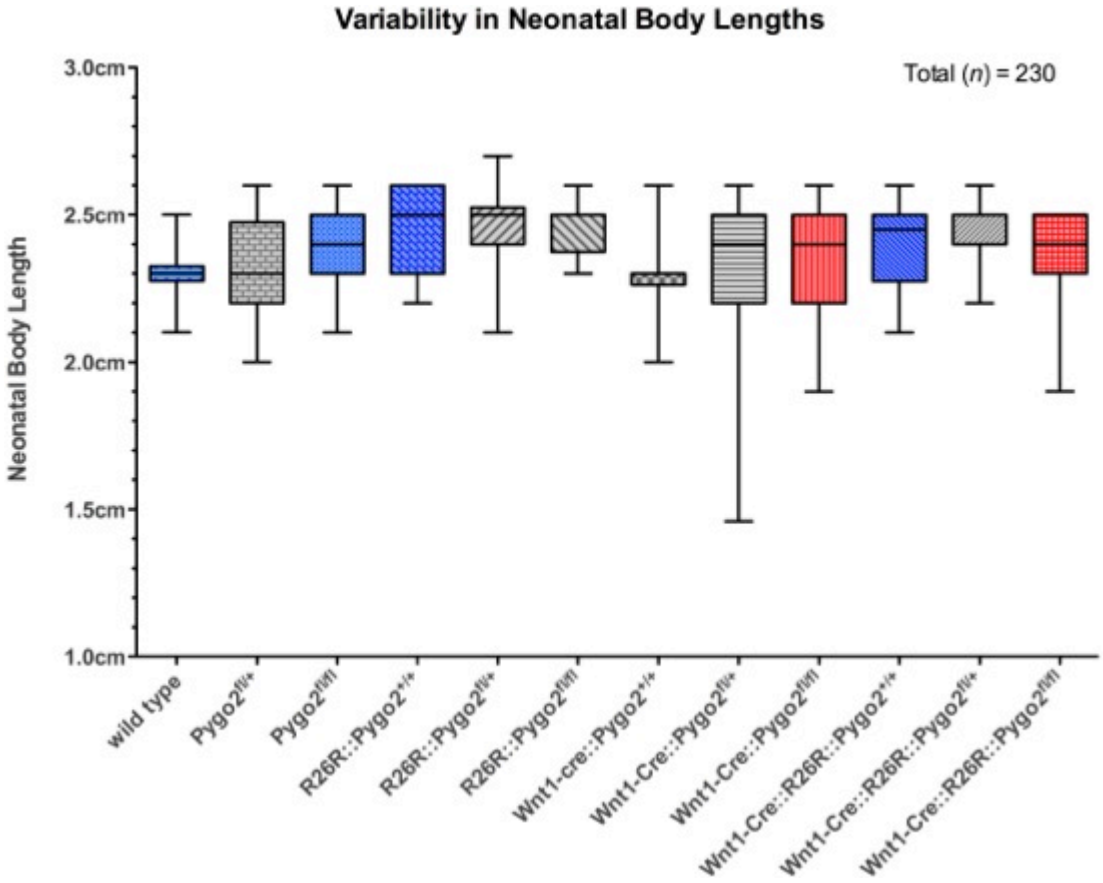

Figure 4-8. Non-uniform variation in body length, amongst and between genotypes
A box and whisker plot of body lengths collected from newborn triple transgenic litters to illustrate variation amongst nonparametric populations. Data from each group is presented uniformly; for each group, the minimum and maximum values are represented by the whiskers, 25th and 75th percentiles by the bottom and top of the box, and the band near the middle of the box is the 50th percentile (the median). Body lengths are measured from the ear to the base of the tail (cm).

4.5.3 Ablation of Pygo2 in a Wnt1-specific manner leads to abdominal bloating and gasping respiration

In addition to lower birth weight and shortened body length, the *Pygo2 null* neonate was also reported to exhibit exencephaly and an eye defect apparent by visual examination (see Chapter 1). In this study, *Pygo2* CKO displayed neither an eye defect nor exencephaly. However, the Wnt1-Cre specific deletion of *Pygo2* led to two anatomically linked phenotypes manifesting shortly after birth.

These phenotypes were not previously observed in the *Pygo2 null* newborns. Whether they were omitted or were physiologically masked is unclear.

Firstly neonatal pups presented with abdominal bloating or gastric torsion (see Figure 4-9). That is, their abdomen or more specifically, their gastro-intestinal tract (GI) was filled with gas or bubbles. This usually extended the entire GI length, from the stomach to the colon. However, in some individuals the stomach and portions of the small intestine were clear of gas and distension. Usually deposits of gas were found in discrete 'bubbles', indicating some amount of torsion had occurred. Additionally, in many of the pups with abdominal bloating, milk was found within the GI, suggesting attempts had been made to feed, and that feeding was possible. Importantly, in all *Pygo2* CKO pups found dead, evidence of abnormal gas deposition, or gastric torsion was identified. This was assumed to be the cause of death, in a manner similar to tympany in ruminants [273,274].

Further to the gastric torsion, *Pygo2* CKO pups also displayed sporadic gasping respiration. This involved a synchronized gasping reflex and large abdominal contractions. In all pups displaying gasping respiration, abdominal bloating was also found. For this reason the two phenotypes were assumed to be associated. This is consistent to other knockout models, whereby gasping respiration is associated with abdominal bloating [275-278]. Curiously, the vast majority of these studies focus on NC-related genes or NC derived tissues.

For example, several knockout models from the *Dlx* (Distal-less homolog) family of homeobox proteins lead to perinatal lethality in combination with abdominal bloating, and gasping respiration [275,279,280]. Interestingly, many of these knockout models display defects in NC derived tissues, including bones of the skull, neurons, ganglia and the GI. In describing the *Dlx-2* phenotype Qiu *et al.* (1995) postulate, the abdominal bloating may have been "caused by a structural obstruction, an abnormality in gut motility, or swallowing excessive air". The same may be said for the apparent phenotype from the Wnt1-Cre mediated deletion of *Pygo2*. However, obstruction of the nasal and oral cavities, for example choanal atresia [281] was excluded as a possibility, given that air was

evident in the entire length of GI tract and newborns were not cyanotic. In other words, air was able to enter the lungs and could be swallowed. This left the remaining possibilities to be investigated.

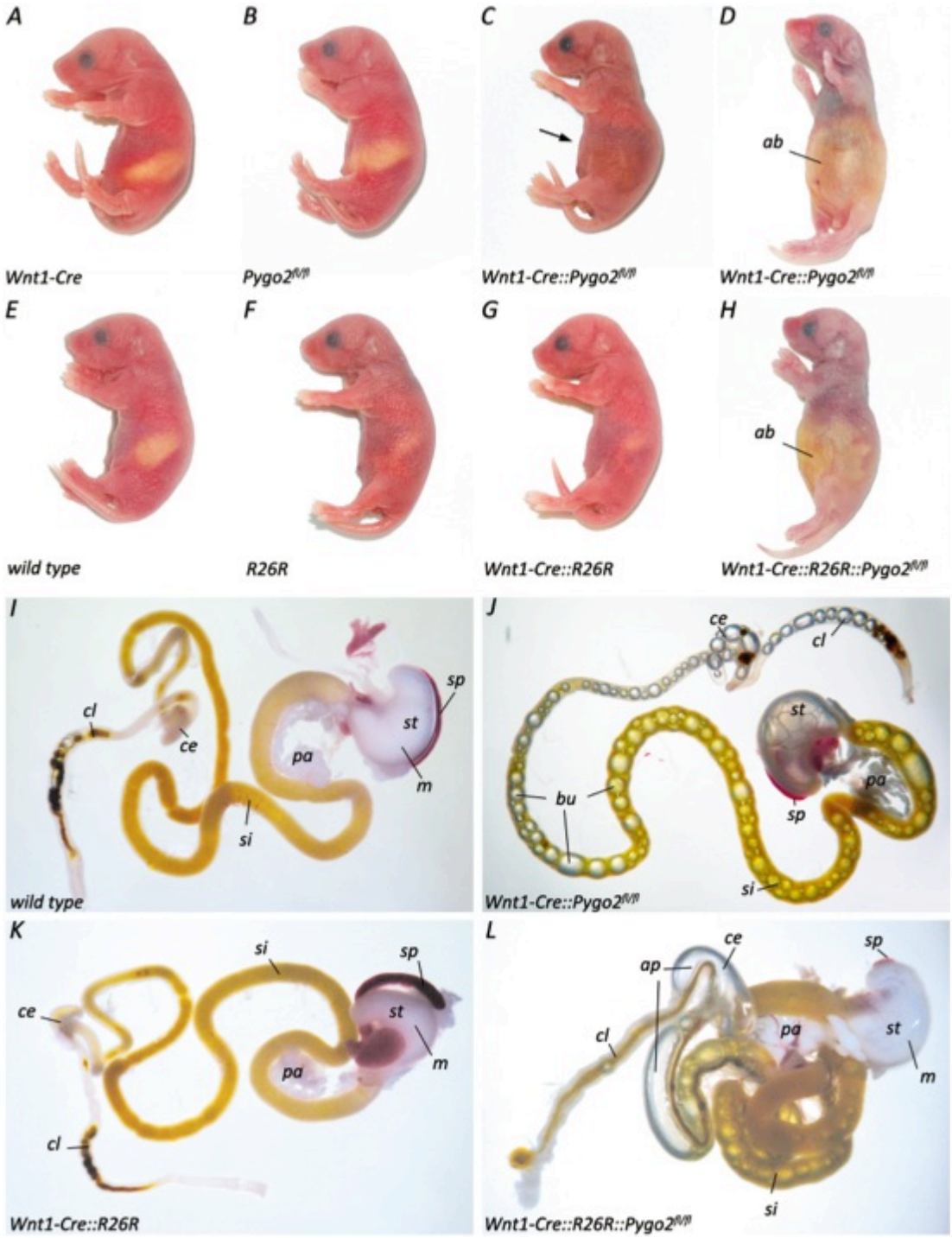

Figure 4-9. Phenotype of newborn mice after Wnt1-Cre mediated inactivation of Pygo2
Lateral view of neonatal transgenic pups (A-H). Both double (D) and triple (H) *Pygo2* CKO develop abdominal bloating (a) or gastric torsion, and this is usually accompanied by gasping respiration and eventually death. Abdominal bloating manifests shortly after birth as bubbles within the GI, sometimes visible through the abdominal wall (arrow). Dissected GI from wild type (I) and *Pygo2* CKO pups (J). Abdominal bloating is caused by large air pockets (ap) or bubbles (bu) within the GI. In some cases, evidence of prior feeding (m; milk in the GI) is also present. st, stomach; pa, pancreas; sp, spleen; si, small intestine; ce, cecum; cl, colon.

4.5.4 Reduction in skull length and calcification of the styloid process

Cranio-facial defects define all of the previous studies wherein mutants exhibit gasping respiration, abdominal bloating and perinatal death. The *Pax9* mutant fails to develop teeth, and shows clefting of the secondary palate [277,282]. Arginyltransferase (*Ate1*) and *Ryk* ('related to tyrosine kinases') *null* mice also develop defects in secondary palate formation together with abnormalities in bones of the skull [276,278]. Despite this, only a single *Pygo2* CKO pup was found with cleft palate in this study (see Appendix X).

Mice have six *Dlx* genes that are found as linked pairs within the genome (*Dl1/2*, *Dlx3/4*, *Dlx5/6*) [283]. CNCC that migrate along the first pharyngeal arch rely upon their expression to gather positional and patterning cues. For example, in mid-gestation, the *Dlx* genes are expressed in the maxillary (upper jaw) and mandibular (lower jaw) arches in a nested pattern along the proximodistal axis. For instance, *Dlx1/2* are expressed throughout much of the arch, while the expression of *Dlx5/*6 are restricted distally to *Dlx1/2* and *Dlx3/4* are further restricted distally to *Dlx5/6*. In this manner, they create a nested gradient of *Dlx* expression along the length of the pharyngeal arch [284].

In many of the *Dlx* mutant studies, the primary phenotypes reported include exencephaly and a range of defects in bones of the skull [275,279,285-288]. Some of these are hypoplastic and ectopic transformations of bones in the middle ear (styloid, incus, stapes, timpanic ring) and nasal bones, homeotic transformations of upper jaws into lower jaws, and loss of parietal (skull) bones. In addition, other cranio-facial abnormalities included primary and secondary cleft palate, alongside defects in the hyoid and thyroid cartilage of the throat. In all cases, these phenotypes culminated in death of the mutant together with abdominal bloating. Thus, these studies provide evidence that abdominal bloating may be caused either through a palate defect, or abnormalities in the bones and cartilage of the head and neck.

To determine if the NC derived bones and cartilage of the head and neck were affected in the *Pygo2* CKO pups, skeletal preparations were produced utilizing the Alcian blue and Alizarin red staining technique (described in Chapter 2).

Using this protocol, whole skeletons are prepared, with ossified bone staining red and cartilage staining blue following an alkaline clearing of soft tissues. As Figure 4-10 shows, *Pygo2* CKO pups develop the normal complement of bones and cartilage in the spine, rib cage and limbs. This is an expected result as NC contributes to bone and cartilage of the head and neck only. Interestingly, the skull appeared smaller in the Wnt1-Cre::Pygo2$^{fl/fl}$ pups when compared to control and wild type littermates.

To quantify this reduction, the total length of the skull from the nasal bone to the occipital bone, and the skull height, from the sphenoid to the parietal/frontal bone were measured, similar to previous descriptions [289]. In addition to the length and height, the mandible length was also measured. In the Wnt1-Cre::Pygo2$^{fl/fl}$ pups, both the skull and mandible mean lengths are reduced. This was found to be statistically significant using ANOVA, skull length, ($F(3,37) = 7.418$, $P = 0.00015$) and mandible length ($F(3,37) = 6.147$, $P = 0.0017$).

Using Tukey's multiple comparison test (post-hoc), a significant difference between the Wnt1-Cre::Pygo2$^{fl/fl}$ and controls was also seen in skull length and mandible length. While there was an apparent trend for a reduction in skull height as seen in Figure 4-11, no significant difference between the means was found using ANOVA, ($F(3,37) = 1.228$, $P = 0.31$).

A closer inspection of the skull revealed another two related phenotypes, not previously reported in either *Pygo1/2* null study. Firstly, within the cartilage of the middle ear, unilateral or bilateral calcification of the styloid process was observed in 7 out of 12 (58%) *Pygo2* CKO studied (3 bilateral). Calculi were observed in all pups that died prior to collection. Additionally, elongation of the styloid process was observed in nearly half of those with Calculi (3/7). Importantly, the styloid process is NC derived [290,291] and abnormalities can lead to symptoms of pain and discomfort in swallowing [292,293]. In humans, calcification of the styloid process is associated with Eagle's syndrome and been reported to cause stroke through compression of the carotid arteries [294].

The stapes was also found fused to the styloid process (see Figure 4-10) in 4 out of the 7 *Pygo2 CKO* pups found with calcification of the styloid process. The dual *Dlx5/6 null* mouse also develops defects in the styloid ligament [285] and this model led to the discovery that the *Dlx5/6* genes, together with *Dlx1/2,* regulate the expression of Pou3f3 [283]. *Pou3f3* is a member of the class III POU family of transcription factors and is specifically expressed within the CNS [295]. Intriguingly, the *Pou3f3 null* mouse develops a fused stapes and styloid process [283], a rare phenotype replicated by the Wnt1-Cre specific deletion of *Pygo2* in this study. In corroboration with this finding, the *Dlx* family of genes regulate both Pou3f3 and Wnt1 and may suggest an interaction between the Wnt pathway and Pou3f3 in formation of the stapes and styloid process [283,296].

Furthermore, the *Noggin* knockout mouse also develops a fused stapes and styloid process. And again, Noggin is a downstream target of the *Wnt* pathway, providing further evidence that *Pygo2* is required in a context dependent manner for appropriate Wnt signaling.

Given the observation that cranio-facial defects lead to abdominal bloating in other NC mutant models, and together with symptoms of Eagle's syndrome, it is likely that the calcification of the styloid process is the primary cause of gasping respiration and ultimately death in the *Pygo2* CKO pups. This assertion is supported by the close mortality rate (60%) and frequency of the styloid calculi found in *Pygo2* CKO pups (58%). Additionally, no mean difference was seen in body length of *Pygo2* CKO, and so it is unlikely that the shorter skull length is due to the pups being smaller (Section 4.5.2). Furthermore, it is possible that the shorter body length (~10% reduction) seen in the *Pygo2 null* mice reported by Li *et al.* (2007) [116] was primarily due to a shorter skull length.

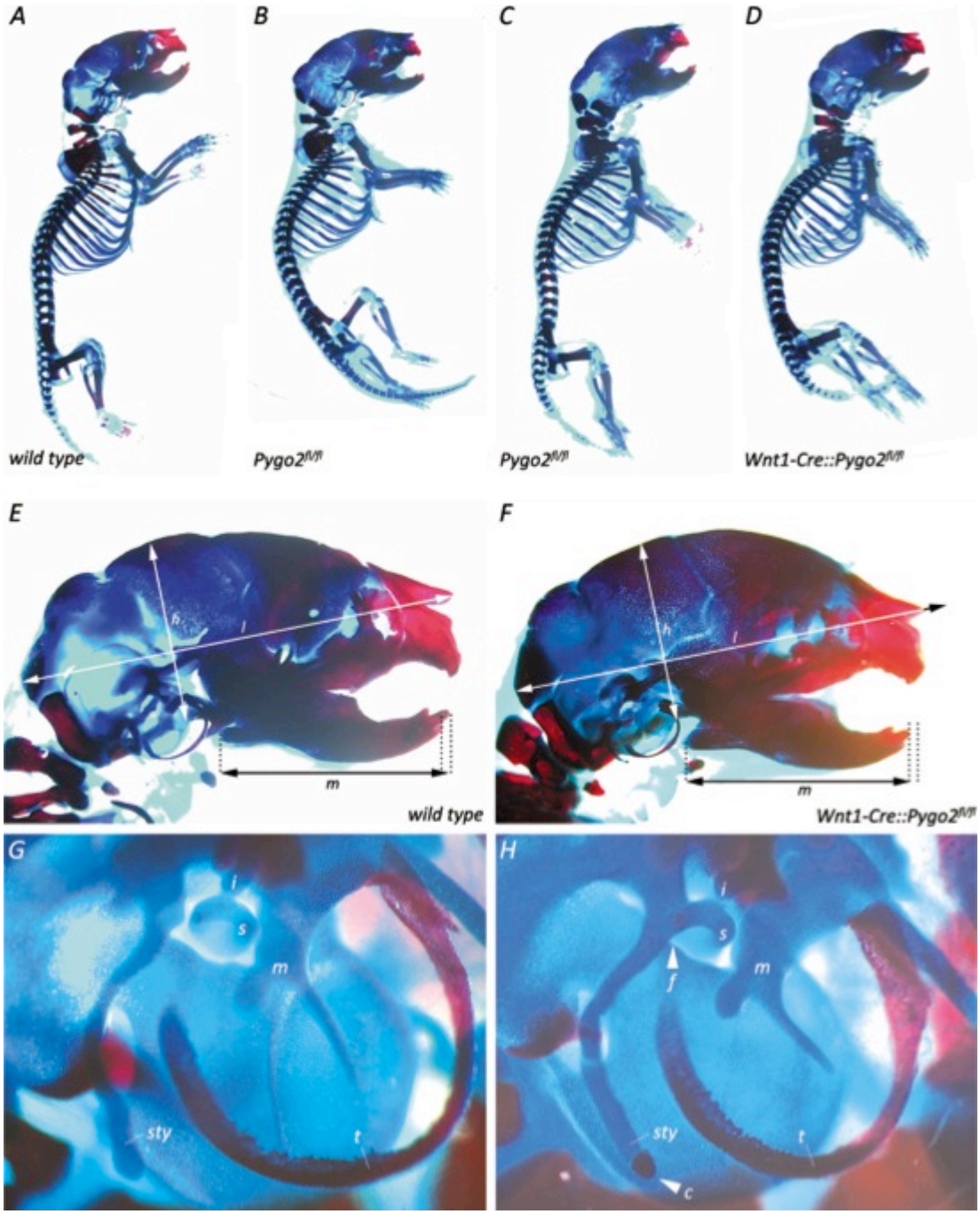

Figure 4-10. *Pygo2* CKO display a reduction in skull length together with calcification of the styloid process and fusion of the stapes

Alcian Blue staining of cartilage (& connective tissue) and Alizarin Red S staining of ossified bone in skeletal preparations from wild type (A), Wnt1-Cre (B), Pygo2$^{fl/fl}$ (C), Wnt1-Cre::Pygo2$^{fl/fl}$ (D) neonatal pups. Panels E and F display cartilage and bone of the middle ear enlarged from A & B (boxed regions). Calcification of the styloid process is indicated in H (c) and fusion of the stapes (f). Example measurements of skull length (l), skull height (h) and mandible length (m) are indicated in E,F by arrows.

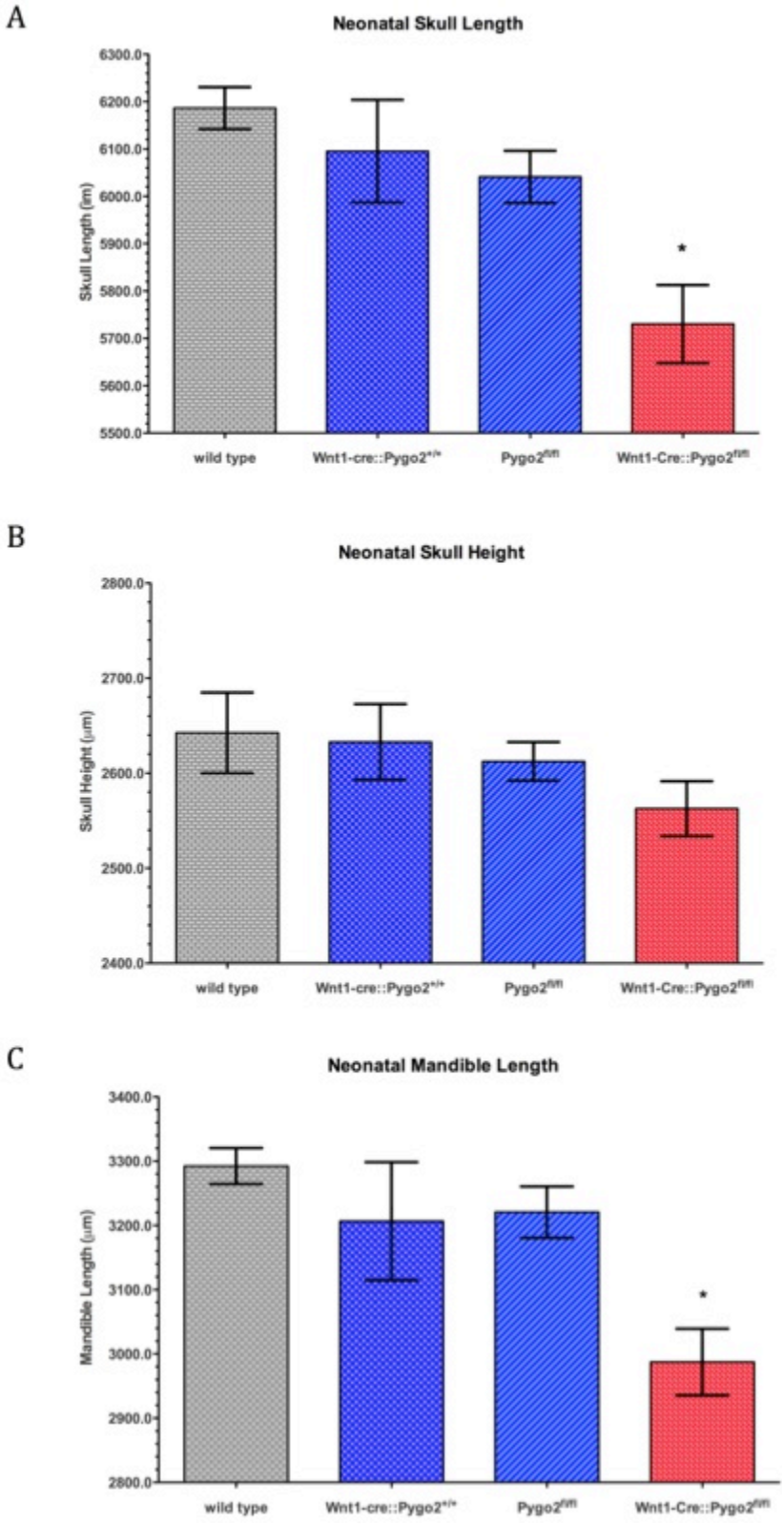

Figure 4-11. Skull and mandible length are significantly reduced in *Pygo2* CKO newborn pups
Bar charts representing the mean length from morphometric analyses of newborn skulls. Standard error (SEM) for each genotype is marked by error bars and statistical significance by an asterisk (*).

4.5.5 Reduced NC cell density in the colon

In line with the postulate that the abdominal bloating may be caused by excessive swallowing or abnormal gut motility, the contribution of NC in the GI was investigated. The NC is solely responsible for colonizing the GI during development and forming the enteric nervous system (ENS). The ENS provides motor innervation to the mucosal layers of the GI tract. A lack of neurons in the GI can cause obstruction through a failure of the colon to relax. Hirschsprung's disease is an example of this, and results from a failure of NC to migrate and correctly form neurons in the colon [69,297].

To test whether there is evidence for aganglionic colons in *Pygo2* conditional knockout pups, β-gal staining of colons was performed in a manner similar to Section 4.4.1. As Figure 4-12 shows, the *Pygo2* CKO pups exhibited a reduction in the intensity of β-gal staining. Thus indicating fewer NC derived neurons are present within the ENS of Wnt1-Cre::R26R::Pygo2$^{fl/fl}$ pups. In addition, the reduction in cell density incorporates the entire length of the GI, including the stomach, small intestine, cecum and colon.

In order to measure the loss of neurons in the colon, image quantification was performed on colour photographs by thresholding pixel intensity values with ImageJ software. Briefly, GI tracts were dissected from newborn pups, fixed and stained following the X-gal protocol. The contents from the lumen of the GI often stained positive for β-gal activity, and in some instances this led to non-specific staining of the mucosal layer. To combat this, GI tracts were routinely cut longitudinally and flattened; the contents and mucosal layer were scraped away to remove non-specific background stain. Once the GI contents and mucosal layer had been removed, wild type GI tracts showed no staining with X-gal. While many of the *Pygo2* CKO GI tracts were initially distend with air (see Section 4.5.3), they returned to an apparent normal size following this procedure. Thus, no obvious difference was observed between control and *Pygo2* CKO GI length, or area.

With this method of quantification, the area covered by positive X-gal staining in the *Pygo2* conditional knockouts was reduced by 43% compared to control

levels, represented in Figure 4-13. Using an independent-samples t-test, the difference between areas stained in Wnt1-Cre::R26R::Pygo2$^{+/+}$ (M=73%, SEM=12, n=8) and Wnt1-Cre::R26R::Pygo2$^{fl/fl}$ (M=42%, SEM=9.1, n=9) colons was found to be significant; t(2.1)=15, p=0.0271. Whilst needing further confirmation, this is consistent with the phenotype and further suggests lack of neural proliferation within the GI or of the progenitor population of neurons.

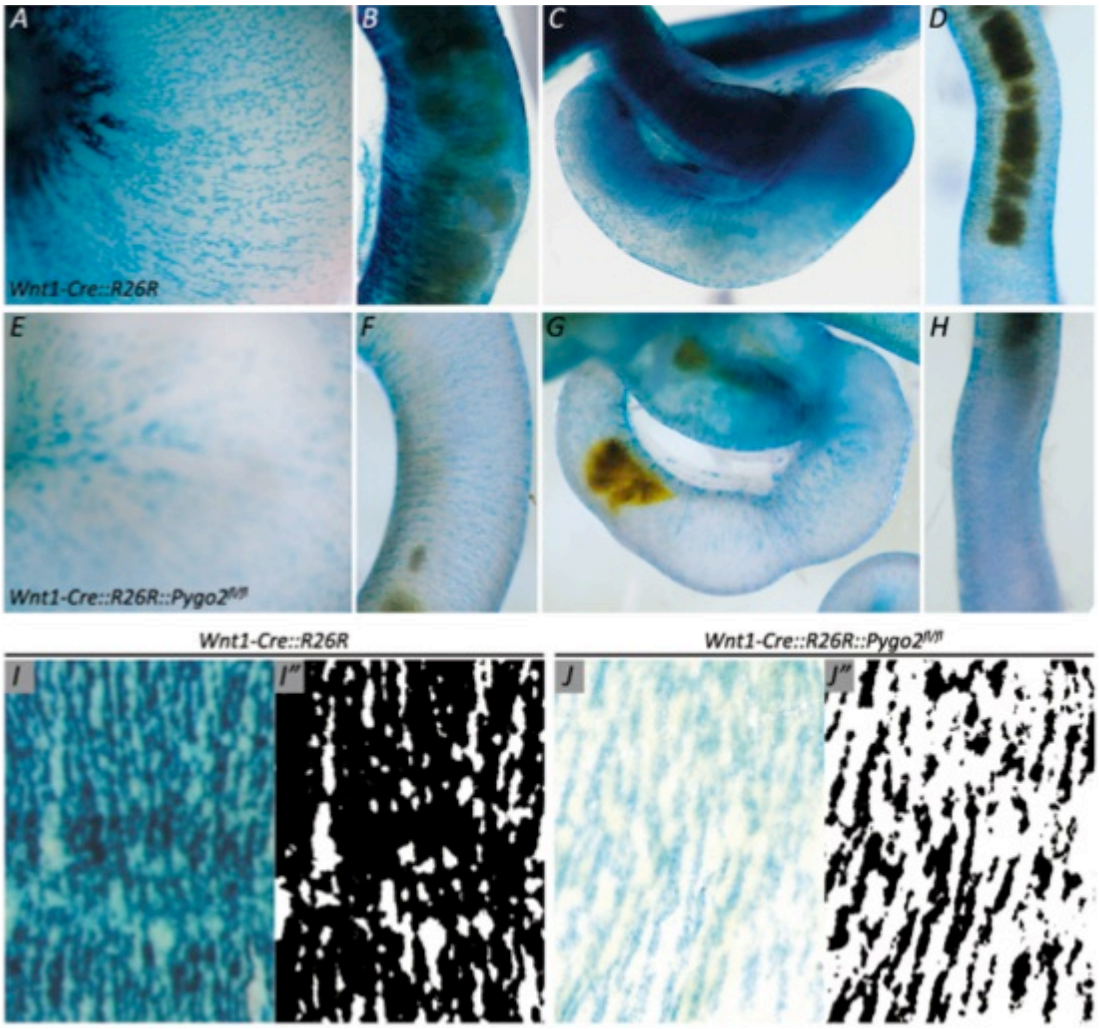

Figure 4-12. Reduction in NCC density within the GI tracts of *Pygo2* CKO neonatal pups
X-gal staining of control (A-D, I) and *Pygo2* CKO (E-H, J) GI tissue reveals a reduction in the intensity and area covered by the staining reaction. A reduction is apparent the entire length of the *Pygo2* CKO GI, including the stomach (A,E), the small intestine (B,F), the cecum (C,G) and the colon (D,H). The area and intensity of the stain is assumed to be directly proportional to the number of NC derived neurons present in the tissue. To quantify the density of neurons in the colon, ImageJ software was used to calculate the area stained, after applying a colour threshold (I", J") to acquired images (I, J). Area calculated to be X-gal positive is displayed in black versus the unstained area in white.

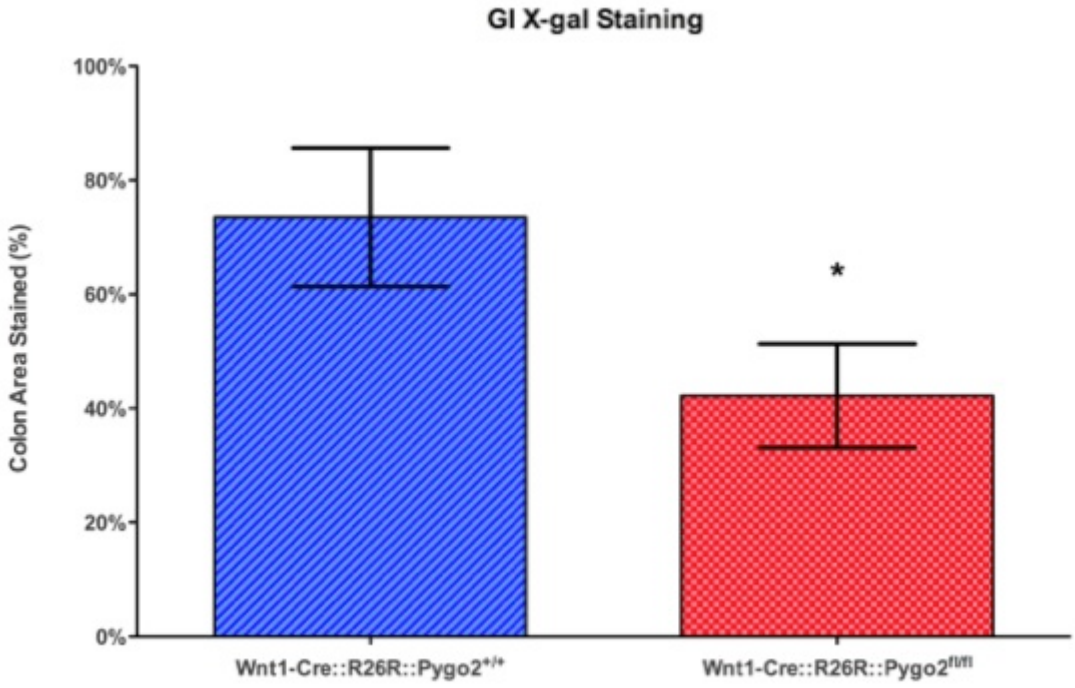

Figure 4-13. Neuronal cell density is reduced in the colon of *Pygo2* CKO neonates
Pygo2 CKO pups display a 43% reduction in the density of NC derived cells within the colon. The reduction in staining area was significantly reduced in Wnt1-Cre::R26R::Pygo2$^{fl/fl}$ (M=42%, SEM=9.1, *n*=9) versus Wnt1-Cre::R26R control animals (M=73%, SEM=12, *n*=8); t(15)=2.1, p=0.0271.

4.5.6 Loss of Pygo2 in a Wnt-1 specific manner leads to cardiac hypertrophy

The NC is important in mammals for two aspects of cardiogenesis. NC contributes to (1) patterning the pharyngeal arches and its derivatives, the aortic arch, and coronary arteries and (2) septation of the cardiac outflow tracts (OFT) by forming the outflow septum, and the arterial and atrioventricular valves [19,298-300]. Consistent with these two roles, mutagenesis and ablation of NC in chick and mouse models provide two major categories of cardiac defects: absence of OFT septation and alignment defects. For example, persistent truncus arteriosus (PTA) is defined by a lack of outflow septum. While double outlet right ventricle (DORV) defects often form a normal outflow septum, but are misaligned over the right ventricle [301,302]. However,

disruption of normal CaNCC processes leads to a spectrum of related cardiac and aortic arch artery defects of variable severity (reviewed in [20,303-305]).

These disruptions may include autonomous and non-autonomous insults directly to the NCSC population, their migration or differentiation. For instance, the *splotch* mutant (*Pax3*) fails to develop outflow septation (PTA) yet cardiogenesis is completely unaffected in a Wnt1-specific deletion of *Pax3* [306]. This suggests that *Pax3* is required for NC morphogenesis in the progenitor population of NCSC prior to Wnt1 expression, but not in subsequent migration nor OFT septation. Thus, Conway et al. (2000) conclude that the conotruncal malformations in the *splotch* mutant are due decreased NCSC expansion [306,307].

Yet Wnt1-mediated deletion of *Hand2* (Heart and neural crest expressed derivatives 2), causes misalignment of the aortic arch arteries and outflow tract, provoking development of DORV and ventricular septal defects (VSD) [308]. *Hand2* is expressed within the primary and secondary heart fields and CaNCC. However, this result suggests that CaNCC contain multiple sub-populations required for distinct functions in cardiogenesis.

Aside from the heart and vasculature, the NC is also critical for formation of the cardiac plexus, forming the neurons and supporting cells of the cardiac ganglia that innervate the heart [19]. While NC is not thought to form the conductive system of the heart, a loss of NC does influence the definitive conductive system [309]. This raises an interesting possibility that functional defects observed in NC ablated embryos may involve the cardiac plexus and the central and peripheral conduction system. This is primarily because abnormal myocardial function occurs in NC ablated embryos, long before the stage when septation occurs [310,311].

To identify if any cardiac abnormalities appear in *Pygo2* CKO mice, 16 newborn hearts (8 controls hearts, Wnt1-Cre::R26R::Pygo2$^{+/+}$ & 8 Pygo2 CKO hearts, Wnt1-Cre::R26R::Pygo2$^{fl/fl}$) were sectioned in coronal or transverse planes (4 of each genotype per plane). While these sectioned hearts showed no gross

abnormality in the cardiac plexus, pulmonary valves, OFT or ventricular septation, they did present with thicker ventricle walls and thickening of the ventricular septum (see Figure 4-14).

Again, using ImageJ software, photomicrographs of the sectioned hearts were measured and cell nuclei counted. The ventricular walls were separated into the compact and trabecular layers as shown in Figure 4-14, and measurements were taken from 8 serially aligned sections at the midpoint of the plane of section. Additionally, the number of nuclei per 1 000μm^2 was counted from 8 random regions along the ventricle walls.

As Figure 4-15 demonstrates, it was found that trabeculae from both left and right ventricles, and the septum were significantly thicker (9-17%) in the Wnt1-Cre::R26R::Pygo2$^{fl/fl}$ than the Wnt1-Cre::R26R control hearts. This was also reflected in an overall increase in the total width (9%) of the heart, even with a 19% reduction in the right ventricle space. The compact cell layers were largely unchanged, along with the overall height of the heart. While there was no change in the number or density of cells within the ventricular walls, the overall cardiac volume was increased, suggesting there must be an increase in the number of cells within the myocardium. This suggests the thickening in ventricle walls and septum may be due to hypertrophy or hyperplasia processes during cardiogenesis.

The NC does not contribute to the myocardium of the ventricle walls and so it is likely the thickening of trabeculae is a secondary effect. Hypertrophy is generally regarded as a compensatory mechanism to increased load, or pathology [312,313]. However, *in utero* hypertrophy is often preceded by hyperplasia in mouse and rat models of cardiomyopathy [314-316]. Curiously, NC ablation leads to poor contractility, adversely affecting cardiac function before NC dependent septation and patterning occurs [310,311,317]. However, the trigger for this remains unclear. Despite this, myocyte hypertrophy and contractility are intrinsically linked [318,319]. Thus the *Pygo2* CKO mouse may provide an ideal model to further investigate the role of NC disruptions causing functional defects in cardiogenesis.

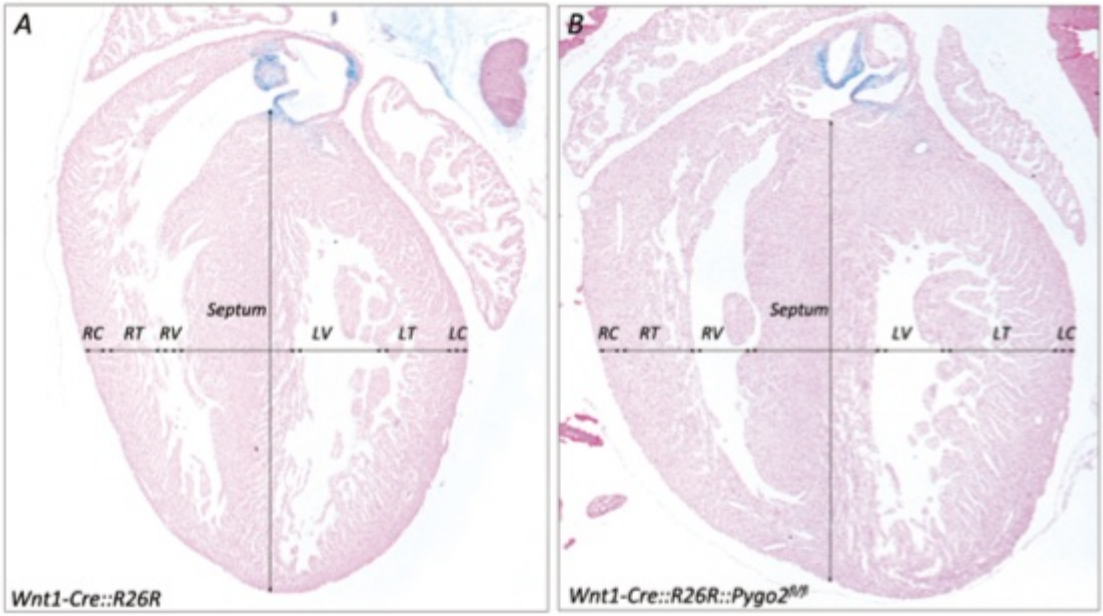

Figure 4-14. *Pygo2* CKO hearts exhibit thickened ventricle walls and cardiac septum
Coronal sections of Wnt1-Cre::R26R control (A) and *Pygo2* CKO (B) newborn hearts stained with X-gal and counter stained with nuclear fast red. Morphometric analysis of hearts measured the cardiac height from the apex to the pulmonary pole. The outer ventricular walls were separated into the right compact cell layer (RC), right trabeculae (RT), left trabeculae (LT) and left compact cell layer (LC). RV = right ventricle; LV = left ventricle.

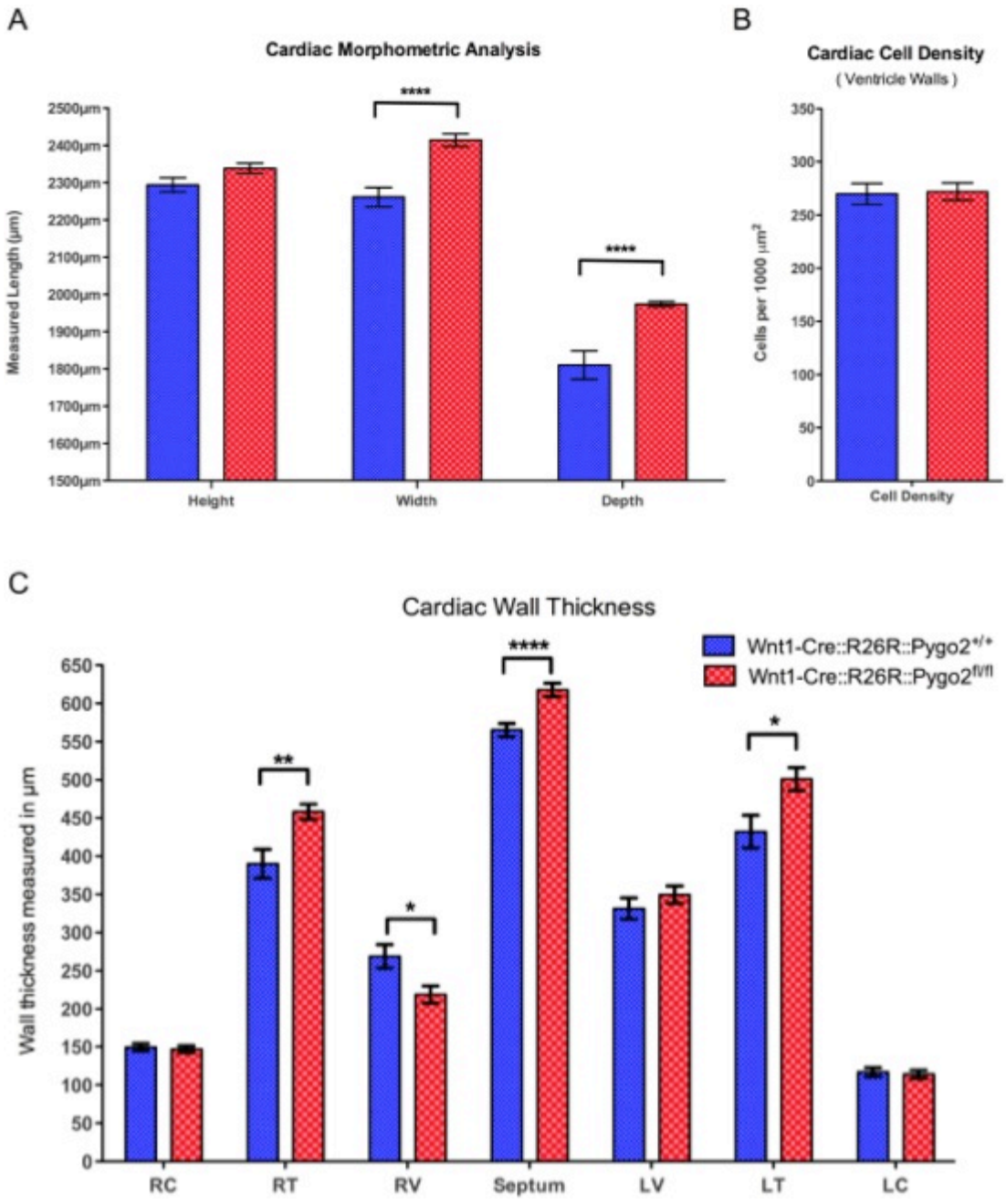

Figure 4-15. Morphometric analyses of newborn hearts reveals both hypertrophic and hyperplastic defects

Bar charts representing the morphometric analyses of the newborn hearts reveal a significant increase in cardiac width and depth. Cell density in the ventricular walls is unchanged. Significant increases in the trabeculae of the right and left ventricles (RT, LT) together with the septum contribute to the overall increase in heart size. The increase in size, together with an unchanged cell density, suggests newborn hearts are hyperplastic. Error bars denote SEM. Statistical significance is indicated by an asterisk (* = $p<0.05$; ** = $p<0.01$; *** = $p<0.001$; **** = $p<0.0001$).

4.5.7 The respiratory system is morphologically normal and is innervated by the NC in Pygo2 CKO neonates.

The circulatory system and the respiratory system are physiologically linked. Thus it is possible the cardiac thickening observed previously, may be associated with a lung or diaphragmatic defect, leading to increased arterial stress. In addition, the gasping respiration phenotype observed in *Pygo2* CKOs may also indicate a problem within the airways or lungs of neonatal pups. In support of this, Li et al (2007) observed defects in branching morphogenesis within the lungs of Pygo2 null mice [116]. For these reasons, lungs and diaphragms were investigated to identify if any respiratory involvement exists in the *Pygo2* CKO phenotype.

Maekawa *et al.* (1999) studied the ATF-2 knockout mouse model that displays various parallels to this study [320]. Primarily, neonates died shortly after birth and presented with gasping respiration. However, it was discovered that their lungs were filled with meconium. While the gasping phenotype is similar to what is observed in the *Pygo2* CKO pups, there was no abdominal bloating reported in their study. Nevertheless, in an attempt to identify if the lungs of *Pygo2 CKO* neonates were filled with fluid or air, they were subjected to a floatation test. In a manner similar to Maekawa *et al.* (1999), newborns lungs were floated on PBS to determine this fact. All lungs tested (n = 6) from both control and *Pygo2* CKO pups floated easily in PBS suggesting that the airways were clear of fluid and patent. Importantly, 4 out of the 6 *Pygo2* CKO lungs were from pups exhibiting abdominal bloating.

Previous studies of the *Pygo2 null* mouse have shown a marked decrease in the size of the newborn lung, with the airways terminating in smooth walled cylindrical alveoli, together with an increase in interstitial tissue. This was suggested to be similar to other mouse models in which the Wnt pathway had been inhibited [116]. In contrast to this earlier finding, *Pygo2* CKO lungs were of comparative size to controls, and histological analysis showed no change in the morphology of terminal alveoli (n=8; see Figure 4-16). Thus, it is likely that the

defect observed by Li *et al* (2007) represents a NC independent function of *Pygo2*.

This finding is not unexpected, given that the lung is derived from an outgrowth of endoderm forming the gut, and the only contribution by NC is the intrinsic innervation. This has recently been highlighted in both mouse and human lungs, where NC derived neurons have been found supporting the smooth muscle of the bronchi [321-324]. As Figure 4-16 demonstrates, *Pygo2* CKO have a normal distribution of neurons in the branching airways. Specifically, NC derived cells closely associated to the bronchi were found in both control and *Pygo2* CKO lungs across the entire length of the lungs studied (*n*=8).

Finally, to assess whether the respiratory system is defective in *Pygo2* CKO newborns, the structure and innervation of the diaphragm was investigated. The diaphragm is critical for breathing. During inhalation, contraction of the thoracic diaphragm increases the thoracic cavity volume, leading to a lowering of the intra-thoracic pressure, and subsequently drawing air into the lungs. Adopting a similar methodology as previous studies in this chapter, diaphragms from neonatal pups were dissected and stained with X-gal to detect NC derived cells expressing β-gal. Again, no gross defect was observed between the *Pygo2* CKO and control diaphragms in terms of structure or NC contribution (see Figure 4-16).

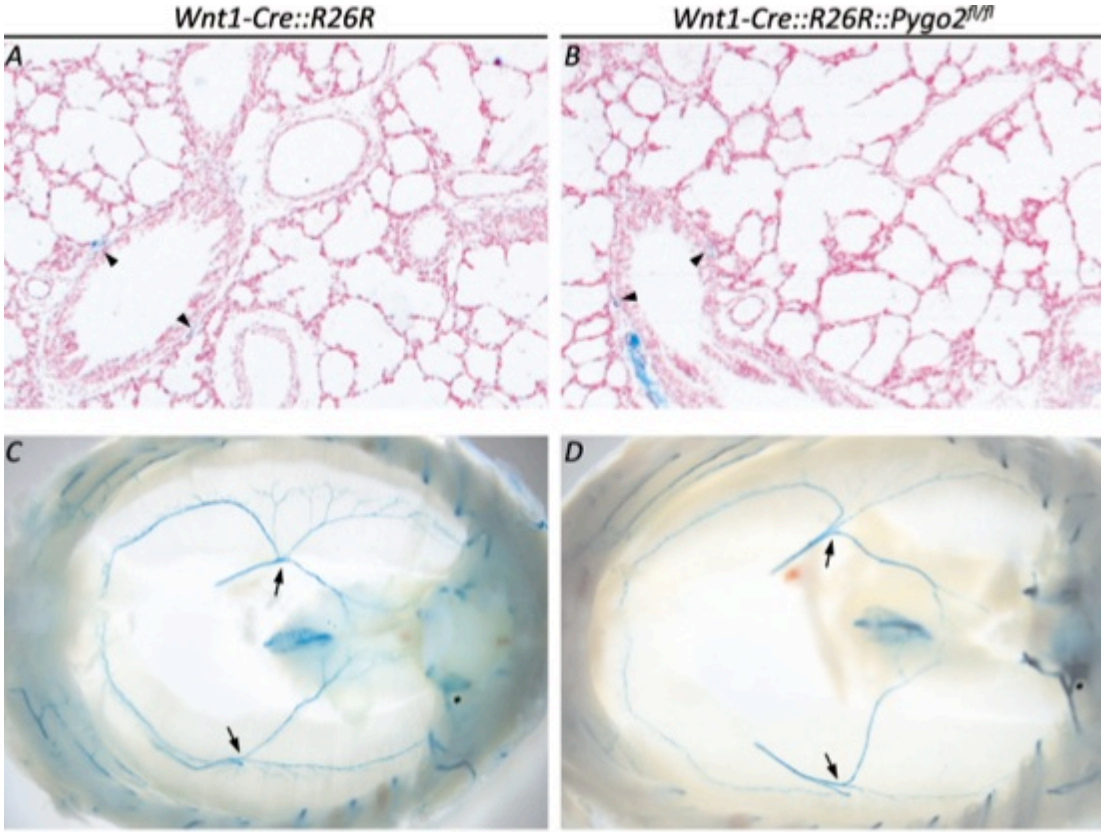

Figure 4-16. The structure and NC contribution to the lung and diaphragm is normal in *Pygo2* CKO
Transverse sections through control (A) and *Pygo2* CKO (B) lungs stained with X-gal and counterstained with nuclear fast red. NC derived neurons are found supporting the smooth muscle of the bronchi (arrowheads). Development and innervation of the diaphragm is normal, comparing control (C) and *Pygo2* CKO (D) diaphragm and phrenic nerve (arrows).

4.5.8 Abnormal hair follicle development in Pygo2 CKO mice

To date, NC derived cells have been found within the bulge and dermal papilla of the hair follicle, sensory neurons, and basement membrane of the skin [45]. Within these locations they form glia, melanocytes, and Merkel cells [325]. Although, the correct ontology of Merkel cells still remains controversial [325,326]. In addition to these differentiated cell types, the bulge and dermal papillae also contain multiple stem cell populations, amongst numerous other progenitor populations [327] and at least one of these stem cell niches is of NC origin, namely EPI-NCSC (see Chapters 1 & 5).

Intriguingly, *Pygo2* highly is expressed in the skin, in particular within the developing hair follicle. Li *et al* (2007) found that *Pygo2 null* mice were born with a 30% reduction in hair follicles, including many that were developmentally delayed. In light of this, and given that *Pygo2* is a signature gene of EPI-NCSC, there exists the possibility of a similar defect in the *Pygo2* CKO newborns. To address this idea, skin samples from the back of newborn mice were collected for morphometric analysis. In total, samples from 3 Wnt1-Cre::R26R::Pygo2$^{+/+}$ and 3 Wnt1-Cre::R26R::Pygo2$^{fl/fl}$ were processed for histological staining and subsequent image quantification using ImageJ software.

Using micrographs of longitudinal sections stained with H&E, follicle numbers were counted per mm^2 of tissue as a measure of follicle density. At the same time, the area of each follicle was measured to ascertain follicular size or thickness. *Pygo2* CKO newborn skin displayed a significant reduction in hair density (18%), control (2.7 ± 0.11 n=33) versus *Pygo2* CKO (2.2 ± 0.09 n=31); $t(62)=3.153$, $p=0.0025$. The reduction in density was observed together with a significant reduction in follicle area, control (458.0 ± 6.9 n=676) versus *Pygo2* CKO (429.3 ± 7.9 n=575); $t(1249)=2.745$, $p=0.006$. This reduction in area may be directly correlated to a reduction in follicle thickness, approximately 5% as illustrated by Figure 4-17 and Figure 4-18.

The skin of mice produces four major hair types contributing to the adult coat, plus many specialized hairs such as the vibrissae of the whisker pad [328]. The formation of hair follicles is induced in three successive waves with specific patterning giving rise to each hair type [329]. The primary hairs (guard hairs or tylotrichs) are first induced by the expression of *Edar* in the placode and *Eda* in the non-placodal ectoderm around 14.5 dpc [330]. While the induction of the primary hairs is uniquely dependent on *Eda/Edar* expression, secondary and tertiary hair formation still requires their expression later in morphogenesis for appropriate determination of hair type. For example, mutations in *Eda/Edar* lead to a loss of guard hairs, yet secondary and tertiary placodes improperly form only awl-like hairs [328,331,332].

The second wave occurs at 16-17.5 dpc in a process requiring *Noggin* and *Troy* expression that produces the awl hair type [333]. Interestingly, skin grafts from *Noggin* knockout embryos onto SCID mice develop primary placodes, but development is halted at this stage [334]. This suggests that while *Noggin* is not required for primary hair patterning, it is required for their continued development. The Wnt pathway gene *Lef1* is a downstream target of Noggin. *Lef1* knockout mice form primary placodes, yet lack secondary and tertiary hair formation [335]. Interestingly, β-catenin expression is required by all hair types, yet the dependence on *Lef1* expression is unique to the formation of awls and tertiary zig zag hairs.

Finally the formation of tertiary hair types again requires Noggin and subsequent Lef1 expression at 18 dpc to P1. In contrast to secondary hairs, the over expression of Edar prevents the bending and further maturation of zig zag hairs, although *Eda/Edar* expression is still required [336-338]. The formation of the fourth hair type, the auchenes, occurs during either the secondary or tertiary wave of induction in a process that is yet to be determined.

In summary, the morphogenesis of hair follicles requires a finely balanced interplay across subsequent waves of gene expression. Each wave of expression induces distinct hair type formation. At birth or P0, the neonatal skin contains multiple hair types in differing stages of morphogenesis. These stages are well described by Paus *et al* (1999). Importantly, this raises the possibility that the loss of *Pygo2* expression, a transducer of the Wnt signal, may play a part in the formation of a specific hair type. Intriguingly, awls account for approximately 30% of the adult coat, with the remainder composed of zig zags (65-70%), guards (1-3%) and auchenes (0.1%). Thus, a simple explanation for the loss of follicles would be from a failure of appropriate Wnt signaling to induce either awl or zig zag hair formation.

To investigate this possibility in the *Pygo2* CKO pups, cross sections of neonatal skin from 3 control, and 3 *Pygo2* CKO neonates were sectioned, stained and analysed. Follicles were staged from multiple photomicrographs containing approximately 300 follicles (in total), according to the methodology described

by Paus *et al* (1999) [164]. For each photomicrograph, two different people applied the staging criteria, in a randomized blind manner.

A significant difference in the relative number of follicles was revealed between stages 3 and 4 (see Figure 4-18). There are fewer *Pygo2* CKO follicles in stage 4, and surprisingly more in the less developed stage 3. This result is more consistent with a general delay or arrest in the development of tertiary hairs, rather than a specific loss of any particular hair type. If for example, there were a loss or reduction in the number of awl hairs, this would presumably be reflected by a reduction in the later staged hair follicles and relatively little or no change in the number of earlier staged follicles.

The reduction in stage 4 follicles is likely to represent reduced numbers of the more mature tertiary hairs. Yet, this is accompanied by an increase in stage 3 follicles, suggesting the reduced number of stage 4 follicles is due to a delay rather than an actual loss. Interestingly, this may also suggest an arrest in development of these tertiary hairs. However, this remains unclear due to the inability to study follicle maturation after birth.

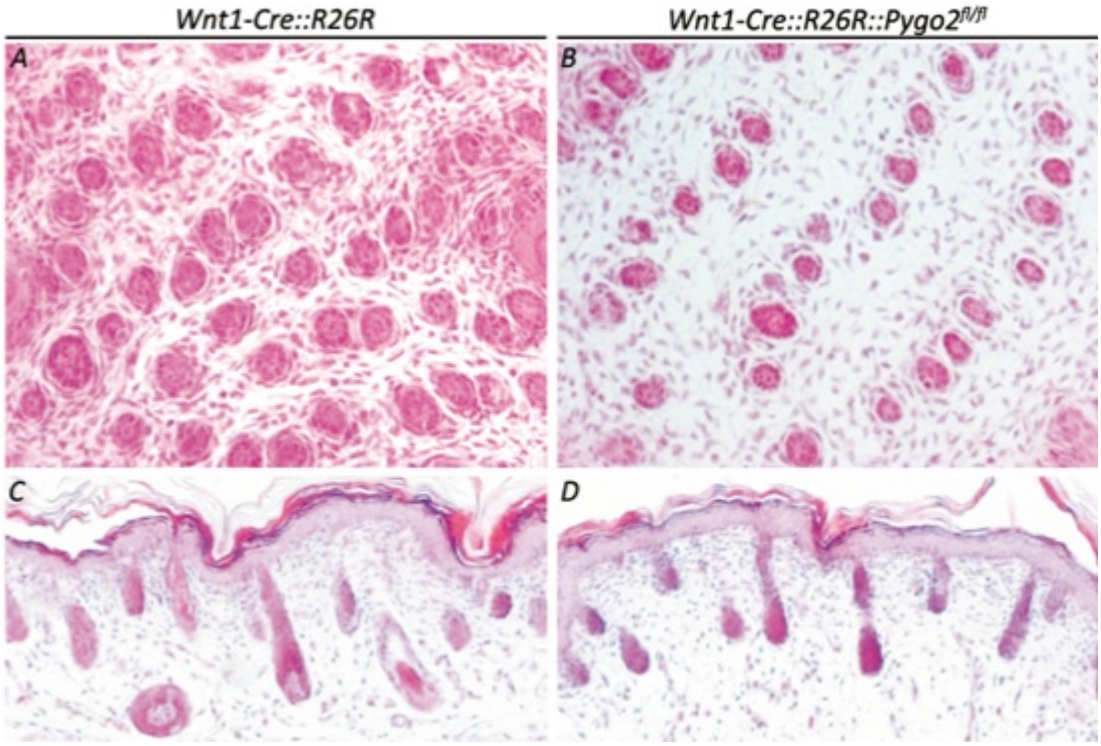

Figure 4-17. Abnormal pelage follicle morphology in *Pygo2* CKO newborn back skin
H&E longitudinal sections of neonatal back skin from control (A) and *Pygo2 CKO* (B), reveals significant reduction in hair follicle density and thickness. Similarly, cross-sections of control (C) and *Pygo2* CKO (D) back skin display fewer, less developed follicles.

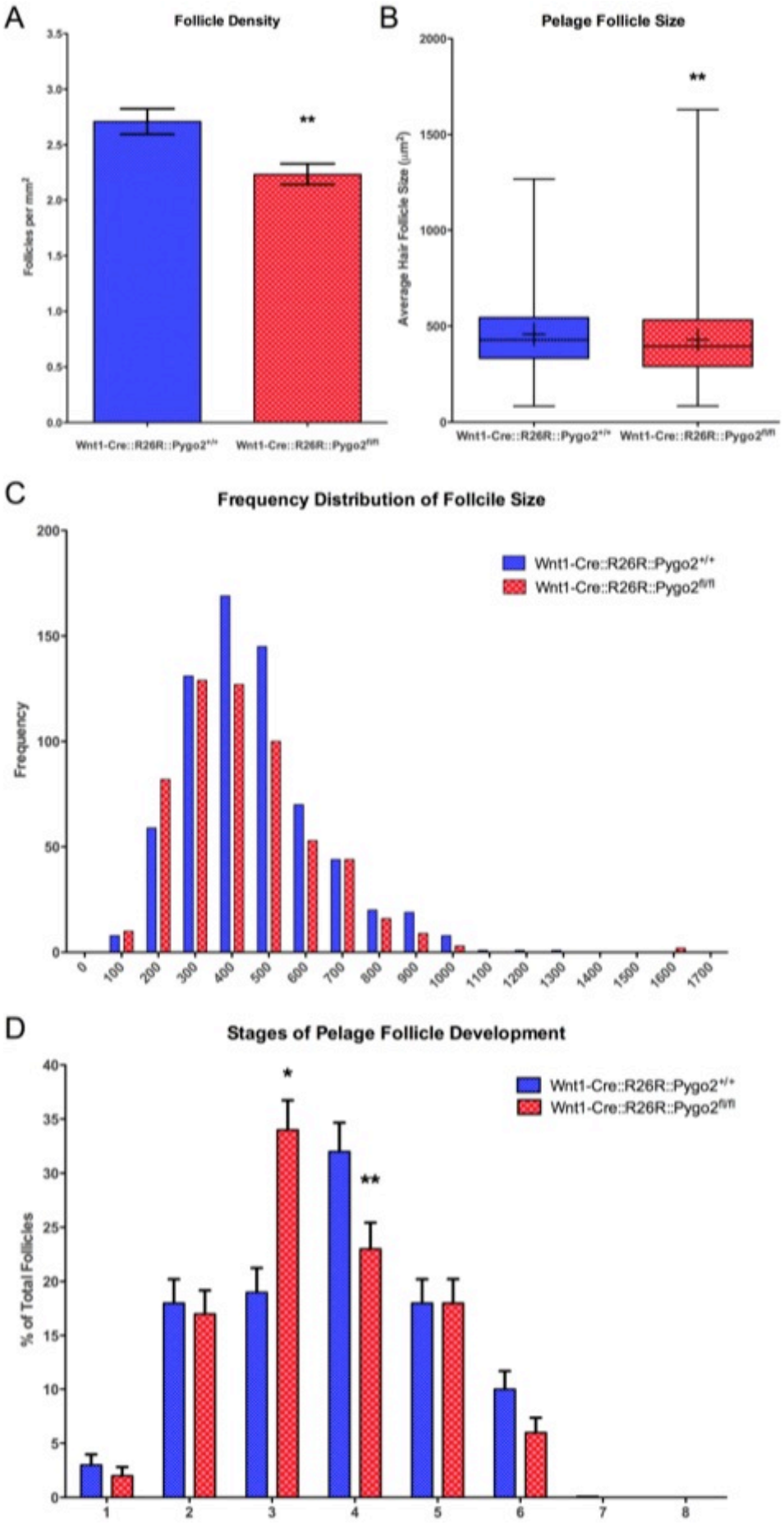
A
Follicle Density
Follicles per mm²
3.5
3.0
2.5
2.0
1.5
1.0
0.5
0.0
**
Wnt1-Cre::R26R::Pygo2+/+
Wnt1-Cre::R26R::Pygo2fl/fl
B
Pelage Follicle Size
Average Hair Follicle Size (μm²)
2000
1500
1000
500
0
**
Wnt1-Cre::R26R::Pygo2+/+
Wnt1-Cre::R26R::Pygo2fl/fl
C
Frequency Distribution of Follcile Size
Frequency
200
150
100
50
0
Wnt1-Cre::R26R::Pygo2+/+
Wnt1-Cre::R26R::Pygo2fl/fl
0
100
200
300
400
500
600
700
800
900
1000
1100
1200
1300
1400
1500
1600
1700
D
Stages of Pelage Follicle Development
% of Total Follicles
40
35
30
25
20
15
10
5
0
*
**
Wnt1-Cre::R26R::Pygo2+/+
Wnt1-Cre::R26R::Pygo2fl/fl
1
2
3
4
5
6
7
8

Figure 4-18. Morphometric analyses of pelage follicle development
Hair follicle density is significantly reduced in *Pygo2* CKO neonates by 18% (A). Average follicle size (B) as a measure of area is also significantly reduced by 5% in *Pygo2* CKO. (C) Histogram of follicle sizes illustrating a shift in medium sized follicles towards the smaller sizes. Stage 4 of hair follicle development (D) are delayed in *Pygo2* CKO pups, with more follicles in stage 3 than controls.

4.5.9 Pygo2 CKO develop hydrocephaly and display a reduction in the number of neurons in the trigeminal mesencephalic nucleus

As most of the CNS is derived from the neural ectoderm (neural tube), the presence of a phenotype in the brain of *Pygo2* CKO newborns is not surprising. In this study, *Pygo2* CKO neonatal brain displayed an enlargement of the cerebral aqueduct together with a reduction in the number of NC derived neurons in the mesencephalic trigeminal nucleus (Me5).

The brains of *Pygo2* CKO newborns were investigated for a number of reasons. Firstly, the reduction in follicle density and size seen in the previous study may be linked to a requirement for *Lef1* in hair follicle induction and maturation. Given that, *Pygo2* binds to TCF/Lef at the transcriptional level, a loss of *Pygo2* may phenocopy aspects of the *Lef1* knockout. Loss of function studies by Van Genderen et al. (1994)[335] on Lef1 also described a loss of the Me5 in addition to defects in the hair follicles. The loss of Lef1 was associated with an inability to feed properly, and may also be linked to the gasping phenotype of *Pygo2* CKOs. And finally, the Me5 is largely viewed as being of NC origin [339,340].

Results from quail-chick chimaera studies, and in embryonic mice have provided evidence for the assertion that the Me5 is derived from the NC [341-343]. However, this has been challenged by studies where there was a lack of responsiveness to nerve growth factor, and NC markers in cluding HNK-1 and Ap-2α [344,345].

The trigeminal nerve is responsible for innervation in the head and neck, providing motor innervation for mastication or suckling reflexes [346]. The

central processes of the nerve are distributed to three sensory nuclei, namely the spinal tract nucleus, main sensory nucleus and the Me5. However, the cells bodies that co-ordinate biting, suckling, mastication and dietary behavior are found specifically within the Me5 [162]. The neurons of the Me5 are large, round to ovoid shaped, unipolar cells [347]. In previous studies, Burns and Delalande (2005)[322] have shown that NGFR p75 may be used to label cells of NC origin. Taking these two points together with the likely NC origin of Me5 neurons, and the Atlas of Brain development [348], the presence of Me5 neurons was investigated in control and *Pygo2* CKO newborn brains. Three separate techniques were utilized.

Firstly, Nissl bodies of both neurons and glia were stained (Cresyl violet) on coronal sections (Figure 4-19). A reduction or loss of the Me5 was observed in all three *Pygo2* CKO studied. Secondly, antibody staining of the nerve growth factor receptor p75 (NGFR p75) was also used to identify the Me5 location. NGFR p75 is a transmembrane glycoprotein that binds nerve growth factor and other neurotrophins [349]. It is vital for neuronal growth, differentiation and cell death, and is primarily expressed in neurons and Schwann cells. Stemple *et al* (1992) have previously used NGFR p75 to successfully identify cells of NC origin and the Me5 [47,322]. Finally, X-gal staining was also used to identify the Me5, being of NC origin (Figure 4-19).

All three techniques showed either a reduction or a near loss of the Me5 in *Pygo2* CKO newborn brains, illustrated in Figure 4-19 & Figure 4-20. It is also interesting to note the widespread expression of β-gal in both control and *Pygo2* CKO brain, visualized with X-gal staining. However, it is important to reiterate that within the CNS, the expression of Wnt1 is not limited to the NC, but may also include cells derived from the dorsal neural tube, especially within the midbrain boundaries (see Chapter 1).

In order to quantify the perceived reduction, the number of cells, and the area of each Me5, from 3 images of each genotype were measured. Statistical analysis showed a significant reduction in both the number and area of Me5 neurons in *Pygo2* CKO mice (Figure 4-20). Hence, although a Wnt1-specific inactivation of

Pygo2 does not cause a complete loss of the Me5, it did result in a significant reduction (28%) in the number of *Pygo2* CKO neurons (13 ± 0.89, *n*=9) compared to control (18 ± 1.7, *n*=9); t(16)=2.5, p=0.0237. In addition, using ImageJ software to automate the measurements, gave a significant reduction (40%) in *Pygo2* CKO Me5 area (3613 μm^2 ± 502.7 *n*=9) when compared to control samples (2137 μm^2 ± 316.5 *n*=9); t(16)=2.48, p=0.0245.

In addition to the reduction in the Me5, an enlargement of the cerebral aqueduct was observed (see Figure 4-19). This enlargement was consistent in all *Pygo2* CKO animals examined and extended from the fourth ventricle through to the third ventricles. The cerebral aqueduct also known as the aqueduct of Sylvius, is a channel in the mesencephalon connecting the third and the fourth ventricles. Together these form the ventricular system that is continuous with the central canal of the spinal cord and harbors cerebrospinal fluid (CSF), which cushions the central nervous system. In addition to the cerebral enlargement, a reduction in the space between the brain and the skull plate, was observed as illustrated in Figure 4-19.

This enlargement or hydrocephaly, may be due to defective tight junctions between the choroidal epithelial cells responsible for maintaining the blood CSF barrier [350]. In addition, the choroid plexus is responsible for secretion of CSF into the ventricular space [351]. Moreover, these cells lining the ventricles and the cerebral aqueduct possess cilia that maintain the proper flow of CSF in the central nervous system. While it is not known if these cells are of NC origin, they do express Wnt1 during development accounting for the intense stain seen in Figure 4-19.

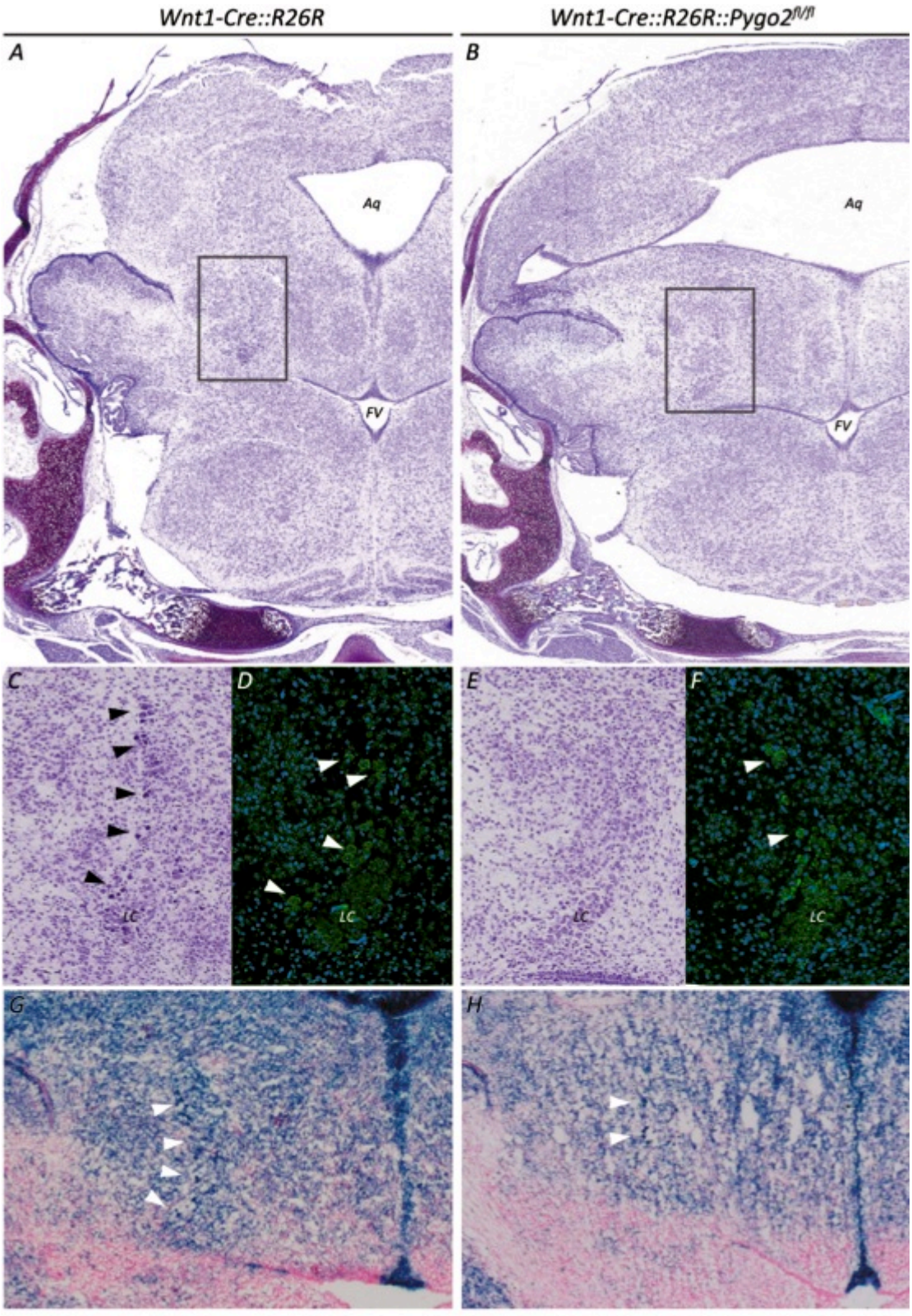

Figure 4-19. Reduction in the NC derived neurons of the Me5 within *Pygo2* CKO brain
Coronal sections through the mid-brain of control (A) and null (B) neonatal pups. Sections A, B, C and E are stained using Cresyl Violet to view Nissl bodies and nerve-cell constituents. (A) *Pygo2* CKO pups show an enlargement of the cerebral aqueduct (Aq) when compared to control littermates (*n*=3). Analysis of the Me5 using Nissl stain (C, E), NGFR p75 antibody (D, F), and (G, H) X-gal staining of NC derived tissue. Arrowheads indicate neurons of the Me5 region (C-H) and illustrate a significant reduction (28%) in the number of neurons in *Pygo2* CKO Me5 versus control littermates (*n*=9).

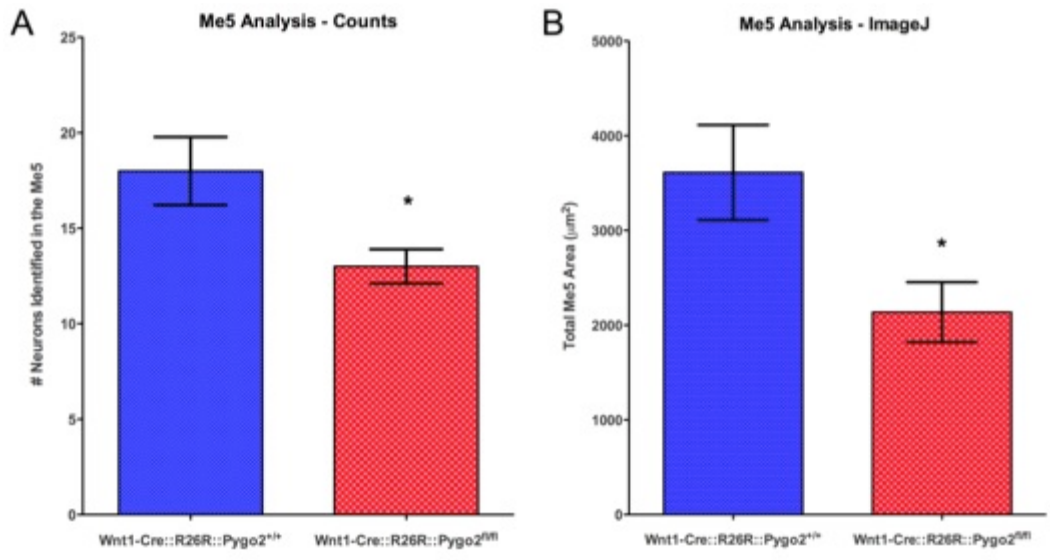

Figure 4-20. Significant loss of neurons in the Me5 of *Pygo2* CKO neonatal brain
The reduction in Me5 neurons was quantified by counting individual neurons from photomicrographs of the Me5 (A) and using ImageJ software to automatically acquire the area of Me5 staining (B). In both cases, significant reductions of between 28% and 40% were observed in *Pygo2* CKO Me5 neurons.

4.6 Rare *Pygo2* CKO survivors display cranio-facial abnormalities

Due to the high level of mortality seen in neonatal pups, the majority of studies conducted during this project were on neonatal *Pygo2* CKO pups. However, in rare cases, *Pygo2* CKO pups survived past weaning into early adult maturity (<10 weeks), before being sacrificed for analysis.

Three females and one male mouse were studied for possible phenotypes. Bearing in mind that 60% of neonatal pups die within the first 24 hours, it is likely that survivors will present with a lessened phenotype and represent a partial penetrance of many of the previously described *Pygo2* CKO phenotypes. Overall, the *Pygo2* CKO adults appeared normal and healthy. They were capable of independent feeding, and were housed without special care alongside littermates. However, in all cases, the *Pygo2* CKO mice were slightly lighter and shorter than their control littermates.

Interestingly, *Pygo2* CKO mice displayed a similar cranio-facial phenotype to the neonates. Their nose and jaws were shorter or stunted (see Figure 4-21). Despite these similarities to *Pygo2* CKO neonates, no defects in the styloid process or middle ear ossicles were observed.

However, as displayed in Figure 4-21, the upper and lower incisors of *Pygo2* CKO display a defect in appropriate tooth formation. Both upper and lower incisors are misaligned, shorter, and translucent, in a manner similar to dentinogenesis imperfecta (DI). DI is a hereditary disorder in which the teeth are unusually discoloured and translucent, and weaker, making them prone to rapid damage or loss [352,353]. The primary cause of DI is due to aberrant development of the tooth dentine in both primary and secondary dentitions. It is generally understood that the support tissue and the dentine, pulp, cementum and periodontal ligament, are of NC origin from NC lineage tracing using the Wnt1-Cre::R26R mouse model [253,354]. This is also supported by Di-I labeling studies in rat [355]. However, it has recently been proposed that NC also contribute to enamel formation [39].

With NC contributing to tooth morphogenesis and the observation of misaligned, translucent teeth in the *Pygo2* CKO adult, it is likely that these mice are lacking normal dentin. Intriguingly, mutations in *Dlx3* and *Msx2* lead to abnormalities in hair, bone and teeth, and the presentation of DI [356,357]. Given that newborn *Pygo2* CKO phenotypes described previously (section 4.5.4), are similar to other *Dlx* mutations, and *Msx2* is a signature gene of EPI-NCSC (see Chapter 1), this provides support for *Pygo2* having a role in NC tooth morphogenesis. Moreover, DI is commonly associated with hearing loss [352,358,359] and may be mechanistically similar to the styloid-stapes fusion seen in *Pygo2* CKO pups.

While DI and *Pygo2* CKO share a similar set of associated genes, the precise tooth defect in *Pygo2* CKO still remains to be identified. Whether it is in the dentin, the pulp or enamel, it is certainly NC derived. Unfortunately, with the rare occurrence of *Pygo2* CKO pups living to adult age, closer inspection of the

tooth structure, and the ultrastructure of the tooth defect, was outside the investigative scope of this project.

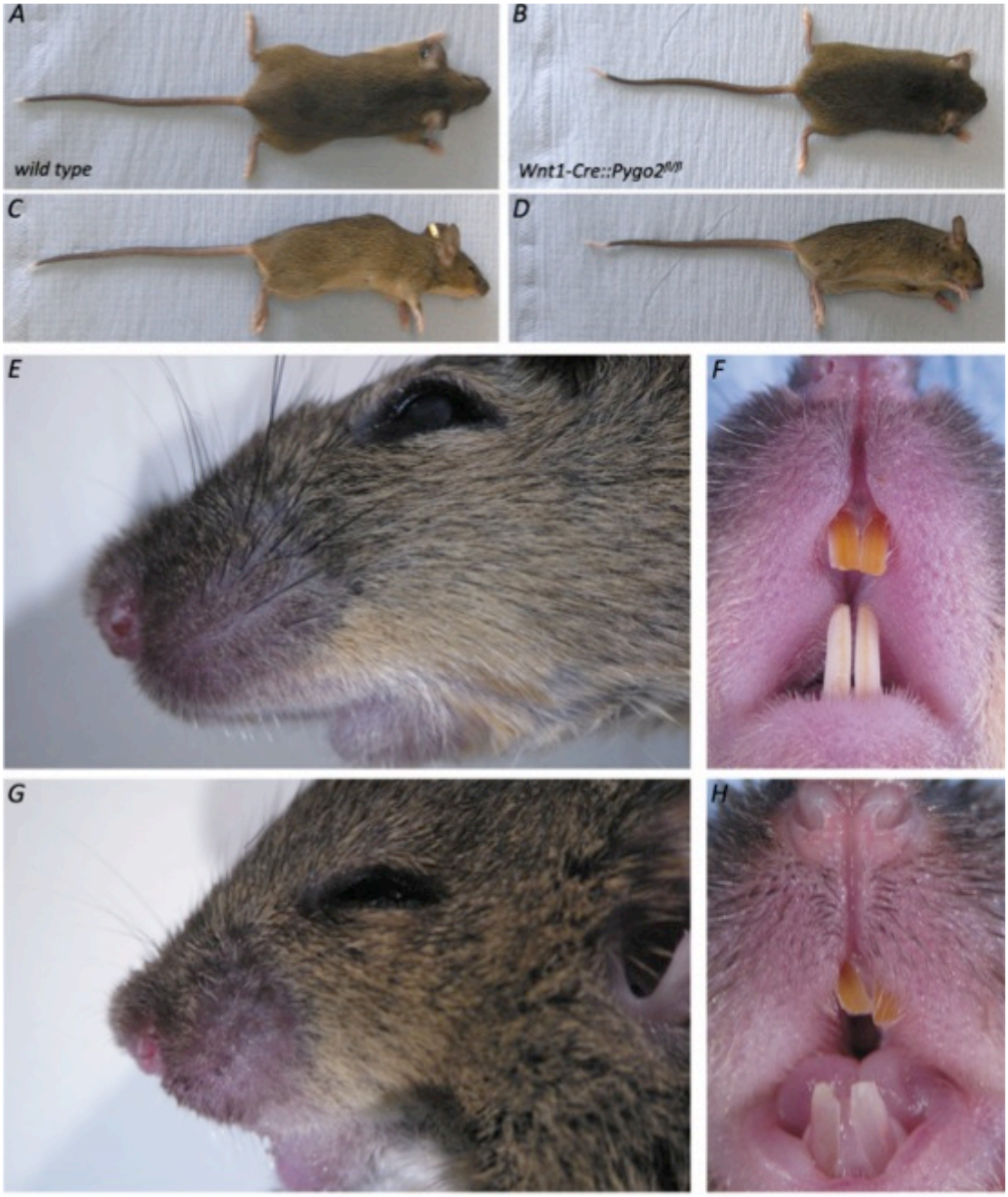

Figure 4-21. Pygo2 CKO adult mouse with shortened skull and jaw, together with abnormal incisors
Wild type (A, C, E, G) and a rare *Pygo2* CKO (B, D, F, H) adult mouse (10 weeks) from the dorsal (A, B) and lateral (C, D) aspect. *Pygo2* CKO are smaller than littermates and develop abnormal incisors, similar to dentinogenesis imperfect in humans.

4.7 Discussion

In this study, a triple transgenic mouse model was used to carry out a loss-off-function investigation into the role or requirement of *Pygo2* in murine NC development, whilst simultaneously marking the Wnt1 cell lineage. The Wnt1-specific knockout of *Pygo2* led to multi-organ birth defects in numerous NC derived tissues and organs. For most of these defects, it is the first time they have been reported in the context of *Pygo2* biology. Likewise, few of the defects reported in the *Pygo2* null (see Chapter 1) are present in *Pygo2* CKO. However, neonatal lethality and the reduction in hair follicle development do resemble those observed in *Pygo2 null* mice. Interestingly, this illustrates the pleiotropic nature of *Pygo2* in murine development.

The expression of *Pygo2* in the EPI-NCSC molecular signature provided the basis for the hypothesis that *Pygo2* is required for NC development. However, *Pygo2* CKO defects are quantitative rather than qualitative/absolute, for example recall the reduction in Me5, enteric neurons and bone morphogenesis of the skull. Similarly, the tissues described previously in the *Pygo2 null* also show mild abnormalities, such as reduced branching morphogenesis within the kidney [131].

There are a few possible reasons for this. Firstly, *Pygo1* may provide a 'rescue' in specific tissues. Although this is unlikely when presented with the evidence from the original *Pygo1/2* double knockout, only a handful of organs were analysed by Schwab *et al* (2007) [131]. Of particular note is the lack of heart analysis. A recent conference report citing Aguet *et al.* [360] reports OFT abnormalities in a separate double *Pygo1/2* knockout mouse model. Moreover, analysis of *Pygo1* expression by this study further supports the possibility of *Pygo1* functioning in place of *Pygo2*, within specific organs/tissues (see Appendix A). Taken together this suggests a Wnt1-specific deletion of *Pgyo1/2* may produce a more severe heart phenotype (similar to the OFT abnormalities reported by Aguet *et al.,* 2006.) together with other organ defects.

The background strain of mice provides an alternative explanation for the variation and penetrance in defects. This is particularly relevant when using a

triple transgenic model. Unknown modifier genes may be present in some strains that may affect the expression or function of *Pygo2*. For example, mouse models of *Wilms' tumour suppressor 1* (*Wt1*) exhibit variable phenotype penetrance, dependent upon the strain used. This can affect their fertility [361], development of the spleen and pericardium [271], and the presentation of diffuse mesangial sclerosis [362] and Denys-Drash syndrome [363,364]. Another extreme example of this is the targeted disruption of the *EGF receptor* (*Egfr*). Dependent on the strain used, the *Egfr null* mouse is lethal at pre-implantation, mid-gestation or 3 weeks after birth [272]. However, strain variance occurring through genetic drift is unavoidable, within inbred populations housed separately, or under differing conditions [269,270]. This may explain the high level of variance observed in the weight and length measurements between the various genotypes in this study, while also providing evidence for strain variance (compare R26R neonate body length to wild type and Wnt1-Cre genotypes; Figure 4-8).

It is encouraging to note that many of the abnormalities in the *Pygo2* CKO phenotype not only resemble other NC ablation models, but Wnt pathway knockout models too. As previously mentioned, many of the *Pygo2* CKO defects were not reported by the previous *Pygo2* null studies. Taken together, this may suggest a much closer association between the role of *Pygo2* and the NC than previously anticipated. However, this is not entirely surprising, given the crucial roles of the Wnt pathway in NC development (see Chapter 1).

The physiological effects of the *Pygo2* CKO include perinatal lethality, gasping respiration, abdominal bloating and the increased thickness of the ventricular walls and cardiac septum. It is likely these represent secondary effects and it is tempting to suggest they are functionally linked. The perinatal lethality is almost certainly due to the gasping respiration, together with the abdominal bloating. This is supported by the observation that all dead or dying *Pygo2* CKO pups have excessive air in their GI tract. A recent study by Turgeon *et al* (2009) reports that air in the GI tract can lead to death through an inability to feed within 12-24 hours of birth [365]. In contrast, for the vast majority of defects

analysed in the respiratory, circulatory or neuro-muscular systems, death was generally immediate or shortly after birth (<60 minutes).

This assertion raises the question of what causes the abdominal bloating. Calcification of the styloid process was identified in *Pygo2* CKO newborns with the proportion of styloid process defects being almost the same as the mortality rate. Thus, providing further evidence for this conclusion. The calcification of the styloid process is a cause of Eagle's syndrome in humans, and can often lead to compression of the carotid artery [294]. It is possible, that this may in turn lead to increased strain on the embryonic heart, triggering the compensatory combined hypertrophy and hyperplasia (see Section 4.5.6). An alternative possibility is that a delayed or aberrant morphogenic event leads to the increased workload. For instance, fewer CaNCC in the OFT may delay the normal septation event, and lead to the thickening of the cardiac walls and septum.

This possibility highlights a group of defects that may be due to abnormal proliferative processes. These include, the shortened skull and mandible, the reduction in neurons within the colon and Me5, the reduction in hair follicle number and size, and the possible lack of dentine in the incisors. Overall these defects could be attributed to a reduction in the size or number of NC derived cells. Irrespective of the mechanism, these tissues are lacking the normal complement of cellular mass. This may be analogous to the Pax3 mouse model in which a lack of proliferation in the NC progenitor pool, before migration, leads to various patterning defects in the heart [307]. It is possible this may represent a common mechanism in a subset of neurocristopathies. Interestingly the timing of Wnt1 expression may also be critical to the Pygo2 phenotype. It is possible that the variable phenotype of *Pygo2* CKO mice is due to a partial overlap of the temporal requirement for Wnt1 and Pygo2 in NCSC. If, for instance Pygo2 is required by NCSC close to the time when Wnt is first being expressed. This could lead to a defect in a portion of NCSC, and variable penetrance or severity. It would be interesting to test this possibility in a manner similar to Conway *et al* (2000), using alternative NC specific mouse Cre strains.

In summary, the aims of this chapter were to determine a role for *Pygo2* in NC and EPI-NCSC. While perinatal lethality of *Pygo2* CKO pups prevented a study in EPI-NCSC, a NC dependent role for *Pygo2* has been identified, together with multiple models of human diseases. These included a model for Eagle's syndrome, with calcification of the styloid process, and perhaps Hirschsprung's Disease, recalling the reduction of neurons in the colon. In addition, a NC ablation model for studying cardiac function, separate from conotruncal malformations has also been revealed.

Importantly, a unique role for NC in hair follicle development has been identified and further supports the important role of *Pygo2* in NC development. This finding represents an entirely novel aspect of NC and hair follicle development. Taken together, this study supports the central hypothesis of this thesis. In addition, it is tempting to speculate that *Pygo2* is required for normal NC development through regulation of proliferation in the embryonic NCSC pool prior to migration.

Chapter 5. The role of Pygo2 in EPI-NCSC migration, proliferation and maintenance

5.1 Introduction

Having described a number of *Pygo2* mutant phenotypes in zebrafish (see Chapter 3) and mouse (see Chapter 4), that strongly correlate to a defect in NC and Wnt signalling during development, an *in vitro* model was sought to further investigate the possible mechanism involved. Given that *Pygo2* has previously been shown to affect cellular proliferation [149,366,367], it was hypothesised that the process underpinning the phenotypes observed in zebrafish and mouse might also be related to aberrant cellular proliferation.

To this end, an *ex vivo* model was generated to investigate the role of *Pygo2* using EPI-NCSC cultures. Intriguingly, the loss of *Pygo2* had only a mild effect on EPI-NCSC proliferation within 7 days of culture, albeit in direct contrast to previous reports of *Pygo2* ablation leading to a suppression of cell cycling [135,149,367] and proliferation [144,149,261,367].

5.1.1 Stem cells of the mammalian skin

In early development, stem cells (SC) are found abundantly within the embryo. SC are essential for their innate ability to self-renew and provide specialised or differentiated cell types, required during embryogenesis. However, throughout the adult organism, SC become restricted to particular regions, thought to regulate their proliferation and differentiation [368-370]. Specifically, these regions or environments are often referred to as SC niches, providing a protective environment for slow cycling SC [371]. Ultimately, the role of the SC niche in the adult organism is to provide cells for maintaining homeostasis and regenerating tissues, following injury or damage.

The skin is in a constant state of regeneration. It constantly sloughs terminally differentiated keratinocytes from the surface, driven by frequent abrasive

forces [372,373]. The top layers of cells are flattened, anucleated, keratinised dead cells, which protect against dehydration, pathogens and form a semi-permeable barrier to the external environment. In this capacity, the skin is required to deliver rapid repair, in response to injury or damage. So it is not surprising that epidermis harbours numerous SC types, and multiple SC niches [374].

In mammals, skin consists of an upper stratified squamous epithelial layer, known as the epidermis, which sits atop the basement membrane and the underlying dermis. Interspersed laterally throughout the epithelium are numerous complex structures known as appendages. These appendages are generally found at regularly spaced intervals and include, hair follicles, arrector pilli (follicular muscles), sebaceous glands, sweat glands and nails [375]. While discrete stem cell niches have been identified in many appendages of the skin [376-378], the location of the primary epithelial niche still remains unclear [379]. It is thought that the basal epidermal cells, attached to the basement membrane, maintain the upward flow of differentiating keratinocytes [380,381]. However, studies of label retaining cells show that 95% of the infrequently cycling cells in the epidermis are found within the bulge of the hair follicle [382], suggesting that the bulge of the hair follicle may be the primary niche for resident skin stem cells.

The hair follicle bulge was first described more than 100 years ago [383]. It is an epidermal structure of the hair follicle, contained between the outer root sheath (ORS) and the inner root sheath. In this way, the hair follicle consists of layers, much like an onion, with the ORS, inner root sheath and the hair shaft in the centre of the follicle. The ORS is continuous with the epidermis and attached to the basal lamina [382]. However, the base of the hair follicle extends deeper, past the basal lamina, into the dermis. Here, a population of transit amplifying cells or matrix progenitors form a bulb that encases a cluster of mesenchymal cells, known as the dermal papilla (see Figure 5-1) [384,385].

Mature hair follicles undergo cyclic episodes of generation (anagen), destruction (catagen) and rest (telogen). During anagen, the hair shaft grows

from the dermal papilla, while the dermal papilla migrates downwards, deep into the dermis and subcutis [386]. Catagen begins after the anagen growth phase. The papilla detaches from the bulb and moves upward together with the shaft in a process of tightly co-ordinated apoptosis and cell differentiation prior to telogen [387]. At the beginning of telogen, the follicle does not extend much deeper than the uppermost portion of the dermis (see Figure 5-1). At this stage, the dermal papilla is extracellular matrix poor, and the club hair/shaft is now attached at the base to the ORS. At this point, the follicle maintains a resting period before the next anagen phase and loss of the club hair (exogen). However, the growth of a new hair shaft does not depend on exogen, as it is common for new hairs to grow before the old ones fall out. New hairs generally form from an outgrowth of the bulge region [388].

So throughout the hair follicle growth cycle, the dermal papilla is undergoing continual movement through the basal lamina and dermis, reshaping of the extracellular matrix, and proliferation and apoptotic processes within the bulb (refer Figure 5-1). Importantly, the movement of the dermal papilla in hair cycling, places the dermal papilla immediately below the bulge region at the beginning of anagen, and throughout telogen. Between the dermal papilla and the bulge populations, lays the secondary hair germ, which is thought to be where transit-amplifying cells are produced in the following hair cycle [389].

Early studies on the dermal papilla predicted it would be the permanent source of hair follicle stem cells. An assertion that is supported by the ability of dermal papilla cells to generate new follicles in transplantation assays [384,385]. Yet, during catagen, epithelial cells at the dermal papilla base undergo apoptosis, and the cells of the dermal papilla remain largely unscathed [390,391]. It is also thought that they do not generally divide [392], so it seems unlikely that they contribute directly to the resident SC population.

It is now believed that the bulge harbours the primary SC niche of the epidermis for two reasons. Firstly, as previously mentioned, the cells within the bulge are known to be slow cycling [382]. And secondly, the bulge contributes cells to the secondary hair germ prior to anagen. While the dermal papilla activates the

secondary hair germ, leading to the growth of a new hair shaft and downward movement of the dermal papilla [382], at the onset of anagen, both damage to the epidermis and normal hair cycling has been shown to stimulate migration of resident bulge cells, upward to the epidermis and downward to the dermal papilla [79,393,394]. It is likely these are, presumptive secondary hair germ cells migrating from the bulge during the transition from catagen to telogen, meeting the dermal papilla. These cells subsequently reside as a distinct population during telogen [389,395]. Moreover, bulge populations can give rise epidermis, hair follicles and sebaceous glands in transplants [394].

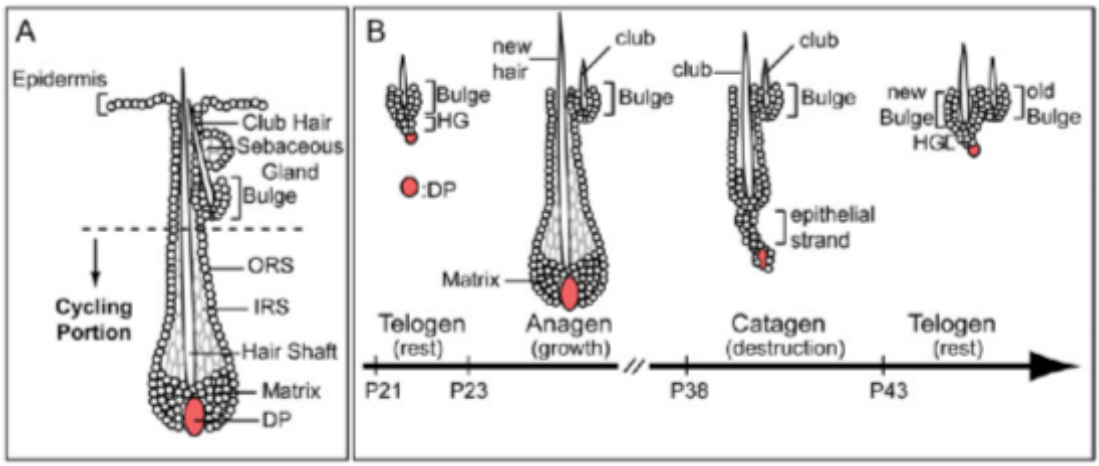

Figure 5-1. Structure of a hair follicle, showing the cycling and permanent portions
Following morphogenesis, the hair follicle enters continual cycles of growth, rest and destruction. (A) Structure of mature hair follicle during anagen, showing hair bulge and bulb with matrix cells surrounding the DP. The bulge region resides above the cycling portion, in the permanent portion of the hair follicle. (B) At P21 (postnatal day 21) in the mouse, all hair follicles are synchronised in telogen. During catagen, the matrix and DP regress towards the epidermis, where it remains throughout telogen, until the growth phase anagen. *Source: Pasolli, H*ilda *A. (2011)*[327].

5.1.2 Bulge populations of the mammalian hair follicle

The possibility of therapeutic applications based on SC derived from the skin [78,396] has led to increased interest in the hair follicle bulge niche, both in terms of the niche origin, and characterising the resident SC within. Despite this, it is still unclear how the niche is formed, where it originates and its exact composition. Recent evidence suggests that the ORS replenishes the bulge population during cycling [378]. However, it is clear that there are at least two distinct populations of SC within the bulge. While it is possible that these populations may derive from a common SC population, further characterisation of this niche is required to fully disseminate its components.

Blanpain *et al* (2004) have shown two distinct populations within the bulge, one in close contact to the basal lamina, and the other resting directly above it [374]. These populations were extracted and sorted using flow cytometry based on α6-integrin and $CD34^+$ expression. Subsequently it has been demonstrated these cells are multipotent, capable of self-renewal [374] and can give rise to multiple epithelial appendages [79,394,397,398].

Interestingly, $CD34^+$ is a marker of haematopoietic progenitor cells and is also expressed by another bulge SC population, known as nestin-expressing cells. *Nestin* (*Nes*) is generally a marker of neural stem cells, and the discovery of nestin-expressing cells has raised the possibility that some cells within the bulge may even be pluripotent [399]. *Nes* is also expressed by EPI-NCSC [75], found within the bulge, and skin derived precursors (SKP)[400], which are found exclusively within the dermal papilla [401]. Given that these cells share similar markers of cell identity [400], have both been successfully used in spinal cord and peripheral nerve injury models [400,402], and are both multipotent *in vitro* [401], it is difficult to deny that SKPs constitute the same SC population as EPI-NCSC.

Importantly a distinction may be made, by the manner in which they are derived. *Nes* and $CD34^+$ cells require *in vivo* labelling, and FACS (fluorescent activated cell sorting) to enrich *in vitro* cell populations. While SKP's are cultured from dissociated bulge cells and form spheres in culture [403,404].

Whereas EPI-NCSC emigrate from bulge explants as a highly pure population and do not require enrichment prior to harvesting.

5.1.3 Pygo2 may play a role in EPI-NCSC regulation

Previously a requirement for *Pygo2* in normal vertebrate development has been demonstrated with phenotypes exhibiting defects in NC related structures or tissues by others [123,131,163,261] and by this project (see Chapters 3 & 4). These defects are often suggestive of a developmental impairment in the proliferation or migration of the NC or progenitor population of cells. For example, the mouse model (*Pygo2* CKO) displays shorter bones of the skull, and this may reflect a failure of the mandible progenitor population to adequately drive extension through a dampened proliferative potential.

A role for *Pygo2* in regulating cell cycle, proliferation and cancer progression is also implied by *in vitro* studies (see Chapter 1). Briefly, *Pygo2* expression is up-regulated in breast cancer cell lines [136,144], is required for growth of ovarian cancer cells [147] and is a target of known tumour suppressor genes [405]. Furthermore, *Pygo2* is a signature gene of EPI-NCSC, enabling these multipotent SC to be identified from other SC within the bulge niche. The NC specific defects observed in newborn mice harbouring a deletion in *Pygo2*, together with those observed *in vitro*, suggest that EPI-NCSC (a NC derivative and *in* vitro cultured SC) may also rely on *Pygo2* expression for homeostasis.

5.2 Aims of the study

To further understand the basis for the defects observed in the zebrafish morphant and transgenic mouse models requires investigation of the molecular and cellular mechanisms involved. In turn, an in-depth understanding of the molecular interactions and function of *Pygo2* is required to determine an appropriate assay. However, the direct transcriptional targets of *Pygo2* still remain largely unknown, in addition to its requirement by the vertebrate Wnt pathway. Furthermore, with the possibility that *Pygo2* may be involved in Wnt independent processes (see Chapter 1), elucidation of the mechanism of Pygo2's action in these *in vivo* models remains difficult.

A suitable *ex vivo* model to utilise (in terms of biological relevance) would be EPI-NCSC harvested from the whisker follicles of a *Pygo2 null* mouse. However, the neonatal lethality observed in both the ubiquitous and the Wnt1-Cre specific *Pygo2* knockout models, prevents the isolation of EPI-NCSC from adult animals.

Embryonic NCSC, however, would not provide a suitable system for establishing an *ex vivo* model of *Pygo2* deletion. NCSC are difficult to culture for extended periods of time [406], resistant to transfection (genetic manipulation with transgenes), and are prone to spontaneous differentiation *in vitro* [46,406]. Primary cultures of NCSC are also highly heterogeneous and may further hinder or confound downstream assays.

With the attractive therapeutic potential of EPI-NCSC, it is essential that further characterisation of these cells is continued. Human EPI-NCSC already show great promise for usage in translational therapies, with directed differentiation into osteoblasts and dopaminergic neurons [72]. For example, differentiated EPI-NCSC may be useful in autologous transplants for simple bone fractures, or other defective repair mechanisms. Despite this, long-term cultures, bulk cellular expansion and genetic manipulation of these cells has not been attempted to date, in either mouse or human cultures. Importantly these procedures will need to be perfected before any possible applications are of clinical use in treating diseases like cancer, congenital defects or age-related pathology.

With this in mind, a suitable *ex vivo Pygo2* ablation model, utilising EPI-NCSC was developed to investigate the role of *Pygo2* in the maintenance, proliferation and migration of NC derived SC.

Specifically, the aims of this chapter were:

1. *Identify and develop an ex vivo model for the genetic manipulation of murine EPI-NCSC*
2. *Further characterise the culturing conditions of mouse EPI-NCSC ex vivo*
3. *Determine if Pygo2 functions in the migration of EPI-NCSC ex vivo*
4. *Determine whether Pygo2 plays a role in EPI-NCSC proliferation ex vivo*
5. *Determine if Pygo2 is required for maintenance of key EPI-NCSC marker genes expression ex vivo*

5.3 Experimental outline

In order to identify a model for the effective knockout of *Pygo2* in EPI-NCSC, a number of options were considered. These included targeted deletion or knockdown of *Pygo2* expression, in both a stable or transient manner. Firstly, gene knockdown may be achieved with RNA interference (RNAi) using shRNA (short hairpin-RNA)[407] or MO [408]targeted to the *Pygo2* mRNA transcript. However, these methods do not achieve a complete ablation of gene expression. In contrast, with access to the $Pygo2^{fl/fl}$ mouse strain (as described in Chapter 5), complete deletion of the gene, in a permanent manner was possible through the transient expression of Cre. While both methods rely upon efficient transfection, the targeted deletion of *Pygo2* with Cre is advantageous, compared to methods relying on RNAi as it can deliver a complete loss of function.

Following on from this, only standard transient transfection techniques were considered to identify the most efficient means of transiently introducing a transgene into EPI-NCSC. Whilst stable transfection methods like Lentiviral infection [409], or antibiotic resistance selection, can achieve very high levels of transfection in difficult-to-transfect cells lines, they often raise the significant issue of clonal variation amongst the cells being analysed – that is not such a problem with "transient transfection". Furthermore, circumventing the need for host DNA integration may also provide useful information concerning transfection methodology of relevance to future studies aimed at translation of

EPI-NCSC biology to the clinic. For this reason, human EPI-NCSC are routinely cultured within the laboratory using xeno-free (free of animal products) or GMP (Good Manufacturing Practice) compliant media and reagents [72]. In addition, stable transfection or methods based on genome integration take longer to develop and are ultimately more expensive.

In summary, to address the aims of this study, EPI-NCSC were harvested from Pygo2$^{fl/fl}$ mice. Cells were grown for 7 days, allowing them to emigrate from the bulge in culture, after which they were subsequently transfected with a Cre-GFP expression plasmid. This plasmid expressed a Cre-GFP fusion protein, to simultaneously remove *Pygo2* from the cell genome, and mark transfected cells through fluorescence of GFP. EPI-NCSC positive for Cre-GFP expression were isolated using FACS, and cultured for another 7 days. During this time, cells were assayed for their proliferation, migratory potential and maintenance of signature gene expression. This has been outlined in Figure 5-2.

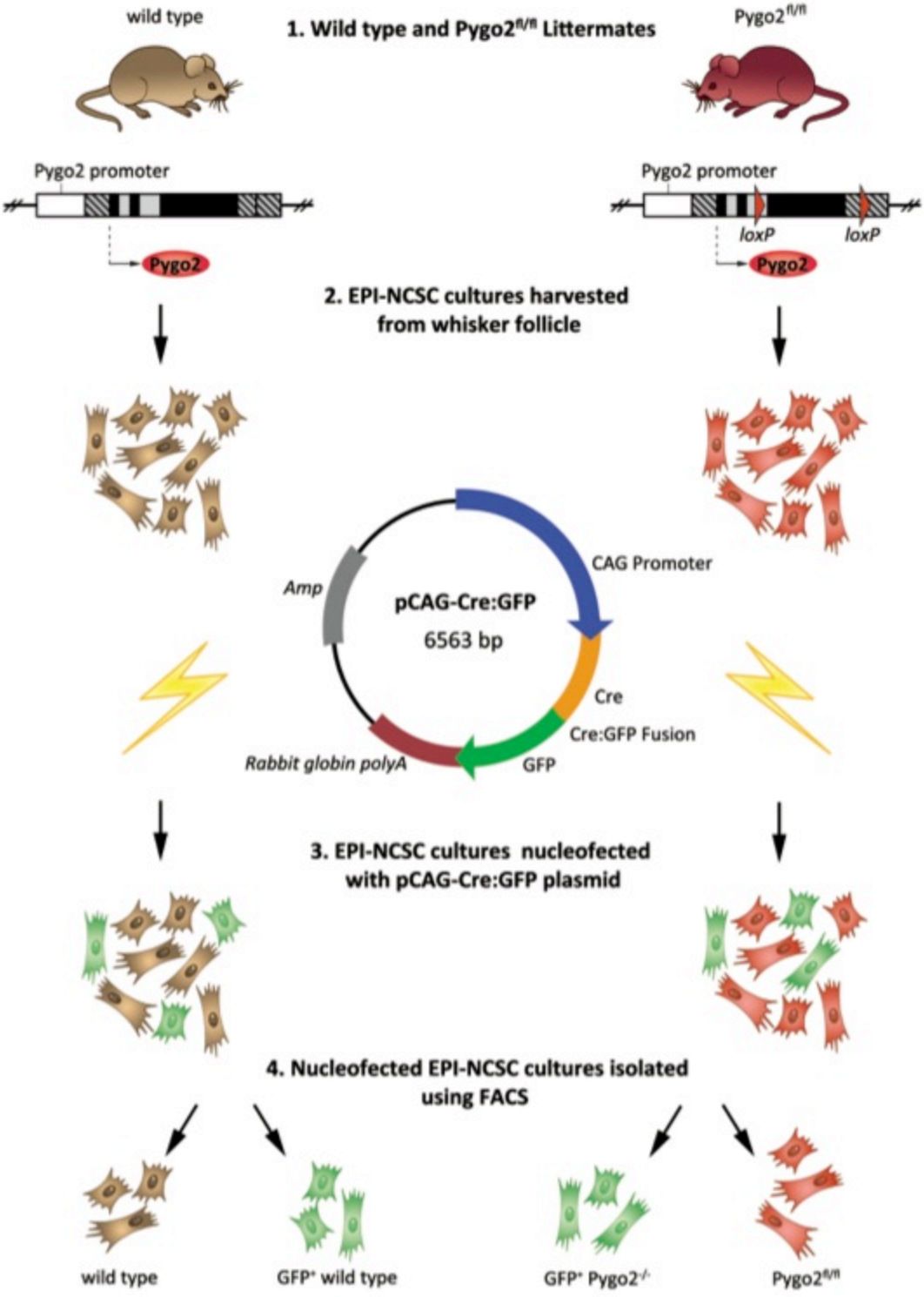

Figure 5-2. Flow diagram of the method developed for the FACS isolation of wild type and *Pygo2*$^{-/-}$ EPI-NCSC for downstream proliferation, migration and maintenance assays

5.4 Further optimisation of the EPI-NCSC model

5.4.1 EPI-NCSC may be harvested from the bulge of adult Pygo2$^{fl/fl}$ mouse whisker follicles

EPI-NCSC are not only defined by their molecular signature, but also by their unique culturing conditions (see also Chapter 2). Briefly, hair follicles are removed, and micro-dissected to isolate the bulge region (see Figure 5-3A-D). The bulge is then dried onto a collagen-coated dish, and cultured at 37°C for 7 days in a media consisting of CEE, FBS and αMEM. The CEE is specifically enriched for the neural components of the chick embryo. These conditions were empirically derived [76], based on the standard conditions required for deriving embryonic NCSC from mouse spinal cord *ex vivo* [406] and have been successfully employed to obtain human EPI-NCSC [71]. Interestingly, Clewes *et al* (2011) have used a proprietary neural stem cell medium (NeuroCult®, Stem Cell Technologies) and synthetic collagen replacement (CellStart™, Invitrogen) to derive human EPI-NCSC in xeno-free conditions, suggesting that EPI-NCSC may not be reliant on CEE nor collagen for optimal growth [72]. However, CEE and proprietary media consist of a cocktail of active factors, and are not easily defined. Nor is their composition freely available. Ultimately this makes it difficult to characterise EPI-NCSC-specific cell signalling and basal requirements for *in vitro* cultivation. Furthermore, reliance on FBS in media and collagen-coated plastic-ware can interfere with many downstream applications.

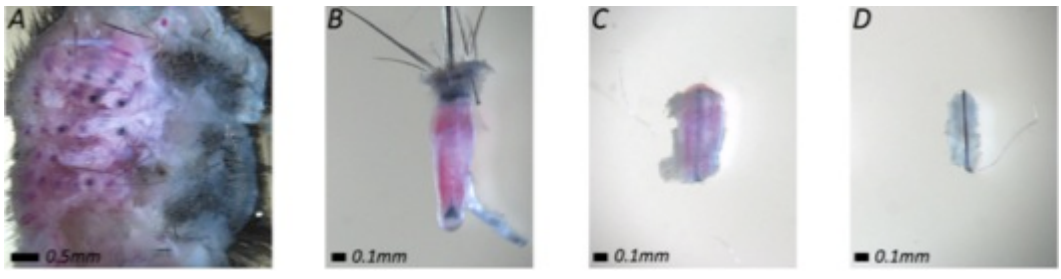

Figure 5-3. Isolation of bulges from the whisker follicles of mice
Whisker follicles are removed from the base of the whisker pad (A) and connective tissue and fat trimmed away (B), before cutting away the DP (C) and above the ring sinus. The bulge (D) is released by cutting the remaining follicle longitudinally.

These previous findings prompted the questions, are mouse EPI-NCSC able to grow on non-collagen surfaces? And are mouse EPI-NCSC reliant upon CEE for growth? To answer these questions, dissected bulge regions from wild type and *Pygo2*$^{fl/fl}$ whisker follicles, were cultured under the following conditions, (1) Standard EPI-NCSC Emigration Media (ED1), (2) Standard mammalian cell culture medium (DMEM), (3) Feeder independent embryonic stem cell medium (GTES), 1-3 all on CellStart™ coated 6-well plates, with the following conditions in ED1 medium, (4) 6-well gelatin replacement plates (CellBind), and (5) 6-well uncoated tissue culture plates.

The culture conditions and results from these experiments have been summarised in Table 5-1 and Figure 5-4. Under the conditions originally defined by Sieber-Blum *et al.* (2004), EPI-NCSC emigrated from bulges in ED1 media as expected on CellStart™ coated plasticware. This suggests that, like human EPI-NCSC, mouse EPI-NCSC may be derived on a collagen-replacement coating, like CellStart™. Yet, the expansion of EPI-NCSC was not possible on the gelatin replacement surface. Gelatin is routinely used in the culturing of feeder independent mouse embryonic stem cells (mESC) to assist cell adhesion [410-412]. Given that EPI-NCSC normally grow as a monolayer, it is interesting to note that while some cells initially migrated, and adhered to the plate, their continual growth and expansion was limited (Figure 5-4 & Figure 5-5). Moreover, bulge cultures were not obtained in the uncoated conditions (not shown in Figure 5-5). While these experimental conditions are not exhaustive, these results provide preliminary evidence for a collagen requirement, or factors associated with collagen in the maintenance of EPI-NCSC, but not in the emigration of cells from the bulge. It is interesting to note other SC within the bulge niche are known to express α6-integrin [374]. It is possible that EPI-NCSC may also express a similar integrin/receptor specific for collagen binding/attachment.

DMEM is a standard culture medium that contains elevated levels of essential amino acids, vitamins and glucose. With the removal of CEE it was envisaged supplementation with greater nutrient levels may assist emigration and growth of EPI-NCSC. However, as Figure 5-4 demonstrates, while a small number of

cells emigrated from the bulge initially, they did not continue to emigrate or proliferate as well as those in ED1 media.

In contrast, cells in the GTES medium emigrated, were morphologically similar to EPI-NCSC, and were maintained in GTES for at least 8 passages (see Chapter 2). After this time, the cells were frozen, stored in LN_2 for two weeks and were subsequently capable of continued growth. Thus suggesting that GTES is capable of yielding, and sustaining EPI-NCSC. However, extended culture past 8 passages was not tested (growth rate and viability). Intriguingly, GTES is routinely used for the culture of pluripotent embryonic stem cells. There are a number of differences between GTES and ED1. These in include the base medium used, the addition of CEE to ED1 and βME and LIF to GTES. Despite this, the primary active ingredient in GTES for maintenance of mESC is LIF. This seems to suggest that LIF is capable of replacing the requirement for the CEE in the initial emigration, and of basic FGF-2, NT-3, SCF, and EGF in the expansion of EPI-NCSC (compare XP1 medium to GTES).

Table 5-1. EPI-NCSC culturing conditions

Condition	Media		Plastic-ware	
	Emigration	Expansion	Pre-treatment	Cultivation plate
1	ED1	XP1	CellStart™	Standard 6-well plate
2	DMEM	DMEM	CellStart™	Standard 6-well plate
3	GTES	GTES	CellStart™	Standard 6-well plate
4	ED1	XP1	-	CellBIND® (Gelatin Replacement)
5	ED1	XP1	-	Standard 6-well plate

Conditions tested for the emigration and continued support of cell growth of EPI-NCSC over 14 days in culture. Bulges were cultured in emigration media for the initial 7 days until the first sub-culture (see Chapter 2).

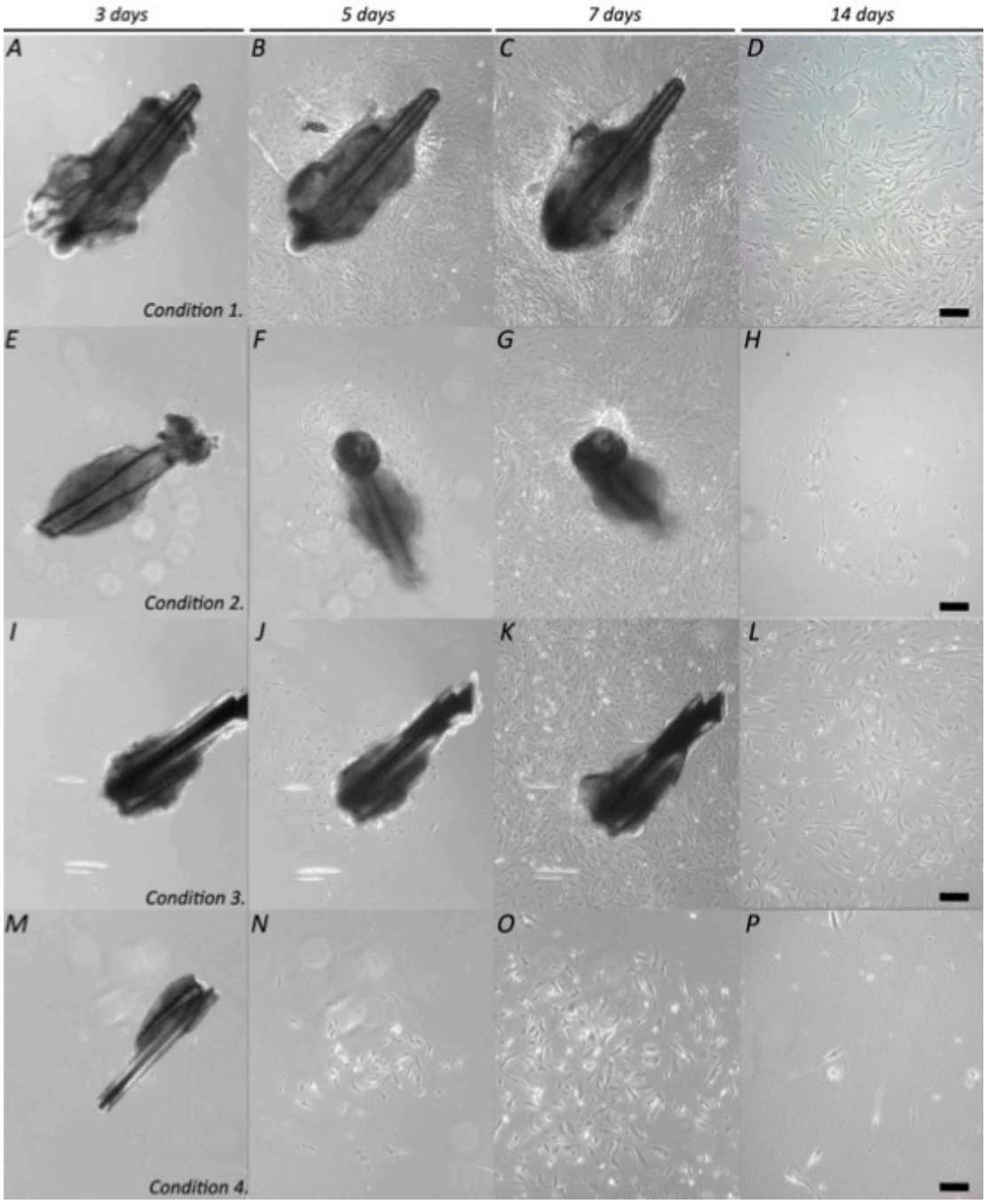

Figure 5-4. Optimisation of EPI-NCSC culturing conditions
Multiple culturing conditions were tested (see Table 5-1) over the initial 7 days of emigration up to 14 days in culture. After the initial emigration, (1-7 days), bulge cultures were routinely sub-cultured. Growth of EPI-NCSC in standard conditions (A-D), and in GTES media (I-L) yields emigrating cultures and supported growth over 14 days. Yet growth in DMEM (E-H) and on CellBIND® plates (M-P) does not. Culturing bulges on uncoated plates (Condition 5; Table 5-1) was unsuccessful (*not shown*). *Scale bar = 150µm.*

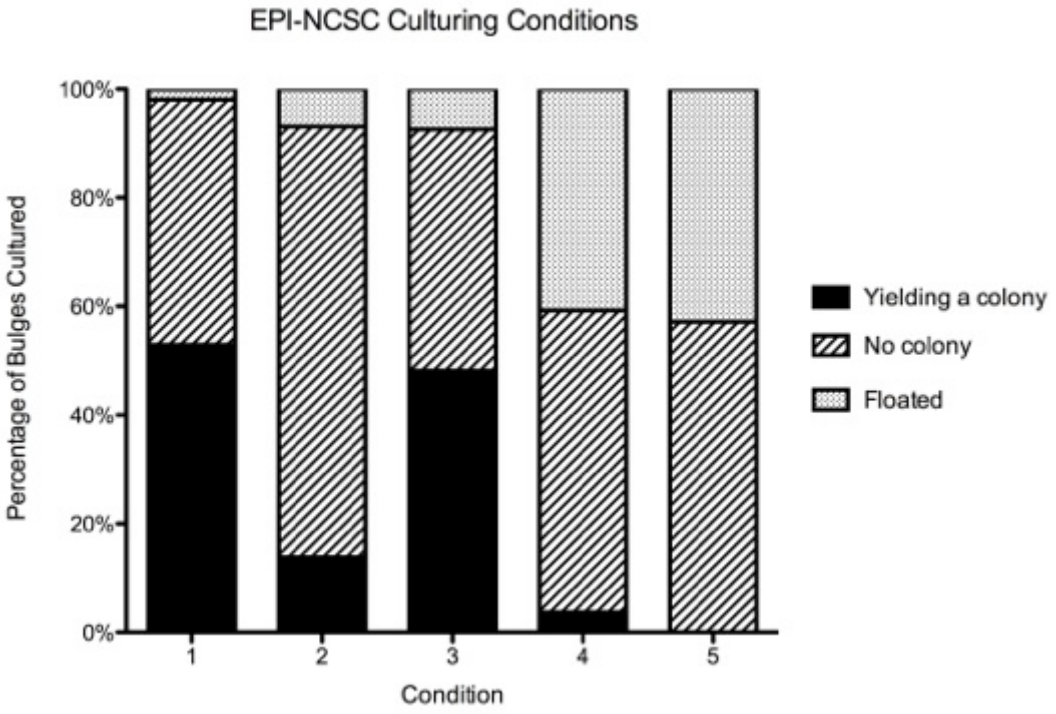

Figure 5-5. Efficiency of culturing conditions used for EPI-NCSC derivation
Stacked bar chart illustrating the efficiency of different culturing conditions tested for derivation of EPI-NCSC following 7 days in culture. The standard culturing conditions (1) were equally as efficient at obtaining cultures as GTES media (condition 3), while DMEM (condition 2) is less efficient than ED1 or GTES media. Using a non-collagen based substrate (condition 4) to coat plates leads to decreased bulge attachment, and reduced *ex vivo* cultures. In all conditions a minimum of 30 bulges were tested ($n > 30$).

5.4.2 Nucleofection provides an inefficient method for transfection of murine EPI-NCSC

Two different methods were tested empirically for the efficient transfection of EPI-NCSC cultures. Both methods were focussed on bulge cultures following 7 days in culture. This was usually 3-4 days after the first emigration of EPI-NCSC at which point, bulge cultures usually consisted of approximately 1-2 x 10^4 cells per bulge, determined using the V-CELL XP instrument prior to transfection/nucleofection.

Initially a number of commercially available products were tested for liposomal-based transfection. This method relies upon the formation of a lipid bilayer that encases the negatively charged nucleic acid, or transgene, to form a liposome-like structure. Liposome-mediated delivery offers many advantages, such as efficiency of gene transfer, ability to transfect a range of cell types and successful delivery of DNA of all sizes from oligonucleotides to yeast artificial chromosomes [413]. Additionally, liposome-mediated nucleic acid delivery may be used for *in vivo* transfection of DNA and RNA to animals and humans [414].

For this study, both standard and stem cell specific liposomal-based reagents were used. These included, Lipofectamine™ 2000, Lipofectamine™ LTX, Xfect™ (mESC), and X-tremeGENE HP (see also Chapter 2). Additionally, a readily transfectable immortalised cell line (Human Embryonic Kidney, HEK293) and EPI-NCSC were transfected with a positive control plasmid, expressing GFP from a CMV promoter (pmaxGFP®), and the Cre:GFP fusion construct expressed from a CAG promoter (pCAG-Cre:GFP).

Transfection efficiency was assessed by the percentage of cells displaying green fluorescence within 24 to 48 hours post transfection. While the HEK293 cells were consistently transfected at levels between 65%-80%, with either plasmid vector, EPI-NCSC remained resistant, with only rare cells exhibiting green fluorescence. The highest level of transfection achieved in EPI-NCSC with this method was approximately 5% with the pmaxGFP vector (10μg) and 3.5% with the pCAG-Cre:GFP vector (10μg), using Lipofectamine™ LTX (see Figure 5-5).

The Amaxa Nucleofector™ system was the second method used to test transient transfection of EPI-NCSC. This system is a modified electroporation technique, which allows rapid optimisation of electrical pulses and transduction buffers required for optimisation. Electroporation is generally regarded as a 'physical' transfection method, as opposed to biochemical techniques like liposomal transfection. The penetration of DNA is enhanced via the high electric field, essentially pushing the vector through the cellular membrane [415]. Two different buffers were tested from the Neural Stem Cell, and Mouse Embryonic Stem Cell kits (see Chapter 2). Numerous programs were tested with the control

plasmid pmaxGFP, supplied with the buffered solutions, using 1 x 10^5 EPI-NCSC in each assay.

To assess the efficiency of these transfections, three random images were taken 30 hours post nucleofection from each experiment arm. It was found that the T-020 program yielded the highest number of green fluorescent EPI-NCSC following transfection. Interestingly the T-020 program, together with the Mouse SC buffers, led to the least cell loss and overall represents the most efficient method for transfecting EPI-NCSC. These results have been summarised in Figure 5-6.

From Table 5-2, it can be seen that differences in efficiency were minimal between the buffered solutions used. Yet, a greater difference was observed when different nucleofection programs were used. Considering all transient transfection methods tested on EPI-NCSC, nucleofection was the most efficient method. Thus, all subsequent transfections were performed using the T-020 nucleofection program, in the Mouse SC buffered solution. However, nucleofection represents a relatively inefficient method for transfection of EPI-NCSC, when compared to HEK293 cells where up to 80% efficiency is obtainable using lipofection protocols (Figure 5-5).

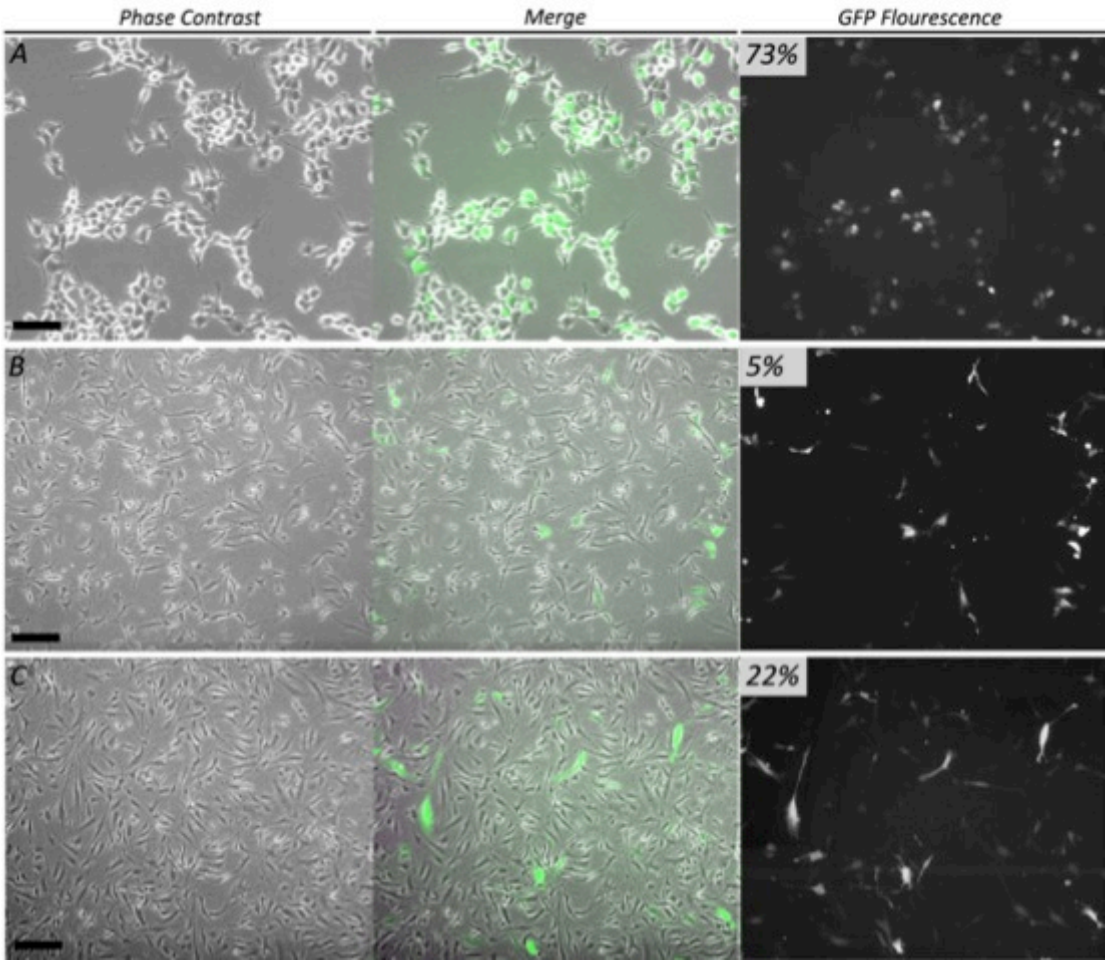

Figure 5-6. Transfection and nucleofection of EPI-NCSC
(A) Transfection of HEK293 cells with Lipofectamine™ LTX achieves approximately 65-80% cells expressing Cre:GFP. EPI-NCSC transfected with Lipofectamine™ LTX (B) and nucleofected using Mouse SC buffer/T-020 program yield approximately 5% and 22% transfection efficiencies, respectively. *Scale bar = 100μm.*

Table 5-2. Nucleofection efficiencies in EPI-NCSC

Electroporation Program	Mouse ESC Buffer	Neural Stem Cell Buffer
G-013	14.3%	14.6%
O-005	8.4%	8.8%
T-020	**22.1% ***	19.3%
X-001	18.5%	14.8%

Efficiency of nucleofection assessed by GFP fluorescence in EPI-NCSC after 48hr assessing different electroporation programs and buffers. * Program used for subsequent nucleofection of EPI-NCSC.

5.4.3 Transfected EPI-NCSC may be isolated based on GFP expression

Fluorescence-activated cell sorting (FACS) was employed to enrich the population of nucleofected cells that express Cre:GFP. FACS, a specialised form of flow cytometry, is regularly used to profile cell populations based on the expression of cell surface markers, or intracellular protein expression, and subsequently sort these populations into separate containers. Briefly, single cells are suspended in a stream of fluid, excited by lasers and passed by a photo-detector. Using fluorescently labelled antibodies targeted to cell surface antigens, or endogenously expressed fluorescent proteins, discrete sub-populations of cells may be identified. A small charge may be applied, based on this fluorescence profile, to an individual droplet containing a single cell. Electromagnets can then separate these droplets into the appropriate container.

Using this method, untransfected and nucleofected (with the pCAG-Cre:GFP plasmid) EPI-NCSC were used to setup three profiling gates for subsequent FACS isolation of GFP positive (GFP^+) cells. As Figure 5-7A demonstrates, EPI-NCSC were first isolated from suspended debris and other particles by analysis of the forward and side scatter pulse areas. Forward scatter (FSC) correlates to particle volume, and Side Scatter (SSC), to the granularity or complexity of the particle. Both are measures of how much light is refracted, at a particular angle, by a particle and together may be used to judge the size and basic shape of a particle. In this way, cells may be separated from irregular and smaller particles within the stream or flow.

It has been demonstrated that single cells may be further isolated from doublets by plotting area versus the height of SSC pulses, SSC-A and SSC-H respectively [416]. This is particularly important for EPI-NCSC where gentle disaggregation is used when passaging cultures *in vitro* [417] and thus, more likely to contain cell aggregates or doublets than in other standard cell preparations. This may cause a problem if doublets contain a nucleofected cell, and other non-nucleofected cells, which may lead to false positive sorting of cells and subsequent contamination of the sorted population. Thus, a second gate selecting for proportional height and area signals was applied (Figure 5-7B).

Finally, a gate to select nucleofected cells was applied based on their fluorescence at 515 - 545nm, from the endogenous expression of Cre:GFP. This gate was positioned according to the untransfected EPI-NCSC background fluorescence, to capture all cells exhibiting GFP fluorescence above background levels (Figure 5-7C). As can be seen comparing Figure 5-7D and Figure 5-8D, approximately 20% of EPI-NCSC exhibited GFP fluorescence at 488nm when nucleofected with Cre:GFP. This is a similar rate of nucleofection, and reflects what was previously found when optimising the initial transfection conditions (see Section 5.4.2). In addition, it can be seen that EPI-NCSC contain a heterogeneous population of cells based on FSC and SSC, as there are no distinct sub-populations evident, and they display a broad FSC/SSC scatter profile. This is not entirely surprising, as they have previously been shown to contain 70% multipotent cells, with varying capacity to spontaneously differentiate into multiple cell types. Interestingly, this is also similar to what is observed in flow cytometry of neurospheres cultures [418].

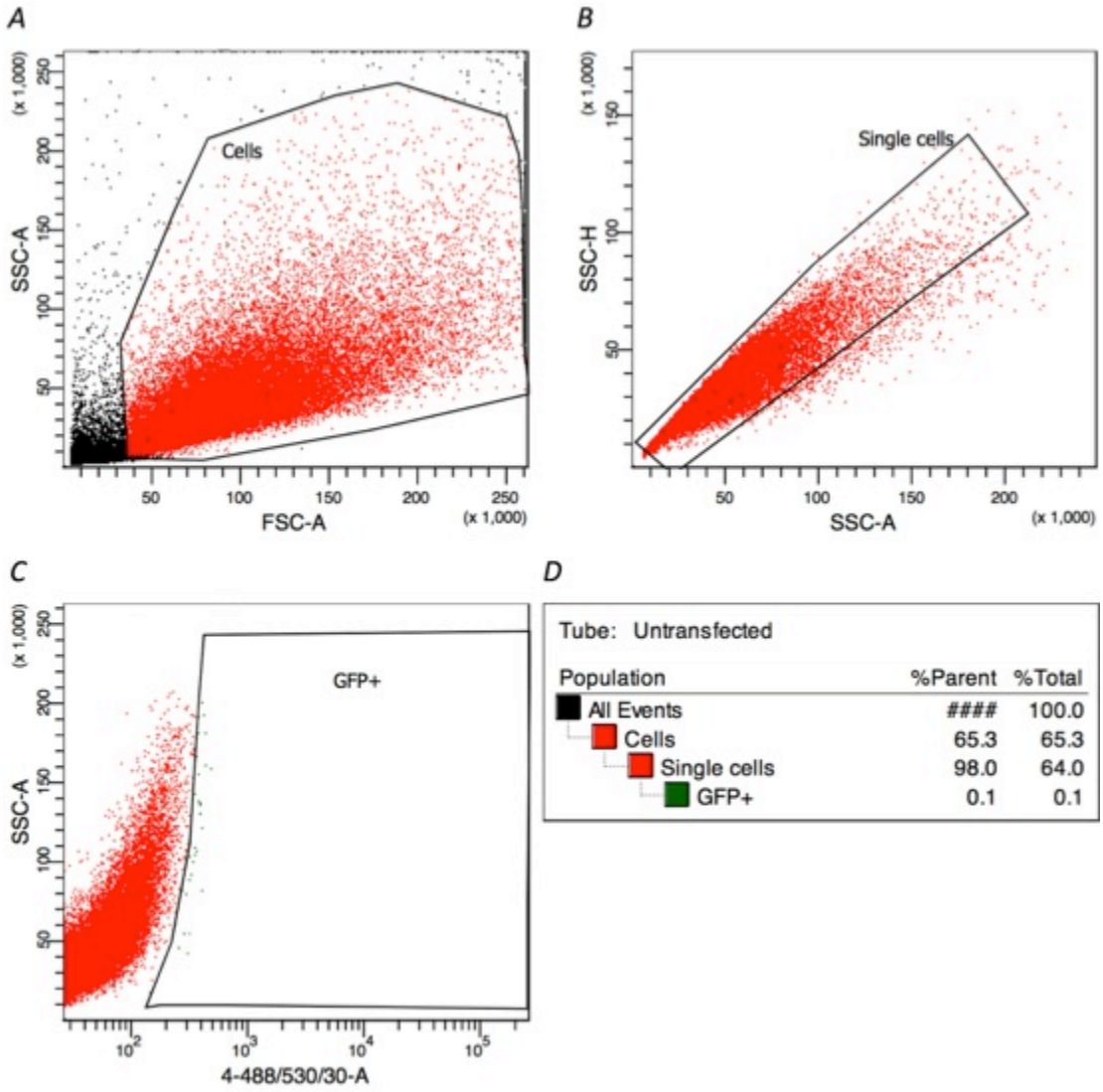

Figure 5-7. Flow cytometry of EPI-NCSC

Flow cytometry of EPI-NCSC showing a heterogeneous population of cells (A), comparing FSC versus SSC. Using SSC area versus height (B), single cells are isolated from suspended doublets. The background level of GFP fluorescence is calibrated (C) on the negative population of EPI-NCSC. Cell populations from the gates setup in A, B and C are displayed as a proportion of the total or parental population. *Gated cell events = 200000.*

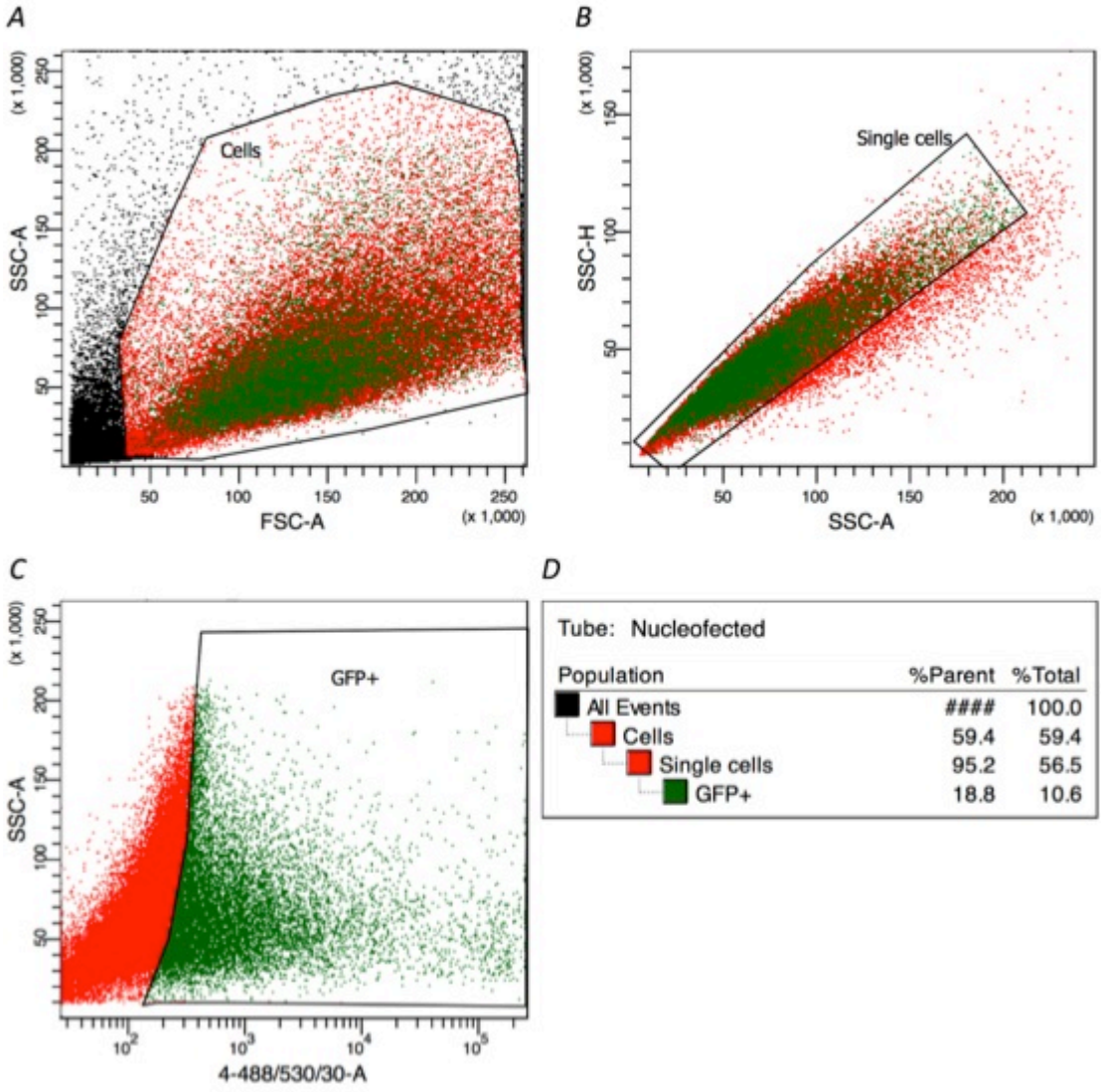

Figure 5-8. Flow cytometry of nucleofected EPI-NCSC with the pCAG-Cre:GFP plasmid vector
The gating strategy setup in panels A, B and C isolate a single cell population of GFP fluorescent cells comprising 18.8% of the total suspension. *Gated cell events = 200000.*

5.4.4 Expression of Cre:GFP efficiently mediates excision of floxed sequences

With the FACS gating strategy setup, EPI-NCSC derived from R26R mice (a Cre reporter strain allowing inducible expression of the *lacZ* gene and activating the expression of β-gal as can be shown by X-gal chromogenic staining, referred to in more detail in Chapter 4) were used to verify that a highly enriched population of GFP^+ cells could be successfully sorted from nucleofected cells. Cells were initially nucleofected and cultured for two days before GFP^+ and GFP negative (GFP^-) populations were isolated and reseeded on CellStart™ treated plates. After cells adhered, they were imaged using a standard fluorescent microscope to verify their GFP expression (Figure 5-9). Following another two days in culture, cells were subsequently stained following the X-gal staining procedure (see Chapter 4). As Figure 5-9 shows, EPI-NCSC were successfully isolated based on their GFP expression. In addition, GFP^+ EPI-NCSC were also found to be positive for β-gal expression. Thus, demonstrating that the Cre:GFP had successfully activated the expression of β-gal through Cre-mediated excision of the *neo* cassette (refer Chapter 4). In addition, all sorted populations contained cells with spindle morphology and closely-associated spherical cells, typical of EPI-NCSC cultures. Furthermore, these populations were maintained in cultures used for X-gal staining. These observations provide support for three important conclusions. Firstly, the heterogeneity of EPI-NCSC reported previously, and observed in the FACS profile, is maintained after FACS without substantial bias. Nucleofection and FACS is an effective method for isolating transfected EPI-NCSC. And finally, Cre:GFP is efficient at mediating loxP recombination in EPI-NCSC.

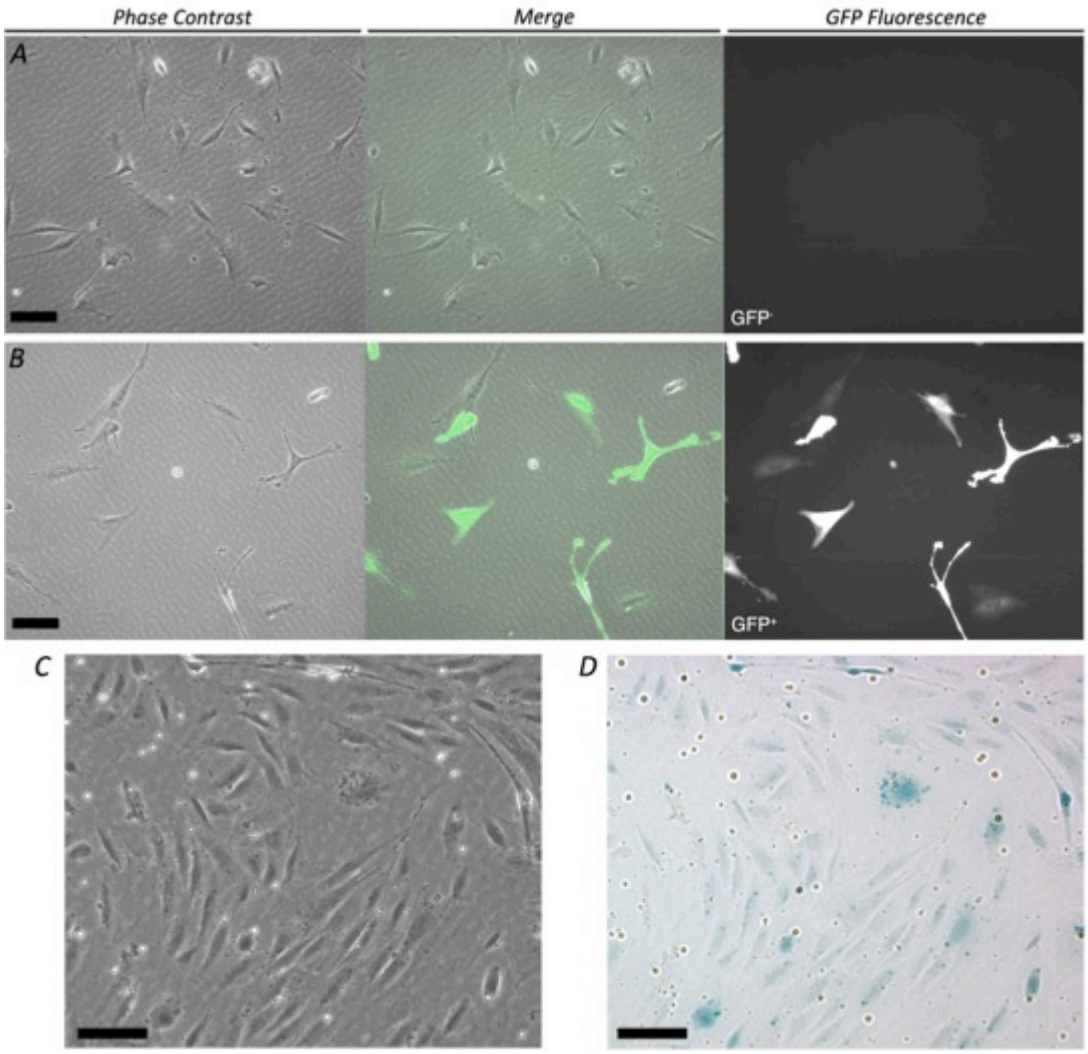

Figure 5-9. Cre:GFP efficiently mediates floxed sequence excision in GFP$^+$ cells isolated using FACS
EPI-NCSC derived from R26R mice (A, B) nucleofected with pCAG-Cre:GFP and isolated using GFP FACS into GFP$^-$ and GFP$^+$ populations. The GFP fluorescence is also verified in the last panel of each row. GFP$^+$ cells grown for two days (C) were stained with X-gal (D) to verify Cre excision of the floxed *neo* cassette and subsequent expression of β-gal. *Scale bar = 50μm*

5.5 Pygo2 is functionally important to EPI-NCSC cultivation

5.5.1 Generation of four Pygo2$^{-/-}$ EPI-NCSC lines

In order to assess the primary aim of this study, murine EPI-NCSC were harvested from the whisker follicles of four wild type and four Pygo2$^{fl/fl}$ littermates at 12 weeks old. Bulge cultures from the same mouse were combined after 7 days in culture, prior to nucleofection. To provide a comparative analysis (between wild type and Pygo2$^{-/-}$) and provide a control for culturing conditions, EPI-NCSC were harvested concurrently in four pairs of wild type and Pygo2$^{fl/fl}$. For example, each day, bulge cultures from one wild type and one Pygo2$^{fl/fl}$ mouse were setup using the same conditions. Nucleofection, FACS and downstream assays were all conducted as a comparison between these pairs (refer to Table 5-3). Using the transfection method developed previously, EPI-NCSC were successfully nucleofected with pCAGCre:GFP and isolated using GFP FACS. Table 5-3 provides a summary of the cell lines generated, and the number of cells recovered through FACS.

Table 5-3. EPI-NCSC cell lines generated by GFP FACS

Cell line	Genotype	Culture Pair	Cell Events	Single Cell Events	GFP$^+$ Events
28	*Pygo2$^{fl/fl}$*	A	2.4 x 10^5	1.8 x 10^5	2.3 x 10^4
32	wild type	A	1.5 x 10^5	9.2 x 10^4	1.6 x 10^4
42	*Pygo2$^{fl/fl}$*	B	6.5 x 10^5	4.9 x 10^5	5.5 x 10^4
44	wild type	B	6.0 x 10^5	4.2 x 10^5	5.5 x 10^4
43	*Pygo2$^{fl/fl}$*	C	1.1 x 10^5	4.2 x 10^4	8.0 x 10^3
45	wild type	C	1.1 x 10^5	7.1 x 10^4	1.7 x 10^4
51	*Pygo2$^{fl/fl}$*	D	8.5 x 10^5	6.2 x 10^5	7.7 x 10^4
50	wild type	D	4.8 x 10^5	3.6 x 10^5	4.4 x 10^4

EPI-NCSC were nucleofected and cultured in pairs, for direct comparison between wild type and Pygo2$^{fl/fl}$ cells. Each cell line was successfully nucleofected and sorted based on GFP fluorescence.

Prior to nucleofection, each of the EPI-NCSC cell lines were genotyped using two standard genomic PCR assays (see Figure 5-10). Immediately following FACS isolation, a small number of cells from both GFP^+ and GFP^- fractions were again assayed via genomic PCR. The Pygo2 FLOX PCR (see Figure 5-10A) flanks the 5' loxP site (of the $Pygo2^{fl/fl}$ allele), and produces a PCR product for wild type (393bp) and a larger product from $Pygo2^{fl/fl}$ (~530bp) attributable to additional nucleotides from the incorporation of loxP site and gene targeting construct.

As shown in Figure 5-10, the larger fragment is no longer obtainable from the GFP^+ $Pygo2^{fl/fl}$, owing to the successful removal of the floxed *Pygo2* gene. The Pygo2 NULL PCR provides a positive control for removal of this genomic region, as it will produce a large fragment (~500bp), only when this region is removed. Again, Figure 5-10 demonstrates that sorted GFP^+ $Pygo2^{fl/fl}$ EPI-NCSC lines do not contain wild type or floxed *Pygo2* allele sequences, yet consist only of *Pygo2*$^{-/-}$. Conversely, the GFP^+ wild type EPI-NCSC contain only wild type Pygo2 alleles in genomic sequences.

To further verify the deletion of Pygo2, RT-PCR was used with primers specific (Pygo2 CDS) to exons 2 and 3 of the *Pygo2* mRNA transcript (see Figure 5-10B). Again, GFP^+ $Pygo2^{fl/fl}$ cultures fail to produce a PCR product. However, all cultures produce a product for the *Pygo2* UTR (outside of the deleted region), demonstrating that the expression of the *Pygo2* transcript is maintained.

In summary, four GFP^+ Pygo2 knockout EPI-NCSC lines (GFP^+ $Pygo2^{-/-}$) were successfully generated and sorted, based upon transient GFP fluorescence, together with four GFP^+ wild type EPI-NCSC lines.

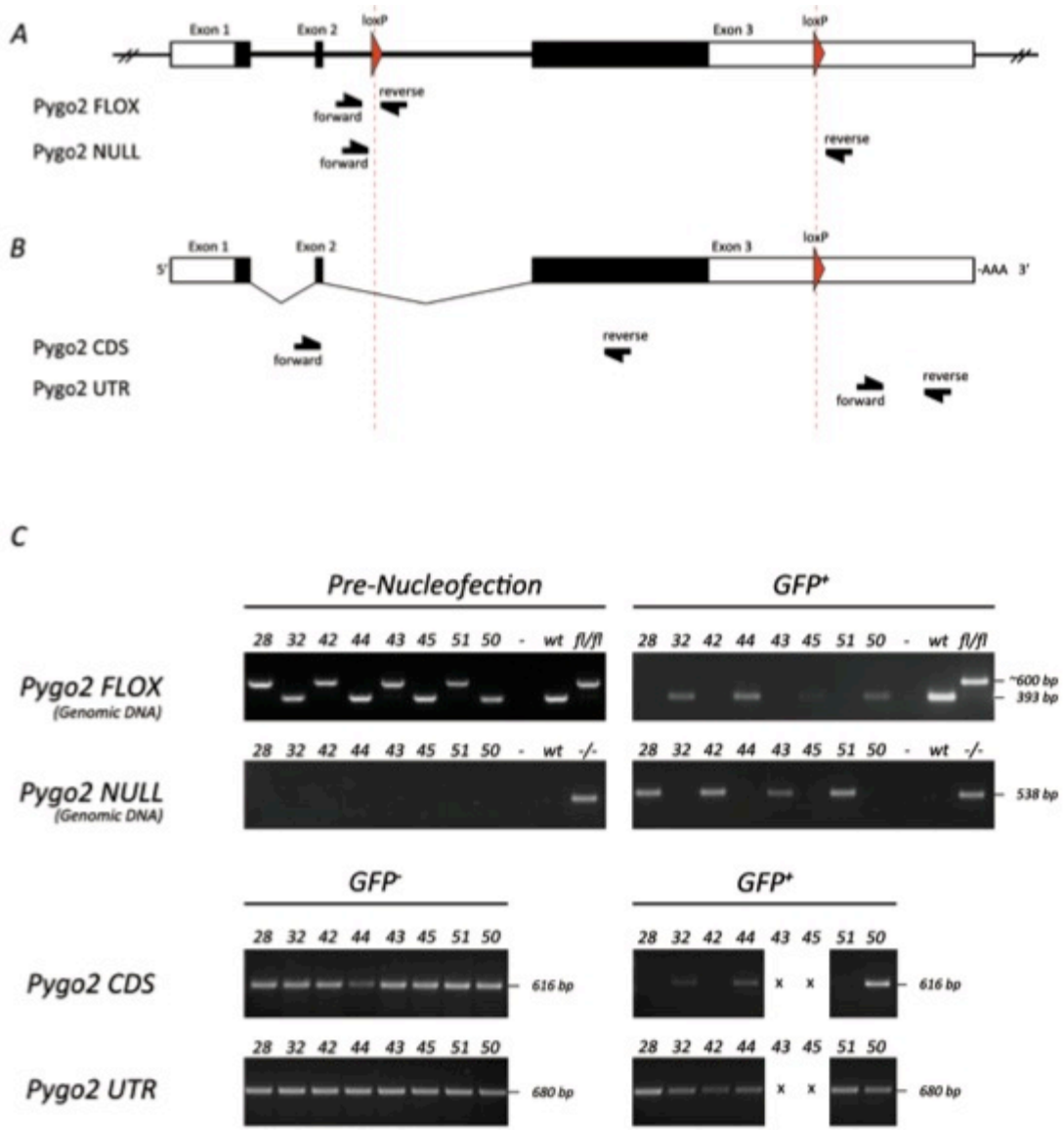

Figure 5-10. Verification of *Pygo2* knockout in EPI-NCSC
The genomic structure of *Pygo2* (A) is represented as a scaled diagram with exons illustrated as boxes. Protein coding sequences are shown as black, while un-translated regions are white filled. The approximate relative positions of primer binding sites (*primer size not to scale*) to the loxP sites are illustrated below as pairs: Pygo2 FLOX and Pygo2 NULL. Likewise, the mRNA (cDNA) structure of *Pygo2* is illustrated in B, with the approximate binding position of primer pairs, Pygo2 CDS and Pygo2 UTR. Genomic and RT-PCR screening of EPI-NCSC (C) derived from wild type and $Pygo2^{fl/fl}$ mice. Pygo2 FLOX PCR primers were used to identify wild type and $Pygo2^{fl/fl}$ cultures. Following nucleofection, GFP^{+} $Pygo2^{-/-}$ cultures no longer contain the *Pygo2* floxed genomic sequence, indicating Cre excision was successful. Pygo2 NULL primers flank both loxP sites (outside) and produce a product when Cre-mediated recombination has occurred as in the GFP^{+} $Pygo2^{fl/fl}$, but not wild type. Pygo2 CDS primers amplify exons 2 and 3 in wild type, but not GFP^{+} $Pygo2^{fl/fl}$ cultures, again suggesting Cre recombination was successful (Cell lines 43 & 45 were not tested due to limited cell availability). Pygo2 UTR provide a control for *Pygo2* expression as they are outside the deleted region.

5.5.2 EPI-NCSC are alkaline phosphatase negative

The expression of alkaline phosphatase is commonly associated with pluripotent stem cells and is often used as a marker of stemness in differentiation assays [419]. Mouse embryonic stem cells express high levels of alkaline phosphatase (ALP) that may be assayed biochemically. Interestingly, the mouse hair follicle also maintains alkaline phosphatase expression, with varying levels throughout development and normal hair cycling [401]. While in the dermal papilla, expression remains consistently high. Yet, SKPs and Nestin-expressing cells derived from hair follicles are negative when assayed for ALP. In addition, EPI-NCSC do not express ALP when assayed by RT-PCR. However, this has not previously been verified biochemically. Interestingly, when SKPs [400] and human EPI-NCSC are induced down an osteogenic pathway, they begin to express ALP [72]. This suggests that changes in their differentiative capacity may be reflected by the expression of ALP. To test this possibility, GFP^{+} wild type and GFP^{+} $Pygo2^{-/-}$ EPI-NCSC were assayed for ALP (see Chapter 2) after 7 days in culture following FACS. As Figure 5-11 demonstrates, mouse EPI-NCSC are negative for ALP and the loss of *Pygo2* does not affect this status. Loosely this may suggest that their differentiative program remains unchanged in the absence of *Pygo2* expression, for example, they are not moving towards and osteogenic lineage.

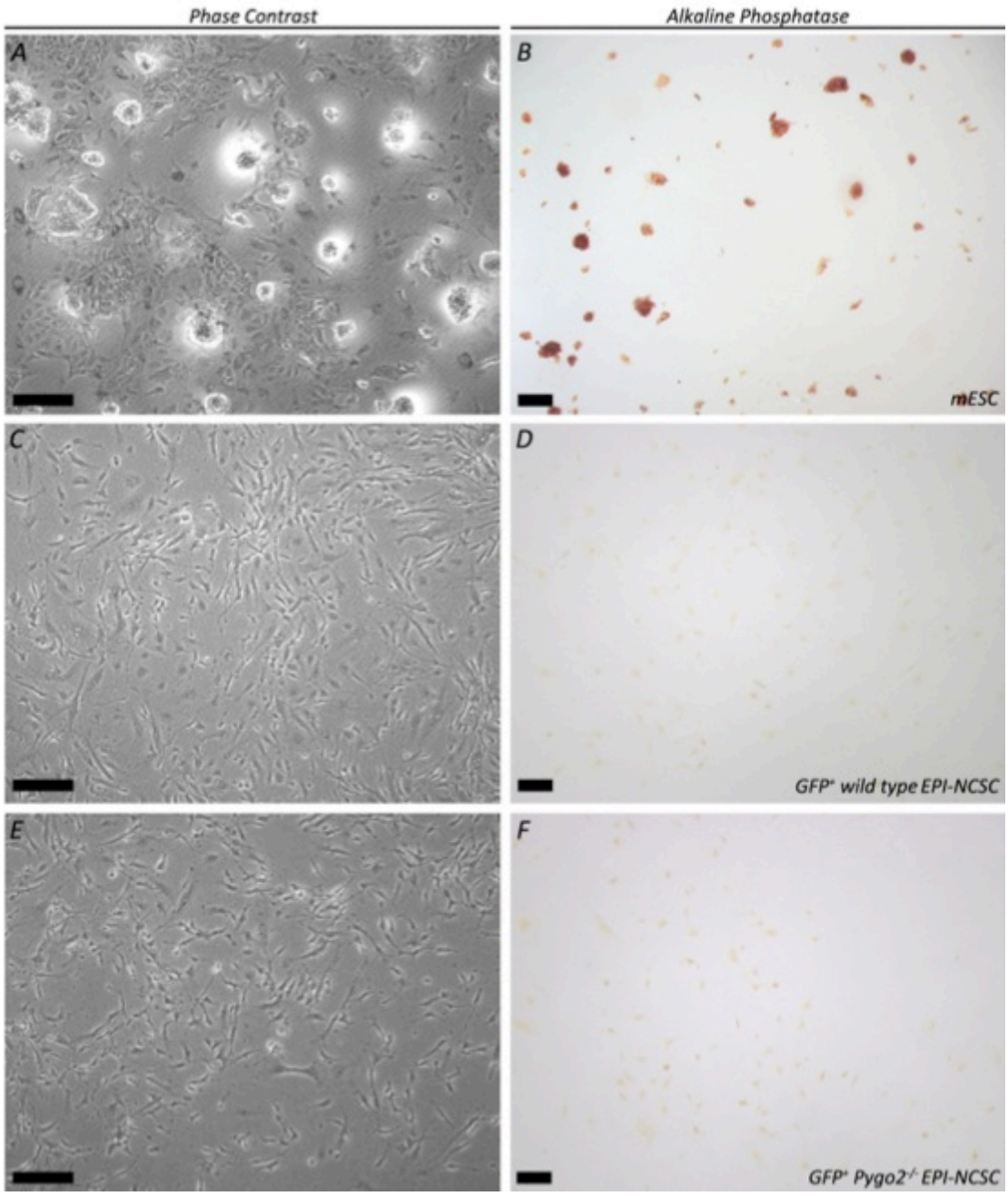

Figure 5-11. Alkaline phosphatase reactivity in EPI-NCSC
Phase contrast images (A, C, E) and ALP staining (B, D, F) of mESC (A,B), GFP+ wild type (C, D), and GFP+ Pygo2$^{-/-}$ (E, F) EPI-NCSC, 7 days after GFP+ FACS isolation. mESC provide a positive control for ALP reactivity, staining dark red (B), while both GFP+ Pygo2$^{fl/fl}$ and GFP+ wild type EPI-NCSC remain negative for ALP expression. *Scale bar = 150μm*

5.5.3 High seeding density promotes spontaneous sphere formation

The ability to form spherical cellular aggregates in a suspension culture has been well documented in pluripotent ESC and multipotent neural SC cultures. By withdrawing LIF from ESC cultures, differentiation can be stimulated via seeding cells as a hanging drop, or on non-adherent plastic-ware. ESCs will spontaneously form aggregates, termed embryoid bodies that replicate many of the early embryonic signalling and development programs, forming rudimentary germ layers [420,421].

Neural SC also share the ability to form spherical aggregates in suspension culture [422,423]. They are multipotent, heterogeneous cultures, and express the neural precursor, *Nes* together with CD34, CD31 and *Tie2* [418,424]. In contrast to ESC, primary cultures of neural SC derived from embryonic and adult mouse brain spontaneously form aggregates, termed neurospheres. Interestingly, their growth as a suspension culture is required to maintain multipotency [425]. Spheres plated onto normal tissue culture plastic will adhere and cells will migrate out from the sphere and subsequently differentiate [418].

Recently KrejčI *et al*. (2010) demonstrated that human EPI-NCSC can form spheres under non-adherent conditions [71]. The exact composition of these cell aggregates was not described. However, it was demonstrated that plating spheres yielded new migrating cultures, and trypinization, followed by adherent culture gave cultures with similar immunohistochemical properties as EPI-NCSC [71]. Thus, the stem cell properties had been maintained by suspension culture, in a manner similar to neurospheres.

The same phenomenon was observed in this study as illustrated in Figure 5-12. Cultures of EPI-NCSC seeded at high density (>1 x 10^4 cells per cm^2), on CellStart™ treated plastic-ware, routinely migrated towards neighbouring cells. This migration created a net-like pattern (Figure 5-12A), with bundles of EPI-NCSC, creating large round regions devoid of cells. The EPI-NCSC bundles subsequently formed spherical aggregates and lifted off the base of the dish as free-floating spheres (see Figure 5-12B, C) over a period 3-5 days in culture.

This raised the possibility that spheres may also form under non-adherent conditions as previously demonstrated in human EPI-NCSC [71]. Thus, each of the GFP^+ $Pygo2^{-/-}$ and GFP^+ wild type EPI-NCSC lines were plated as hanging drops, and on non-adherent plates (suspension seeding) to test their ability to form suspension cell aggregates. As can be seen in Figure 5-12C a number of larger spheres form together with smaller suspended aggregates. However, these were presumably removed by the method of medium exchange (see Chapter 2). Briefly, spheres were allowed to settle for 5min and all but 0.5ml of media was exchanged for fresh medium. Spheres were fed every 48-72hr over the 14 days.

In both conditions, spheres readily formed. In addition, spheres were capable of generating new EPI-NCSC adherent colonies after 2 weeks in suspension (Table 5-1 and Figure 5-12D). In a manner similar to Gritti *et al.* (1996), the sphere forming ability was measured by counting the number of spheres generated, and the proportion of spheres able to produce a new EPI-NCSC culture (in adherent conditions; [422]). As Table 5-4 illustrates, no overt difference was observed, and both wild type and $Pygo2^{-/-}$ cells were able to produce equivalent numbers of spheres, and new EPI-NCSC secondary cultures.

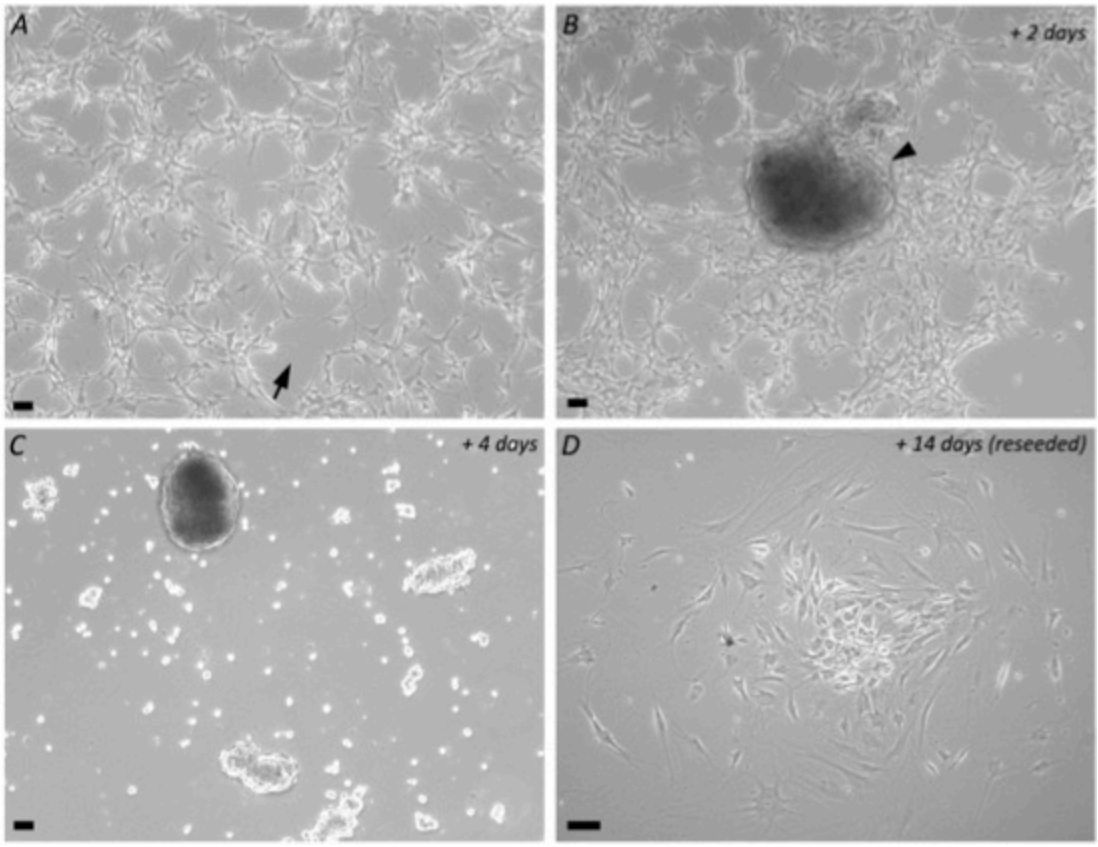

Figure 5-12. EPI-NCSC spontaneously form spheres in high seeding density
EPI-NCSC at high seeding density migrate to form bundles (A), leaving large spaces (arrow), followed by cellular aggregates (B; arrowhead) after 2 days. After 3-5 days, aggregates begin floating in suspension (C). Suspension spheres may be reseeded on CellStart™ coated dishes and will continue growing as an adherent culture (D) after 14 days as a suspension culture. *Scale bar = 100μm*

Table 5-4. Sphere forming ability of EPI-NCSC cultures following *Pygo2* ablation

Cell line	Suspension	2° Colonies	%	Hanging Drop	2° Colonies	%
28	157	27	17.20%	75	16	21.33%
32	143	24	16.78%	63	18	28.57%
42	149	19	12.75%	69	14	20.29%
44	165	24	14.55%	86	11	12.79%
43	108	17	15.74%	27	6	22.22%
45	97	21	21.65%	23	5	21.74%
51	132	24	18.18%	8	2	25.00%
50	110	16	14.55%	31	7	22.58%

EPI-NCSC grown as a suspension culture or hanging drops and transferred to low-adherent plates, spontaneously form spherical aggregates. After 14 days grown as a suspension culture, they are also capable of forming new EPI-NCSC colonies.

5.5.4 The migration of EPI-NCSC is unchanged

As explored previously (Chapter 1), the migratory behaviour of the NC is one of its many distinguishing features. The NC migrates large distances during embryonic development to colonise and contribute to organs and tissues throughout the entire organism (see Chapter 1). There are many models of human disease that are caused by a failure of NC migration. For example, Hirschsprung's disease is due to aberrant TNC and SNC advancement into the cecum and colon [426]. Importantly, the migratory behaviour of NCC in culture is harnessed to isolate many NC derivatives, including neural SC [427] and EPI-NCSC [1].

The Wnt pathway is critical for cell migration, including NC migration. Primarily the PCP or non-canonical pathway is implicated in directional migration of NC *in vivo* [428]. To consider the possibility that *Pygo2* may have roles outside of the canonical Wnt pathway, the migratory ability of GFP^{+} *Pygo2*$^{-/-}$ and wild type EPI-NCSC was investigated.

There exist a number of methods to assay cells *in vitro* for their migratory ability. One common method is the scratch assay. In this procedure, semi-

confluent cell cultures are displaced with a blunt instrument, for example a pipette tip may be used to remove cells from a region. The ability of cells to migrate and re-colonise the 'scratch' are measured over time. However, this assay also provides a measure of the cells to repair, or heal following a physical insult. Despite this, GFP^{+} *Pygo2*$^{-/-}$ and wild type EPI-NCSC were tested for their ability to repopulate following a scratch displacement. Yet, initial attempts using this method were unsuccessful. The scratch either led to complete removal of EPI-NCSC as a sheet of cells, or cells did not regrow over the scratch. It is likely this was due to removal of the collagen substrate. This is supported by the inability of EPI-NCSC to grow on untreated, or synthetic adherent plastic ware (see Section 5.4.1).

An alternative to the scratch assay is the chamber assay or boyden chamber [429]. Cells are restricted or seeded into a chamber separated by physical or chemical barrier. Chemo-attractants may also be used to induce cells to migrate through or into the barrier [429]. However, this assay primarily tests the ability of cells to invade the barrier, in addition to their migratory potential. It also relies upon an understanding of soluble factors that may induce or control migration. This aspect of EPI-NCSC biology remains unclear. Thus, the boyden chamber does not represent an appropriate system in this instance.

Finally, time-lapse photography may be used to follow the migration of individual cells or an entire cell population over time. In this study, EPI-NCSC were seeded onto a CellStart™ treated 30mm dish within a cloning ring (internal ⌀6 mm). This created a high-density culture of approximately 30% confluency, which is very high for EPI-NCSC as they are routinely maintained below 70% to prevent differentiation (see also Chapter 2). The cloning ring restricted EPI-NCSC attachment to the enclosed area, with the remaining surface becoming an exclusion zone (illustrated in Figure 5-13).

After 1hr cells attached, and the cloning ring was removed. The exclusion zone was checked to verify it was free of cells and cultures were subsequently photographed after 6, 24, and 48 hours. The number of cells outside of the initial seeding area were counted and have been represented by roseplots

illustrating the number and direction of migrating cells in Figure 5-15. However, as Table 5-5 also demonstrates, no overt difference in the migratory ability of GFP^{+} $Pygo2^{-/-}$ was observed when directly compared to wild type and control cells. In summary, the distance migrated by all cells irrespective of *Pygo2* status, was consistent when compared within experimental arms, and suggests that *Pygo2* is not required for EPI-NCSC migration *ex vivo*.

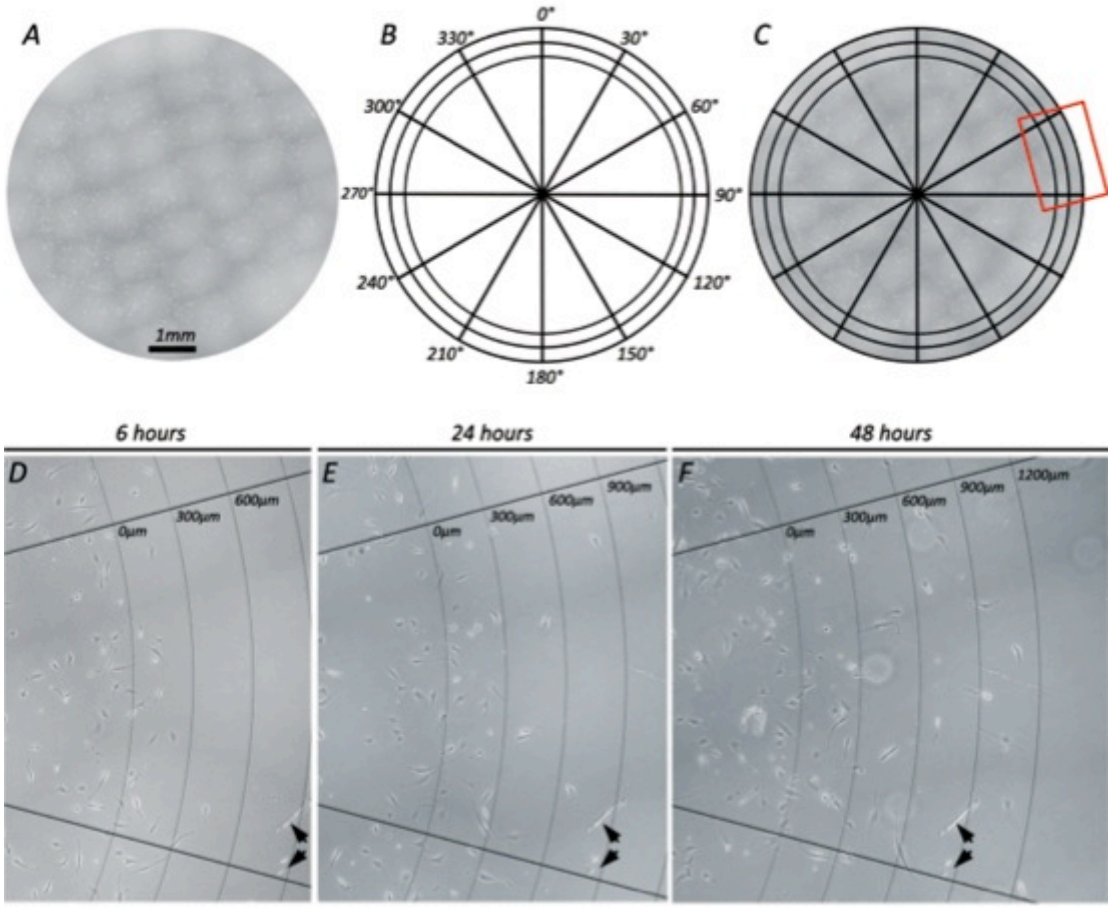

Figure 5-13. Outline of migration assay used to test EPI-NCSC
EPI-NCSC are seeded at high density within a cloning ring and allowed to attach for 1 hour. The cloning ring is removed and the exclusion zone (area delineated by ≥ 0µm arc) created by the ring is checked to make sure no cells are within it. Mosaic images are prepared (A), and measurement guide (B) is overlaid onto the mosaic image (C) to count the number of cells, distance migrated into the exclusion zone, and the direction of migration (angle within 30°). The measurement guide creates 12x 30° segments, subdivided by increasing distance from the edge of the exclusion zone. Cells within each region are counted at 6 (D), 24 (E) and 48 (F) hours, enlarged from C (red box). Scratch marks are used to align mosaic images (arrows).

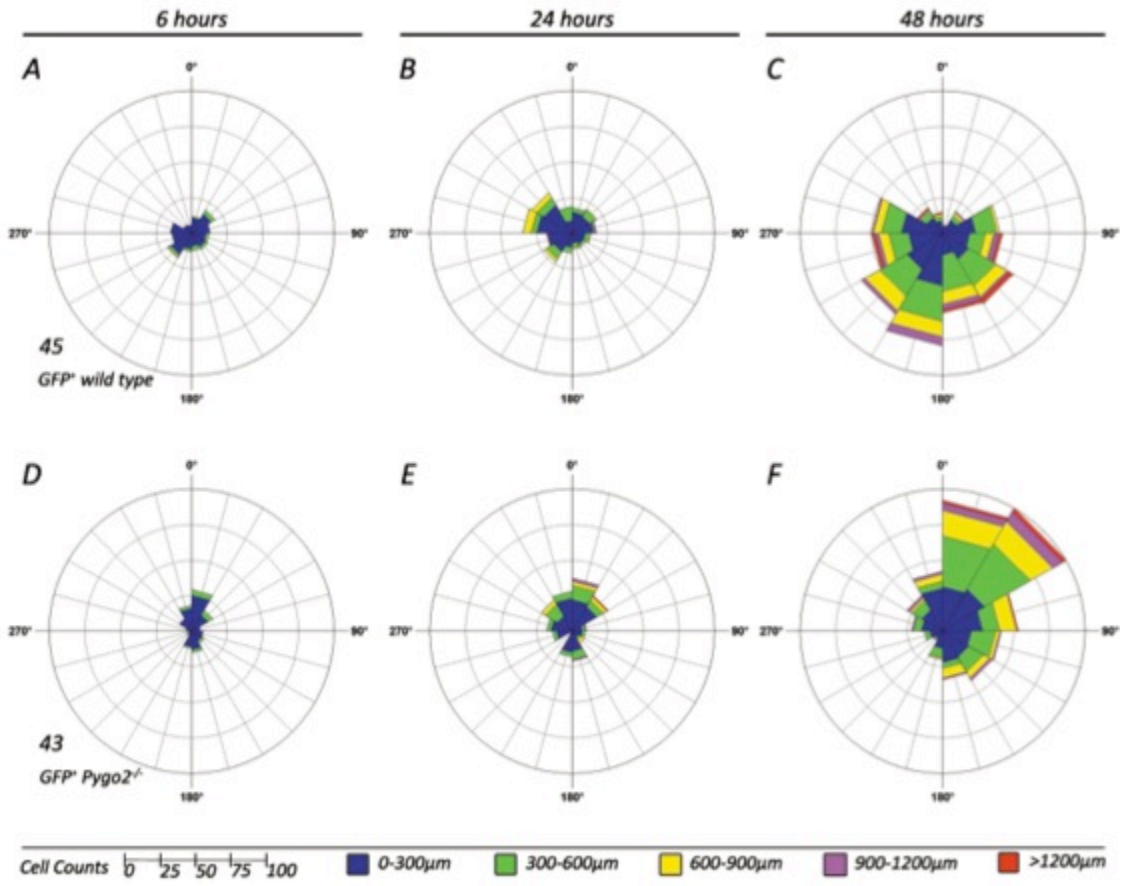

Figure 5-14. GFP+ Pygo2-/- EPI-NCSC migrate normally under standard culture conditions
Rose plots or circular histograms illustrate the direction, and magnitude of EPI-NCSC migration after ablation of *Pygo2*. The direction of cell movement is indicated by the angle of each stacked bar, sub-divided into 30° regions. The radial length of each stacked bar represents the total number of cells migrating in a particular direction. The distance migrated is indicated by the colour of each bar within the stack; blue, 0-300µm; green, 300-600µm; yellow, 600-900µm; purple, 900-1200µm; red, >1200µm. Migration of GFP^{+} wild type (cell line 45) EPI-NCSC (A, B, C) over 6, 24 and 48hr versus the unperturbed migration of GFP^{+} Pygo2$^{-/-}$ (cell line 43) EPI-NCSC (D, E, F) over same time.

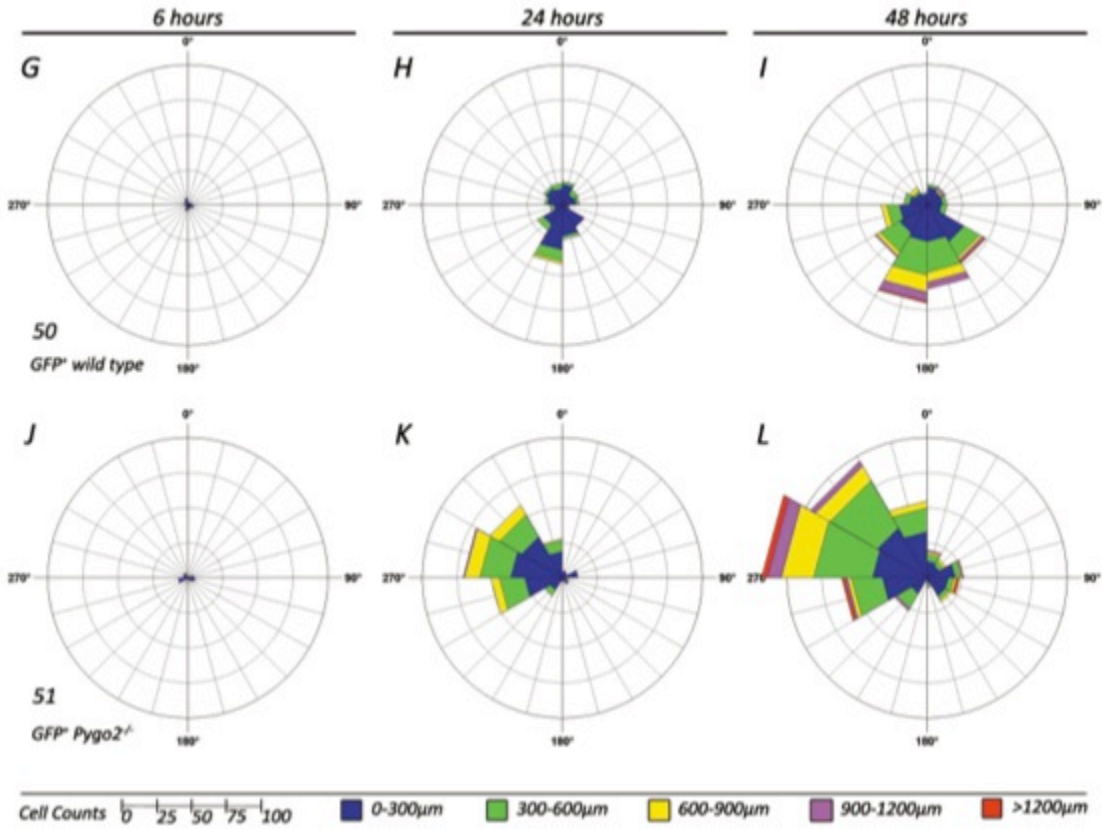

Figure 5-15. GFP$^+$ Pygo2$^{-/-}$ EPI-NCSC migrate normally under standard culture conditions (cont'd)
(Cont'd) Rose plots or circular histograms illustrate the direction, and magnitude of EPI-NCSC migration after ablation of *Pygo2*. The direction of cell movement is indicated by the angle of each stacked bar, sub-divided into 30° regions. The radial length of each stacked bar represents the total number of cells migrating in a particular direction. The distance migrated is indicated by the colour of each bar within the stack; blue, 0-300µm; green, 300-600µm; yellow, 600-900µm; purple, 900-1200µm; red, >1200µm. Compare the migration of GFP$^+$ wild type (cell line 50) EPI-NCSC (A, B, C) over 6, 24 and 48hr versus the unperturbed migration of GFP$^+$ Pygo2$^{-/-}$ (cell line 51) EPI-NCSC (D, E, F) over the same time.

Table 5-5. Total number of EPI-NCSC migrating outside of the initial exclusion zone over time

Cell Line	45 GFP$^+$ wild type	43 GFP$^+$ Pygo2$^{-/-}$	50 GFP$^+$ wild type	51 GFP$^+$ Pygo2$^{-/-}$
6 hours	155	134	32	29
1 day	231	221	205	258
2 day	499	493	333	469

The total number of cells migrating into the exclusion, irrespective of direction suggests that *Pygo2* status does not affect the ability of EPI-NCSC to migrate.

5.5.5 Pygo2 knockout EPI-NCSC display abnormal Proliferation

Participation of the Wnt pathway in promoting cell proliferation is well documented and is the basis for its oncogenic role [430]. This has been demonstrated *in vivo* [431-433] and *in vitro* through studies specifically blocking or activating Wnt signalling [434-436]. This is often achieved by targeting components like β-catenin [437] or genes outside the pathway, such as those involved in the β-catenin destruction complex [438]. In general, the canonical Wnt pathway is understood to promote cell proliferation, through β-catenin-mediated transcriptional activation of target genes, such as Cyclin-D1 [439] and c-Myc [440]. While non-canonical Wnt signals have been shown to antagonise canonical activation of cellular proliferation in murine kidney development [441]. Interestingly, the canonical Wnt pathway appears to be repressed in human ESC by OCT4 [442] and up-regulated upon their differentiation [443]. This is in direct contrast to earlier reports wherein activation of the canonical Wnt pathway in murine and human ESC prevented differentiation [444] (into neurons) and maintained their self-renewal ability (pluripotency) [445].

As previously discussed in Chapter 1, *Pygo2* has been shown to regulate proliferation and cell cycle, as a transcriptional co-activator of the canonical Wnt pathway. Briefly, using antisense MO targeted to *PYGO2*, Andrews et al. (2007) demonstrated that the colony forming ability and growth rate of human breast cancer cell lines was reduced by nearly 50% compared to controls [144]. In rat glioma cells *Pygo2* is over-expressed within the cell nuclei, and transfection of cells with a Pygo2 expression construct leads to enhanced proliferation [136]. Furthermore, siRNA mediated knockdown of *PYGO2* within human glioblastoma cells also led to reduced proliferation *in vitro* [149].

To better understand the role of *Pygo2* in EPI-NCSC, *ex vivo* expansion of these cells was investigated using low and high density seeding. Wild type and *Pygo2*$^{-/-}$ EPI-NCSC were analysed using the Vi-CELL XR instrument to measure cell viability and total cell mass from cultures after 7 days in culture from an initial 5 x 10^3 seeded cells. Cells used in the migration assays were also used in this

assay and represent the high density cells, as the same number of cells were seeded in the same volume of media, but initially restricted to a smaller attachment area. As Figure 5-16 shows, GFP$^+$ Pygo2$^{-/-}$ display an enhanced proliferation compared to GFP$^+$ wild type. Comparing the mean GFP$^+$ *Pygo2*$^{-/-}$ cell counts, 9.8 ± 1.5 x 10^4 cells per well, to GFP$^+$ wild type, 6.4 ± 0.5 x 10^4 cells per well narrowly misses significance ($p = 0.056$, $n = 8$). However, in all cases the nucleofection led to a reduction in GFP$^+$ cell numbers, comparing the GFP$^+$ sorted cells to the negative control populations (GFP$^-$; untransfected) cultured alongside each other following GFP$^+$ FACS.

It is also interesting to note this dramatic reduction in proliferation following nucleofection of EPI-NCSC. Seemingly the uptake and expression of the Cre:GFP plasmid, has reduced overall proliferation in the GFP$^+$ cells independent of *Pygo2* status. Importantly, this requires further investigation to identify if the transfection of EPI-NCSC will be tolerated by the cells, before any possible therapeutic usage is possible. Yet, GFP$^+$ Pygo2$^{-/-}$ cells in all instances displayed a mild proliferative advantage. Whether this is due to an enhanced resistance to the nucleofection procedure, or modulating cell cycle/proliferation remains to be elucidated. This will require an accurate assessment of EPI-NCSC at the single cell level, using flow cytometry analysis of cell cycle and proliferation.

Overall, this data is in direct contrast to the hypothesis that a loss of *Pygo2* would lead to a reduction in cell proliferation. There are a number of possibilities for this. *Pygo2* is known to function outside of the canonical Wnt pathway [123], possibly in the non-canonical or separate entirely from Wnt signal transduction. Non-canonical signalling has also been shown to antagonise the proliferative signal produced by the canonical pathway (as mentioned previously [441]). So it is possible that a loss of *Pygo2* in EPI-NCSC causes a reduction in non-canonical signalling, leading to a relative increase in canonical Wnt signalling and proliferation. A direct assessment at the molecular level will be required to further investigate this possibility.

Furthermore, FGF is a target of Wnt signalling in many developmental programs [446-448]. Because, FGF-2 is added routinely to the media used to expand EPI-

NCSC, t is possible that this may lead to restoration or protection from the loss of *Pygo2* in the maintenance of EPI-NCSC. There are also many other factors, many of which are unknown, present in the EPI-NCSC media that may underlie the differences reported herein with those published on cancer cells. This highlights the importance of defining a basal medium for future experiments based on EPI-NCSC.

Moreover, these results highlight differences between EPI-NCSC and cancer cells. *In vitro* and *in vivo* cancer cells are highly proliferative, with multiple cell cycling pathways activated in an aberrant manner. The reduced proliferative potential of EPI-NCSC may reflect differences in the normal cellular signalling state, versus that found in cancerous cell lines *in vitro*.

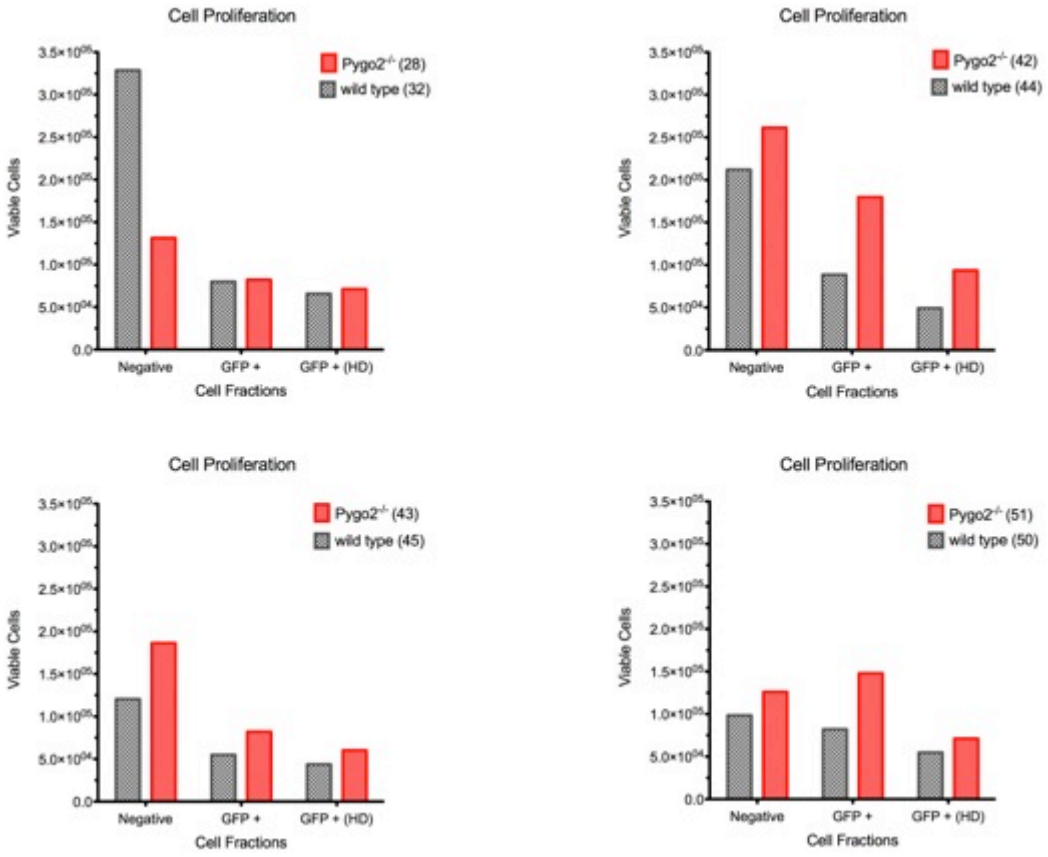

Figure 5-16. Proliferation of EPI-NCSC following GFP FACS
Gross viable cell counts of GFP$^+$ Pygo2$^{-/-}$ and GFP$^+$ wild type EPI-NCSC following 7 days in culture after GFP FACS isolation.

5.5.6 Maintenance of EPI-NCSC gene expression

EPI-NCSC are primarily defined by their molecular signature, in addition to their method of their isolation. For this reason, the expression of a number of key marker genes for were verified by RT-PCR including *Msx2* from the EPI-NCSC signature. In addition, the following general markers were assayed; Neural Crest (*Sox10*, *Snai2*, *Twist1*, *Nes*); neural SC (*Nes, Id3*); induced and pluripotent SC (CD34, *Nes, c-Myc*, *Oct4*, *Sox2*, *Klf4*); proliferation (*PCNA, Id3, Ki-67*).

In all cases, the expression of these markers was maintained in the GFP$^+$ Pygo2$^{-/-}$ and GFP$^+$ wild type EPI-NCSC compared with the equivalent untransfected

cells prior to nucleofection, with the exception of *Sox10* and *Oct4*. However, it has been shown previously that the expression of Sox10 is rapidly lost after initial emigration from bulge cultures [74,75]. In addition, the expression of *Oct4* is only observed using real-time PCR (qPCR) in human and mouse EPI-NCSC and is more than 100-fold less than of other stem cell markers [72,74].

Overall this suggests that the nucleofection of EPI-NCSC did not substantially alter their expression profile, nor did the loss of *Pygo2*. However, this would require further gene profiling to accurately determine expression changes in other genes that may be affected independently of these key markers.

Interestingly, untransfected and GFP^+ EPI-NCSC express CD34. This is in direct contrast to a previous report of EPI-NCSC lacking CD34 expression [74]. However, the primer pair used to assess CD34 expression in the prior study to does not produce a significant similarity when verified directly against mouse CD34 mRNA variants (NM_001111059.1 and NM_133654.3). This may help to explain the discrepancy. Therefore expression of CD34 by mouse EPI-NCSC in this study adds further evidence that EPI-NCSC may be similar to other bulge SC described previously [374].

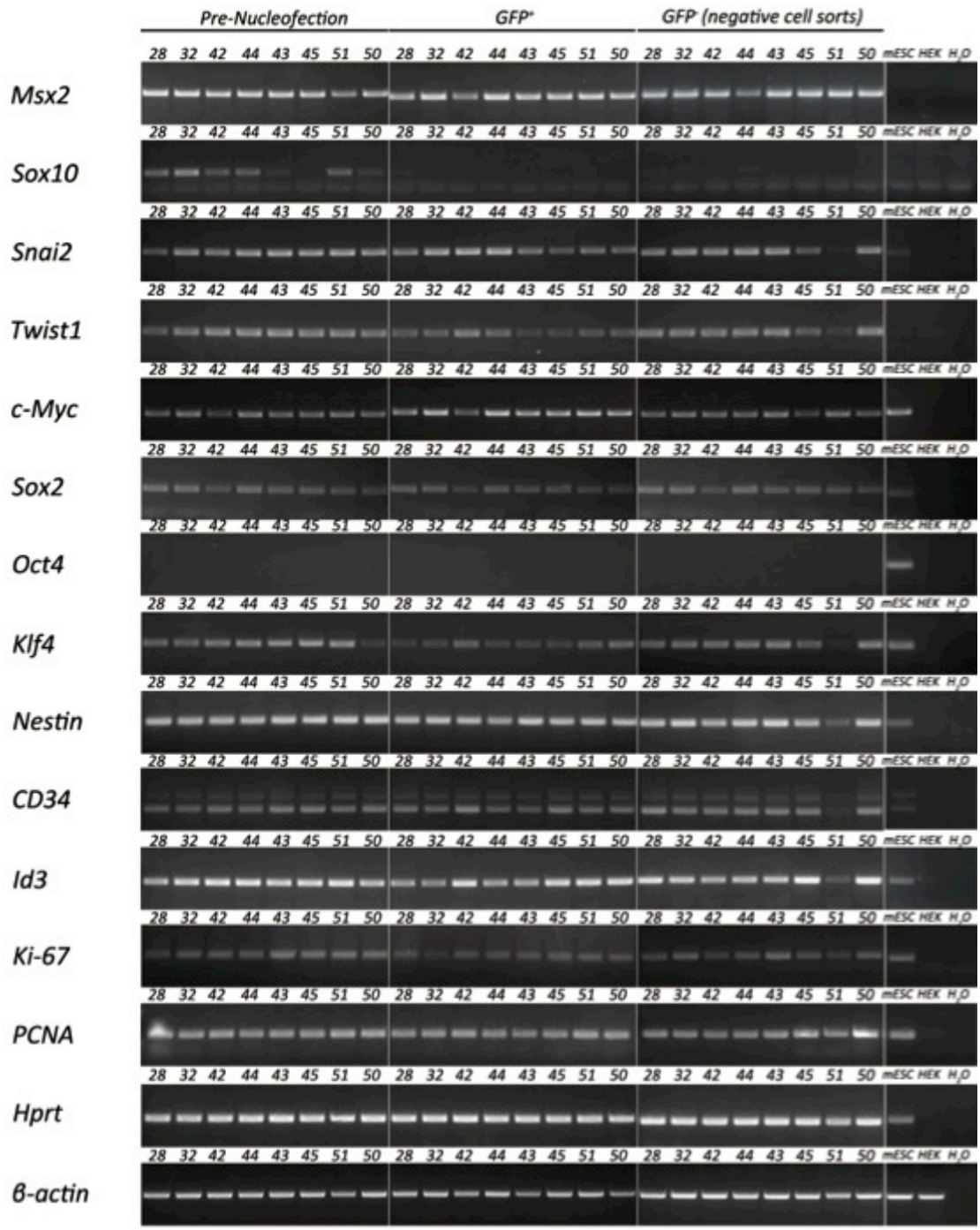

Figure 5-17. Maintenance of gene expression in expanded EPI-NCSC
RT-PCR analysis of key markers of Neural Crest (*Sox10*, *Snai2*, *Twist1*, *Nes*); neural SC (*Nes, Id3*); induced and pluripotent SC (CD34, *Nes,* (*c-Myc*, *Oct4*, *Sox2*, *Klf4*); proliferation (*PCNA3, Id3, Ki-67*).

5.6 Discussion

While EPI-NCSC were first identified in mice, the focus has rapidly shifted to deriving and characterising human cells. However, mouse EPI-NCSC are still largely uncharacterised despite the power of mouse genetics and the tools available to the developmental biologist. This study has provided a number of novel assays with which to further explore mouse EPI-NCSC and EPI-NCSC biology, in general. For example, the sphere forming ability of EPI-NCSC has been reported in human cells, but not in mouse. In addition, the spontaneous formation of spheres in high-density cultures has not previously been observed in either system.

Observations from this study also show parallels to neural SC and other bulge resident SC. The ability to form spheres in suspension culture is shared by neural SC and SKPs. In addition, the expression of CD34 adds further evidence for being derivatives of a common SC in the hair follicle bulge niche [374].

The development of this *ex* vivo model to study genetic manipulation of EPI-NCSC was successful. EPI-NCSC were transfected, and it has been demonstrated that these cells may be enriched on this basis. However, this study has also highlighted the importance of further characterisation of these cells, in particular defining a basal medium and their basic physiology. Additionally, the mild proliferative enhancement/protection in GFP^{+} $Pygo2^{-/-}$ cells suggests drawing parallels between the role of Pygo2 in development and cancer should be approached with caution. Importantly the *ex vivo* system provides a unique model in which to further investigate the role of *Pygo2* in Wnt signalling and to understand the biology of EPI-NCSC.

In summary, this study has developed a model for the genetic manipulation of murine EPI-NCSC cultures, whilst providing preliminary steps towards a defined culture medium and *in vitro* assays of EPI-NCSC biology. In addition, evidence for a role of *Pygo2* in EPI-NCSC proliferation *ex vivo* has been determined to successfully address the aims of this study.

Chapter 6. Final Discussion

Pygo2 is an intriguing gene. It is required for invertebrate and vertebrate development [81,83,84], suggestive of a highly critical function, yet it displays a pleiotropic response to loss of function studies [118,123,131,163,261]. It is highly conserved across all vertebrates, suggesting a common function, yet is required in a differing spatio-temporal manner by each species during development. Furthermore, it is one of only 19 signature genes [74], unique to NC derived EPI-NCSC found in the bulge of the hair follicle, suggestive of a critical requirement by EPI-NCSC, yet its deletion leads only to variable proliferation within those cells.

The *pygo* gene was originally identified in a screen for Wnt pathway members within flies [81,83,84]. Shortly after, mouse knockout models demonstrated a requirement for *Pygo2* in mammalian development [116,131]. At the same time, it was identified in a molecular screen as a genetic marker of NC derived adult SC (EPI-NCSC; [74]. The NC relies heavily upon the Wnt pathway for its specification, migration, proliferation and differentiation during embryogenesis. With this in mind, it raised the possibility that *Pygo2* may be required for NC development, and led to the central hypothesis of this research project; *Pygo2* is required for the normal specification, migration, proliferation and maintenance of NCSC. The evidence presented in this thesis supports aspects of this hypothesis, in addition to other facets of Pygo2 biology in general.

6.1 *Pygo2* is required for NC development

Three different model systems were used in this project to determine the role of *Pygo2* in NC. In zebrafish, a loss of *pygo* homologs caused craniofacial defects and a failure in gastrulation during early embryogenesis. While it is unlikely the gastrulation defect is directly related to NC, the irregular extension of the mandible and hyoid bones of the zebrafish jaw is certainly NC associated. The sox10:GFP zebrafish strain allowed visualization of NC migration and NC

derived structures, including the bones of the cranium and jaw. It was demonstrated that the hyoid and mandible bones were inappropriately patterned ant they failed to extend properly in *pygo1* morphants.

Using the Wnt1-Cre mouse model, multiple organ defects were observed in *Pygo2* CKO newborns. The majority of these abnormalities displayed were associated with a reduction in cell number or density. For example, the reduction in mandible and skull length, exhibits a failure of the NC derived tissue to extend during development. Other examples included the reduction in neurons within the GI tract, and the Me5 within the brain. In terms of the evolutionary conservation of *pygo* function, the finding that both zebrafish and mouse models display cranio-facial defects is important.

Intriguingly the defects displayed in *pygo1* morphants are within derivatives of the first and second (hyoid) pharyngeal arches, namely the mandibular and hyoid bones [186,187]. In mammals, the comparative bones (from the first and second arch) are found within the ear [449,450], mandible and hyoid bones. Remarkably, the *Pygo2* CKO displays defects in these bones too, with calcification of the styloid process (attached to the hyoid via the stylohyoid ligament), fusion of the stapes, and reduction in the mandible length. Add to this the recent finding that a chromosomal duplication including *PYGO2* leads to mandibulofacial dysostosis (Treacher-Collins syndrome) and microtia (undeveloped ear) in a newborn [143,451]. Treacher-Collins syndrome is often caused by haploinsufficiency of *Treacle* (*Tcof1*), resulting in a depletion of NC (or failure to proliferate) prior to migration of NCC into the first and second pharyngeal arches [452]. Taken together, these findings strongly suggest a conserved role across vertebrates, for *pygo* homologs within development of the first and second pharyngeal arches.

In addition, this evidence strongly supports a conserved role of *pygo* homologs within the NC and more broadly in neural tissues, with the reduction in neurons observed in *Pygo2* CKO (Me5 and GI tract). This evidence is further strengthened by previous studies in *Xenopus* where *pygo2α/β* play an important role in embryonic brain and dorsal axis patterning [118]. Furthermore, the

ubiquitous knockout of *Pygo2* mice leads to exencephaly as a direct result of abnormal neural tube closure [116,131]. Moreover, the dual *Pygo1/2* mouse knockout displays cardiac OFT tract defects, again possibly reflecting a critical NC role [360].

6.2 A role for *Pygo2* in NC proliferation

The role of Pygo2 in NC development raises an important question, what is the underlying cellular mechanism? To investigate this further, the major unifying features of NCSC (migration, proliferation and multipotency) were analysed *ex vivo* in EPI-NCSC assays. Neither migration nor differentiation capacity was altered in these cells. Both wild type and Pygo2$^{-/-}$ cells migrated with comparable ability as shown in the migration assays. The maintenance of NC and SC markers suggested no change in their transcriptional profile. Taken together with their ability to re-populate following sphere formation, this led to the conclusion that their capacity for differentiation was also maintained. These results are largely mirrored by the *in vivo* studies. In zebrafish and mouse, the NC underwent specification and normal migration. This was observed in the migration of DRG within the sox10:GFP zebrafish tail, and in X-gal staining and neurofilament staining, of embryonic *Pygo2* CKO mice.

Despite this, a mild enhancement of proliferation was observed in *Pygo2-/-* EPI-NCSC. In contrast, other studies *in vitro* using rat and human cancer cell lines have identified a requirement for *PYGO2* in promoting cell cycle regulation and proliferation [136,149,366,367]. This conflict highlights an important point regarding EPI-NCSC. It is likely that EPI-NCSC are very different from NCSC. They are far removed from the embryonic NC both in terms of location, and timing of appearance. Yet, the difference in proliferation is not inconsolable. It has been suggested that the entire Wnt pathway (both canonical and non-canonical) should be viewed as a regulatory network, rather than separate, linear signaling cascades [105]. It is possible that in EPI-NCSC cultures, extra-cellular factors may affect the final output of the Wnt pathway, providing a seemingly conflicting result in this study. However, further interrogation of this is required at the molecular level.

Further evidence for a *Pygo2* role in proliferation was found in the zebrafish and mouse *in vivo* models investigated by this project. Defects in both organisms may be attributed to a lack of proliferation driving the extension of cranio-facial bones. In addition, the reduction in neurons in the GI tract and Me5 point to a failure of proliferation in the NC derived neurons. Interestingly, Jonckheere *et al.* (2008) have also shown that in *Pygo2 null* mice there is a reduction in the proliferation of cells of the pancreas during development [261]. Taken together with the mild abnormality in EPI-NCSC (which represent a much older population of NC derived cells), it is tempting to speculate that the NC requirement for *Pygo2* occurs much earlier in development. A proliferative defect in the early NC population would also provide a mechanism for the common NC derived cellular reduction observed in multiple organs within the *Pygo2* CKO mouse.

The *Splotch/Pax3* mutant may be considered analogous to this. Several mouse models of *Pax3* mutations lead to CaNCC-associated conotruncal heart defects and early studies showed that a lack of CaNCC caused septation and OFT abnormalities during cardiogenesis [306,307,453]. Initially it was demonstrated that these defects were due to a failure of NC migration and proliferation within the heart. Yet, after more than 10 years studying *Pax3* mutations, Olaopa *et al*. (2011) have conclusively demonstrated that these defects are due to a failure of the NC to proliferate in the dorsal neural tube, prior to migration [306]. In turn, leading to a reduction in the population of CaNCC that migrate to and finally colonise the heart. A number of NC specific Cre mouse models were used to delete Pax3 in a NC-specific manner. Interestingly, Wnt1-Cre mediated deletion of *Pax3* led to no cardiac defects. Yet, the Ap2α-Cre deletion of *Pax3* in earlier pre-migratory NC resulted in DORV defects.

These results reported by Olaopa *et al.* (2011) highlight two important points concerning the role of *Pygo2* in NC. Firstly, is the Wnt1-Cre mediated deletion of *Pygo2* early enough in NC formation to capture the complete phenotype of *Pygo2* ablation within the NC? And secondly, if the requirement of *Pygo2* is in the early NC progenitor population, are EPI-NCSC an appropriate model? To answer these questions, further studies of Pygo2 in early NC development is

required. The definitive experiment would be to use the Ap2α-Cre mouse, together with the *Pygo1/2* floxed mouse, to investigate the NC requirement at any earlier stage of NCSC development in a similar fashion Olaopa et al. (2011)[306].

6.3 Pygo2 and the Wnt pathway

In addition to the central hypothesis, evidence from this project also raises interesting evidence for the role of *Pygo2* within the Wnt pathway. Early experiments in flies demonstrated an essential requirement for pygo in the transduction of the canonical Wnt signal [83]. While subsequent studies in higher vertebrates (frog and mouse) showed a modulatory role, amplifying the Wnt signal [116,118,119,131]. In *Pygo1/2* knockout mice, a reduction in the Wnt signal, not a complete loss was demonstrated using the Bat-Gal reporter. In this way, many of the defects observed within this project, in both zebrafish and mouse, may be attributed to a reduction in Wnt signaling. In particular, the possible proliferative defect, is likely to be a result of reduced Wnt signaling. This is based upon the primary role of canonical Wnt signaling in promoting cell proliferation and that *Cyclin D1* is the best candidate target gene of Pygo2 regulation from prior Pygo2 ablation studies *in vivo* and *in vitro* [131,135,136,144,149].

Despite this role in canonical Wnt signaling, recent evidence has demonstrated Pygo2 interactions with chromatin associated proteins. For example, chromatin immunoprecipitation assays have revealed Pygo2 binds to the promoters of multiple histones and enhances acetylation of histone H3 [135,366]. This would suggest an additional regulatory mechanism of Pygo2 at the epigenetic level and may go some way towards explaining the differences between the invertebrate and vertebrate Wnt signaling. The defect in gastrulation identified by knockdown of *pygo2* in zebrafish also provides evidence for a function in the non-canonical Wnt pathway. The non-canonical pathway is important during early embryonic gastrulation events of many vertebrate embryos [86]. Further evidence for the β-catenin independent function of *Pygo2* has been revealed by others, specifically within embryonic axis patterning of the frog, and in murine

eye development [119,261]. In this way, the epigenetic role of Pygo2 adds an additional aspect to Wnt pathway regulation [136].

Whilst the *pygo* homologs exhibit a pleiotropic nature, their functions are intrinsically linked to the Wnt pathway. In all loss of function models studied to date, from invertebrate to vertebrates, morphological defects may be attributed to either the canonical or non-canonical Wnt signaling cascades [83,116,118,131]. Furthermore, this study has demonstrated that the *pygo* gene appeared simultaneously in metazoans, in an evolutionary context, alongside other members of the Wnt pathway. With its variable roles, and close association to the Wnt pathway, it is likely the role of *Pygo2* in Wnt signal transduction is context dependent. For instance, the defects observed in pygo ablation studies appear to be dependent upon the organism, tissue, or ultimately the cell autonomous and non-autonomous signaling environment. In this way, the context dependent nature of the *pygo* homologs' various roles are supported by theory of the Wnt 'regulatory network' responding to various signaling inputs in a context dependent manner as suggested by van Amerongen and Nusse (2009)[105].

Interestingly, EPI-NCSC may yet provide insight into this possibility. The surprising mild proliferative enhancement of these cells, is likely due to an unrecognized external factor, or intracellular signal modulating the Wnt pathway. This project has provided the preliminary steps towards defining a basal culture medium vital for future studies on the cell-autonomous signaling environment. With this in mind, transcriptional and epigenetic profiling may yet identify these unknown co-operating factors and further interrogate the complexity of the Wnt regulatory network. For example, differential microarray analysis may identify members of specific pathways, or signaling receptors required for the maintenance and proliferation of EPI-NCSC.

6.4 Pygo2 and functional redundancy

Evidence from the initial knockout studies in mice by [116,131] suggested a largely redundant function of *Pygo1* in mammalian development. *Pygo1*

knockout mice are viable and fertile and display no overt phenotype. Yet the Bat-Gal reporter showed a greater reduction of Wnt signaling in the combined *Pygo1/2* knockout versus the *Pygo2* alone. Furthermore, others have reported cardiac defects in dual *Pygo1/2* knockouts suggesting *Pygo1* may function in a compensatory manner in mice.

Evidence produced by this thesis has shown knockdown of both *pygo* homologs in zebrafish demonstrate distinct roles in cranio-facial development and gastrulation. Interestingly, both zebrafish and mouse models also displayed cardiac abnormalities, including a reduced heart rate and looping, in the *pygo2* zebrafish morphant, and a thickening of the cardiac walls in the *Pygo2* CKO mouse. In particular, the calcification of the styloid process in newborn *Pygo2* CKO mice, may lead to compression of the carotid artery and subsequent heart strain during embryonic development leading to hypertrophy or alternatively, this may be due to a delay in OFT septation during development of the *Pygo2* CKO mouse. While these defects may be secondary effects, they still provide support for the OFT abnormalities reported by Aguet *et al.* (2006)[360] in the combined *Pygo1/2* knockout.

Previous reports of *Pygo1* embryonic expression are limited. However, this report has identified that *Pygo1* expression is found in comparable levels to the newborn heart across nearly all organs studied (see Appendix A). Moreover, the expression of *Pygo1* may be up-regulated in some of these tissues. Other studies have also shown an extended expression pattern for *Pygo1* in the mouse [120-125]. With this in mind, it is possible that in the mammalian context, *Pygo1* may provide a compensatory or gene dosage function.

In general, the evolutionary conservation, expression pattern and defects in zebrafish and mouse models would suggest that *Pygo1* is important in the vertebrate system and that this may yet again be in a context dependent manner. For example, the loss of *Pygo2* lead to minor cardiac abnormalities in the *Pygo2* CKO unlikely to cause death, yet ablation of both homologs reportedly leads to OFT defects, in a NC-related manner [360]. Assuming that the heart of

the *Pygo1* knockout mouse was not analysed, in the prior study by Scwab *et al.* (2007)[131], it is likely it too may display a mild phenotype.

Alternatively, the context dependent nature of *Pygo2* function may also affect the role of *Pygo1*. For example, most of the defects found during this project were not previously reported in the *Pygo2 null* mouse. These include the gasping respiration, abdominal bloating, cranio-facial abnormalities, reduction of neurons in the GI tract and Me5, and thickening of the cardiac walls. In a similar manner, a NC specific knockout of *Pygo1* may yield additional phenotypes.

6.5 A novel role for NC and the Wnt pathway in hair follicle formation

An important finding by this project was the reduction in hair follicle density and thickness in the *Pygo2* CKO neonate. While it is well documented that the Wnt pathway is crucial for formation of the primary placodes in hair follicle morphogenesis [329], a role for NC in hair follicle formation has not previously been reported. This represents an entirely novel aspect of NC biology and warrants further investigation.

This result together with the finding that *Pygo2* is a signature gene of EPI-NCSC, naturally leads to the hypothesis that *Pygo2* would be relevant for EPI-NCSC biology. While this may still be the case, the mild proliferative enhancement of EPI-NCSC *ex vivo* seem to suggest the contrary. It is possible this is due to the manner in which the signature genes were originally identified. The signature genes represent the unique transcriptional signature of both NCSC and EPI-NCSC after subtraction of genes in common with other SC. It is possible that this process has led to the removal of many of the functionally relevant genes required by EPI-NCSC and SC in general. This further highlights that *Pygo2* expression may be required much earlier in NC formation, and like other NC-related genes in EPI-NCSC, its expression is a remnant of these earlier processes. For example, *Nes* is highly expressed in EPI-NCSC cultures, yet it is normally expressed early in embryonic development and knockout mice are embryonic lethal [454].

6.6 Concluding remarks

In summary, this project has addressed the aims set out in the introduction and provided evidence in support of aspects of the core hypothesis, that *Pygo2* is required for the normal formation, maintenance, migration, development and differentiation of NCSC. Specifically, it has provided a broader understanding of the evolutionary context of *pygo* homologs, determined their role in zebrafish development and highlighted the function of *Pygo2* in murine NC development and EPI-NCSC. In addition, it delivers clarification for many of the inconsistencies initially observed amongst vertebrate pygo homologs. Substantial evidence for the hypothesis has also been revealed leading to the conclusion that *Pygo2* is required for the normal development of vertebrate NC. Finally, the data presented by this thesis provides an invaluable contribution to the fields of NC and Wnt biology alike and suggests by analogy to Pax3, *Pygo2* may play a critical role in NC progenitor proliferation.

Appendix A

I. Pygo1 is universally expressed in wild type and Pygo2 CKO newborn organs

The current understanding of the role of *Pygo1* is limited. Following the discovery of the two mouse *pygo* homologs, the majority of studies have focused entirely on *Pygo2* and omitted *Pygo1*. This is likely due to the early study conducted by Schwab *et al.* (2007) that concluded the role of *Pygo1* is largely redundant. They found *Pygo1 null* mice were viable and displayed no overt phenotype. When *Pygo2 null* mice were bred on a *Pygo1* deficient background, there was reportedly no difference in phenotype or severity, compared to the *Pygo2 null*, apart from a mild reduction in Wnt signal transduction. Because the combined knockout of both *pygo* homologs did not yield a synergistic effect, it was suggested that *Pygo1* is likely redundant.

Early evidence from the cloning and expression of *Pygo1* found a relatively low expression of *Pygo1* increasing in the later stages of embryonic development (17.5 dpc), and eventually restricted to the heart of adult mice (see Chapter 1). More recently expression in the pharyngeal arches, brain, eye, limbs, kidney and gonads has been demonstrated [120-122]. This raises an important question. Could some of the relatively mild defects and partially penetrant phenotype of the *Pygo2* CKO, be due to partial rescue by *Pygo1*? This would however, require an expanded expression pattern for *Pygo1* than is currently known.

To explore this possibility further, a number of NC derived, and non-NC derived tissues were collected from 2 wild type newborn pups. Using oligonucleotide primers specific to the *Pygo1* transcript, the relative expression of *Pygo1* to housekeeping genes was analysed using quantitative real-time PCR (qPCR) in triplicate assays.

The overall expression of *Pygo1* was relatively low, consistently around 5% of the level of the housekeeping genes, HPRT and β-Actin. Despite this, expression of *Pygo1* was found in all tissues analysed, varying from 50% to 200% relative

to the level of expression found in newborn heart. This is important, as heart is the only site of *Pygo1* expression found in the adult mouse. Interestingly, some tissues with NC contributions had elevated levels of *Pygo1* compared to the heart. For example, expression in back skin and adrenal tissues was on average >2 fold-higher than the heart as illustrated in Figure A.

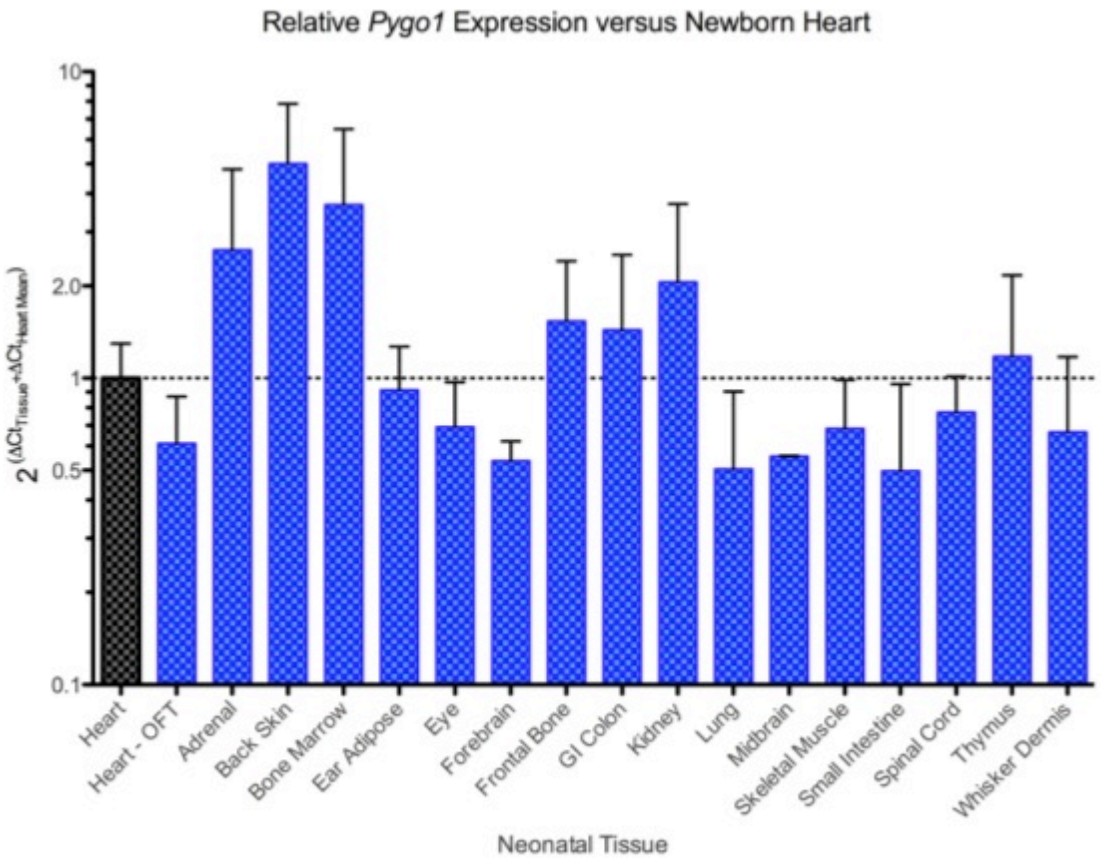

Figure I. Relative expression of *Pygo1* in embryonic tissues, relative to the heart
Quantitative real-time PCR reveals variable levels of *Pygo1* expression across neonatal tissues and organs. Levels are expressed relative to embryonic heart and represent triplicate repeats of each sample, from two wild type animals. Importantly, expression is seen in all tissues analysed.

II. Up regulation of Pygo1 in Pygo2 CKO

In addition to the expanded expression pattern in wild type tissues, the level of *Pygo1* in *Pygo2* CKO tissues was analysed. Interestingly, in *Pygo2* CKO tissues the overall level of *Pygo1* appeared to be much higher, approximately 13% of the housekeeping gene expression. This was particularly evident in specific tissues, like back skin, OFT and eye. Despite this, the results were variable between animals. While further validation is required, these results provide provocative evidence for a role of *Pygo1* in murine development, and the possibility of downstream regulation by *Pygo2*. In addition to the expression of *Pygo1* in other tissues, the relative expression of *Pygo1* in mutants is higher.

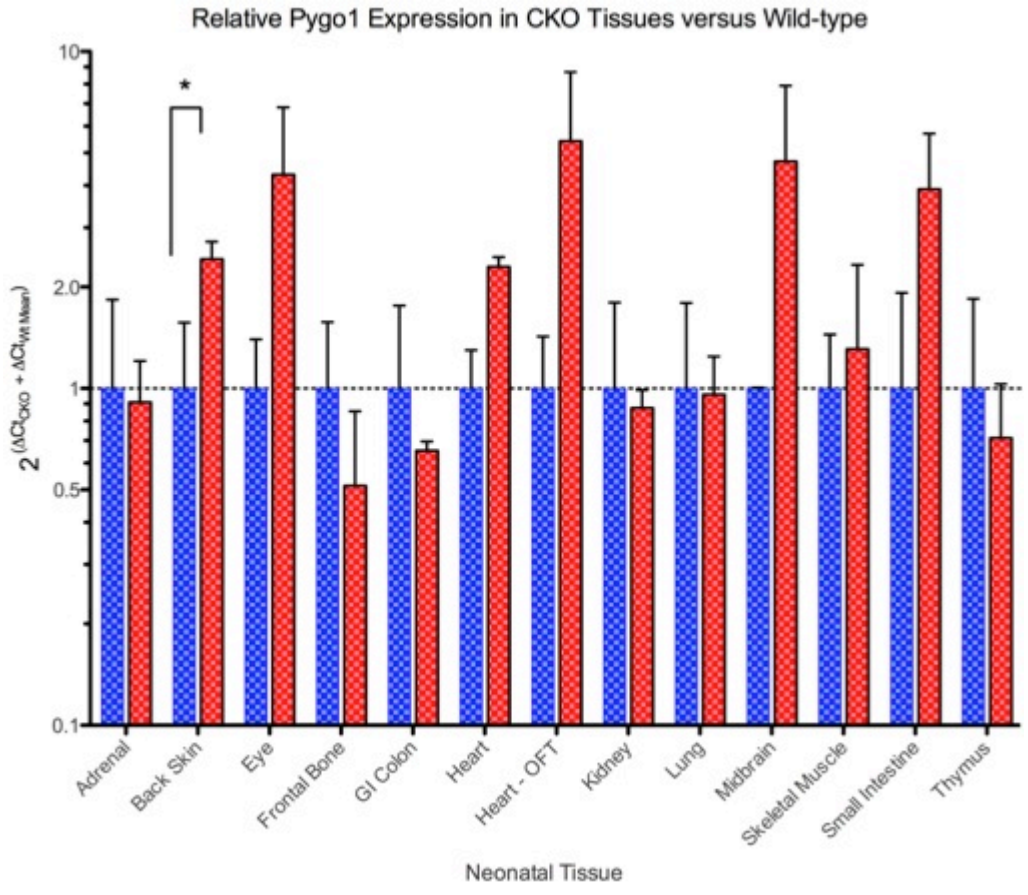

Figure II. Expression of Pygo1 in *Pygo2* CKO is specifically up-regulated by different tissues
Quantitative real-time PCR reveals variable higher levels of *Pygo1* expression in some *Pygo2* CKO tissues compared to wild type.

List of References

1. Sieber-Blum M, Grim M, Hu YF, Szeder V (2004) Pluripotent neural crest stem cells in the adult hair follicle. Dev Dyn 231: 258–269. doi:10.1002/dvdy.20129.

2. Sieber-Blum M, Grim M (2004) The adult hair follicle: cradle for pluripotent neural crest stem cells. Birth Defects Res C Embryo Today 72: 162–172. doi:10.1002/bdrc.20008.

3. Takahashi K, Yamanaka S (2006) Induction of pluripotent stem cells from mouse embryonic and adult fibroblast cultures by defined factors. Cell 126: 663–676. doi:10.1016/j.cell.2006.07.024.

4. Gilbert SF (2010) Developmental biology.

5. Shook DR, Keller R (2008) Epithelial type, ingression, blastopore architecture and the evolution of chordate mesoderm morphogenesis. J Exp Zool B Mol Dev Evol 310: 85–110. doi:10.1002/jez.b.21198.

6. His W (1868) Untersuchungen über die erste Anlage des Wirbeltierleibes. Leipzig: F. C. W. Vogel. pp.

7. Marshall AM (1879) The morphology of the vertebrate olfactory organ. Quarterly Journal of Microscopial Science 19: 300–340.

8. Hall BK (1999) The neural crest in development and evolution. Springer Verlag. pp.

9. Hall BK (2010) The Neural Crest and Neural Crest Cells in Vertebrate Development and Evolution. Springer Verlag. pp.

10. Hall BK (2008) The neural crest and neural crest cells: discovery and significance for theories of embryonic organization. J Biosci 33: 781–793.

11. Gammill LS, Bronner-Fraser M (2003) Neural crest specification: migrating into genomics. Nat Rev Neurosci 4: 795–805. doi:10.1038/nrn1219.

12. Bronner ME, LeDouarin NM (2012) Development and evolution of the neural crest: An overview. Dev Biol. doi:10.1016/j.ydbio.2011.12.042.

13. Betancur P, Bronner-Fraser M, Sauka-Spengler T (2010) Assembling neural crest regulatory circuits into a gene regulatory network. Annu Rev Cell Dev Biol 26: 581–603. doi:10.1146/annurev.cellbio.042308.113245.

14. Sauka-Spengler T, Bronner-Fraser M (2008) A gene regulatory network orchestrates neural crest formation. Nat Rev Mol Cell Biol 9: 557–568. doi:10.1038/nrm2428.

15. Woda JM, Pastagia J, Mercola M, Artinger KB (2003) Dlx proteins position the neural plate border and determine adjacent cell fates. Development 130: 331–342.

16. Donoghue PCJ, Graham A, Kelsh RN (2008) The origin and evolution of the neural crest. Bioessays 30: 530–541. doi:10.1002/bies.20767.

17. McMahon AP, Joyner AL, Bradley A, McMahon JA (1992) The midbrain-hindbrain phenotype of Wnt-1-/Wnt-1- mice results from stepwise deletion of engrailed-expressing cells by 9.5 days postcoitum. Cell 69: 581–595.

18. Knecht AK, Bronner-Fraser M (2002) Induction of the neural crest: a multigene process. Nat Rev Genet 3: 453–461. doi:10.1038/nrg819.

19. Jiang X, Rowitch DH, Soriano P, McMahon AP, Sucov HM (2000) Fate of the mammalian cardiac neural crest. Development 127: 1607–1616.

20. Snider P, Olaopa M, Firulli AB, Conway SJ (2007) Cardiovascular development and the colonizing cardiac neural crest lineage. ScientificWorldJournal 7: 1090–1113. doi:10.1100/tsw.2007.189.

21. Bellmeyer A, Krase J, Lindgren J, LaBonne C (2003) The protooncogene c-myc is an essential regulator of neural crest formation in xenopus. Dev Cell 4: 827–839.

22. Kee Y, Bronner-Fraser M (2005) To proliferate or to die: role of Id3 in cell cycle progression and survival of neural crest progenitors. Genes Dev 19: 744–755. doi:10.1101/gad.1257405.

23. Panda DK, Miao D, Lefebvre V, Hendy GN, Goltzman D (2001) The transcription factor SOX9 regulates cell cycle and differentiation genes in chondrocytic CFK2 cells. J Biol Chem 276: 41229–41236. doi:10.1074/jbc.M104231200.

24. Theveneau E, Mayor R (2012) Neural crest delamination and migration: From epithelium-to-mesenchyme transition to collective cell migration. Dev Biol: 1–21. doi:10.1016/j.ydbio.2011.12.041.

25. Casini P, Nardi I, Ori M (2011) Hyaluronan is required for cranial neural crest cells migration and craniofacial development. Dev Dyn: n/a–n/a. doi:10.1002/dvdy.23715.

26. Kuriyama S, Mayor R (2008) Molecular analysis of neural crest migration. Philos Trans R Soc Lond, B, Biol Sci 363: 1349–1362. doi:10.1098/rstb.2007.2252.

27. Burstyn-Cohen T, Kalcheim C (2002) Association between the cell cycle and neural crest delamination through specific regulation of G1/S transition. Dev Cell 3: 383–395.

28. Burstyn-Cohen T, Stanleigh J, Sela-Donenfeld D, Kalcheim C (2004) Canonical Wnt activity regulates trunk neural crest delamination linking BMP/noggin signaling with G1/S transition. Development 131: 5327–5339. doi:10.1242/dev.01424.

29. Vega S, Morales AV, Ocaña OH, Valdés F, Fabregat I, et al. (2004) Snail blocks the cell cycle and confers resistance to cell death. Genes Dev 18: 1131–1143. doi:10.1101/gad.294104.

30. Hall BK, Hörstadius S (1988) The neural crest. Oxford University Press, USA. pp.

31. Serbedzija GN, Bronner-Fraser M, Fraser SE (1992) Vital dye analysis of cranial neural crest cell migration in the mouse embryo. Development 116: 297–307.

32. Noden DM (1983) The role of the neural crest in patterning of avian cranial skeletal, connective, and muscle tissues. Dev Biol 96: 144–165. doi:10.1016/0012-1606(83)90318-4.

33. Johnston MC (1966) A radioautographic study of the migration and fate of cranial neural crest cells in the chick embryo. Anat Rec 156: 143–155. doi:10.1002/ar.1091560204.

34. Hammond WS, Yntema CL (1964) Depletions of Pharyngeal Arch Cartilages Following Extirpation of Cranial Neural Crest in Chick Embryos. Acta Anat (Basel) 56: 21–34.

35. KIRBY M (1989) Plasticity and predetermination of mesencephalic and trunk neural crest transplanted into the region of the cardiac neural crest. Dev Biol 134: 402–412. doi:10.1016/0012-1606(89)90112-7.

36. Chan WY, Cheung CS, Yung KM, Copp AJ (2004) Cardiac neural crest of the mouse embryo: axial level of origin, migratory pathway and cell autonomy of the splotch (Sp2H) mutant effect. Development 131: 3367–3379. doi:10.1242/dev.01197.

37. Le Lièvre CS, Le Douarin NM (1975) Mesenchymal derivatives of the neural crest: analysis of chimaeric quail and chick embryos. J Embryol Exp Morphol 34: 125–154.

38. Pomeranz HD, Rothman TP, Gershon MD (1991) Colonization of the post-umbilical bowel by cells derived from the sacral neural crest: direct tracing of cell migration using an intercalating probe and a replication-deficient retrovirus. Development 111: 647–655.

39. Wang X, Chan AKK, Sham M-H, Burns AJ, Chan WY (2011) Analysis of the

sacral neural crest cell contribution to the hindgut enteric nervous system in the mouse embryo. Gastroenterology. doi:10.1053/j.gastro.2011.06.002.

40. Le Douarin NM, Teillet M-A (1973) The migration of neural crest cells to the wall of the digestive tract in avian embryo. J Embryol Exp Morphol 30: 31–48.

41. Serbedzija GN, Bronner-Fraser M, Fraser SE (1994) Developmental potential of trunk neural crest cells in the mouse. Development 120: 1709–1718.

42. Bronner-Fraser M, Fraser SE (1988) Cell lineage analysis reveals multipotency of some avian neural crest cells. Nature 335: 161–164. doi:10.1038/335161a0.

43. Baroffio A, Dupin E, Le Douarin NM (1988) Clone-forming ability and differentiation potential of migratory neural crest cells. Proc Natl Acad Sci USA 85: 5325–5329.

44. Dupin E, Calloni GW, Le Douarin NM (2010) The cephalic neural crest of amniote vertebrates is composed of a large majority of precursors endowed with neural, melanocytic, chondrogenic and osteogenic potentialities. Cell Cycle 9: 238–249.

45. Le Douarin NM, Calloni GW, Dupin E (2008) The stem cells of the neural crest. Cell Cycle 7: 1013–1019.

46. Sieber-Blum M, Cohen AM (1980) Clonal analysis of quail neural crest cells: they are pluripotent and differentiate in vitro in the absence of noncrest cells. Dev Biol 80: 96–106.

47. Stemple DL, Anderson DJ (1993) Lineage diversification of the neural crest: in vitro investigations. Dev Biol 159: 12–23. doi:10.1006/dbio.1993.1218.

48. Trentin A, Glavieux-Pardanaud C, Le Douarin NM, Dupin E (2004) Self-renewal capacity is a widespread property of various types of neural crest precursor cells. Proc Natl Acad Sci USA 101: 4495–4500. doi:10.1073/pnas.0400629101.

49. Sieber-Blum M, Ito K, Richardson MK, Langtimm CJ, Duff RS (1993) Distribution of pluripotent neural crest cells in the embryo and the role of brain-derived neurotrophic factor in the commitment to the primary sensory neuron lineage. J Neurobiol 24: 173–184. doi:10.1002/neu.480240205.

50. Duff RS, Langtimm CJ, Richardson MK, Sieber-Blum M (1991) In vitro clonal analysis of progenitor cell patterns in dorsal root and sympathetic ganglia of the quail embryo. Dev Biol 147: 451–459.

51. Sieber-Blum M (1989) Commitment of neural crest cells to the sensory neuron lineage. Science 243: 1608–1611.

52. Ito K, Sieber-Blum M (1991) In vitro clonal analysis of quail cardiac neural crest development. Dev Biol 148: 95–106.

53. Ito K, Sieber-Blum M (1993) Pluripotent and developmentally restricted neural-crest-derived cells in posterior visceral arches. Dev Biol 156: 191–200. doi:10.1006/dbio.1993.1069.

54. Raible DW, Eisen JS (1996) Regulative interactions in zebrafish neural crest. Development 122: 501–507.

55. Baker CV, Bronner-Fraser M, Le Douarin NM, Teillet MA (1997) Early- and late-migrating cranial neural crest cell populations have equivalent developmental potential in vivo. Development 124: 3077–3087.

56. Le Douarin NM, Teillet MA (1974) Experimental analysis of the migration and differentiation of neuroblasts of the autonomic nervous system and of neurectodermal mesenchymal derivatives, using a biological cell marking technique. Dev Biol 41: 162–184.

57. Nakamura H, Ayer-le Lievre CS (1982) Mesectodermal capabilities of the trunk neural crest of birds. J Embryol Exp Morphol 70: 1–18.

58. Le Lièvre CS, Schweizer GG, Ziller CM, Le Douarin NM (1980) Restrictions of developmental capabilities in neural crest cell derivatives as tested by in vivo transplantation experiments. Dev Biol 77: 362–378.

59. Calloni GW, Glavieux-Pardanaud C, Le Douarin NM, Dupin E (2007) Sonic Hedgehog promotes the development of multipotent neural crest progenitors endowed with both mesenchymal and neural potentials. Proceedings of the National Academy of Sciences 104: 19879–19884. doi:10.1073/pnas.0708806104.

60. McGonnell IM, Graham A (2002) Trunk neural crest has skeletogenic potential. Curr Biol 12: 767–771.

61. Spix C, Pastore G, Sankila R, Stiller C, Steliarovafoucher E (2006) Neuroblastoma incidence and survival in European children (1978–1997): Report from the Automated Childhood Cancer Information System project. European Journal of Cancer 42: 2081–2091. doi:10.1016/j.ejca.2006.05.008.

62. Stiller CA, Parkin DM (1992) International Variations in the Incidence of Neuroblastoma. Int J Cancer 42: 538.

63. Powell JE, Estève J, Mann JR, Parker L, Frappaz D, et al. (1998) Neuroblastoma in Europe: differences in the pattern of disease in the UK. The Lancet 352: 682–687. doi:10.1016/S0140-6736(97)11239-9.

64. H Schroeder JWHLSRCRBLPNLTC (2009) Unchanged incidence and increased survival in children with neuroblastoma in Denmark 1981–2000: a population-based study. British Journal of Cancer 100: 853. doi:10.1038/sj.bjc.6604922.

65. Quatresooz P, Vandenbossche G, Piérard-Franchimont C, Piérard GE (2008) [Skin and its main neurocristopathies]. Rev Med Liege 63: 354–358.

66. Prada CE, Rangwala FA, Martin LJ, Lovell AM, Saal HM, et al. (2012) Pediatric plexiform neurofibromas: impact on morbidity and mortality in neurofibromatosis type 1. J Pediatr 160: 461–467. doi:10.1016/j.jpeds.2011.08.051.

67. Filippini G (2012) Epidemiology of primary central nervous system tumors. Handb Clin Neurol 104: 3–22. doi:10.1016/B978-0-444-52138-5.00001-3.

68. Yutzey KE (2010) DiGeorge syndrome, Tbx1, and retinoic acid signaling come full circle. Circ Res 106: 630–632. doi:10.1161/CIRCRESAHA.109.215319.

69. Druckenbrod NR, Epstein ML (2009) Age-dependent changes in the gut environment restrict the invasion of the hindgut by enteric neural progenitors. Development 136: 3195–3203. doi:10.1242/dev.031302.

70. Festen C (2000) Hirschsprungs disease. J Pediatr Surg 35: 1409.

71. Krejčí E, Grim M (2010) Isolation and characterization of neural crest stem cells from adult human hair follicles. Folia Biol (Praha) 56: 149–157.

72. Clewes O, Narytnyk A, Gillinder KR, Loughney AD, Murdoch AP, et al. (2011) Human Epidermal Neural Crest Stem Cells (hEPI-NCSC)-Characterization and Directed Differentiation into Osteocytes and Melanocytes. Stem Cell Rev. doi:10.1007/s12015-011-9255-5.

73. Sieber-Blum M (2004) Cardiac neural crest stem cells. Anat Rec A Discov Mol Cell Evol Biol 276: 34–42. doi:10.1002/ar.a.10132.

74. Hu YF, Zhang Z-J, Sieber-Blum M (2006) An epidermal neural crest stem cell (EPI-NCSC) molecular signature. Stem cells (Dayton, Ohio) 24: 2692–2702. doi:10.1634/stemcells.2006-0233.

75. Sieber-Blum M, Hu Y (2008) Epidermal neural crest stem cells (EPI-NCSC) and pluripotency. Stem Cell Rev 4: 256–260. doi:10.1007/s12015-008-9042-0.

76. Sieber-Blum M, Schnell L, Grim M, Hu YF, Schneider R, et al. (2006) Characterization of epidermal neural crest stem cell (EPI-NCSC) grafts in the lesioned spinal cord. Mol Cell Neurosci 32: 67–81.

doi:10.1016/j.mcn.2006.02.003.

77. Hu YF, Gourab K, Wells C, Clewes O, Schmit BD, et al. (2010) Epidermal neural crest stem cell (EPI-NCSC)--mediated recovery of sensory function in a mouse model of spinal cord injury. Stem Cell Rev 6: 186–198. doi:10.1007/s12015-010-9152-3.

78. Sieber-Blum M (2010) Epidermal neural crest stem cells and their use in mouse models of spinal cord injury. Brain Res Bull 83: 189–193. doi:10.1016/j.brainresbull.2010.07.002.

79. Tumbar T, Guasch G, Greco V, Blanpain C, Lowry WE, et al. (2004) Defining the epithelial stem cell niche in skin. Science 303: 359–363. doi:10.1126/science.1092436.

80. Prieve MG, Waterman ML (1999) Nuclear localization and formation of beta-catenin-lymphoid enhancer factor 1 complexes are not sufficient for activation of gene expression. Molecular and Cellular Biology 19: 4503–4515.

81. Thompson B, Townsley F, Rosin-Arbesfeld R, Musisi H, Bienz M (2002) A new nuclear component of the Wnt signalling pathway. Nat Cell Biol 4: 367–373. doi:10.1038/ncb786.

82. Kramps T, Peter O, Brunner E, Nellen D, Froesch B, et al. (2002) Wnt/wingless signaling requires BCL9/legless-mediated recruitment of pygopus to the nuclear beta-catenin-TCF complex. Cell 109: 47–60.

83. Belenkaya TY, Han C, Standley HJ, Lin X, Houston DW, et al. (2002) pygopus Encodes a nuclear protein essential for wingless/Wnt signaling. Development 129: 4089–4101.

84. Parker DS, Jemison J, Cadigan KM (2002) Pygopus, a nuclear PHD-finger protein required for Wingless signaling in Drosophila. Development 129: 2565–2576.

85. Logan CY, Nusse R (2004) The Wnt signaling pathway in development and disease. Annu Rev Cell Dev Biol 20: 781–810. doi:10.1146/annurev.cellbio.20.010403.113126.

86. Tada M, Concha ML, Heisenberg CP (2002) Non-canonical Wnt signalling and regulation of gastrulation movements. Semin Cell Dev Biol 13: 251–260.

87. Tada M, Kai M (2009) Noncanonical Wnt/PCP signaling during vertebrate gastrulation. Zebrafish 6: 29–40. doi:10.1089/zeb.2008.0566.

88. McNeill H (2009) Planar cell polarity and the kidney. J Am Soc Nephrol 20: 2104–2111. doi:10.1681/ASN.2008111173.

89. Tzahor E (2007) Wnt/beta-catenin signaling and cardiogenesis: timing does matter. Dev Cell 13: 10–13. doi:10.1016/j.devcel.2007.06.006.

90. Clevers H (2009) Eyeing up new Wnt pathway players. Cell 139: 227–229. doi:10.1016/j.cell.2009.09.027.

91. Basch ML, Bronner-Fraser M, García-Castro MI (2006) Specification of the neural crest occurs during gastrulation and requires Pax7. Nature 441: 218–222. doi:10.1038/nature04684.

92. de Calisto J, Araya C, Marchant L, Riaz CF, Mayor R (2005) Essential role of non-canonical Wnt signalling in neural crest migration. Development 132: 2587–2597. doi:10.1242/dev.01857.

93. Zhang Y, Ruest LB (2012) Analysis of Neural Crest Cell Fate During Cardiovascular Development Using Cre-Activated lacZ/β-Galactosidase Staining. Methods Mol Biol 843: 125–138. doi:10.1007/978-1-61779-523-7_12.

94. Stoick-Cooper CL, Moon RT, Weidinger G (2007) Advances in signaling in vertebrate regeneration as a prelude to regenerative medicine. Genes Dev 21: 1292–1315. doi:10.1101/gad.1540507.

95. Stoick-Cooper CL, Weidinger G, Riehle KJ, Hubbert C, Major MB, et al. (2007) Distinct Wnt signaling pathways have opposing roles in appendage regeneration. Development 134: 479–489. doi:10.1242/dev.001123.

96. Secreto FJ, Hoeppner LH, Westendorf JJ (2009) Wnt signaling during fracture repair. Current osteoporosis reports 7: 64–69.

97. Katoh M, Katoh M (2007) WNT signaling pathway and stem cell signaling network. Clin Cancer Res 13: 4042–4045. doi:10.1158/1078-0432.CCR-06-2316.

98. Reya T, Clevers H (2005) Wnt signalling in stem cells and cancer. Nature 434: 843–850. doi:10.1038/nature03319.

99. Sierra J, Yoshida T, Joazeiro CA, Jones KA (2006) The APC tumor suppressor counteracts beta-catenin activation and H3K4 methylation at Wnt target genes. Genes Dev 20: 586–600. doi:10.1101/gad.1385806.

100. MacDonald BT, Tamai K, He X (2009) Wnt/beta-catenin signaling: components, mechanisms, and diseases. Dev Cell 17: 9–26. doi:10.1016/j.devcel.2009.06.016.

101. Klaus A, Birchmeier W (2008) Wnt signalling and its impact on development and cancer. Nat Rev Cancer 8: 387–398. doi:10.1038/nrc2389.

102. Chen W, Chen M, Barak LS (2010) Development of small molecules

targeting the Wnt pathway for the treatment of colon cancer: a high-throughput screening approach. Am J Physiol Gastrointest Liver Physiol 299: G293–G300. doi:10.1152/ajpgi.00005.2010.

103. Moon RT, Kohn AD, de Ferrari GV, Kaykas A (2004) WNT and beta-catenin signalling: diseases and therapies. Nat Rev Genet 5: 691–701. doi:10.1038/nrg1427.

104. Kikuchi A, Yamamoto H, Sato A (2009) Selective activation mechanisms of Wnt signaling pathways. Trends Cell Biol 19: 119–129. doi:10.1016/j.tcb.2009.01.003.

105. van Amerongen R, Nusse R (2009) Towards an integrated view of Wnt signaling in development. Development 136: 3205–3214. doi:10.1242/dev.033910.

106. McMahon AP, Moon RT (1989) Ectopic expression of the proto-oncogene int-1 in Xenopus embryos leads to duplication of the embryonic axis. Cell 58: 1075–1084.

107. Angers S, Moon RT (2009) Proximal events in Wnt signal transduction. Nat Rev Mol Cell Biol 10: 468–477. doi:10.1038/nrm2717.

108. Lu W, Yamamoto V, Ortega B, Baltimore D (2004) Mammalian Ryk is a Wnt coreceptor required for stimulation of neurite outgrowth. Cell 119: 97–108. doi:10.1016/j.cell.2004.09.019.

109. Hikasa H, Sokol SY (2004) The involvement of Frodo in TCF-dependent signaling and neural tissue development. Development 131: 4725–4734. doi:10.1242/dev.01369.

110. Mosimann C, Hausmann G, Basler K (2009) Beta-catenin hits chromatin: regulation of Wnt target gene activation. Nat Rev Mol Cell Biol 10: 276–286. doi:10.1038/nrm2654.

111. Mieszczanek J, La Roche de M, Bienz M (2008) A role of Pygopus as an anti-repressor in facilitating Wnt-dependent transcription. Proc Natl Acad Sci USA 105: 19324–19329. doi:10.1073/pnas.0806098105.

112. Gao C, Chen Y-G (2010) Dishevelled: The hub of Wnt signaling. Cell Signal 22: 717–727. doi:10.1016/j.cellsig.2009.11.021.

113. Song H, Hu J, Chen W, Elliott G, Andre P, et al. (2010) Planar cell polarity breaks bilateral symmetry by controlling ciliary positioning. Nature 466: 378–382. doi:10.1038/nature09129.

114. Petersen LF, Ninomiya H, Winklbauer R (2008) Regulation of convergent extension by non-canonical Wnt signaling in the Xenopus embryo. Methods Mol Biol 469: 477–484. doi:10.1007/978-1-60327-469-2_30.

115. Purro SA, Ciani L, Hoyos-Flight M, Stamatakou E, Siomou E, et al. (2008) Wnt regulates axon behavior through changes in microtubule growth directionality: a new role for adenomatous polyposis coli. J Neurosci 28: 8644–8654. doi:10.1523/JNEUROSCI.2320-08.2008.

116. Li B, Rhéaume C, Teng A, Bilanchone V, Munguia JE, et al. (2007) Developmental phenotypes and reduced Wnt signaling in mice deficient for pygopus 2. genesis 45: 318–325. doi:10.1002/dvg.20299.

117. Bienz M (2006) The PHD finger, a nuclear protein-interaction domain. Trends Biochem Sci.

118. Lake BB, Kao KR (2003) Pygopus is required for embryonic brain patterning in Xenopus. Dev Biol 261: 132–148.

119. Kennedy MW, Cha S-W, Tadjuidje E, Andrews PG, Heasman J, et al. (2010) A co-dependent requirement of xBcl9 and Pygopus for embryonic body axis development in Xenopus. Dev Dyn 239: 271–283. doi:10.1002/dvdy.22133.

120. Edgar R, Domrachev M, Lash AE (2002) Gene Expression Omnibus: NCBI gene expression and hybridization array data repository. Nucleic Acids Res 30: 207–210.

121. Little MH, Brennan J, Georgas K, Davies JA, Davidson DR, et al. (2007) A high-resolution anatomical ontology of the developing murine genitourinary tract. Gene Expr Patterns 7: 680–699. doi:10.1016/j.modgep.2007.03.002.

122. Baldock RA, Bard JBL, Burger A, Burton N, Christiansen J, et al. (2003) EMAP and EMAGE: a framework for understanding spatially organized data. Neuroinformatics 1: 309–325. doi:10.1385/NI:1:4:309.

123. Song N, Schwab KR, Patterson LT, Yamaguchi T, Lin X, et al. (2007) pygopus 2 has a crucial, Wnt pathway-independent function in lens induction. Development 134: 1873–1885. doi:10.1242/dev.001495.

124. Gray PA, Fu H, Luo P, Zhao Q, Yu J, et al. (2004) Mouse brain organization revealed through direct genome-scale TF expression analysis. Science 306: 2255–2257. doi:10.1126/science.1104935.

125. Nair M, Nagamori I, Sun P, Mishra DP, Rhéaume C, et al. (2008) Nuclear regulator Pygo2 controls spermiogenesis and histone H3 acetylation. Dev Biol 320: 446–455. doi:10.1016/j.ydbio.2008.05.553.

126. Aasland R, Gibson TJ, Stewart AF (1995) The PHD finger: implications for chromatin-mediated transcriptional regulation. Trends Biochem Sci 20: 56–59.

127. Thompson B (2004) A complex of armadillo, legless, and pygopus coactivates dTCF to activate wingless target genes. Curr Biol 14: 458–

466. doi:10.1016/j.cub.2004.02.026.

128. Städeli R, Basler K (2005) Dissecting nuclear Wingless signalling: recruitment of the transcriptional co-activator Pygopus by a chain of adaptor proteins. Mech Dev 122: 1171–1182. doi:10.1016/j.mod.2005.07.004.

129. Hoffmans R, Städeli R, Basler K (2005) Pygopus and legless provide essential transcriptional coactivator functions to armadillo/beta-catenin. Curr Biol 15: 1207–1211. doi:10.1016/j.cub.2005.05.054.

130. Cadigan KM, Peifer M (2009) Wnt signaling from development to disease: insights from model systems. Cold Spring Harb Perspect Biol 1: a002881. doi:10.1101/cshperspect.a002881.

131. Schwab KR, Patterson LT, Hartman HA, Song N, Lang RA, et al. (2007) Pygo1 and Pygo2 roles in Wnt signaling in mammalian kidney development. BMC Biol 5: 15. doi:10.1186/1741-7007-5-15.

132. Nakamura Y, Umehara T, Hamana H, Hayashizaki Y, Inoue M, et al. (2007) Crystal structure analysis of the PHD domain of the transcription co-activator Pygopus. J Mol Biol 370: 80–92. doi:10.1016/j.jmb.2007.04.037.

133. Miller TCR, Rutherford TJ, Johnson CM, Fiedler M, Bienz M (2010) Allosteric remodelling of the histone H3 binding pocket in the Pygo2 PHD finger triggered by its binding to the B9L/BCL9 co-factor. J Mol Biol 401: 969–984. doi:10.1016/j.jmb.2010.07.007.

134. Andrews PGP, He Z, Popadiuk C, Kao KR (2009) The transcriptional activity of Pygopus is enhanced by its interaction with cAMP-response-element-binding protein (CREB)-binding protein. Biochem J 422: 493–501. doi:10.1042/BJ20090134.

135. Gu B, Watanabe K, Dai X (2012) Pygo2 regulates histone gene expression and H3 K56 acetylation in human mammary epithelial cells. Cell Cycle 11: 79–87. doi:10.4161/cc.11.1.18402.

136. Chen J, Luo Q, Yuan Y, Huang X, Cai W, et al. (2010) Pygo2 associates with MLL2 histone methyltransferase and GCN5 histone acetyltransferase complexes to augment Wnt target gene expression and breast cancer stem-like cell expansion. Molecular and Cellular Biology 30: 5621–5635. doi:10.1128/MCB.00465-10.

137. Horsley V (2009) Epigenetics, Wnt signaling, and stem cells: the Pygo2 connection. J Cell Biol 185: 761–763. doi:10.1083/jcb.200904125.

138. La Roche de M, Bienz M (2007) Wingless-independent association of Pygopus with dTCF target genes. Curr Biol 17: 556–561. doi:10.1016/j.cub.2007.01.063.

139. Carrera I, Janody F, Leeds N, Duveau F, Treisman JE (2008) Pygopus activates Wingless target gene transcription through the mediator complex subunits Med12 and Med13. Proc Natl Acad Sci USA 105: 6644–6649. doi:10.1073/pnas.0709749105.

140. Wright KJ, Tjian R (2009) Wnt signaling targets ETO coactivation domain of TAF4/TFIID in vivo. Proc Natl Acad Sci USA 106: 55–60. doi:10.1073/pnas.0811914106.

141. Sustmann C, Flach H, Ebert H, Eastman Q, Grosschedl R (2008) Cell-type-specific function of BCL9 involves a transcriptional activation domain that synergizes with beta-catenin. Molecular and Cellular Biology 28: 3526–3537. doi:10.1128/MCB.01986-07.

142. Mosimann C, Hausmann G, Basler K (2006) Parafibromin/Hyrax activates Wnt/Wg target gene transcription by direct association with beta-catenin/Armadillo. Cell 125: 327–341. doi:10.1016/j.cell.2006.01.053.

143. Zhang Y, Dai Y, Liu Y, Ren J (2010) Mandibulofacial dysostosis, microtia, and limb anomalies in a newborn: a new form of acrofacial dysostosis syndrome? Clin Genet 78: 570–574. doi:10.1111/j.1399-0004.2010.01427.x.

144. Andrews PGP, Lake BB, Popadiuk C, Kao KR (2007) Requirement of Pygopus 2 in breast cancer. Int J Oncol 30: 357–363.

145. Andrews PGP, Kennedy MW, Popadiuk CM, Kao KR (2008) Oncogenic activation of the human Pygopus2 promoter by E74-like factor-1. Mol Cancer Res 6: 259–266. doi:10.1158/1541-7786.MCR-07-0068.

146. Skawran B, Steinemann D, Weigmann A, Flemming P, Becker T, et al. (2008) Gene expression profiling in hepatocellular carcinoma: upregulation of genes in amplified chromosome regions. Mod Pathol 21: 505–516. doi:10.1038/modpathol.3800998.

147. Popadiuk CM, Xiong J, Wells MG, Andrews PG, Dankwa K, et al. (2006) Antisense suppression of pygopus2 results in growth arrest of epithelial ovarian cancer. Clin Cancer Res 12: 2216–2223. doi:10.1158/1078-0432.CCR-05-2433.

148. Roose J, Clevers H (1999) TCF transcription factors: molecular switches in carcinogenesis. Biochim Biophys Acta 1424: M23–M37.

149. Wang Z-X, Chen Y-Y, Li B-A, Tan G-W, Liu X-Y, et al. (2010) Decreased pygopus 2 expression suppresses glioblastoma U251 cell growth. J Neurooncol 100: 31–41. doi:10.1007/s11060-010-0144-6.

150. Thorne CA, Hanson AJ, Schneider J, Tahinci E, Orton D, et al. (2010) Small-molecule inhibition of Wnt signaling through activation of casein kinase 1α. Nat Chem Biol 6: 829–836. doi:10.1038/nchembio.453.

151. Drummond A, Ashton B, Buxton S, Cheung M, Cooper A, et al. (2010) Geneious: 1–160. Available:http://www.geneious.com.

152. Edgar RC (2004) MUSCLE: multiple sequence alignment with high accuracy and high throughput. Nucleic Acids Res 32: 1792–1797. doi:10.1093/nar/gkh340.

153. Eddy SR (2004) Where did the BLOSUM62 alignment score matrix come from? Nat Biotechnol 22: 1035–1036. doi:10.1038/nbt0804-1035.

154. Carney TJ, Dutton KA, Greenhill E, Delfino-Machín M, Dufourcq P, et al. (2006) A direct role for Sox10 in specification of neural crest-derived sensory neurons. Development 133: 4619–4630. doi:10.1242/dev.02668.

155. Kimmel CB, Ballard WW, Kimmel SR, Ullmann B, Schilling TF (1995) Stages of embryonic development of the zebrafish. Dev Dyn 203: 253–310. doi:10.1002/aja.1002030302.

156. Eisen JS, Smith JC (2008) Controlling morpholino experiments: don't stop making antisense. Development 135: 1735–1743. doi:10.1242/dev.001115.

157. Nüsslein-Volhard C, Dahm R (2002) Zebrafish. Oxford University Press, USA. pp.

158. Danielian PS, Muccino D, Rowitch DH, Michael SK, McMahon AP (1998) Modification of gene activity in mouse embryos in utero by a tamoxifen-inducible form of Cre recombinase. Curr Biol 8: 1323–1326.

159. Soriano P (1999) Generalized lacZ expression with the ROSA26 Cre reporter strain. Nat Genet 21: 70–71. doi:10.1038/5007.

160. McLeod MJ (1980) Differential staining of cartilage and bone in whole mouse fetuses by alcian blue and alizarin red S. Teratology 22: 299–301. doi:10.1002/tera.1420220306.

161. Pennisi DJ, Wilkinson L, Kolle G, Sohaskey ML, Gillinder KR, et al. (2007) Crim1KST264/KST264 mice display a disruption of the Crim1 gene resulting in perinatal lethality with defects in multiple organ systems. Dev Dyn 236: 502–511. doi:10.1002/dvdy.21015.

162. Ishii M, Han J, Yen H-Y, Sucov HM, Chai Y, et al. (2005) Combined deficiencies of Msx1 and Msx2 cause impaired patterning and survival of the cranial neural crest. Development 132: 4937–4950. doi:10.1242/dev.02072.

163. Li B, Mackay D, Ma J, Dai X (2004) Cloning and developmental expression of mouse pygopus 2, a putative Wnt signaling component. Genomics 84: 398–405. doi:10.1016/j.ygeno.2004.04.007.

164. Paus R, Müller-Röver S, van der Veen C, Maurer M, Eichmüller S, et al. (1999) A comprehensive guide for the recognition and classification of distinct stages of hair follicle morphogenesis. J Invest Dermatol 113: 523–532. doi:10.1046/j.1523-1747.1999.00740.x.

165. Spraggon L (n.d.) The development of genetic models to understand the role of the Wilms' tumour suppressor gene, WT1.

166. Matsuda T, Cepko CL (2007) Controlled expression of transgenes introduced by in vivo electroporation. Proc Natl Acad Sci USA 104: 1027–1032. doi:10.1073/pnas.0610155104.

167. Chang CH, Moog F (1972) Alkaline phosphatases of the chicken duodenum. I. Isolation and partial characterization of the multiple forms of duodenal phosphatase in pre- and post-hatching stages. Biochim Biophys Acta 258: 154–165.

168. Laale HW (1977) The biology and use of zebrafish, Brachydanio rerio in fisheries research. A literature review. Journal of Fish Biology 10: 121–173. Available:http://onlinelibrary.wiley.com/doi/10.1111/j.1095-8649.1977.tb04049.x/abstract.

169. Lieschke GJ, Currie PD (2007) Animal models of human disease: zebrafish swim into view. Nat Rev Genet 8: 353–367. doi:10.1038/nrg2091.

170. Henken DB, Rasooly RS, Javois L, Hewitt AT (2004) The National Institutes of Health and the Growth of the Zebrafish as an Experimental Model Organism. Zebrafish 1: 105–110. doi:10.1089/zeb.2004.1.105.

171. Streisinger G, Walker C, Dower N, Knauber D (1981) Production of clones of homozygous diploid zebra fish (Brachydanio rerio). Nature.

172. Hammerschmidt M, Haffter P, Nüsslein-Volhard C (1994) Large-scale mutagenesis in the zebrafish: in search of genes controlling development in a vertebrate. Current Biology.

173. Driever W, Fishman MC (1996) The zebrafish: heritable disorders in transparent embryos. J Clin Invest 97: 1788–1794. doi:10.1172/JCI118608.

174. Vogel G (2000) Sanger will sequence Zebrafish genome. Science.

175. Schier AF, Neuhauss SC, Harvey M, Malicki J, Solnica-Krezel L, et al. (1996) Mutations affecting the development of the embryonic zebrafish brain. Development 123: 165–178.

176. Sprague J (2006) The Zebrafish Information Network: the zebrafish model organism database. Nucleic Acids Res 34: D581–D585. doi:10.1093/nar/gkj086.

177. Bradford Y, Conlin T, Dunn N, Fashena D, Frazer K, et al. (2011) ZFIN: enhancements and updates to the Zebrafish Model Organism Database. Nucleic Acids Res 39: D822–D829. doi:10.1093/nar/gkq1077.

178. Campos-Ortega J (1994) On the formation of the neural keel and neural tube in the zebrafishDanio (Brachydanio) rerio. Development Genes and Evolution.

179. Schmitz B, Papan C, Campos-Ortega JA (1993) Neurulation in the anterior trunk region of the zebrafish Brachydanio rerio. Roux's Arch Dev Biol 202: 250–259. doi:10.1007/BF00363214.

180. West-Eberhard MJ (2003) Developmental Plasticity and Evolution. 1st ed. Oxford University Press, USA. pp.

181. Glass AS, Dahm R (2004) The Zebrafish as a Model Organism for Eye Development. Ophthalmic Res 36: 4–24. doi:10.1159/000076105.

182. Bakkers J (2011) Zebrafish as a model to study cardiac development and human cardiac disease. Cardiovasc Res 91: 279. doi:10.1093/cvr/cvr098.

183. Pereira TCB, Rico EP, Rosemberg DB, Schirmer H, Dias RD, et al. (2011) Zebrafish as a Model Organism to Evaluate Drugs Potentially Able to Modulate Sirtuin Expression. Zebrafish 8: 9–16. doi:10.1089/zeb.2010.0677.

184. William Norton LB-C (2010) Adult zebrafish as a model organism for behavioural genetics. BMC Neuroscience 11: 90. doi:10.1186/1471-2202-11-90.

185. Briggs JP (2002) The zebrafish: a new model organism for integrative physiology. Am J Physiol Regul Integr Comp Physiol 282: R3–R9. doi:10.1152/ajpregu.00589.2001.

186. Schilling TF, Piotrowski T, Grandel H, Brand M, Heisenberg CP, et al. (1996) Jaw and branchial arch mutants in zebrafish I: branchial arches. Development 123: 329–344.

187. Piotrowski T, Schilling TF, Brand M, Jiang YJ, Heisenberg CP, et al. (1996) Jaw and branchial arch mutants in zebrafish II: anterior arches and cartilage differentiation. Development 123: 345–356.

188. Artinger KB, Chitnis AB, Mercola M, Driever W (1999) Zebrafish narrowminded suggests a genetic link between formation of neural crest and primary sensory neurons. Development 126: 3969–3979.

189. Raible DW, Wood A, Hodsdon W, Henion PD, Weston JA, et al. (1992) Segregation and early dispersal of neural crest cells in the embryonic zebrafish. Dev Dyn 195: 29–42. doi:10.1002/aja.1001950104.

190. Dutton KA, Pauliny A, Lopes SS, Elworthy S, Carney TJ, et al. (2001) Zebrafish colourless encodes sox10 and specifies non-ectomesenchymal neural crest fates. Development 128: 4113–4125.

191. Knaut H, Blader P, Strähle U, Schier AF (2005) Assembly of trigeminal sensory ganglia by chemokine signaling. Neuron 47: 653–666. doi:10.1016/j.neuron.2005.07.014.

192. Ghysen A, Dambly-Chaudière C (2004) Development of the zebrafish lateral line. Curr Opin Neurobiol 14: 67–73. doi:10.1016/j.conb.2004.01.012.

193. Sato M, Yost HJ (2003) Cardiac neural crest contributes to cardiomyogenesis in zebrafish. Dev Biol 257: 127–139.

194. Sato M, Tsai H-J, Yost HJ (2006) Semaphorin3D regulates invasion of cardiac neural crest cells into the primary heart field. Dev Biol 298: 12–21. doi:10.1016/j.ydbio.2006.05.033.

195. Li Y-X, Zdanowicz M, Young L, Kumiski D, Leatherbury L, et al. (2003) Cardiac neural crest in zebrafish embryos contributes to myocardial cell lineage and early heart function. Dev Dyn 226: 540–550. doi:10.1002/dvdy.10264.

196. Yelon D, Ticho B, Halpern M, Ruvinsky I (2000) The bHLH transcription factor hand2 plays parallel roles in zebrafish heart and pectoral fin development. ….

197. Stewart RA, Sanda T, Widlund HR, Zhu S, Swanson KD, et al. (2010) Phosphatase-dependent and -independent functions of Shp2 in neural crest cells underlie LEOPARD syndrome pathogenesis. Dev Cell 18: 750–762. doi:10.1016/j.devcel.2010.03.009.

198. Kelsh RN (2006) Sorting out Sox10 functions in neural crest development. Bioessays 28: 788–798. doi:10.1002/bies.20445.

199. Dutton JR, Antonellis A, Carney TJ, Rodrigues FSLM, Pavan WJ, et al. (2008) An evolutionarily conserved intronic region controls the spatiotemporal expression of the transcription factor Sox10. BMC Dev Biol 8: 105. doi:10.1186/1471-213X-8-105.

200. Shimeld SM, Holland PW (2000) Vertebrate innovations. Proc Natl Acad Sci USA 97: 4449–4452.

201. Kessler R, Hausmann G, Basler K (2009) The PHD domain is required to link Drosophila Pygopus to Legless/beta-catenin and not to histone H3. Mech Dev 126: 752–759. doi:10.1016/j.mod.2009.04.003.

202. Fiedler M, Sánchez-Barrena MJ, Nekrasov M, Mieszczanek J, Rybin V, et al. (2008) Decoding of methylated histone H3 tail by the Pygo-BCL9 Wnt signaling complex. Mol Cell 30: 507–518.

doi:10.1016/j.molcel.2008.03.011.

203. NCBI, editor (n.d.) How to: Find a homolog for a gene in another organism. National Centre for Biotechnology Information. pp. Available:http://www.ncbi.nlm.nih.gov/guide/howto/find-homolog-gene/. Accessed April 2011.

204. NCBI, editor (2009) Homologene. National Centre for Biotechnology Information. pp. Available:http://www.ncbi.nlm.nih.gov/sites/entrez?db=homologene. Accessed 6 April 2011.

205. NCBI, editor (2011) Gene. National Centre for Biotechnology Information. pp. Available:http://www.ncbi.nlm.nih.gov/sites/entrez?db=gene. Accessed 6 April 2011.

206. NCBI, editor (2010) Protein. National Centre for Biotechnology Information. pp. Available:http://www.ncbi.nlm.nih.gov/sites/entrez?db=protein. Accessed 6 April 2011.

207. NCBI, editor (2010) Nucleotide. National Centre for Biotechnology Information. pp. Available:http://www.ncbi.nlm.nih.gov/nuccore. Accessed 7 April 2011.

208. Pruitt KD, Tatusova T, Klimke W, Maglott DR (2009) NCBI Reference Sequences: current status, policy and new initiatives. Nucleic Acids Res 37: D32–D36. doi:10.1093/nar/gkn721.

209. Madden T (2002) The BLAST Sequence Analysis Tool. The NCBI Handbook. Bethesda (MD): National Library of Medicine.

210. Cooper PS, Lipshultz D, Matten WT, McGinnis SD, Pechous S, et al. (2010) Education resources of the National Center for Biotechnology Information. Brief Bioinformatics 11: 563–569. doi:10.1093/bib/bbq022.

211. Altschul S, Madden T, Schäffer A (1997) Gapped BLAST and PSI-BLAST: a new generation of protein database search programs. Nucleic acids ….

212. Edgar RC, Sjolander K (2004) A comparison of scoring functions for protein sequence profile alignment. Bioinformatics 20: 1301–1308. doi:10.1093/bioinformatics/bth090.

213. Taylor JS, Braasch I, Frickey T, Meyer A, de Peer Van Y (2003) Genome duplication, a trait shared by 22000 species of ray-finned fish. Genome Res 13: 382–390. doi:10.1101/gr.640303.

214. Fitch WM (1970) Distinguishing homologous from analogous proteins. Systematic Zoology 19: 99–113.

215. Thompson JD, Gibson TJ, Higgins DG (2002) Multiple sequence alignment using ClustalW and ClustalX. Curr Protoc Bioinformatics Chapter 2: Unit2.3. doi:10.1002/0471250953.bi0203s00.

216. Nusse R (2001) An ancient cluster of Wnt paralogues. Trends Genet 17: 443.

217. Smith AV (2012) Genetic Analysis: Moving between Linkage and Association. Cold Spring Harbor Protocols 2012: pdb.top067819–pdb.top067819. doi:10.1101/pdb.top067819.

218. Flicek P, Aken BL, Ballester B, Beal K, Bragin E, et al. (2010) Ensembl's 10th year. Nucleic Acids Res 38: D557–D562. doi:10.1093/nar/gkp972.

219. Spudich G, Fernández-Suarez XM, Birney E (2007) Genome browsing with Ensembl: a practical overview. Brief Funct Genomic Proteomic 6: 202–219. doi:10.1093/bfgp/elm025.

220. Gans C, Northcutt RG (1983) Neural crest and the origin of vertebrates: a new head. Science 220: 268–273. doi:10.1126/science.220.4594.268.

221. Tang R, Dodd A, Lai D, McNabb WC, Love DR (2007) Validation of zebrafish (Danio rerio) reference genes for quantitative real-time RT-PCR normalization. Acta Biochim Biophys Sin (Shanghai) 39: 384–390.

222. Gerety SS, Wilkinson DG (2011) Morpholino artifacts provide pitfalls and reveal a novel role for pro-apoptotic genes in hindbrain boundary development. Dev Biol 350: 279–289. doi:10.1016/j.ydbio.2010.11.030.

223. Ekker SC, Larson JD (2001) Morphant technology in model developmental systems. genesis 30: 89–93.

224. Robu ME, Larson JD, Nasevicius A, Beiraghi S, Brenner C, et al. (2007) p53 activation by knockdown technologies. PLoS Genet 3: e78. doi:10.1371/journal.pgen.0030078.

225. Danilova N, Kumagai A, Lin J (2010) p53 Upregulation Is a Frequent Response to Deficiency of Cell-Essential Genes. PLoS ONE 5: e15938. doi:10.1371/journal.pone.0015938.g006.

226. Nakaya N, Lee H-S, Takada Y, Tzchori I, Tomarev SI (2008) Zebrafish olfactomedin 1 regulates retinal axon elongation in vivo and is a modulator of Wnt signaling pathway. J Neurosci 28: 7900–7910. doi:10.1523/JNEUROSCI.0617-08.2008.

227. Barembaum M, Moreno TA, LaBonne C, Sechrist J, Bronner-Fraser M (2000) Noelin-1 is a secreted glycoprotein involved in generation of the neural crest. Nat Cell Biol 2: 219–225. doi:10.1038/35008643.

228. Moreno TA, Bronner-Fraser M (2005) Noelins modulate the timing of neuronal differentiation during development. Dev Biol 288: 434–447.

doi:10.1016/j.ydbio.2005.09.050.

229. Jopling C, Hertog JD (2005) Fyn/Yes and non-canonical Wnt signalling converge on RhoA in vertebrate gastrulation cell movements. EMBO Rep 6: 426–431. doi:10.1038/sj.embor.7400386.

230. Dellaporta SL (2006) Mitochondrial genome of Trichoplax adhaerens supports Placozoa as the basal lower metazoan phylum. Proceedings of the National Academy of Sciences 103: 8751–8756. doi:10.1073/pnas.0602076103.

231. Croce JC, Wu S-Y, Byrum C, Xu R, Duloquin L, et al. (2006) A genome-wide survey of the evolutionarily conserved Wnt pathways in the sea urchin Strongylocentrotus purpuratus. Dev Biol 300: 121–131. doi:10.1016/j.ydbio.2006.08.045.

232. Heisenberg CP, Tada M, Rauch GJ, Saúde L, Concha ML, et al. (2000) Silberblick/Wnt11 mediates convergent extension movements during zebrafish gastrulation. Nature 405: 76–81. doi:10.1038/35011068.

233. Vijayaragavan K, Bhatia M (2007) Early cardiac development: A Wnt beat away. Proceedings of the National Academy of Sciences 104: 9549–9550. doi:10.1073/pnas.0703731104.

234. Rao TP, Kühl M (2010) An updated overview on Wnt signaling pathways: a prelude for more. Circ Res 106: 1798–1806. doi:10.1161/CIRCRESAHA.110.219840.

235. Oakley DJ, Iyer V, Skarnes WC, Smedley D (2011) BioMart as an integration solution for the International Knockout Mouse Consortium. Database 2011: bar028–bar028. doi:10.1093/database/bar028.

236. Nusse R, van Ooyen A, Cox D, Fung YK, Varmus H (1984) Mode of proviral activation of a putative mammary oncogene (int-1) on mouse chromosome 15. Nature 307: 131–136.

237. Morata G, Lawrence PA (1977) The development of wingless, a homeotic mutation of Drosophila. Dev Biol 56: 227–240. doi:10.1016/0012-1606(77)90266-4.

238. Rijsewijk F, Schuermann M, Wagenaar E, Parren P, Weigel D, et al. (1987) The Drosophila homology of the mouse mammary oncogene int-1 is identical to the segment polarity gene wingless. Cell 50: 649–657. doi:10.1016/0092-8674(87)90038-9.

239. Nusse R, Brown A, Papkoff J, Scambler P, Shackleford G, et al. (1991) A new nomenclature for int-1 and related genes: the Wnt gene family. Cell 64: 231.

240. Jakobovits A, Shackleford GM, Varmus HE, Martin GR (1986) Two proto-oncogenes implicated in mammary carcinogenesis, int-1 and int-2, are

independently regulated during mouse development. Proc Natl Acad Sci USA 83: 7806–7810.

241. Shackleford GM, Varmus HE (1987) Expression of the proto-oncogene int-1 is restricted to postmeiotic male germ cells and the neural tube of mid-gestational embryos. Cell 50: 89–95.

242. Wilkinson DG, Bailes JA, McMahon AP (1987) Expression of the proto-oncogene int-1 is restricted to specific neural cells in the developing mouse embryo. Cell 50: 79–88.

243. Thomas KR, Capecchi MR (1990) Targeted disruption of the murine int-1 proto-oncogene resulting in severe abnormalities in midbrain and cerebellar development. Nature 346: 847–850. doi:10.1038/346847a0.

244. Thomas KR, Musci TS, Neumann PE, Capecchi MR (1991) Swaying is a mutant allele of the proto-oncogene Wnt-1. Cell 67: 969–976.

245. Barrow JR, Howell WD, Rule M, Hayashi S, Thomas KR, et al. (2007) Wnt3 signaling in the epiblast is required for proper orientation of the anteroposterior axis. Dev Biol 312: 312–320. doi:10.1016/j.ydbio.2007.09.030.

246. Mulroy T, McMahon JA, Burakoff SJ, McMahon AP, Sen J (2002) Wnt-1 and Wnt-4 regulate thymic cellularity. Eur J Immunol 32: 967–971. doi:10.1002/1521-4141(200204)32:4<967::AID-IMMU967>3.0.CO;2-6.

247. augustine KA (n.d.) Interactions of Wnt-1 and Wnt-3a are essential fo... [Teratology. 1995] - PubMed - NCBI.

248. Lekven AC, Buckles GR, Kostakis N, Moon RT (2003) Wnt1 and wnt10b function redundantly at the zebrafish midbrain-hindbrain boundary. Dev Biol 254: 172–187.

249. Echelard Y, Vassileva G, McMahon AP (1994) Cis-acting regulatory sequences governing Wnt-1 expression in the developing mouse CNS. Development 120: 2213–2224.

250. Kothary R, Clapoff S, Darling S, Perry MD, Moran LA, et al. (1989) Inducible expression of an hsp68-lacZ hybrid gene in transgenic mice. Development 105: 707–714.

251. Danielian PS, Echelard Y, Vassileva G, McMahon AP (1997) A 5.5-kb enhancer is both necessary and sufficient for regulation of Wnt-1 transcription in vivo. Dev Biol 192: 300–309. doi:10.1006/dbio.1997.8762.

252. Rowitch DH, Echelard Y, Danielian PS, Gellner K, Brenner S, et al. (1998) Identification of an evolutionarily conserved 110 base-pair cis-acting regulatory sequence that governs Wnt-1 expression in the murine

neural plate. Development 125: 2735–2746.

253. Chai Y, Jiang X, Ito Y, Bringas P, Han J, et al. (2000) Fate of the mammalian cranial neural crest during tooth and mandibular morphogenesis. Development 127: 1671–1679.

254. Sauer B (1987) Functional expression of the cre-lox site-specific recombination system in the yeast Saccharomyces cerevisiae. Molecular and Cellular Biology 7: 2087–2096.

255. Gu H, Marth JD, Orban PC, Mossmann H, Rajewsky K (1994) Deletion of a DNA polymerase beta gene segment in T cells using cell type-specific gene targeting. Science 265: 103–106.

256. Porras D, Brown CB (2008) Temporal-spatial ablation of neural crest in the mouse results in cardiovascular defects. Dev Dyn 237: 153–162. doi:10.1002/dvdy.21382.

257. Nassenstein C, Taylor-Clark TE, Myers AC, Ru F, Nandigama R, et al. (2010) Phenotypic distinctions between neural crest and placodal derived vagal C-fibres in mouse lungs. J Physiol (Lond) 588: 4769–4783. doi:10.1113/jphysiol.2010.195339.

258. Behr B, Panetta NJ, Longaker MT, Quarto N (2010) Different endogenous threshold levels of Fibroblast Growth Factor-ligands determine the healing potential of frontal and parietal bones. Bone 47: 281–294. doi:10.1016/j.bone.2010.05.008.

259. Gagan JR, Tholpady SS, Ogle RC (2007) Cellular dynamics and tissue interactions of the dura mater during head development. Birth Defects Res C Embryo Today 81: 297–304. doi:10.1002/bdrc.20104.

260. Jiang X, Iseki S, Maxson RE, Sucov HM, Morriss-Kay GM (2002) Tissue origins and interactions in the mammalian skull vault. Dev Biol 241: 106–116. doi:10.1006/dbio.2001.0487.

261. Jonckheere N, Mayes E, Shih H-P, Li B, Lioubinski O, et al. (2008) Analysis of mPygo2 mutant mice suggests a requirement for mesenchymal Wnt signaling in pancreatic growth and differentiation. Dev Biol 318: 224–235. doi:10.1016/j.ydbio.2008.03.014.

262. Ramirez A, Page A, Gandarillas A, Zanet J, Pibre S, et al. (2004) A keratin K5Cre transgenic line appropriate for tissue-specific or generalized cre-mediated recombination. genesis 39: 52–57. doi:10.1002/gene.20025.

263. Lomelí H, Ramos Mejía V, Gertsenstein M, Lobe CG, Nagy A (n.d.) Targeted insertion of Cre recombinase into the TNAP gene: Excision in primordial germ cells. genesis 26: 116–117. doi:10.1002/(SICI)1526-968X(200002)26:2<116::AID-GENE4>3.0.CO;2-X.

264. Matthaei KI (2007) Genetically manipulated mice: a powerful tool with

unsuspected caveats. J Physiol (Lond) 582: 481–488. doi:10.1113/jphysiol.2007.134908.

265. Rassoulzadegan M, Grandjean V, Gounon P, Vincent S, Gillot I, et al. (2006) RNA-mediated non-mendelian inheritance of an epigenetic change in the mouse. Nature Publishing Group 441: 469–474. doi:10.1038/nature04674.

266. Turlo KA, Gallaher SD, Vora R, Laski FA, Iruela-Arispe ML (2010) When Cre-mediated recombination in mice does not result in protein loss. Genetics 186: 959–967. doi:10.1534/genetics.110.121608.

267. Schwenk F, Baron U, Rajewsky K (1995) A cre-transgenic mouse strain for the ubiquitous deletion of loxP-flanked gene segments including deletion in germ cells. Nucleic Acids Res 23: 5080–5081.

268. Moss TH, Lewkowicz SJ (1983) The axon reaction in motor and sensory neurones of mice studied by a monoclonal antibody marker of neurofilament protein. J Neurol Sci 60: 267–280.

269. Bailey DW (1977) Genetic drift: the problem and its possible solution by frozen-embryo storage. Ciba Found Symp 52: 291–303.

270. Sluyter F, Marican CC, Crusio WE (1999) Further phenotypical characterisation of two substrains of C57BL/6J inbred mice differing by a spontaneous single-gene mutation. Behav Brain Res 98: 39–43.

271. Herzer U, Crocoll A, Barton D, Howells N, Englert C (1999) The Wilms tumor suppressor gene wt1 is required for development of the spleen. Curr Biol 9: 837–840.

272. Threadgill DW, Dlugosz AA, Hansen LA, Tennenbaum T, Lichti U, et al. (1995) Targeted disruption of mouse EGF receptor: effect of genetic background on mutant phenotype. Science 269: 230–234.

273. Panciera RJ, Boileau MJ, Step DL (2007) Tympany, acidosis, and mural emphysema of the stomach in calves: report of cases and experimental induction. J Vet Diagn Invest 19: 392–395.

274. Kümper H (1994) [New therapy for acute abomasal tympany in calves]. Tierarztl Prax 22: 25–27.

275. Qiu M, Bulfone A, Martinez S, Meneses JJ, Shimamura K, et al. (1995) Null mutation of Dlx-2 results in abnormal morphogenesis of proximal first and second branchial arch derivatives and abnormal differentiation in the forebrain. Genes Dev 9: 2523–2538.

276. Kurosaka S, Leu NA, Zhang F, Bunte R, Saha S, et al. (2010) Arginylation-dependent neural crest cell migration is essential for mouse development. PLoS Genet 6: e1000878. doi:10.1371/journal.pgen.1000878.

277. Kist R, Greally E, Peters H (2007) Derivation of a mouse model for conditional inactivation of Pax9. genesis 45: 460–464. doi:10.1002/dvg.20295.

278. Halford MM, Armes J, Buchert M, Meskenaite V, Grail D, et al. (2000) Ryk-deficient mice exhibit craniofacial defects associated with perturbed Eph receptor crosstalk. Nat Genet 25: 414–418. doi:10.1038/78099.

279. Qiu M (1997) Role of the Dlx Homeobox Genes in Proximodistal Patterning of the Branchial Arches: Mutations of Dlx-1, Dlx-2, and Dlx-1 and -2 Alter Morphogenesis of Proximal Skeletal and Soft Tissue Structures Derived from the First and Second Arches. Dev Biol 185: 165–184. doi:10.1006/dbio.1997.8556.

280. Acampora D, Merlo GR, Paleari L, Zerega B, Postiglione MP, et al. (1999) Craniofacial, vestibular and bone defects in mice lacking the Distal-less-related gene Dlx5. Development 126: 3795–3809.

281. Dupé V, Matt N, Garnier J-M, Chambon P, Mark M, et al. (2003) A newborn lethal defect due to inactivation of retinaldehyde dehydrogenase type 3 is prevented by maternal retinoic acid treatment. Proc Natl Acad Sci USA 100: 14036–14041. doi:10.1073/pnas.2336223100.

282. Kist R, Watson M, Wang X, Cairns P, Miles C, et al. (2005) Reduction of Pax9 gene dosage in an allelic series of mouse mutants causes hypodontia and oligodontia. Hum Mol Genet 14: 3605–3617. doi:10.1093/hmg/ddi388.

283. Jeong J, Li X, McEvilly RJ, Rosenfeld MG, Lufkin T, et al. (2008) Dlx genes pattern mammalian jaw primordium by regulating both lower jaw-specific and upper jaw-specific genetic programs. Development 135: 2905–2916. doi:10.1242/dev.019778.

284. Depew MJ, Lufkin T, Rubenstein JLR (2002) Specification of jaw subdivisions by Dlx genes. Science 298: 381–385. doi:10.1126/science.1075703.

285. Beverdam A, Merlo GR, Paleari L, Mantero S, Genova F, et al. (2002) Jaw transformation with gain of symmetry after Dlx5/Dlx6 inactivation: mirror of the past? genesis 34: 221–227. doi:10.1002/gene.10156.

286. Depew MJ, Liu JK, Long JE, Presley R, Meneses JJ, et al. (1999) Dlx5 regulates regional development of the branchial arches and sensory capsules. Development 126: 3831–3846.

287. Depew MJ, Simpson CA, Morasso M, Rubenstein JLR (2005) Reassessing the Dlx code: the genetic regulation of branchial arch skeletal pattern and development. J Anat 207: 501–561. doi:10.1111/j.1469-7580.2005.00487.x.

288. Merlo GR, Paleari L, Mantero S, Genova F, Beverdam A, et al. (2002) Mouse model of split hand/foot malformation type I. genesis 33: 97–101. doi:10.1002/gene.10098.

289. Richtsmeier JT, Baxter LL, Reeves RH (2000) Parallels of craniofacial maldevelopment in Down syndrome and Ts65Dn mice. Dev Dyn 217: 137–145. doi:10.1002/(SICI)1097-0177(200002)217:2<137::AID-DVDY1>3.0.CO;2-N.

290. Trainor PA, Krumlauf R (2000) Box 1 : Patterning the cranial neural crest: Hinbrain segmentation and : hox: gene plasticity : Nature Reviews Neuroscience. Nat Rev Neurosci 1: 116–124. doi:10.1038/35039056.

291. Jeong J (2004) Hedgehog signaling in the neural crest cells regulates the patterning and growth of facial primordia. Genes Dev 18: 937–951. doi:10.1101/gad.1190304.

292. Bouguila J, Khonsari RH, Pierrefeu A, Corre P (2011) Eagle syndrome: a rare and atypical pain. Rev Stomatol Chir Maxillofac 112: 348–352.

293. Jain D, Chauhan JS, Jain S, Goel G (2011) Elongated styloid process: an unusual cause of neck pain and difficulty in swallowing. J Orofac Pain 25: 269–271.

294. Cumali Gokce YSMS (2008) Styloid Process Elongation or Eagle's Syndrome: Is There Any Role for Ectopic Calcification? European Journal of Dentistry 2: 224.

295. Hara Y, Rovescalli AC, Kim Y, Nirenberg M (1992) Structure and evolution of four POU domain genes expressed in mouse brain. Proc Natl Acad Sci USA 89: 3280–3284.

296. Iler N, Rowitch DH, Echelard Y, McMahon AP, Abate-Shen C (1995) A single homeodomain binding site restricts spatial expression of Wnt-1 in the developing brain. Mech Dev 53: 87–96.

297. Druckenbrod NR, Epstein ML (2007) Behavior of enteric neural crest-derived cells varies with respect to the migratory wavefront. Dev Dyn 236: 84–92. doi:10.1002/dvdy.20974.

298. Nakamura T, Colbert MC, Robbins J (2006) Neural crest cells retain multipotential characteristics in the developing valves and label the cardiac conduction system. Circ Res 98: 1547–1554. doi:10.1161/01.RES.0000227505.19472.69.

299. Poelmann RE, Gittenberger-de Groot AC (1999) A subpopulation of apoptosis-prone cardiac neural crest cells targets to the venous pole: multiple functions in heart development? Dev Biol 207: 271–286. doi:10.1006/dbio.1998.9166.

300. Kirby ML, Waldo KL (1995) Neural crest and cardiovascular patterning.

Circ Res 77: 211–215.

301. Farrell M, Waldo K, Li YX, Kirby ML (1999) A novel role for cardiac neural crest in heart development. Trends Cardiovasc Med 9: 214–220.

302. Hutson MR, Kirby ML (2003) Neural crest and cardiovascular development: A 20-year perspective. Birth Defects Res C Embryo Today 69: 2–13. doi:10.1002/bdrc.10002.

303. Kirby ML, Hunt P, Wallis K, Thorogood P (1997) Abnormal patterning of the aortic arch arteries does not evoke cardiac malformations. Dev Dyn 208: 34–47. doi:10.1002/(SICI)1097-0177(199701)208:1<34::AID-AJA4>3.0.CO;2-2.

304. Stoller JZ, Epstein JA (2005) Cardiac neural crest. Semin Cell Dev Biol 16: 704–715. doi:10.1016/j.semcdb.2005.06.004.

305. Obler D, Juraszek AL, Smoot LB, Natowicz MR (2008) Double outlet right ventricle: aetiologies and associations. J Med Genet 45: 481–497. doi:10.1136/jmg.2008.057984.

306. Olaopa M, Zhou H-M, Snider P, Wang J, Schwartz RJ, et al. (2011) Pax3 is essential for normal cardiac neural crest morphogenesis but is not required during migration nor outflow tract septation. Dev Biol 356: 308–322. doi:10.1016/j.ydbio.2011.05.583.

307. Conway SJ, Bundy J, Chen J, Dickman E, Rogers R, et al. (2000) Decreased neural crest stem cell expansion is responsible for the conotruncal heart defects within the splotch (Sp(2H))/Pax3 mouse mutant. Cardiovasc Res 47: 314–328.

308. Holler KL, Hendershot TJ, Troy SE, Vincentz JW, Firulli AB, et al. (2010) Targeted deletion of Hand2 in cardiac neural crest-derived cells influences cardiac gene expression and outflow tract development. Dev Biol 341: 291–304. doi:10.1016/j.ydbio.2010.02.001.

309. Gurjarpadhye A, Hewett KW, Justus C, Wen X, Stadt H, et al. (2007) Cardiac neural crest ablation inhibits compaction and electrical function of conduction system bundles. Am J Physiol Heart Circ Physiol 292: H1291–H1300. doi:10.1152/ajpheart.01017.2006.

310. Leatherbury L, Connuck DM, Gauldin HE, Kirby ML (1991) Hemodynamic changes and compensatory mechanisms during early cardiogenesis after neural crest ablation in chick embryos. Pediatr Res 30: 509–512.

311. Männer J, Seidl W, Steding G (1993) Correlation between the embryonic head flexures and cardiac development. An experimental study in chick embryos. Anat Embryol 188: 269–285.

312. Kolwicz SC, Tian R (2011) Glucose metabolism and cardiac hypertrophy.

Cardiovasc Res 90: 194–201. doi:10.1093/cvr/cvr071.

313. Finckenberg P, Mervaala E (2010) Novel regulators and drug targets of cardiac hypertrophy. J Hypertens 28 Suppl 1: S33–S38. doi:10.1097/01.hjh.0000388492.73954.0b.

314. Hoff MB, Lekanne Deprez R, Ruijter J, Boer PJ, Tesink-Taekema S, et al. (2004) Increased cardiac workload by closure of the ductus arteriosus leads to hypertrophy and apoptosis rather than to hyperplasia in the late fetal period. Naunyn-Schmiedeberg's Arch Pharmacol 370. doi:10.1007/s00210-004-0955-0.

315. Li F, Wang X, Capasso JM, Gerdes AM (1996) Rapid transition of cardiac myocytes from hyperplasia to hypertrophy during postnatal development. J Mol Cell Cardiol 28: 1737–1746. doi:10.1006/jmcc.1996.0163.

316. Olivetti G, Quaini F, Lagrasta C, Ricci R, Tiberti G, et al. (1992) Myocyte cellular hypertrophy and hyperplasia contribute to ventricular wall remodeling in anemia-induced cardiac hypertrophy in rats. AJPA 141: 227–239.

317. Tomita H, Connuck DM, Leatherbury L, Kirby ML (1991) Relation of early hemodynamic changes to final cardiac phenotype and survival after neural crest ablation in chick embryos. Circulation 84: 1289–1295.

318. Schaub MC, Hefti MA, Zuellig RA, Morano I (1998) Modulation of contractility in human cardiac hypertrophy by myosin essential light chain isoforms. Cardiovasc Res 37: 381–404.

319. KEMI O, HARAM P, LOENNECHEN J, OSNES J, SKOMEDAL T, et al. (2005) Moderate vs. high exercise intensity: Differential effects on aerobic fitness, cardiomyocyte contractility, and endothelial function. Cardiovasc Res 67: 161–172. doi:10.1016/j.cardiores.2005.03.010.

320. Maekawa T (1999) Mouse ATF-2 Null Mutants Display Features of a Severe Type of Meconium Aspiration Syndrome. Journal of Biological Chemistry 274: 17813–17819. doi:10.1074/jbc.274.25.17813.

321. Burns AJ, Thapar N, Barlow AJ (2008) Development of the neural crest-derived intrinsic innervation of the human lung. Am J Respir Cell Mol Biol 38: 269–275. doi:10.1165/rcmb.2007-0246OC.

322. Burns AJ, Delalande J-M (2005) Neural crest cell origin for intrinsic ganglia of the developing chicken lung. Dev Biol 277: 63–79. doi:10.1016/j.ydbio.2004.09.006.

323. Freem LJ, Escot S, Tannahill D, Druckenbrod NR, Thapar N, et al. (2010) The intrinsic innervation of the lung is derived from neural crest cells as shown by optical projection tomography in Wnt1-Cre;YFP reporter mice. J Anat 217: 651–664. doi:10.1111/j.1469-7580.2010.01295.x.

324. Langsdorf A, Radzikinas K, Kroten A, Jain S, Ai X (2010) Neural Crest Cell Origin and Signals for Intrinsic Neurogenesis in the Mammalian Respiratory Tract. Am J Respir Cell Mol Biol. doi:10.1165/rcmb.2009-0462OC.

325. Szeder V, Grim M, Halata Z, Sieber-Blum M (2003) Neural crest origin of mammalian Merkel cells. Dev Biol 253: 258–263.

326. Morrison KM, Miesegaes GR, Lumpkin EA, Maricich SM (2009) Mammalian Merkel cells are descended from the epidermal lineage. Dev Biol 336: 76–83. doi:10.1016/j.ydbio.2009.09.032.

327. Pasolli HA (2011) The hair follicle bulge: a niche for adult stem cells. Microsc Microanal 17: 513–519. doi:10.1017/S1431927611000419.

328. Nakamura M, Sundberg JP, Paus R (2001) Mutant laboratory mice with abnormalities in hair follicle morphogenesis, cycling, and/or structure: annotated tables. Exp Dermatol 10: 369–390.

329. Duverger O, Morasso MI (2009) Epidermal patterning and induction of different hair types during mouse embryonic development. Birth Defects Res C Embryo Today 87: 263–272. doi:10.1002/bdrc.20158.

330. Pummila M, Fliniaux I, Jaatinen R, James MJ, Laurikkala J, et al. (2007) Ectodysplasin has a dual role in ectodermal organogenesis: inhibition of Bmp activity and induction of Shh expression. Development 134: 117–125. doi:10.1242/dev.02708.

331. Stenn KS, Paus R (2001) Controls of hair follicle cycling. Physiol Rev 81: 449–494.

332. Schmidt-Ullrich R, Paus R (2005) Molecular principles of hair follicle induction and morphogenesis. Bioessays 27: 247–261. doi:10.1002/bies.20184.

333. Sharov AA, Sharova TY, Mardaryev AN, Tommasi di Vignano A, Atoyan R, et al. (2006) Bone morphogenetic protein signaling regulates the size of hair follicles and modulates the expression of cell cycle-associated genes. Proc Natl Acad Sci USA 103: 18166–18171. doi:10.1073/pnas.0608899103.

334. Botchkarev VA, Botchkareva NV, Sharov AA, Funa K, Huber O, et al. (2002) Modulation of BMP Signaling by Noggin is Required for Induction of the Secondary (Nontylotrich) Hair Follicles. Journal of Investigative Dermatology 118: 3–10. doi:doi:10.1046/j.1523-1747.2002.01645.x.

335. van Genderen C, Okamura RM, Fariñas I, Quo RG, Parslow TG, et al. (1994) Development of several organs that require inductive epithelial-mesenchymal interactions is impaired in LEF-1-deficient mice. Genes Dev 8: 2691–2703.

336. Cui C-Y, Durmowicz M, Ottolenghi C, Hashimoto T, Griggs B, et al. (2003) Inducible mEDA-A1 transgene mediates sebaceous gland hyperplasia and differential formation of two types of mouse hair follicles. Hum Mol Genet 12: 2931–2940. doi:10.1093/hmg/ddg325.

337. Mustonen T, Pispa J, Mikkola ML, Pummila M, Kangas AT, et al. (2003) Stimulation of ectodermal organ development by Ectodysplasin-A1. Dev Biol 259: 123–136.

338. Zhang M, Brancaccio A, Weiner L, Missero C, Brissette JL (2003) Ectodysplasin regulates pattern formation in the mammalian hair coat. genesis 37: 30–37. doi:10.1002/gene.10230.

339. Straznicky C, Rush RA (1985) The effect of nerve growth factor on developing primary sensory neurons of the trigeminal nerve in chick embryos. Anat Embryol 171: 91–95.

340. Hunter E, Begbie J, Mason I, Graham A (2001) Early development of the mesencephalic trigeminal nucleus. Dev Dyn 222: 484–493. doi:10.1002/dvdy.1197.

341. Narayanan CH, Narayanan Y (1978) Determination of the embryonic origin of the mesencephalic nucleus of the trigeminal nerve in birds. J Embryol Exp Morphol 43: 85–105.

342. Stainier DY, Gilbert W (1990) Pioneer neurons in the mouse trigeminal sensory system. Proc Natl Acad Sci USA 87: 923–927.

343. Louvi A, Yoshida M, Grove EA (2007) The derivatives of the Wnt3a lineage in the central nervous system. J Comp Neurol 504: 550–569. doi:10.1002/cne.21461.

344. Tyndel FJ, Bilbao JM, Tucker WS (1984) Unsuspected lesions in patients with bilateral tic douloureux. The Lancet 1: 1418.

345. Cho DY, Chang CG, Wang YC, Wang FH, Shen CC, et al. (1994) Repeat operations in failed microvascular decompression for trigeminal neuralgia. Neurosurgery 35: 665–669; discussion669–discussion670.

346. Capra NF, Anderson KV, Pride JB, Jones TE (1984) Simultaneous demonstration of neuronal somata that innervate the tooth pulp and adjacent periodontal tissues, using two retrogradely transported anatomic markers. Exp Neurol 86: 165–170.

347. Liem RS, Copray JC, van Willigen JD (1991) Ultrastructure of the rat mesencephalic trigeminal nucleus. Acta Anat (Basel) 140: 112–119.

348. Paxinos G, Halliday G, Watson C, Houtcherov Y, Wang H (2007) Atlas of the Developing Mouse Brain.

349. Rodriguez-Tébar A, Dechant G, Barde YA (1990) Binding of brain-

derived neurotrophic factor to the nerve growth factor receptor. Neuron 4: 487–492.

350. Wolburg H, Lippoldt A (2002) Tight junctions of the blood-brain barrier: development, composition and regulation. Vascul Pharmacol 38: 323–337.

351. Zappaterra MW, Lehtinen MK (2012) The cerebrospinal fluid: regulator of neurogenesis, behavior, and beyond. Cell Mol Life Sci. doi:10.1007/s00018-012-0957-x.

352. Kantaputra PN (2001) Dentinogenesis imperfecta-associated syndromes. Am J Med Genet 104: 75–78.

353. Dhaliwal H, McKaig S (2010) Dentinogenesis imperfecta. Dent Update 37: 364–366, 369–371.

354. Miletich I, Sharpe PT (2004) Neural crest contribution to mammalian tooth formation. Birth Defects Res C Embryo Today 72: 200–212. doi:10.1002/bdrc.20012.

355. Imai H, Osumi-Yamashita N, Ninomiya Y, Eto K (1996) Contribution of early-emigrating midbrain crest cells to the dental mesenchyme of mandibular molar teeth in rat embryos. Dev Biol 176: 151–165. doi:10.1006/dbio.1996.9985.

356. Choi SJ, Song IS, Feng JQ, Gao T, Haruyama N, et al. (2010) Mutant DLX 3 disrupts odontoblast polarization and dentin formation. Dev Biol 344: 682–692. doi:10.1016/j.ydbio.2010.05.499.

357. Aïoub M, Lézot F, Molla M, Castaneda B, Robert B, et al. (2007) Msx2 −/− transgenic mice develop compound amelogenesis imperfecta, dentinogenesis imperfecta and periodental osteopetrosis. Bone 41: 851–859. doi:10.1016/j.bone.2007.07.023.

358. Xiao S, Yu C, Chou X, Yuan W, Wang Y, et al. (2001) Dentinogenesis imperfecta 1 with or without progressive hearing loss is associated with distinct mutations in DSPP. Nat Genet 27: 201–204. doi:10.1038/84848.

359. Patel P (2001) Soundbites. Nat Genet 27: 129–130. doi:10.1038/84728.

360. He X, Axelrod JD (2006) A WNTer wonderland in Snowbird. Development 133: 2597–2603. doi:10.1242/dev.02452.

361. Kreidberg JA, Natoli TA, McGinnis L, Donovan M, Biggers JD, et al. (1999) Coordinate action of Wt1 and a modifier gene supports embryonic survival in the oviduct. Mol Reprod Dev 52: 366–375. doi:10.1002/(SICI)1098-2795(199904)52:4<366::AID-MRD5>3.0.CO;2-Y.

362. Ratelade J, Arrondel C, Hamard G, Garbay S, Harvey S, et al. (2010) A

murine model of Denys-Drash syndrome reveals novel transcriptional targets of WT1 in podocytes. Hum Mol Genet 19: 1–15. doi:10.1093/hmg/ddp462.

363. Patek CE, Brownstein DG, Fleming S, Wroe C, Rose L, et al. (2008) Effects on kidney disease, fertility and development in mice inheriting a protein-truncating Denys-Drash syndrome allele (Wt1tmT396). Transgenic Res 17: 459–475. doi:10.1007/s11248-007-9157-0.

364. Patek CE, Fleming S, Miles CG, Bellamy CO, Ladomery M, et al. (2003) Murine Denys-Drash syndrome: evidence of podocyte de-differentiation and systemic mediation of glomerulosclerosis. Hum Mol Genet 12: 2379–2394. doi:10.1093/hmg/ddg240.

365. Turgeon B, Meloche S (2009) Interpreting neonatal lethal phenotypes in mouse mutants: insights into gene function and human diseases. Physiol Rev 89: 1–26. doi:10.1152/physrev.00040.2007.

366. Gu B, Sun P, Yuan Y, Moraes RC, Li A, et al. (2009) Pygo2 expands mammary progenitor cells by facilitating histone H3 K4 methylation. J Cell Biol 185: 811–826. doi:10.1083/jcb.200810133.

367. Chen Y-Y, Li B-A, Wang H-D, Liu X-Y, Tan G-W, et al. (2010) The role of Pygopus 2 in rat glioma cell growth. Med Oncol. doi:10.1007/s12032-010-9488-1.

368. Lin H (2002) The stem-cell niche theory: lessons from flies. Nat Rev Genet 3: 931–940. doi:10.1038/nrg952.

369. Fuchs E, Tumbar T, Guasch G (2004) Socializing with the neighbors: stem cells and their niche. Cell 116: 769–778.

370. Spradling A, Drummond-Barbosa D, Kai T (2001) Stem cells find their niche. Nature 414: 98–104. doi:10.1038/35102160.

371. Cotsarelis G, Sun TT, Lavker RM (1990) Label-retaining cells reside in the bulge area of pilosebaceous unit: implications for follicular stem cells, hair cycle, and skin carcinogenesis. Cell 61: 1329–1337.

372. Watt FM (2002) The stem cell compartment in human interfollicular epidermis. J Dermatol Sci 28: 173–180.

373. Fuchs E, Raghavan S (2002) Getting under the skin of epidermal morphogenesis. Nat Rev Genet 3: 199–209. doi:10.1038/nrg758.

374. Blanpain C, Lowry WE, Geoghegan A, Polak L, Fuchs E (2004) Self-renewal, multipotency, and the existence of two cell populations within an epithelial stem cell niche. Cell 118: 635–648. doi:10.1016/j.cell.2004.08.012.

375. Niemann C, Watt FM (2002) Designer skin: lineage commitment in

postnatal epidermis. Trends Cell Biol 12: 185–192.

376. Horsley V, O'Carroll D, Tooze R, Ohinata Y, Saitou M, et al. (2006) Blimp1 defines a progenitor population that governs cellular input to the sebaceous gland. Cell 126: 597–609. doi:10.1016/j.cell.2006.06.048.

377. Petschnik AE, Klatte JE, Evers LH, Kruse C, Paus R, et al. (2010) Phenotypic indications that human sweat glands are a rich source of nestin-positive stem cell populations. Br J Dermatol 162: 380–383. doi:10.1111/j.1365-2133.2009.09512.x.

378. Hsu Y-C, Pasolli HA, Fuchs E (2011) Dynamics between stem cells, niche, and progeny in the hair follicle. Cell 144: 92–105. doi:10.1016/j.cell.2010.11.049.

379. Fuchs E (2009) Finding One's Niche in the Skin. Cell Stem Cell 4: 499–502. doi:10.1016/j.stem.2009.05.001.

380. Potten CS, Morris RJ (1988) Epithelial stem cells in vivo. J Cell Sci Suppl 10: 45–62.

381. Potten CS (1974) The epidermal proliferative unit: the possible role of the central basal cell. Cell Tissue Kinet 7: 77–88.

382. Panteleyev AA, Jahoda CA, Christiano AM (2001) Hair follicle predetermination. J Cell Sci 114: 3419–3431.

383. Unna PG (1876) Beitrage zur histologie und entwicklungsge. Arch Mikroskop Anat Entwicklungsmech 12: 665–741.

384. Jahoda CA, Oliver RF (1984) Histological studies of the effects of wounding vibrissa follicles in the hooded rat. J Embryol Exp Morphol 83: 95–108.

385. Jahoda CA, Horne KA, Oliver RF (1984) Induction of hair growth by implantation of cultured dermal papilla cells. Nature 311: 560–562.

386. KLIGMAN AM (1959) The human hair cycle. J Invest Dermatol 33: 307–316.

387. Müller-Röver S, Handjiski B, van der Veen C, Eichmüller S, Foitzik K, et al. (2001) A comprehensive guide for the accurate classification of murine hair follicles in distinct hair cycle stages. J Invest Dermatol 117: 3–15. doi:10.1046/j.0022-202x.2001.01377.x.

388. Paus R, Cotsarelis G (1999) The biology of hair follicles. N Engl J Med 341: 491–497. doi:10.1056/NEJM199908123410706.

389. Ito M, Kizawa K, Hamada K, Cotsarelis G (2004) Hair follicle stem cells in the lower bulge form the secondary germ, a biochemically distinct but functionally equivalent progenitor cell population, at the termination of

catagen. Differentiation 72: 548–557. doi:10.1111/j.1432-0436.2004.07209008.x.

390. Tobin DJ, Gunin A, Magerl M, Handijski B, Paus R (2003) Plasticity and cytokinetic dynamics of the hair follicle mesenchyme: implications for hair growth control. J Invest Dermatol 120: 895–904. doi:10.1046/j.1523-1747.2003.12237.x.

391. Chi WY, Enshell-Seijffers D, Morgan BA (2010) De novo production of dermal papilla cells during the anagen phase of the hair cycle. J Invest Dermatol 130: 2664–2666. doi:10.1038/jid.2010.176.

392. Driskell RR, Clavel C, Rendl M, Watt FM (2011) Hair follicle dermal papilla cells at a glance. J Cell Sci 124: 1179–1182. doi:10.1242/jcs.082446.

393. Taylor G, Lehrer MS, Jensen PJ, Sun TT, Lavker RM (2000) Involvement of follicular stem cells in forming not only the follicle but also the epidermis. Cell 102: 451–461.

394. Morris RJ, Liu Y, Marles L, Yang Z, Trempus C, et al. (2004) Capturing and profiling adult hair follicle stem cells. Nat Biotechnol 22: 411–417. doi:10.1038/nbt950.

395. Greco V, Chen T, Rendl M, Schober M, Pasolli HA, et al. (2009) A two-step mechanism for stem cell activation during hair regeneration. Cell Stem Cell 4: 155–169. doi:10.1016/j.stem.2008.12.009.

396. Biernaskie J (2010) Human hair follicles: "bulging" with neural crest-like stem cells. J Invest Dermatol 130: 1202–1204. doi:10.1038/jid.2009.449.

397. Ramalho-Santos M, Yoon S, Matsuzaki Y, Mulligan RC, Melton DA (2002) "Stemness": transcriptional profiling of embryonic and adult stem cells. Science 298: 597–600. doi:10.1126/science.1072530.

398. Ivanova NB, Dimos JT, Schaniel C, Hackney JA, Moore KA, et al. (2002) A stem cell molecular signature. Science 298: 601–604. doi:10.1126/science.1073823.

399. Li L, Mignone J, Yang M, Matic M, Penman S, et al. (2003) Nestin expression in hair follicle sheath progenitor cells. Proc Natl Acad Sci USA 100: 9958–9961. doi:10.1073/pnas.1733025100.

400. Biernaskie J, Paris M, Morozova O, Fagan BM, Marra M, et al. (2009) SKPs derive from hair follicle precursors and exhibit properties of adult dermal stem cells. Cell Stem Cell 5: 610–623. doi:10.1016/j.stem.2009.10.019.

401. Fernandes KJL, McKenzie IA, Mill P, Smith KM, Akhavan M, et al. (2004) A dermal niche for multipotent adult skin-derived precursor cells. Nat

Cell Biol 6: 1082–1093. doi:10.1038/ncb1181.

402. Amoh Y, Li L, Katsuoka K, Penman S, Hoffman RM (2005) Multipotent nestin-positive, keratin-negative hair-follicle bulge stem cells can form neurons. Proc Natl Acad Sci USA 102: 5530–5534. doi:10.1073/pnas.0501263102.

403. Yu H, Kumar SM, Kossenkov AV, Showe L, Xu X (2010) Stem cells with neural crest characteristics derived from the bulge region of cultured human hair follicles. J Invest Dermatol 130: 1227–1236. doi:10.1038/jid.2009.322.

404. Amoh Y, Li L, Katsuoka K, Hoffman RM (2010) Embryonic development of hair follicle pluripotent stem (hfPS) cells. Med Mol Morphol 43: 123–127. doi:10.1007/s00795-010-0498-z.

405. Fuerer C, Nusse R, Berge ten D (2008) Wnt signalling in development and disease. Max Delbrück Center for Molecular Medicine meeting on Wnt Signaling in Development and Disease. EMBO Rep 9: 134–138. doi:10.1038/sj.embor.7401159.

406. Etchevers H (2011) Primary culture of chick, mouse or human neural crest cells. Nat Protoc 6: 1568–1577. doi:10.1038/nprot.2011.398.

407. Paddison PJ, Caudy AA, Bernstein E, Hannon GJ, Conklin DS (2002) Short hairpin RNAs (shRNAs) induce sequence-specific silencing in mammalian cells. Genes Dev 16: 948–958. doi:10.1101/gad.981002.

408. Summerton J (1999) Morpholino antisense oligomers: the case for an RNase H-independent structural type. Biochim Biophys Acta 1489: 141–158.

409. Pfeifer A, Ikawa M, Dayn Y, Verma IM (2002) Transgenesis by lentiviral vectors: lack of gene silencing in mammalian embryonic stem cells and preimplantation embryos. Proc Natl Acad Sci USA 99: 2140–2145. doi:10.1073/pnas.251682798.

410. Blancas AA, Chen C-S, Stolberg S, McCloskey KE (2011) Adhesive forces in embryonic stem cell cultures. Cell adhesion & migration 5: 472–479. doi:10.4161/cam.5.6.18270.

411. Greenlee AR, Kronenwetter-Koepel TA, Kaiser SJ, Liu K (2005) Comparison of Matrigel and gelatin substrata for feeder-free culture of undifferentiated mouse embryonic stem cells for toxicity testing. Toxicol In Vitro 19: 389–397. doi:10.1016/j.tiv.2004.11.002.

412. Bryja V, Bonilla S, Arenas E (2006) Derivation of mouse embryonic stem cells. Nat Protoc 1: 2082–2087. doi:10.1038/nprot.2006.355.

413. Felgner PL, Gadek TR, Holm M, Roman R, Chan HW, et al. (1987) Lipofection: a highly efficient, lipid-mediated DNA-transfection

procedure. Proc Natl Acad Sci USA 84: 7413–7417.

414. Felgner PL, Tsai YJ, Sukhu L, Wheeler CJ, Manthorpe M, et al. (1995) Improved cationic lipid formulations for in vivo gene therapy. Ann N Y Acad Sci 772: 126–139.

415. Neumann E, Schaefer-Ridder M, Wang Y, Hofschneider PH (1982) Gene transfer into mouse lyoma cells by electroporation in high electric fields. EMBO J 1: 841–845.

416. Hughes OR, Stewart R, Dimmick I, Jones EA (2009) A critical appraisal of factors affecting the accuracy of results obtained when using flow cytometry in stem cell investigations: Where do you put your gates? Cytometry 75A: 803–810. doi:10.1002/cyto.a.20764.

417. Sieber-Blum M, Hu Y (2008) Mouse epidermal neural crest stem cell (EPI-NCSC) cultures. J Vis Exp. doi:10.3791/772.

418. Bez A, Corsini E, Curti D, Biggiogera M, Colombo A, et al. (2003) Neurosphere and neurosphere-forming cells: morphological and ultrastructural characterization. Brain Res 993: 18–29.

419. O'Connor MD, Kardel MD, Iosfina I, Youssef D, Lu M, et al. (2008) Alkaline phosphatase-positive colony formation is a sensitive, specific, and quantitative indicator of undifferentiated human embryonic stem cells. Stem cells (Dayton, Ohio) 26: 1109–1116. doi:10.1634/stemcells.2007-0801.

420. Martin GR, Evans MJ (1975) Differentiation of clonal lines of teratocarcinoma cells: formation of embryoid bodies in vitro. Proc Natl Acad Sci USA 72: 1441–1445.

421. Coucouvanis E, Martin GR (1995) Signals for death and survival: a two-step mechanism for cavitation in the vertebrate embryo. Cell 83: 279–287.

422. Gritti A, Parati EA, Cova L, Frolichsthal P, Galli R, et al. (1996) Multipotential stem cells from the adult mouse brain proliferate and self-renew in response to basic fibroblast growth factor. J Neurosci 16: 1091–1100.

423. Reynolds BA, Weiss S (1992) Generation of neurons and astrocytes from isolated cells of the adult mammalian central nervous system. Science 255: 1707–1710.

424. Lobo M-VT, Alonso FJM, Redondo C, López-Toledano MA, Caso E, et al. (2003) Cellular Characterization of Epidermal Growth Factor-expanded Free-floating Neurospheres. Journal of Histochemistry & Cytochemistry 51: 89–103. doi:10.1177/002215540305100111.

425. Suslov ON, Kukekov VG, Ignatova TN, Steindler DA (2002) Neural stem

cell heterogeneity demonstrated by molecular phenotyping of clonal neurospheres. Proc Natl Acad Sci USA 99: 14506–14511. doi:10.1073/pnas.212525299.

426. Druckenbrod NR, Epstein ML (2005) The pattern of neural crest advance in the cecum and colon. Dev Biol 287: 125–133. doi:10.1016/j.ydbio.2005.08.040.

427. Thomas S, Thomas M, Wincker P, Babarit C, Xu P, et al. (2008) Human neural crest cells display molecular and phenotypic hallmarks of stem cells. Hum Mol Genet 17: 3411–3425. doi:10.1093/hmg/ddn235.

428. Carmona-Fontaine C, Matthews H, Mayor R (2008) Directional cell migration in vivo: Wnt at the crest. Cell adhesion & migration 2: 240–242.

429. Falasca M, Raimondi C, Maffucci T (2011) Boyden chamber. Methods Mol Biol 769: 87–95. doi:10.1007/978-1-61779-207-6_7.

430. Teo J-L, Kahn M (2010) The Wnt signaling pathway in cellular proliferation and differentiation: A tale of two coactivators. Adv Drug Deliv Rev 62: 1149–1155. doi:10.1016/j.addr.2010.09.012.

431. Chen D, Jarrell A, Guo C, Lang R, Atit R (2012) Dermal β-catenin activity in response to epidermal Wnt ligands is required for fibroblast proliferation and hair follicle initiation. Development 139: 1522–1533. doi:10.1242/dev.076463.

432. Chen Y, Guan Y, Liu H, Wu X, Yu L, et al. (2012) Activation of the Wnt/β-catenin signaling pathway is associated with glial proliferation in the adult spinal cord of ALS transgenic mice. Biochem Biophys Res Commun. doi:10.1016/j.bbrc.2012.03.006.

433. Giraldez AJ (2003) Wingless and Notch signaling provide cell survival cues and control cell proliferation during wing development. Development 130: 6533–6543. doi:10.1242/dev.00904.

434. Qin X, Zhang H, Zhou X, Wang C, Zhang H, et al. (2007) Proliferation and migration mediated by Dkk-1/Wnt/β-catenin cascade in a model of hepatocellular carcinoma cells. Translational Research 150: 281–294. doi:10.1016/j.trsl.2007.06.005.

435. Nteliopoulos G, Marley SB, Gordon MY (2009) Influence of PI-3K/Akt pathway on Wnt signalling in regulating myeloid progenitor cell proliferation. Evidence for a role of autocrine/paracrine Wnt regulation. Br J Haematol 146: 637–651. doi:10.1111/j.1365-2141.2009.07823.x.

436. Kawano Y (2003) Secreted antagonists of the Wnt signalling pathway. J Cell Sci 116: 2627–2634. doi:10.1242/jcs.00623.

437. Saldanha G, Ghura V, Potter L, Fletcher A (2004) Nuclear beta-catenin in

basal cell carcinoma correlates with increased proliferation. Br J Dermatol 151: 157–164. doi:10.1111/j.1365-2133.2004.06048.x.

438. Wang X, Goode EL, Fredericksen ZS, Vierkant RA, Pankratz VS, et al. (2008) Association of genetic variation in genes implicated in the beta-catenin destruction complex with risk of breast cancer. Cancer Epidemiol Biomarkers Prev 17: 2101–2108. doi:10.1158/1055-9965.EPI-08-0134.

439. Zhang J, Gill AJM, Issacs JD, Atmore B, Johns A, et al. (2011) The Wnt/β-catenin pathway drives increased cyclin D1 levels in lymph node metastasis in papillary thyroid cancer. Hum Pathol. doi:10.1016/j.humpath.2011.08.013.

440. Liu L, Rao JN, Zou T, Xiao L, Smith A, et al. (2012) Activation of Wnt3a signaling stimulates intestinal epithelial repair by promoting c-Myc-regulated gene expression. AJP: Cell Physiology 302: C277–C285. doi:10.1152/ajpcell.00341.2011.

441. McCoy KE, Zhou X, Vize PD (2011) Non-canonical wnt signals antagonize and canonical wnt signals promote cell proliferation in early kidney development. Dev Dyn 240: 1558–1566. doi:10.1002/dvdy.22626.

442. Davidson KC, Adams AM, Goodson JM, McDonald CE, Potter JC, et al. (2012) Wnt/β-catenin signaling promotes differentiation, not self-renewal, of human embryonic stem cells and is repressed by Oct4. Proceedings of the National Academy of Sciences 109: 4485–4490. doi:10.1073/pnas.1118777109.

443. Dravid G, Ye Z, Hammond H, Chen G, Pyle A, et al. (2005) Defining the role of Wnt/beta-catenin signaling in the survival, proliferation, and self-renewal of human embryonic stem cells. Stem cells (Dayton, Ohio) 23: 1489–1501. doi:10.1634/stemcells.2005-0034.

444. Aubert J, Dunstan H, Chambers I, Smith A (2002) Functional gene screening in embryonic stem cells implicates Wnt antagonism in neural differentiation. Nat Biotechnol 20: 1240–1245. doi:10.1038/nbt763.

445. Sato N, Meijer L, Skaltsounis L, Greengard P, Brivanlou AH (2004) Maintenance of pluripotency in human and mouse embryonic stem cells through activation of Wnt signaling by a pharmacological GSK-3-specific inhibitor. Nat Med 10: 55–63. doi:10.1038/nm979.

446. Wang Y, Song L, Zhou CJ (2011) The canonical Wnt/β-catenin signaling pathway regulates Fgf signaling for early facial development. Dev Biol 349: 250–260. doi:10.1016/j.ydbio.2010.11.004.

447. Yin Y, White AC, Huh S-H, Hilton MJ, Kanazawa H, et al. (2008) An FGF–WNT gene regulatory network controls lung mesenchyme development. Dev Biol 319: 426–436. doi:10.1016/j.ydbio.2008.04.009.

448. Shu W, Guttentag S, Wang Z, Andl T, Ballard P, et al. (2005) Wnt/β-catenin signaling acts upstream of N-myc, BMP4, and FGF signaling to regulate proximal–distal patterning in the lung. Dev Biol 283: 226–239. doi:10.1016/j.ydbio.2005.04.014.

449. Takechi M, Kuratani S (2010) History of studies on mammalian middle ear evolution: a comparative morphological and developmental biology perspective. J Exp Zool B Mol Dev Evol 314: 417–433. doi:10.1002/jez.b.21347.

450. Kuratani S (2004) Evolution of the vertebrate jaw: comparative embryology and molecular developmental biology reveal the factors behind evolutionary novelty. J Anat 205: 335–347. doi:10.1111/j.0021-8782.2004.00345.x.

451. Liu Y-H, Shi S-Q, Zhang Y-L, Dai Y, Shang X, et al. (2010) [Prenatal diagnosis of a fetus in a family with mandibulofacial dysostosis]. Zhonghua Yi Xue Yi Chuan Xue Za Zhi 27: 437–440. doi:10.3760/cma.j.issn.1003-9406.2010.04.017.

452. Dixon J, Jones NC, Sandell LL, Jayasinghe SM, Crane J, et al. (2006) Tcof1/Treacle is required for neural crest cell formation and proliferation deficiencies that cause craniofacial abnormalities. Proc Natl Acad Sci USA 103: 13403. doi:10.1073/pnas.0603730103.

453. Conway SJ, Henderson DJ, Copp AJ (1997) Pax3 is required for cardiac neural crest migration in the mouse: evidence from the splotch (Sp2H) mutant. Development 124: 505–514.

454. Park D, Xiang AP, Mao FF, Zhang L, Di C-G, et al. (2010) Nestin is required for the proper self-renewal of neural stem cells. Stem cells (Dayton, Ohio) 28: 2162–2171. doi:10.1002/stem.541.

"To kill an error is as good a service as, and sometimes even better than, the establishing of a new truth or fact."

Charles Darwin, 1880.